4-D CLOUD PROPERTIES FROM PASSIVE SATELLITE DATA AND

APPLICATIONS TO RESOLVE THE FLIGHT ICING THREAT TO AIRCRAFT

By

William L. Smith Jr.

A dissertation submitted in partial fulfillment of

the requirements for the degree of

Doctor of Philosophy

(Atmospheric and Oceanic Sciences)

at the

UNIVERSITY OF WISCONSIN-MADISON

2014

Date of final oral examination: 07/22/14

This dissertation is approved by the following members of the Final Oral Committee:
Steve Ackerman, Professor, Atmospheric and Oceanic Sciences
Ralf Bennartz, Professor, University of Wisconsin-Madison
Tristen L'Ecuyer, Professor, Atmospheric and Oceanic Sciences
Michael Morgan, Professor, Atmospheric and Oceanic Sciences
Paul Menzel, University of Wisconsin-Madison
Bruce Doddridge, NASA Langley Research Center

Abstract

The threat for aircraft icing in clouds is a significant hazard that routinely impacts aviation operations. Accurate diagnoses and forecasts of aircraft icing conditions requires identifying the location and vertical distribution of clouds with super-cooled liquid water (SLW) droplets, as well as the characteristics of the droplet size distribution. Traditional forecasting methods rely on guidance from numerical models and conventional observations, neither of which currently resolve cloud properties adequately on the optimal scales needed for aviation. Satellite imagers provide measurements over large areas with high spatial resolution that can be interpreted to identify the locations and characteristics of clouds, including features associated with adverse weather and storms. This thesis develops new techniques for interpreting cloud products derived from satellite data to infer the flight icing threat to aircraft. For unobscured low clouds, the icing threat is determined using empirical relationships developed from correlations between satellite imager retrievals of liquid water path and droplet size with icing conditions reported by pilots (PIREPS). For deep ice over water cloud systems, ice and liquid water content (IWC and LWC) profiles are derived by using the imager cloud properties to constrain climatological information on cloud vertical structure and water phase obtained apriori from radar and lidar observations, and from cloud model analyses. Retrievals of the SLW content embedded within overlapping clouds are mapped to the icing threat using guidance from an airfoil modeling study. Compared to PIREPS and ground-based icing remote sensing datasets, the satellite icing detection and intensity accuracies are approximately 90% and 70%, respectively. The satellite-derived icing boundaries capture the reported altitudes over 90% of the time. Mean differences between the imager IWC retrievals with those derived from CloudSat and CALIPSO profiling data are less than 30% for a wide range of cloud conditions. This level of closure in the cloud water budget

can only be achieved by correcting for errors in the imager retrievals due to the simplifying but poor assumption that deep optically thick clouds are single-phase and vertically homogeneous. When applied to geostationary satellite data, the profiling method provides a real-time characterization of clouds in 4-D. This research should improve the utility of satellite imager data for quantitatively diagnosing and predicting clouds and their effects in weather and climate applications.

Acknowledgements

I would like to thank my father for his support, encouragement and companionship throughout my career. Despite a significant interest in weather as a young man, I initially resisted the idea of following the same career path that he had. Luckily, I had an intervention. As a civil engineering undergraduate at the University of Wisconsin-Madison (UW) in the mid-80's, I had the privilege of working with Dr. Paul Menzel and Dr. Don Wylie as a student hourly at the Space Science and Engineering Center. It was there that I was first introduced to the Man-computer Interactive Data Access System (McIDAS), a revolutionary tool developed at the UW Space Science and Enginerring Center (SSEC) for visualizing satellite data and geophysical satellite retrievals in concert with a wide variety of conventional weather observations and numerical model outputs. My career path epiphany occurred rather abruptly one day while transitioning from my engineering studies (mass sludge flow calculations to be specific) to my 'really cool' job at a McIDAS terminal analyzing and validating cloud properties derived from satellite data. The next semester I declared a major in Meteorology.

I would like to thank Gary Wade, Tom Achtor, Jim Nelson, Tony Schreiner and Chris Velden for their patience in teaching me how to use McIDAS at the Cooperative Institute for Meteorological Satellite Studies, and for piquing my early interests in satellite meteorology.

I am grateful to Dr. Patrick Minnis, particularly for his friendship, mentorship and inspiration, but also for his support in bringing McIDAS to NASA, where it has played a critical role, not only in developing this dissertation, but in developing and advancing satellite programs to improve our understanding of clouds and their impacts on weather and climate. Without

McIDAS, many of our discoveries and advances at NASA would have been more difficult or possibly not have occurred at all.

I appreciate all of the hard work by those at SSEC who pioneered the development and portability of McIDAS and who continue to keep it viable.

I thank my thesis committee, Dr. Ralf Bennartz, Dr. Tristan L'Ecuyer, Dr. Paul Menzel, Dr. Michael Morgan and particularly my advisor, Dr. Steve Ackerman. At NASA, the support and encouragement of Mr. Gary Gibson, Dr. Bruce Doddridge and all of my managers and co-workers, but particularly Dr. Cecilia Fleeger, Mr. Doug Spangenberg, Mr. Walt Miller, Mr. Louis Nguyen, Mr. Pat Heck, Mr. Rabindra Palikonda, Ms. Mandy Khaiyer, and Ms. Sunny Sun-Mack are greatly appreciated.

Finally, I thank my wife Nitchie for all of her support, her willingness to move to Madison for two years with our two boys Jake and Nick, and for sticking with me after that. As I already knew from experience, moving away from the great people and city of Madison is not an easy thing to do.

Table of Contents

List of Figures

List of Tables

1 Introduction

Clouds influence the dynamics and thermodynamics of the atmosphere and thus affect the weather and climate of the Earth in many ways. They modulate the flow of solar and thermal energy, which impacts local air temperatures, they influence large-scale circulations through the release of latent heat, and they play a critical role in the overall balance of the Earth's energy budget (Ramanathan et al., 1989; Stephens 2005). Clouds are a key element in the hydrologic cycle (e.g., Stephens 2006), producing precipitation to transport fresh water to the surface. They are often associated with adverse weather conditions that can be disruptive and even dangerous to human life. Because of their profound influence, an accurate representation of clouds is needed in order to accurately predict the weather and climate with numerical models (Tripoli and Cotton 1982; Cess et al., 1989). Observing clouds with in-situ sensors (e.g., Baumgardner 1983; Twohy et al., 1987; Baumgardner et al., 2002; Baker and Lawson 2006), ground-based remote sensors (e.g., Sassen 1991; Matrosov et al., 1992; Clothiaux et al., 1995, 2000; Mace et al. 1998) and satellite remote sensing systems (e.g., Menzel et al., 1994; Barnes et al., 1998; Stephens et al., 2002; Winker et al., 2002), all contribute to an understanding of the composition and distribution of clouds in the atmosphere. Current satellite data provide a wealth of global cloud-related information (e.g., Rossow and Schiffer 1991; Minnis et al., 1995 and 2011b; Han et al., 1998; King et al. 2003; Bennartz 2007; Mace et al., 2009; Stephens et al., 2008). Increased computer power is allowing for more advanced representations of clouds in numerical models (e.g., Meyers et al., 1995; Reisner at al., 1998; Thompson et al., 2004; Hashino and Tripoli, 2007) and an improved understanding of cloud processes.

Despite these important advances, many challenges remain in adequately characterizing clouds and their effects in numerical weather analyses and forecast models from both a

theoretical and practical standpoint (e.g., Khain et al., 2000; Errico et al., 2007). In general, this is due to a number of factors, including; (1) the microphysical processes of formation and growth, and the interaction of aerosols, liquid and ice hydrometeors is poorly understood in certain conditions, (2) the mathematical formulations or parameterizations used to describe these complex processes in models and relate them to dynamic air motions are inadequate, and (3) the 3-dimensional distribution of cloud hydrometeors in the atmosphere are poorly observed and not accurately prescribed in model initial conditions.

Satellite imager data taken from scanning passive radiometric sensors flown on operational weather and other research satellites can help address the last factor. Satellites are the only observing platform with the capability to observe characteristics of the Earth and atmosphere over large areas and at the spatial and temporal scales needed by many weather related applications. Under many conditions, observations from satellite imagers offer the ability to accurately detect the location of clouds (Ackerman et al., 1998; Minnis et al., 2008a) and estimate their altitudes (Smith and Platt, 1978; Holz et al., 2008; Smith et al., 2008; Minnis et al., 2008c), optical and macro-physical properties (Nakajima and King, 1990; Minnis et al., 1995; King et al., 1997; Minnis et al., 2011b). These techniques were largely pioneered in the United States and developed under the auspices of satellite programs designed to monitor and improve our understanding of clouds on the Earth's climate. Despite the vast amount of work and resources expended in developing cloud property retrievals from imager data, they remain underutilized, particularly in weather applications and decision support systems (DSS).

A major objective of this dissertation is to demonstrate that satellite-derived cloud products can and should play a more important role in weather applications and DSS. This is accomplished by developing new methods that utilize operational satellite cloud retrievals to

improve the instantaneous resolution of cloud vertical structure and to estimate the flight icing threat to aircraft in a wide range of cloud conditions. This document is organized in the following way. The motivation and objectives for this work are discussed in Section 2. Section 3 describes the models and data used in this study. In Section 4, satellite-derived cloud properties are compared to cloud properties derived in an advanced mesoscale numerical modeling system. The comparisons are meant to illustrate some of the outstanding issues associated with models and observations, and to highlight the potential benefits for satellite cloud retrievals in weather applications. In section 5, a cloud water content profiling capability is developed. Section 6 describes a series of algorithms developed to estimate the flight icing threat to aircraft using satellite cloud retrievals as the primary inputs. The key findings and potential implications are summarized in Section 7 along with suggestions for future work needed to refine the methods.

2 Motivation and Objectives

This dissertation is partially motivated by the fact that despite the vast amount of work and resources expended in developing cloud property retrievals from imager data for climate applications, they remain underutilized in weather applications and DSS. An example of such a system is the 4-D weather cube, a concept in development for the Next Generation Transportation System (NextGen). Accurate diagnoses and predictions of clouds and associated weather conditions are urgently needed by the transportation industry, particularly aviation, in order to improve operational safety and efficiency. Adverse weather accounts for nearly 70% of all air traffic delays within the U.S. National Airspace System (Bureau of Transportation Statistics). The Federal Aviation Administration (FAA) has determined that as much as two thirds of weather-related delays are potentially avoidable with better weather information and roughly 20% of all aviation accidents are weather related (FAA NASDAC). The concept of a 4-

D weather cube is being developed to address that need by integrating observed and forecasted weather information into a shared 4-D database, providing an integrated and nationally consistent weather picture for a variety of users and to support operational decision support systems. However, satellite data are currently only slated to play a rudimentary role with respect to characterizing clouds and their impacts, both directly via specific applications and indirectly via improved numerical cloud analyses. Participation by the satellite community in developing the 4-D cube is also largely void. There are a few possible reasons for this. First, many routine satellite derived products are not considered to be 'operational' since they do not meet some pre-determined availability criteria set by program managers for use in DSS. The criteria seem to vary from program to program. For example, products that are approved for operational use by the National Weather Service (NWS), are not approved for use by the FAA (Marcia Politovitch, UCAR, personal communication). Second, while satellite data have long been recognized for their utility in observing the horizontal and temporal distribution of clouds, their utility for describing quantitatively, or constraining, the vertical distribution of cloud properties has not been demonstrated. This is important because clouds and their impacts on both the weather and climate systems are of course a three-dimensional spatial problem. Thus, while the weather forecast community recognizes the need for improved observations of clouds and cloud properties, the lack of apparent vertical resolution may be a barrier to more widespread use. A common theme that has been propagating in program management and research evolution plans within the NWS and the FAA is that higher resolution models and improved cloud microphysics schemes will improve the resolution of clouds. As a result, much of the available funding within the FAA and National Oceanic and Atmospheric Administration (NOAA) has been directed to two places; (1) modeling centers to improve model resolutions/physics and (2) to satellite and

radar programs to improve observations. However, relatively little funding has been directed toward improved assimilation and incorporation of satellite cloud retrievals in models and DSS. While model improvements could lead to modest gains in some cases, the more fundamental problem is the latter, which is the fact that current observational information on clouds is not being adequately assimilated or utilized to initialize forecast models. More frequent and tighter collaboration between the satellite cloud retrieval and weather forecasting communities is needed. It is also possible that the satellite cloud retrieval community has not yet done an adequate job of characterizing errors and uncertainties in order to better promote the more effective use of satellite products in weather applications. It should be pointed out that NOAA is working to break down and address some of these barriers in their next generation Geostationary Operational Environmental Satellite (GOES) program (GOES-R). For GOES-R, NOAA is sponsoring and promoting the development of an operational cloud retrieval system and demonstrating new satellite products and applications for the NWS via well-designed and focused 'Proving Ground' experiments.

In this study, new methods to derive cloud water content (CWC) profiles and to infer the flight icing threat to aircraft from the satellite retrievals are developed and demonstrated. Accurate diagnoses and forecasts of atmospheric icing conditions not only require knowledge of the location of clouds, but also require knowledge of the vertical distribution of super-cooled liquid water (SLW) and the associated characteristics of the SLW droplet size distribution. In this work, an approach is taken that utilizes traditional satellite-derived cloud properties, including microphysical parameters, to infer the potential existence and density of SLW embedded in a wide variety of cloud types, including deep mixed-phase ice over water cloud systems often associated with synoptic scale storm systems. In order to accomplish this, an

improved understanding of the satellite product uncertainties is developed and empirical methods are employed to improve their overall accuracies. Better information on cloud vertical structure, which is typically void in traditional passive satellite retrievals, is also required. For deep ice over water cloud systems, imager cloud properties are used to constrain climatological information on cloud vertical structure and water phase obtained apriori from radar and lidar observations, and from cloud model analyses. The motivation for this synergistic approach is the fact that in many instances, no single observing system or numerical modeling capability can realistically capture or predict cloud properties with the optimal resolution and accuracy needed. Therefore, the unique, but complementary information on clouds that is captured from multiple observing and modeling systems is assessed independently and combined and constrained with operational satellite retrievals to improve the four dimensional characterization of clouds for weather and climate applications.

Icing reports from pilots (PIREPS) and case studies conducted at the time of several serious aviation incidents are used to validate the satellite icing threat estimates. Ice water content (IWC) profiles derived from the satellite imager data in a wide range of cloud conditions are compared to CloudSat and CALIPSO retrievals. The level of agreement found with CloudSat/CALIPSO in the upper troposphere along with the degree of correspondence with icing PIREPS in the lower troposphere provides a closure test for the profiling method and demonstrates how well passive satellite observations can be used to infer the vertical distribution of cloud water in the atmosphere using the new methods developed here.

Although optically thick ice over water clouds occur relatively infrequently in most locations, they contain a significant fraction of the total cloud mass found over large areas of the Earth, are commonly associated with hazardous weather and precipitation, and are therefore a

major weather concern and a central focus in numerical weather prediction (NWP). Thus, an additional potential benefit of this study is a new synergistic method for estimating the global distribution of cloud ice and liquid water content that is unlike any method previously developed and that could play a future role in helping to validate weather and climate models.

3 Models and Data

3.1 NOAA GSD/ESRL Assimilation and Modeling System

The Rapid Update Cycle (RUC), and its successor, the Rapid Refresh (RAP), are NOAA/NCEP (National Centers for Environmental Prediction) operational weather prediction systems developed at the Earth Systems Research Laboratory (ESRL) in the NOAA Global Systems Division (GSD) in Boulder, Colorado. The RUC and RAP serve users needing frequently updated short-range weather forecasts, including those in the US aviation community, the U.S. severe weather forecasting community and the renewable energy industry. The RUC and RAP are key elements of the FAA Aviation Weather Research Program. They are used in this aviation weather focused study because the cloud analysis scheme, which incorporates satellite-derived cloud products in the model's assimilation system, is relatively advanced with respect to the volume of cloud observations ingested. The RAP replaced the RUC as the NOAA hourly-updated assimilation/modeling system operational at NCEP starting 1 May 2012. Therefore, cloud fields developed from both systems in the native 50-level vertical coordinate have been evaluated with respect to satellite observations at different times during the course of this study.

The RUC numerical forecast model is an advanced version of the hydrostatic primitive equation model described by Bleck and Benjamin (1993) configured in a hybrid

isentropic/terrain following vertical coordinate system (Benjamin et al., 2004a). The NCEP RAP uses a configuration of the Weather Research and Forecasting (WRF) model in a 1-hour cycle system with updated RUC-like physics (Grell-G3 convection, Thompson/NCAR microphysics, RRTM longwave radiation, Goddard shortwave radiation, MYNN-Olsen turbulent mixing, RUC-Smirnova land-surface model). Like the RUC, it is run at 13-km horizontal resolution with 50 vertical levels in a sigma coordinate system but over a considerably expanded domain in all directions, notably to include Alaska. The RUC and RAP processing domains are shown in Figure 1. The Gridpoint Statistical Interpolation (GSI) system configured for the RAP includes a similar cloud/hydrometeor analysis that was developed for the RUC (Benjamin et al., 2004b). In this system, a wide variety of observations including rawindsonde, surface, aircraft, radar and satellite data are assimilated. The RUC and RAP cycle 1-hourly at full-resolution five microphysical species (q_c - cloud water, q_i - cloud ice, q_r - rain water, q_s - snow, and q_g - graupel, where q is the species mixing ratio) and have the capability for updating these fields using observations. The current assimilation technique for the RUC and RAP uses Meteorological Terminal Aviation routine weather Report (METAR) cloud and visibility data, and GOES cloud-top data to modify the 1-h forecast (background) 3-d hydrometeor and water vapor fields. The RUC assimilation of GOES cloud-top pressure and temperature (Benjamin et al., 2004b) is based on the creation of a 3-D gridded cloud logical field indicating volumes where: 1) it is known that clouds do not exist, 2) it is known that clouds do exist, or 3) the presence of clouds is indeterminate. The same logical structure used for GOES cloud assimilation is used again with METAR observations, which further improves the 3-d hydrometeor yes/no/unknown field when compared to observations. In the current cloud-building scheme, a layer depth of 50 hPa is assumed unless the same METAR observation reports precipitation, in which case, the depth is

set at 150 hPa. In this study, we compute and utilize the ice and liquid water contents (IWC and LWC) and water paths (IWP and LWP) computed from the cloud mixing ratios. Cloud ice (i), snow (s), and graupel (g) are combined to form the total IWC while cloud water (c) and rain (r) are combined to form the total LWC. That is,

$$LWC(z_i) = q_c(z_i)\rho_{air} + q_r(z_i)\rho_{air} \quad \text{for i=1,2,3,...,50 levels,} \tag{1}$$

$$IWC(z_i) = q_i(z_i)\rho_{air} + q_s(z_i)\rho_{air} + q_g(z_i)\rho_{air} \quad \text{for i=1,2,3,...,50 levels.} \tag{2}$$

The total cloud water content (CWC) at a particular level is

$$CWC(z_i) = LWC(z_i) + IWC(z_i). \tag{3}$$

Cloud water path (CWP) is the vertical integral of the CWC profile between the cloud top and base altitudes (Z_t and Z_b) computed as

$$CWP = \int_{Z_b}^{Z_t} CWC(z_i)\,dz. \tag{4}$$

3.2 Satellite Data and Products

The primary satellite datasets used in this study consist of cloud properties derived from passive sensor data obtained from the Geostationary Operational Environmental Satellite (GOES-10 thru GOES-15) imagers, the Moderate Resolution Imaging Spectroradiometer (MODIS) imager on the Sun-synchronous Aqua satellite, and from active sensor data obtained from the Cloud Profiling Radar (CPR) on CloudSat, and the Cloud-Aerosol Lidar with Orthogonal Polarization (CALIOP) on the CALIPSO satellite. AQUA, CloudSat, and CALIPSO are three satellites flown in the tightly coordinated National Aeronautics and Space Administration (NASA) A-Train formation. Brief descriptions of the various cloud products and the retrieval methods are given below.

3.2.1 GOES and MODIS

The passive satellite cloud retrieval algorithms were developed for the NASA Clouds and Earth's Radiant Energy System (CERES; Wielicki et al. 1996) climate program at NASA Langley Research Center (LaRC). A critical aspect in developing CERES cloud and radiation datasets for climate studies is that the algorithms and calibrations be consistent across satellite platforms. Thus, the retrieval algorithms were designed to nominally use just 4 or 5 channels common to the various satellite imagers. For MODIS, which is a 36-channel imager taking data with a nominal resolution of 1-km (250-m for the visible band), the critical bands for the cloud property retrievals used here are centered near 0.64 (visible, VIS), 3.7 (shortwave- infrared, SIR), 10.8 (infrared, IR), 12.0 (split window, SW) and 13.3 (CO_2) μm. Similar channels are available on the GOES imagers with a 4-km (1-km for the visible band) nominal resolution beginning with GOES-8, which was launched in 1994. The primary GOES channels are at 0.65, 3.9, 10.8, and at either 12.0 or 13.3 μm. The CO_2 channel replaced the SW channel beginning with GOES-12. The GOES radiances are calibrated to MODIS following the approach of Minnis et al. (2002, 2008b). The biggest impact of the calibration is to account for degradation in the GOES visible channel.

The retrieval algorithms used to derive cloud properties from the MODIS and GOES radiance data are the VISST (Visible Infrared Solar-infrared Split-window Technique) and SIST (Solar-infrared Infrared Split Window Technique). The VISST operates during the daytime using the VIS, SIR, IR, and SW or CO2 channels while the SIST operates at night using the same channels but without the VIS. These methods are described in Minnis et al. (2011a). The multi-layer VISST (ML-VISST) was implemented to identify multi-layer clouds for situations where optically thin cirrus overlay a lower level opaque cloud deck (Chang et al., 2010a), and to derive

improved cloud boundaries and optical properties of each layer (Chang et al., 2010b; Minnis et al., 2007) versus those that would be retrieved with the single-layer (SL) assumption. In these techniques, cloud parameters are derived using a set of parameterizations of the Earth-atmosphere reflectance (during daytime) and infrared emittance models (day and night) that incorporate cloud contributions for each relevant wavelength in order to match the observed satellite radiances with adding-doubling (AD) radiative transfer calculations, and assuming that each cloud layer is composed entirely of either ice crystals or water droplets. The calculations are conducted a-priori for a wide range of cloud liquid water droplets with effective radii values ranging from 2 to 32 μm, and for randomly oriented hexagonal ice crystal particle size distributions with effective diameters varying from 6 to 135 μm (Minnis et al., 1998). The parameterizations are able to reproduce the AD calculations quite accurately and significantly improve the efficiency of the inverse retrieval problem in routine operational applications.

The observed radiance at a particular wavelength depends to varying degrees on the cloud temperature, its geometric thickness, and microphysical properties, the latter of which includes the shapes of the cloud particles, their size distribution and concentration. For the algorithms described here, the IR radiance primarily depends on the effective cloud temperature (CET), while the VIS channel reflectance is mainly determined by the cloud optical depth (COD or τ), which is the convolution over the thickness of the cloud of the hydrometeor concentration or number density N, the extinction efficiency Q_e, and the effective cross-sectional area of the particle. For water droplets, the last variable is defined as the cross-sectional area of a droplet having the effective radius (CER or r_e),

$$r_e = \frac{\int\limits_{r1}^{r2} \pi r^3 n(r)\,dr}{\int\limits_{r1}^{r2} \pi r^2 n(r)\,dr},$$ (5)

where the integration is over a size distribution having the number density of particles *n(r)* of radius *r* between r_1 and r_2. In this study, r_e is retrieved from the SIR channel. The cloud optical depth is,

$$\tau = \pi Q_e \int\limits_{z1}^{z2} N r_e^2\,dr .$$ (6)

For ice clouds, the r_e is defined for randomly oriented hexagonal ice crystals and for a wide range of potential size distributions as in Minnis et al. 2011(a). The cloud water path can be computed as

$$CWP = 4\rho\tau r_e/(3Q_e),$$ (7)

where ρ is the water density, which is 1.0 and 0.9 g cm^{-3} for liquid and solid water, respectively. For clouds with tops determined to be ice (liquid), CWP is referred to as the IWP (LWP). In this formulation, it is assumed that the r_e is constant throughout the depth of the cloud. Since the value of CER retrieved using the SIR channel corresponds to an optical depth of ~3 or less at the top of the cloud, it is not necessarily representative of the entire cloud. For liquid clouds, the adiabatic approximation

$$LWP = 10\tau r_e/(9Q_e),$$ (8)

has been found to provide more accurate results if r_e is retrieved using the MODIS 2.1-µm channel (Seethala and Horvath, 2010). It is not necessarily more accurate when using the SIR retrieval of r_e. Hereafter, r_e is referred to as CER. In this study, the IWP and LWP are computed using Eq (7), where the extinction efficiency Q_e, ranges from 2.03 to 2.19 for liquid droplets. For

clouds with ice phase tops, the values of Q_e are found in Table 8 of Minnis et al. (1998). Due to the vertical homogeneity assumptions associated with Eq (7) and that no attempt is made to partition the effects of liquid and ice hydrometeors in mixed phase and overlapping cloud conditions, the retrieved values of IWP and LWP in some cloud conditions may not be that representative of the true values occurring in nature. Satellite VIS and SIR retrievals of LWP have been compared extensively and quite favorably with retrievals from microwave radiometer data (e.g., Bennartz, 2007; Dong et al., 2008; Painemal et al., 2012). On the other hand, with the exception of just a few studies (e.g., Mace et al., 1998, 2005), IWP has not been extensively validated. Their uncertainties are explored further in section 4.

CET is the effective radiating temperature of the cloud and typically is located at a distance from cloud top corresponding to a COD value of ~ 1.1 (Holz et al., 2008). It varies with the viewing zenith angle, VZA. The cloud effective height, CEH, is determined from CET using a temperature profile from an NWP analysis. The cloud top temperature, CTT, the geometric thickness, H, and therefore the cloud top and base heights, CTH and CBH, are derived from empirical methods based on CET, phase, and COD (Minnis et al., 2008c, 2010). Thus, the critical cloud parameters derived in this study from GOES (MODIS) data, hereafter the GDCP (MDCP), include for each cloudy pixel, the cloud top phase, the ice or liquid CER, the LWP or IWP, COD, CTT, CTH, H (and thus CBH).   The COD, LWP, IWP, CER, and H can be derived for a wide range of cloud thicknesses during the daytime since the solar-reflectance at visible wavelengths is sensitive to changes in COD from values less than 1 to values near 150. Radiative transfer calculations indicate that the reflectance changes very little with increasing COD beyond this range. Thus, in the LaRC system, the reflectance saturation point occurs at a COD value of 150. Since only infrared channels are available at night, COD, LWP, IWP, CER,

and H are only valid for optically thin clouds (COD < 6) since there is little sensitivity to variations in COD for thick clouds. The majority of this study will focus on the daytime satellite products.

3.2.2 CALIPSO

The CALIPSO satellite, is in the A-train formation and nearly coincident with the Aqua satellite (carrying MODIS) and the CloudSat CPR. CALIPSO carries the nadir-pointing CALIOP lidar (Winker et al., 2009), which measures parallel and perpendicular attenuated backscatter at 532 nm and total backscatter at 1064 nm. The measurements are interpreted at 60-m vertical resolution averaged to ~1.0 km along-track between 8.2 and 20.2 km and at 30-m vertical and 0.333-km along-track resolution below 8.2 km. A number of the CloudSat data products used here incorporate CALIPSO data. These are described in the next section. In addition, IWC profiles from release 3 of the CALIPSO Cloud Profile (CPro) product are used in this study. The CPro product provides a 532 nm backscatter, a 532 nm extinction coefficient, and IWC profiles at 395 vertical bins with a 60 m vertical and a 5 km horizontal resolution. The CALIPSO IWC is derived from an empirical relationship between the extinction coefficient and IWC:

$$IWC = C_0 (\frac{\sigma_{cp}}{1000})^{C_1}, \tag{9}$$

where $C_0 = 119$ g m^{-3} and $C_1 = 1.22$. This relationship was derived from co-located lidar extinction and in situ measurements of cloud particle properties obtained during field experiments (Heymsfield et al., 2005). The extinction coefficient (σ_{cp}) is obtained from the backscatter coefficient (β_{cp}),

$$\sigma_{cp} = S_{cp} \beta_{cp}, \tag{10}$$

where S_{cp} is the particle extinction-to-backscatter (lidar) ratio. In all versions of CALIPSO data (3.01-3.30) used in this study, the lidar ratio is assumed to be constant within the identified layers (features) (Young and Vaughan, 2009). A new parameterization to account for temperature and particle size dependence is being evaluated for a future update to the CALIPSO data products.

3.2.3 CloudSat

The CloudSat CPR is providing unprecedented data describing the vertical structure of cloud systems across the Earth (Stephens et al., 2008). CloudSat is also in the A-train formation with Aqua-MODIS and CALIPSO. The CPR measures the vertical profile of the radar reflectivity factor (Z_e) at a vertical resolution of 240 m between the surface and an altitude of 30-km. The footprint size is approximately 1.3 km across-track by 1.7 km along-track. The CloudSat version 4 data products, which include some MODIS and CALIPSO data in the processing schemes, are used in this study. Specifically, the GEOPROF-Lidar, CWC-RO, CWC-RVOD, and 2C-ICE products are used extensively. The GEOPROF-Lidar product (Mace et al., 2009) provides an accurate global characterization of cloud boundaries by combining the Radar and Lidar cloud masks, taking advantage of their unique sensitivities. The 2C-ICE product (Deng et al., 2010) provides estimates of ice water content derived by combining information from the CPR and CALIOP. The CWC-RO product provides cloud water content profile estimates derived from the radar-only (RO) while the CWC-RVOD uses the MODIS cloud visible optical depth (daytime only) to constrain the radar-only retrieval (RVOD) and is generally thought to be more accurate. Details on the CWC-RO and CWC-RVOD algorithms can be found in Wood (2008) and Austin et al. (2009). The CWC-RO and CWC-RVOD algorithms also provide composite CWC profiles from separate liquid and ice water retrievals. The algorithm assumes that the entire radar signal

profile comes from either liquid or ice phase particles, not a mixture of them (Wood, 2008). Total column profiles are retrieved for both cloud water phases and combined into a single best estimate that depends on the cloud temperature profile. The temperature profiles are from the CloudSat European Center for Medium-Range Weather (ECMWF) Forecasts Auxiliary product. For radar bins colder than 253 K, the bin is assumed to be an ice cloud and the ice profile is applied. For radar range bins warmer than 273 K, the liquid water profile is applied. Between 253 K and 273 K, the ice and liquid profiles are scaled linearly with temperature, and thus the uncertainty increases at these temperatures. In addition, the current version of CloudSat liquid phase retrieval uses an incorrect refractive index and has difficulty resolving cloud hydrometeors close to the surface (below ~ 1 km). Therefore, in this study we primarily focus on the CloudSat retrievals at altitudes above the 253 K level.

3.2.4 CERES C3M

The CERES C3M data product is used to help tune and validate the passive satellite cloud profiling method developed here. C3M merges CloudSat and CALIPSO satellite retrievals with CERES and MODIS cloud and radiation parameters (Kato et al., 2010) derived from AQUA satellite data. All three satellites are flown in the A-Train formation beginning with the AQUA, launched in in 2002, followed by CloudSat and CALIPSO which were launched in 2006. Thus, the A-Train provides a simultaneous multi-sensor view of clouds and radiation. The C3M data product was designed to merge and geo-locate several A-Train datasets containing cloud, aerosol and radiation retrievals, in order to better promote and simplify their use in scientific studies. A full-resolution intermediate product that is available upon request from the CERES program at NASA LaRC is employed here, which includes the CERES MDCP, the CloudSat CWC-RO, and the CALIPSO CPro cloud properties.

4 NWP Cloud Analyses and Forecasts vs. Satellite Observations

4.1 Background

NWP models are often considered the single most important tools used in modern day weather forecasting. However, accurate numerical forecasts depend significantly on how well the initial state of the atmosphere is known and prescribed to the model. Thus, observations of the atmospheric state are just as important in weather forecasting as the models that process the data to make future predictions. Because conventional in-situ observations from radiosondes and surface stations are sparse, relatively high-resolution satellite observations now constitute the vast majority of information assimilated by NWP models. Satellite radiance assimilation in NWP has been used effectively to improve weather forecasts in cloud free regions (e.g., Andersson et al., 1994; Derber and Wu, 1998; Le Marshall et al., 2006), particularly in data sparse regions over the oceans. Nevertheless, much of the satellite information content is not used due to data thinning procedures to overcome cloud contamination, computational resource limits, and other factors. Thus, the improvements in modern day weather forecasting that have been realized since the advent of weather satellites are likely to be modest relative to the potential impact that could still be achieved if more of the available information were utilized.

Clouds are fundamental to our weather, yet in general they remain poorly initialized in models. Some recent studies have demonstrated the potential to improve the initialization of clouds in NWP models by assimilating satellite radiances (e.g., Greenwald et al., 2002; Vukicevic et al., 2004, 2006) and satellite products (e.g., Lipton et al., 1999; Baylor et al., 2000; Benjamin et al., 2004a; Benedetti and Janiskova 2008; Jones et al., 2012), but much more work is needed to implement these advantageously in operational weather forecast systems. While promising, assimilation of cloud affected radiance is problematic because of the difficulties and

resources required to relate the radiances to the cloud variables resolved by the model (e.g., Bennartz and Greenwald, 2011).

Satellite products, rather than radiances, provide an alternative option to incorporate satellite data in NWP since their assimilation may be less resource intensive and they can provide information more directly related to the model variables. The satellite retrieval schemes are also typically optimized to exploit a greater spectrum of information contained in the satellite data, as well as other ancillary statistical and climatologically relevant information. With respect to clouds, for example, the NOAA/GSD-ESRL system (described in sec. 2.1) assimilates satellite derived cloud top heights, and subsequently modifies the hydrometeor and water vapor fields used to initialize the RAP (successor to the RUC) which is operational at NCEP. This method and others that are similar have demonstrated a positive impact in NWP (e.g., Yucel et al., 2002, 2003; Lin et al., 2003), even though crude assumptions are made regarding the vertical extent and density of the modified cloud fields.

In the mid-2000's, the NASA Applied Sciences program had an interest in fostering partnerships to help transition NASA weather satellite products to NOAA operational systems. As a result, a partnership between the satellite cloud remote sensing group at NASA LaRC and the Assimilation and Modeling branch at the NOAA GSD-ESRL was formed to facilitate the transition of new satellite products to an operational numerical weather forecasting center with the goal of improving short-range forecasts of cloud hydrometeors and associated weather conditions. The experimental models being run at GSD-ESRL and the operational model run at NCEP at that time were the RUC. Specific goals were to investigate the potential for assimilating satellite-derived LWP data to improve icing diagnoses and forecasts for low-level clouds and to ingest the cloud top height information that NASA was deriving from GOES

imager data. Cloud top pressure (CTP) data derived operationally over the CONUS from the GOES sounder data at the NOAA National Environmental Satellite, Data, and Information Service (NESDIS) (Schreiner et al., 2001) were already being assimilated into the RUC to help build and clear clouds in the model analysis. The NOAA/NESDIS GOES sounder CTP product provides good information on upper level clouds but over a somewhat limited domain confined to the CONUS. Thus, in the early implementations of the RUC, no satellite coverage was available over southern Canada, for example. Better information on low clouds and increased coverage over a much wider area were needed, particularly as the RUC domain was being significantly expanded for the RAP (see Figure 1). The NASA cloud altitude products derived from the GOES imagers met these needs and eventually replaced or augmented the NESDIS products in some versions of the RUC and RAP implemented at GSD/ESRL and at NCEP. While this collaboration between NASA and NOAA resulted in a number of significant advances, including the development of a system for routinely ingesting the NASA cloud products operationally at NCEP, and generally more accurate representations of clouds in the NOAA models, a number of issues and challenges also became apparent. In this section, a few of the more pertinent of these successes and remaining challenges are highlighted for the primary purpose of illustrating the need for continued work to improve the utility of satellite cloud properties in weather analyses and forecasts. While there are both theoretical and practical reasons that the assimilation of cloud data into models remains a considerably difficult problem (Errico et al., 2007), considering that more information on clouds are now being derived operationally from satellite data (e.g., cloud water path, cloud thickness), greater impacts are certainly possible.

4.2 Cloud Comparisons

In June of 2005 the operational implementation of the RUC at NCEP was updated from the RUC-20 (20 km grid) to the RUC-13 (13-km grid). That update included many changes to the model physics and cloud analysis scheme. Smith et al. (2006) compared cloud fields from each of these versions to the GDCP. The goal was to test the latest implementation (RUC-13) to see if the significant changes made to the cloud analysis code improved the level of agreement between the cloud analyses and forecasts when compared with the satellite products relative to that found in comparisons with the RUC-20. In that study, cloud properties analyzed and predicted by RUC were compared with the satellite estimates. The comparison focused on cloud frequency, cloud water path and cloud top height. The analysis was restricted to satellite products derived at 1445, 1745 and 2045 UTC, and analyzed and predicted (1-hr, 3-hr, and 6-hr forecasts) fields from the RUC valid at 1500, 1800 and 2100 UTC. Spatial matching was accomplished by mapping the satellite pixel-level parameters to the RUC grid. For each grid box, the satellite cloud parameters were averaged for the ice and liquid phases separately. A RUC grid box is either cloudy or clear. A corresponding GOES grid box is overcast, clear or partly cloudy. Cloud frequencies were computed for overcast grid boxes, and then broken down into levels; low (0-3 km), mid (3-7 km) and high (greater than 7 km), and stratified by the cloud phase at cloud top. The main conclusions from that study were that the total cloud cover in both models agreed well with the satellite observations on average for the entire domain. This result was not unexpected when considering that the model assimilation system was assimilating the NOAA-NESDIS CTP product to build and clear clouds in order to help improve the cloud initialization. However, when the comparisons were stratified by cloud top phase, the RUC-13 ice and liquid cloud cover was found to agree less with the satellite observations than that found for the RUC-20. The

RUC-13 was producing considerably more ice cloud and less liquid clouds than both the RUC-20 and that inferred from the satellite observations. These differences were largest at the analysis time and decreased with increasing forecast hour out to 6-hours. This led to the discovery of several bugs in the early implementation of the RUC-13. For example, a logic error was found that resulted in the clearing (removal) of too much oceanic stratocumulus due to a misinterpretation of the NOAA-NESDIS product. A coding error was also found in a relative humidity calculation within the cloud analysis code where a variable was not being properly indexed to account for latitudinal dependencies. It was encouraging at that time to learn that the satellite observations could be used to improve cloud analyses in the RUC via simple inter-comparisons.

Similar cloud comparisons to those conducted in Smith et al. (2006) were performed more recently to test the RAP version-1 (V1) cloud analyses and forecasts in both the GSD implementation as well as the operational implementation at NCEP. RAP analyses and forecasts out to 6-hrs were obtained and matched with the LaRC GDCP over a 7-day period from 12-18 November 2012. A few of the more pertinent results are presented here. The cloud and hydrometeor analysis in the RAP is considerably enhanced relative to its predecessor the RUC. These enhancements include the addition of the LaRC GOES imager CTP product, improvements in the use of METAR cloud ceiling data and in radar reflectivity assimilation among other improvements. More details on the RAP can be found at http://rapidrefresh.noaa.gov. In the GSD RAP, the GOES cloud building logic in the cloud analysis scheme was turned on, whereas in the NCEP RAPv1, the GOES cloud building logic was turned off.

Figure 2 depicts the LaRC CTH derived from GOES (Figure 2b) at 1745 UTC and that derived in the GSD (Figure 2c) and NCEPv1 RAP analysis (Figure 2d) at 1800 UTC on 12 November 2012. An RGB (red-green-blue channel combination) image derived from the VIS, SIR, and IR imager channels on GOES-E and GOES-W is also shown (Figure 2a) which easily distinguishes the clouds from cloud-free areas. The darkest of the pink areas are cloud free but snow-covered (i.e. central Utah, western and northeastern Colorado, and extending northward across eastern Montana, western Nebraska, and across the Dakotas into Canada). Overall and qualitatively, the CTH analyses from the RAP agree reasonably well with the GOES analysis. The most notable discrepancies are found in the areas circled in white in Figure 2. For example, the NCEP RAPv1 produced some high level clouds in eastern Oklahoma and a broad area of middle level clouds between the Yucatan peninsula and Cuba, neither of which are evident in the RGB image or the GOES CTH analysis. The NCEP RAPv1 analysis also severely underestimates the amount of low cloudiness over the mid-western Atlantic. Another interesting discrepancy occurs over northern Wisconsin into southern Canada, where a mid-level SLW cloud was detected from GOES with CTH values ranging from 3-5 km. Both model analyses indicate that this cloud is about 1.5 km lower than the GOES estimate on average, and ranges from about 2-4 km. The GOES CET associated with the higher clouds in this area indicated that the cloud top temperatures were between -20°C to -25°C which corresponds to nearly 5 km in the 12 UTC radiosonde profile obtained near Minneapolis earlier in the day. This supports the satellite estimate in this case. One reason that the CTH in the GSD analysis (GOES cloud building is on) was not adjusted to better match the satellite analysis is that the cloud building logic does not assign significant value to satellite CTH retrievals in the mid-levels. This is because of the well-known 'mid-level' cloud bias commonly found in VIS/IR satellite CTH

retrieval methods. In overlapping conditions (i.e. high cirrus over low-level stratus), these clouds appear as mid-level clouds because they are optically thick, and the warmer low-level cloud heavily influences the CET. The impact of assimilating overlapping clouds as mid-level clouds in the model analysis has dire consequences, and leads to significant overestimates of mid-tropospheric moisture, which is neither an accurate nor desirable model outcome. In this particular case, the satellite data could be trusted, but unless more accurate satellite CTH estimates are obtained in overlapping conditions, or better estimates of uncertainties are provided to flag the more uncertain mid-level cloud retrievals, the modeling community will struggle to use these data most effectively. For the comparisons shown in this section, only the single-layer GDCP are compared to the model output. A long-term goal is to demonstrate improvements in the satellite retrievals when applying multi-layer techniques, but that remains as future work.

Figure 3 depicts the fraction of clouds detected by GOES compared to that found in the model analyses and forecasts for all, low (0-3 km), middle (3-7 km), and high (7+ km) clouds as defined by their CTH. Thus, this comparison is from a satellite perspective, with a top down view, and does not consider cloud overlap. The total cloud fraction detected by GOES is 67% indicating that this particular week in November 2012 was relatively cloudy over the domain. Overall, the total cloudiness is well represented in the two models analyses with respect to GOES, with differences found to be 4% (7%) for the GSD (NCEP) analyses, respectively. Note that the total cloud fraction valid at the analysis time increases with increasing lead-time in the forecasts. This indicates that the cloud clearing done in the model initialization is losing retention as the forecast period increases. Over the entire domain, most of this effect is occurring with high clouds, as the low and mid-level cloud amounts remain relatively constant with forecast hour. The low cloud amounts agree to within a few percent with the satellite analysis,

however the satellite analysis also suggests that there are more mid-level clouds and less high-level clouds than found in the model output. This is partially due to the mid-cloud bias in the satellite observations due to overlapping clouds, but model errors may also contribute. A wide range of biases have been found in other studies when comparing clouds in model analyses with observations but model overestimates (underestimates) of high (middle) level clouds and significant problems with low clouds are consistently found. For example, Lin and Zhang (2004) compared climate model output to International Satellite Cloud Climatology Project (ISCCP) data and found notable underestimates in cloud fraction over the mid-latitude storm track regions and in the sub-tropical dry regions but overestimates in tropical convective regions. They found that the model produced too much (little) high (middle) level cloudiness. They also found that the model produced too many optically thick low clouds and too few optically thinner low clouds. Yoo and Li (2012) compared the NCEP Global Forecast System (GFS) model to MODIS single and multi-layer cloud retrievals, and active sensor data, and found that both mid-level and high clouds are overestimated in the GFS relative to the satellite retrievals. The GFS also had a tendency to underestimate low clouds over the oceans but overestimate low clouds over the continents. Bodas-Salcedo et al. (2008) found that the UK Met Office Unified Model produces to few mid-level clouds compared to CloudSat data. Yoo et al. (2013) examined the marine stratocumulus difference more carefully and found that the GFS underestimates the cloud LWC. Ahlgrimm et al. (2012) compared low cloud properties in the ECMWF to ground-based observations at the Department of Energy (DOE) Atmospheric Radiation Measurement (ARM) site in Lamont, Oklahoma. In that study, the ECMWF LWP was found to be too high in summertime shallow convective clouds but for overcast low clouds in other seasons, the model produced fewer clouds and lower values of LWP than that observed.

A regional comparison between the satellite cloud fraction and the GSD and NCEP model is summarized in Table 1a and Table 1b. In this case, the comparison is stratified for land and ocean, and for three oceanic regions, over the Atlantic, the Pacific and the Gulf of Mexico, where the clouds are expected to be quite different because they are influenced by much different weather regimes. The purpose of this comparison is to see how well the model tracks regional variations in clouds as observed from satellite and to highlight any notable differences between the GSD and NCEP versions of the RAP since GOES cloud building was turned off in the NCEP version. It is assumed that the satellite retrievals, and their uncertainties, are relatively self-consistent over the various regions, which these data and other validation studies indicate. The data shown here indicate that the greatest impact of the cloud building is associated with low clouds over the oceans since much better agreement with GOES is found in the GSD analyses than in the NCEP analyses. These results also suggest that the different cloud processes and cloud types associated with low clouds over these three different oceanic regions may not be that well represented in the model physics since the level of agreement with the satellite observations is so variable. For example, even with cloud building turned on, as in the GSD version, there are 20% more low clouds over the Pacific ocean but 18% fewer low clouds over the Gulf of Mexico than found in the satellite analyses. Furthermore, nearly 50% of the low clouds observed from GOES are missing in the NCEP analyses over the Gulf of Mexico.

Figure 4 further illustrates the problem that models have with retaining assimilated satellite information as a function of forecast hour. Here, the focus is on cloud clearing. This figure depicts the fraction of time that the GSD model grid box is cloud-free relative to the regions that GOES indicates are 100% cloud free. This analysis is broken down by region and forecast hour. For example, over land the model correctly depicts clear areas 90% of the time in the analysis

and 1-hr forecast. This reduces to 83% and 79% in the 3-hr and 6-hr forecasts. The situation is not as good over the oceans, where the model only correctly depicts clear regions 80% of the time in the analysis and less than 40% of the time in the 6-hr forecast. Thus, despite the positive impact of cloud clearing in the model initialization, clouds reappear in areas observed from satellite to be cloud free. This effect is worse over ocean than land (particularly over the Pacific stratocumulus regime) and also worse with increasing forecast lead-time. Over oceans the cloud clearing retention issues are mostly associated with low clouds while over the land they are mostly associated with high clouds (not shown).

One satellite-derived parameter of interest that is not currently used in the RAP assimilation system but has significant potential to improve the representation of clouds and their impacts (e.g., icing forecasts, precipitation) is the cloud water path. As described earlier, this parameter is diagnosed explicitly in the RUC/RAP modeling system and includes the contribution from all five of the species cloud water mixing ratios (ice+liquid+snow+rain+graupel). The CWP derived from GOES and from the RUC are shown in Figure 5a and Figure 5b at 20 UTC on May 6, 2008. The CWP difference is shown in Figure 5c. In this figure, the GOES CWP represents the retrieved LWP for liquid topped clouds and IWP for ice-topped clouds. These results indicate that while the overall representation of CWP produced by the model compares reasonably well with the observations, the instantaneous differences over small spatial scales are quite large. These differences have remained fairly consistent over time and in different implementations of the model cloud analysis system as shown in Figure 5d and Figure 5e, which depict a more recent comparison with the RAP-GSD and RAP-NCEP derived at 18 UTC on Nov 20, 2012. One possible exception is associated with the marine stratocumulus LWP, which in this case seems to agree fairly well, qualitatively, with the satellite observations. While the instantaneous

uncertainty in the satellite LWP retrievals for these clouds is pretty well understood and found to be about 30% (e.g., Dong et al., 2008), previous comparisons (not shown) with earlier versions of the RUC indicated that eastern Pacific marine boundary layer clouds found in the model analyses were often too low (in altitude), too geometrically thin, and thus their CWP was much lower than the satellite retrieved values. Thus, some model improvements for these clouds may be evident here.

Nonetheless, considering the paucity of cloud information being assimilated into models, large instantaneous differences between the model CWP and the satellite observations should be expected. Figure 6 shows the range and variability found in the instantaneous CWP comparison for the entire domain. Here, the comparison is shown in terms of the frequency distribution of the ratio between the instantaneous CWP derived from GOES and that derived from the GSD-RAP during the period from 12-18 Nov 2012. The relative differences are found to be quite variable, depending on both the altitude bin and the region of interest. The mean values for the CWP derived from GOES and those found in the GSD and NCEP model analyses stratified by region is shown in Tables 2a-d for all, low, middle, and high clouds. The ratios of the means and the mean biases are also shown. These results indicate that the domain averaged CWP values agree to some degree but are generally larger on average from GOES than from the model. For all clouds the GSD CWP is within about 25% of the GOES value. A big difference is found in the mean CWP for low clouds where the model value is nearly a factor of 3 smaller than that found from GOES, although as previously noted, good agreement is evident over the Pacific. For high clouds the means are in near perfect agreement overall, but big differences (about a factor of two) are found of opposite sign over the Pacific and over the Gulf of Mexico. For mid-level clouds, the largest discrepancy between the satellite retrievals and the models is over land,

particularly in the GSD version (factor of three difference). Pretty good agreement is found over the Atlantic and Pacific (ratios near 1) but poorer agreement is again found over the Gulf. Even though the data points aggregated in these comparisons are for regions in which both the model and GOES indicate that clouds occur coincidentally and in the same cloud top height bin (low, mid or high), some of the mid-cloud CWP differences shown here may be due to the fact that there are 2.5 times more GOES mid-level clouds due to the overlap problem. Thus, the types of clouds that comprise these samples, particularly in the mid and high level bins, are not that similar in some cases. At high levels, the model analysis produces about 25% more high clouds relative to the amount detected from GOES. Over the same domain during the entire summer of 2012, the GSD-RAP produced 65% more high clouds relative to those detected from GOES (not shown). Some of this difference can be attributed again to the overlap problem but most of the is that the model produces much more very thin high cloud than is detected from GOES. About 14% of the GSD-RUC high clouds found for the 7-day Nov 2008 period have CWP values less than 10 gm^{-2}, whereas only 2% of the high clouds detected from GOES have CWP values this low. Data taken from more highly sensitive active sensors such as CALIOP lidar indicate that there are a lot of thin cirrus that occur in nature with optical depths less than about 0.3. Since these are difficult to detect from passive satellite imagers (e.g., Ackerman et al., 2008), the actual frequency of occurrence diagnosed by the model may in fact be more realistic than the GOES estimates. Nevertheless, the primary purpose for the comparisons shown in this section is to demonstrate that, with respect to clouds that impact our weather (i.e. with appreciable CWP), the clouds diagnosed by the models are not in the right place at the right time. Of course, this may be an acceptable outcome for some applications, but aviation weather is not one of them. Regarding Figure 6, note also that the ratios of the means, tabulated in the figure legend, are

much different (larger) than the apparent mean ratios suggested by the frequency distributions. While the former may be more meaningful than the latter given the lack of correlation at the grid box level, the main purpose of this figure is to illustrate that the instantaneous differences are highly variable and can be as large as an order of magnitude, which significantly exceeds the observational uncertainties. This is further illustrated in Figure 7 which shows the mean and standard deviation in the gridded CWP ratio (GSD RAP divided by GOES) computed between 20-50 °N and 80-120 °W using data valid near 18 UTC over a 3-month period in the summer of 2012, and by varying the grid resolution from the native RAP resolution of 13km to a resolution of 500 km. For all clouds (blue curve), the number of regions that comprise the 90-day mean values ranged from N=142,486 at 13 km resolution to N=32 at a resolution of 500 km. The derivative of these ratios with changing averaging distance varies markedly at lower distances but asymptotes at about 100 km (300 km) for liquid (ice) clouds respectively. This indicates that relative to the satellite observations, the variability in the CWP prescribed by the models is not captured until averaged over a square area of about 10,000 to 90,000 km. In general, these results indicate that clouds in the model analyses are reasonably well correlated with observations at larger (synoptic) scales but are not in the right place at the right time at the smaller scales required by the aviation community. These types of potential errors associated with clouds in models relative to remote sensing observations are not unique to the models explored here, but rather seem to be common in a wide range of models.

In summary, satellite-derived cloud products provide valuable information that can be used to assess NWP cloud analyses and forecasts. It is found that the satellite cloud top height data assimilation in the RUC/RAP improves the model analyses to some degree but appears to have much less impact on short-range forecasts. Together with the METAR assimilation, the greatest

positive impacts appear to be the improved diagnoses of cloud/cloud free areas and more accurate cloud top heights and ceilings in the model analyses. To first order, these are important advances for the aviation weather community. Despite the fact that the RUC and RAP may be considered state of the art with respect to the amount of information on clouds being assimilated operationally over the United States, the critical information on the vertical distribution of cloud mass that is needed to better diagnose and predict icing conditions, precipitation, and other weather hazards associated with clouds remains relatively poor when compared to the potential information contained in the satellite retrievals. In the next section of this study, a profiling technique is developed that has the potential to address this issue. One purpose for the profiling technique is to improve the compatibility between the satellite data and the model cloud variables by projecting the satellite cloud properties into a 3-dimensional system along with guidance that can be used to address the potential partitioning of cloud ice and liquid. While developing and verifying the technique, it is found that significant adjustments are needed in order to improve the accuracy of the satellite products. These are demonstrated below. Thus, another potential benefit of this study is the development of new, more accurate, satellite products that are more consistent with cloud variables in models and therefore more suitable for assimilation. While these datasets may further improve cloud analyses in weather applications, variational approaches will most certainly be needed in order to improve short-range forecasts. This is because the current cloud product assimilation methods do not appear to adequately address the linkage between clouds and the model dynamics and physics that are needed to accurately retain and project the information gained from satellite observations downstream.

5 A Cloud Water Content Profiling Technique

5.1 Background

In this section, a CWC profiling technique is developed for application to satellite imager data. This work is motivated by the many weather applications that require vertical resolution of atmospheric constituents. Data from active sensors, such as that from the CloudSat and CALIPSO satellites, and from radars and lidars deployed at ground sites, provide the capability to resolve the vertical distribution of some cloud parameters (e.g., Austin et al. 2009). When combined, radar and lidar data provide an accurate characterization of cloud boundaries (Mace et al., 2009) in a wide range of conditions, and can also resolve the IWC in upper tropospheric clouds with reasonable accuracy (e.g., Deng et al. 2013). However, this information is only available in a small footprint directly beneath the satellite track or above the ground station, which is of limited direct use in weather applications. Passive satellite imager data provide cloud information and integral cloud parameters with the temporal and spatial resolution needed but lack vertical resolution. This study seeks to exploit the advantages of both the active and passive sensor systems synergistically in order to produce an accurate characterization of clouds in 4-D (vertical cloud structures over wide areas and with high temporal resolution). Smith et al. (2010) introduced a profiling concept for application to weather satellite data. The technique employs climatological vertical distribution functions (VDF's), which are derived from CloudSat CWC profiles and constrains them with satellite imager estimates of cloud boundaries and CWP in order to derive CWC profiles at the imager resolutions. The updated version described below better accounts for retrieval errors and thus improves the accuracy of the imager retrievals and the derived profiles. The CALIPSO, CloudSat and imager (e.g., GOES, MODIS) observations of cloud properties each have notable limitations. The CALIOP is highly sensitive to thin clouds

but fully attenuates at an optical depth of about 3. The CPR sensitivity is not as high as CALIOP, which limits the ability to detect some thin cirrus and low clouds. Difficulties in detecting low clouds are also encountered due to surface clutter. The CPR can penetrate deep optically thick ice over water clouds but attenuation due to encounters with precipitation size hydrometeors which are common in these types of clouds confound the retrieval of accurate vertical profiles. This leads to errors in cloud base detection, cloud typing, a low bias in cloud water content retrievals, and errors in the vertical distribution of cloud water content derived from CloudSat data. Some of these issues are apparent in Figure 8, which shows satellite-derived cloud properties retrieved in two deep cloud systems found along the CloudSat and CALIPSO orbit track over the eastern Dakotas for the 6 May 2008 case shown in Figure 5. With respect to Figure 8a, the CPR reflectivity image shown in panel (a) suggests that both cloud systems are producing precipitation to the surface, particularly near 44°N and 48°N. Next Generation Weather Radar (NEXRAD) and METAR data (not shown) confirm this. The cloud boundaries derived from the radar, the lidar, or both, are indicated by the different colors shown in panel (b). In this case, the CPR detects most of the hydrometeors near the tops of the clouds that were detected by CALIOP. The CloudSat CWC retrievals shown in panels (c) and (d) imply that most of the mass in these clouds is above 5 km. The CWC-RVOD (constrained with MODIS visible COD) retrieval appears to fail in portions of the thickest part of the southern system but provides retrievals to a greater depth below the cloud top, extending down to 2 km or so. The CWC-RO is unable to retrieve cloud properties below about 4 km. Panel (e) shows the corresponding RUC CWC analysis indicating that the cloud boundaries are reasonably well diagnosed for both cloud systems. The magnitude and distribution of CWC found in the RUC analysis agrees well with CloudSat for the northern system, while poor agreement is found for the more severe convective

system to the south. This is reinforced in panel (e) which compares the CWP derived from the RUC with that derived from GOES-12 and from CloudSat (CWC-RVOD). With the exception of the deficiency in the RUC CWP for the southern system, all three systems track the CWP in a similar manner. The deep convective CWP derived from GOES peaks at a value of about 5500 gm^{-2}, whereas the values retrieved from CloudSat are much higher; clearly, care must be taken in how both the active and passive sensor retrievals are interpreted. Accurate imager retrievals of CWP are needed in order to estimate accurate CWC profiles from weather satellite data. Therefore, errors due to the simplifying assumptions in the current imager retrieval techniques also need to be accounted for. For example, large errors occur for optically thick, single-layer (SL) ice over water cloud systems (hereafter, SLIOW clouds) because the imager retrieval techniques assume that the clouds are composed entirely of ice and that they are vertically homogenous. These assumptions are often violated in natural SLIOW clouds because liquid water is in fact often present, which explains the typically large values of COD found for these clouds, and because many observational studies have shown that the mass density (IWC), and size of the cloud ice crystals, typically increase with increasing temperature and distance from cloud top (e.g., Heymsfield et al., 1990; Heymsfield et al., 2007). Thus, the retrieved IWP should not be interpreted as representing the total water path and may not adequately represent the true IWP either. An additional source of error is that the visible reflectance measured by satellite imagers saturates at high COD. In the LaRC cloud retrieval system, this restricts the upper limit of the COD retrievals to 150, which translates to an upper limit of about 5000-6000 gm^{-2} for CWP. These errors and limitations need to be minimized or more properly accounted for in order to use satellite imager estimates of CWP effectively in both weather and climate applications.

To further illustrate the relative importance of these issues for optically thick clouds, consider the global monthly mean CERES AQUA-MODIS cloud property retrievals shown in Figure 9-12 for April 2013. The mean cloud fraction is shown in Figure 9 according to the cloud top phase. Liquid clouds (Figure 9a) are most common in the marine stratocumulus regimes, in a wide area associated with the Asian winter monsoon extending from the Arabian Sea through southern India and China and across the sub-tropical western Pacific Ocean. Relatively frequent liquid cloudiness is also found across much of the North Atlantic, the North Pacific, and over the southern hemisphere mid-latitude oceans. Liquid clouds are generally less frequent over the land areas. Ice clouds (Figure 9b) are most prevalent across the Intertropical Convergence Zone (ITCZ), northern land areas (Canada and Siberia), over the Tibetan plateau, over convective hot spots across South America and northern Africa, and coinciding with convection and mid-latitude storm tracks across the USA and Asia. The corresponding mean CWP for ice clouds (IWP) and liquid clouds (LWP) are shown in Figure 10. Retrieval errors are possible for overlapping clouds due to the poor assumptions discussed earlier and because the optical depth derived from the visible reflectance represents the combined effects of all cloud layers. Since the VIS reflectance is interpreted using a single-layer ice cloud model, the ice cloud optical depth can be significantly overestimated because the underlying water cloud generally increases the reflectance (Minnis et al, 2007). This may lead to an overestimate in the retrieved IWP. On the other hand, the vertical homogeneity assumption regarding the vertical profile of ice particle size, and the reflectance saturation problem, may contribute to potentially significant IWP underestimates. Errors are also possible in the estimates of the global distribution of LWP shown in Figure 9a. This is because these estimates are only comprised of liquid topped clouds.

The potentially significant contributions to the global mean values by liquid clouds that occur beneath overlapping ice clouds are completely excluded in these estimates.

For the data shown in Figure 10, the global non-polar (60 N to 60 S) mean values of IWP and LWP are 199 gm^{-2} and 77 gm^{-2}, respectively. The mean value of the COD is about 10. While the distribution of retrieved values are skewed to the low end, the relative importance of optically thick clouds to the total cloud water budget is still significant. This is illustrated in Figure 11 and Figure 12 which show the relative fraction and the contribution to the total water path for clouds with COD > 50 and for saturated clouds (COD=150). These data indicate that while the relative fraction of optically thick clouds is fairly low, their relative contribution to the mean cloud water path is significant. For example, along the ITCZ, the fraction of saturated clouds is found to be on the order of 5%, while the relative contribution that those clouds make to the total mean CWP is found to be as large as 25% or more. For clouds with COD > 50, the relative contribution to the total mean water path is on the order of 50% or more. In other words, while the fraction of optically thick clouds found across the globe is relatively low, these clouds are significant for weather applications because of their association with storm systems, precipitation and hazardous weather, and they are important for climate applications because they constitute a significant mass fraction in the cloud water budget over large regions of the Earth. Thus, the potentially large errors in satellite observations of CWP, which tend to increase with increasing COD, should not be ignored. The CWC profiling method developed here is uniquely designed to better account for these errors. The goal is to maximize the utility of the information content contained in the imager radiances and cloud property retrievals by improving the accuracy of quantitative cloud water path estimates from passive satellite data.

Two other methods for estimating 3-D cloud fields from satellite data have been developed recently but differ substantially from the current method in design and application. Barker et al. (2011) employ a radiation-similarity approach based on thermal infrared and visible channels to extend the along-track CloudSat vertical profile information to cross-track MODIS pixels. Their technique produces radiatively consistent results when compared to CERES measured top-of-atmosphere broadband fluxes, and provides best results to distances of about 20 km away from the active sensor data. Miller et al. (2014) develops and employs cloud-type dependent information in a similar 3-D cloud characterization that extends the active sensor data to the MODIS along-track retrievals. That method is found to outperform type-independent nearest neighbor methods at the 200-km range for estimating cloud base height. Some CWC vertical structure information are also demonstrated but not validated.

5.2 Cloud Water Path Parameterization

Based on the discussion above and the expectation that the passive satellite retrievals of CWP are underestimated for optically thicker SLIOW clouds due largely to the vertical homogeneity assumption and the reduced sensitivity as the bi-directional cloud reflectance saturates in the VIS, a parameterization is developed in this study to help overcome the retrieval errors. The parameterization is based on correlations between the GDCP and the ARM Continuous Baseline Microphysical Retrieval (MICROBASE) value-added product using a coincident dataset constructed over a 5-year period (2006-2010) at the ARM southern great plains (SGP) site. MICROBASE uses a combination of millimeter-wavelength cloud radar (MMCR), microwave radiometer (MWR), and radiosonde observations to estimate the vertical profiles of the primary microphysical parameters of clouds including the liquid/ice water content and liquid/ice cloud particle effective radius. MICROBASE is a baseline algorithm designed to

apply to most conditions and surface site locations using a single set of parameterizations and a simple determination of water phase based on temperature (Dunn et al., 2011). A long time record is needed to build enough samples from the coincident datasets since the observations from the SGP site that are used in MICROBASE represent a single spatial point measurement and because deep optically thick clouds are relatively rare as shown earlier. Relative to CloudSat and CALIPSO, IWC underestimates in the upper troposphere are certainly possible in the MICROBASE dataset since the MMCR may not detect some thin ice clouds due to its sensitivity settings which are optimized for operational use, and because the signal can also attenuate in optically thick cloud conditions. Much like the satellite cloud property retrievals, the ground-based estimates are the result of inverting remote sensing measurements based on assumptions regarding the particle habits and size distributions, thus all of these have potentially high uncertainties (e.g., Zhao et al., 2012a). The MICROBASE CWC retrieval method uses a simple empirical relationship with the MMCR reflectivity and a temperature dependent scaling to partition the ice and liquid retrievals between 0°C and -16°C. Zhou at al. (2012b) estimate the IWC uncertainty in the MICROBASE product to be 20-110%. Nevertheless, a potentially significant advantage to MICROBASE observations of optically thick clouds is the improved sensitivity to cloud water in the lower troposphere since the MMCR is looking up, and because the derived profiles are constrained with observations of cloud liquid water obtained from the MWR. Thus, for optically thick clouds, the MICROBASE retrievals may contain observations of lower tropospheric cloud liquid and ice water that are not well characterized in the CloudSat datasets.

Figure 13 shows the relationship between the MICROBASE TWP (squares) and IWP (circles) with GOES VISST IWP retrievals over the 5-year study period. The error bars represent

the standard deviation of the MICROBASE TWP values found in each VISST IWP bin. The MICROBASE IWP standard deviations are of similar magnitude but not shown to reduce clutter. The one-to-one line and power law best fits are also shown. It is assumed that the power law fits bracket the relationship between the VISST IWP and the true IWP rather than the true TWP. Due to the MMCR sensitivity, the ice cloud retrieval uncertainties, the MWR LWP uncertainties in optically thick SLIOW clouds, and for reasons that become more apparent later in this study, the line fit to the MICROBASE TWP shown here may underestimate the true TWP for the optically thicker clouds. The relationship between the MWR LWP and the GOES VISST COD is shown in Figure 14 with two power law fits; one for all data points (solid-black) and one that just fits the values at the low end with LWP < 300 gm^{-2} (dashed-black). The standard deviation of the LWP values found in each COD bin are approximately as large as the mean LWP values (not shown). A third curve shown in blue is the fit to the data presented in Minnis et al. (2007). In these analyses, the MICROBASE 20-minute product, which provides cloud property profiles averaged every 20 minutes, was used. The GOES retrievals were averaged in a 20-km radius circle centered on the ARM SGP surface site and matched with the corresponding MICROBASE profile. Only overcast scenes (according to GOES) were included. Periods during which a disdrometer at the ground site indicated that precipitation was falling to the surface were excluded, mainly to reduce the impact of wet optical windows on the retrievals. The data points shown in Figure 13 and Figure 14 were bin-averaged according to the GOES IWP and COD, respectively, to decrease the sampling noise. The results shown here are fairly consistent with our expectations that the VISST IWP underestimates the TWP as discerned from the MICROBASE data, and that the amount of liquid found within overlapping clouds tends to increase with increasing VISST COD. The latter relationship shown in Figure 14 between COD

and LWP agrees with Minnis et al., (2007) (blue curve) for lower values of COD and LWP. That study used Visible and Infrared Scanner (VIRS) and Tropical Rainfall Measuring Mission (TRMM) Microwave Imager (TMI) measurements of lower water-path clouds ($< 300 \text{ gm}^{-2}$) acquired over the Tropics between January and August 1998. The curve fit to the data in that study shown in blue agrees reasonably well to a curve fit to the VISST/MICROBASE comparison when applied to a similar range of values (dashed black curve). Extrapolating these curves over the full range however overestimates the potential LWP at higher values of COD relative to the values suggested by the MWR retrievals at the ARM SGP site (indicated in magenta). The purpose of these analyses is to develop simple parameterizations that can be applied to the VISST retrievals to estimate more realistic values of the IWP and LWP in optically thick ice over water clouds, the sum of which gives the true TWP, which is needed as a constraint in the profiling technique described in the next section. Based on the correlations with the ARM MICROBASE data, the TWP is

$$TWP = LWP_{iow} + IWP_{iow}, \qquad (11)$$

where the LWP for ice over water clouds is

$$LWP_{iow} = 4.699 * COD^{1.1}, \qquad (12)$$

which is the curve fit to the data shown in magenta in Figure 14. The overlapping IWP is

$$IWP_{iow} = 0.305 * IWP^{1.194}. \qquad (13)$$

Note that this is the fit for the TWP (solid) curve shown in Figure 13, which is assumed here to better represent the overlapping IWP and maximizes the parameterized TWP estimates. The impact of this approach to estimating the actual TWP in ice over water clouds is shown in Figure 15. The values are found to be nearly double the values of the VISST IWP at the high end.

The potential to improve global estimates of IWP and LWP from MODIS is illustrated by applying the SLIOW parameterizations given by Eqns. 12 and 13 to MODIS cloud retrievals for all pixels with COD>10. The new estimates and their differences with the original estimates (Figure 10) were derived from the CERES MODIS Edition 4 cloud retrievals during April 2013 and are shown in Figure 16 and Figure 17, respectively. The difference images highlight the impact of the optically thick ice over water cloud overlap parameterizations on the monthly mean LWP and IWP estimates indicating significant increases in some areas when compared with the original estimates. The new MODIS LWP appear to be much more consistent with microwave satellite remote sensing estimates over the world oceans. This is apparent by comparing the LWP estimates from April 2013 shown in Figure 16 with the 5-year (2002-2007) all sky LWP climatology found in Li et al., 2008, which was constructed from Special Sensor Microwave/Imager (SSM/I) shown in Figure 18. While the time period and averaging techniques are different here, the new MODIS estimates and the SSM/I climatology both show consistent relative increases in LWP from the stratocumulus regions to the ITCZ and the storm track areas that are harder to discern in the original MODIS/VISST monthly mean LWP estimates since the latter do not include the liquid found in overlapping cloud conditions. While more direct comparisons with other sensors and retrievals remain as future work, this initial comparison suggests that these new MODIS retrievals of LWP in single-layer overlapping conditions are reasonable. For ice clouds, the largest IWP differences (10-30%) are found over the mid-latitude storm tracks and tropical convective areas associated with the ITCZ where deep SL cloud systems tend to occur. Smaller differences are found in areas where both the ice cloud fraction and optical thickness are low, although the relative differences are large, on the order of 30-40% (not shown). These areas include the large stratocumulus regions found on the west

sides of the major continents for example. It is likely that in these areas the ice clouds are associated with ML systems (i.e. thin cirrus overlapping low level stratus). Minnis et al., (2007) found that the IWP decreased relative to the traditional VISST estimates when accounting for the lower level cloud properties retrieved with a multi-layer technique that incorporated radiative transfer calculation for these types of clouds. Thus, the simple parameterizations applied globally here for demonstration purposes and assuming that all clouds are SL, may lead to IWP overestimates when ML conditions actually occur. A better global solution, which remains as future work, is to integrate the parameterizations for SLIOW clouds developed here with the ML cloud retrieval techniques. For SL clouds, it is found later that the MODIS IWP retrievals that incorporate the SLIOW parameterization are more accurate compared to CALIPSO and CloudSat data than the traditional VISST retrievals. These comparisons are presented below.

5.3 Profiling Methodology

Since CWC profiles are currently impossible to infer directly from passive satellite imager data alone, an indirect approach is developed that employs climatological CWC VDF's, *S*, derived from cloud model and active sensor data as a function of cloud type, and constrains that information with satellite imager estimates of cloud boundaries and CWP. The natural vertical distribution of cloud water content is complex and depends on many factors including the phase of the hydrometeors, temperature, relative humidity, and the influence of the wind field. An attempt to crudely account for these factors is developed here by characterizing the cloud profiles by cloud type, namely the CWP and the cloud top temperature (CTT), since these parameters are common to the active sensing, passive sensing, and modeling retrieval systems. *S* characterizes the magnitude of the CWC, at each profile level, relative to its vertical integral (CWP), and in a

vertical coordinate system defined relative to the cloud top altitude. For each profile, S is computed from the CWC as a function of altitude and normalized by the mean CWC found for the entire profile as

$$S(z^*) = \frac{CWC(z^*)}{\overline{CWC}}, \qquad (14)$$

where

$$\overline{CWC} = \frac{\int_{CBH}^{CTH} CWC(z)\,dz}{CTH - CBH}. \qquad (15)$$

An altitude factor, z^*, is also computed to normalize the vertical coordinate, such that

$$z^* = (z(i) - CBH)/(CTH - CBH), \qquad (16)$$

where z(i) represents the altitude of the observation or retrieval. Thus, z^* is the depth below cloud top normalized to H and is equal to a value of 1 at cloud top and a value of 0 at cloud base, while S represents the CWC profile normalized to its vertical mean. The vertical integral of $S(z^*)$ is unity. $S(z^*)$ is linearly interpolated to a 100-level vertical grid and the mean and standard deviation is computed for about 125 cloud types and stored in lookup tables. The maximum value of $S(z^*)$, S_{max}, is a measure of the degree of heterogeneity in the vertical profile. A value of 1 for S_{max} would indicate a perfectly homogenous vertical profile. The relative vertical position of S_{max} is hereafter referred to as Z_{max}. For example, a vertical profile peaking at the mid-cloud level would have a Z_{max} value of 0.5. Note that the numerator in Eqn. 15 is the CWP and the denominator in Eqns. 15 and 16 is the cloud thickness, H. Since these parameters are retrieved with some skill from passive satellite data in the LaRC cloud retrieval system along with the CTH and CTT, $S(z^*)$ can then be used in a simple retrieval system to derive CWC

profiles in near real-time from operational satellite data that are constrained with passive satellite-derived cloud parameters. Thus,

$$CWC(z^*) = S(z^*) * \frac{CWP}{H}, \tag{17}$$

where CWP and H now represent the passive satellite retrievals and along with CTT also define the cloud type used to select $S(z^*)$ from the lookup table. The actual altitude profile, $z(i)$ is computed from the passive satellite-derived CTH and H by inverting Eqn. 16.

5.4 Climatological Database

For cirrus clouds, $S(z^*)$ is computed from the IWC profiles contained in the CloudSat 2C-ICE and the CWC-RVOD products. Cirrus clouds are defined here to be all clouds with CBH determined from the combination of CPR and CALIOP data to be above the -20°C level. This distinction is made primarily for verification purposes so that uncertainties associated with mixed phase or lower level liquid clouds and precipitation are minimized. $S(z^*)$ is also characterized for all clouds using the CWC-RVOD product and using the explicit cloud hydrometeor profiles computed in the RAP, since ultimately an accurate cloud profiling solution is sought under all cloud conditions. Figure 19 and Figure 20 show the mean and standard deviation of $S(z^*)$ for a wide range of cirrus cloud types determined from the 2C-ICE data product aggregated for 3-months (Jan-Mar) in the winter of 2010 over a large area encompassing the CONUS and southern Canada (20-55°N; 65-150°W). This region is referred to hereafter as the study area. With the exception of a few cloud types that are poorly sampled, the mean profiles are relatively smooth and indicate that the IWC increases with increasing depth into the cloud relative to cloud top, peaking below the mid-cloud level before decreasing toward cloud base. The standard deviation in the cirrus IWC VDF's shown in Figure 20 is found to be on the order of 50-60% of

the mean for each cloud type, and likely includes the combined effect of the natural variability occurring in each cloud type, as well as retrieval errors. Figure 21 shows the mean of $S(z^*)$ found for the same time period in the CWC-RVOD dataset. The results indicate that the vertical distribution of IWC found in the RVOD profiles based on the CPR data is more vertically homogeneous (lower values of S_{max}) than those derived from the combination of CPR and CALIOP data in the 2C-ICE product. Thus, the latter may be more realistic since the 2C-ICE retrievals include the more tenuous cirrus detected near the tops of clouds by the CALIOP that are not detected by the CPR. Otherwise, the two datasets exhibit fairly similar behavior in terms of the dependence of the IWC vertical structure on cloud temperature and IWP. Optically thinner clouds with lower IWP are found to be more vertically homogeneous with lower values of S_{max} than the optically thicker clouds that have larger IWP values. Generally, the maximum IWC is found to be at a lower altitude (with lower values of Z_{max}) within colder clouds and in clouds with higher values of IWP. These are well known characteristics of ice clouds, due to the sedimentation of larger ice crystals, and have been observed in aircraft observations for several decades and are now reinforced by global analyses of cirrus cloud microphysical retrievals from CloudSat and CALIPSO (e.g., Ham et al., 2013).

Figure 22 depicts the mean CWC VDF's derived from the CWC-RVOD product for all SL clouds, including deeper SLIOW clouds and warm liquid water clouds. In this figure, the impact of precipitation size particles and the CPR attenuation on the CWC retrievals is apparent, as there is a dramatic and unrealistic shift in the mass peak to higher levels in the cloud types that have higher CWP's. Note that the CloudSat data products include precipitation flags, which could be used to help eliminate clouds with precipitation size particles from this analysis. The problem with that approach is that it effectively eliminates most of the naturally occurring optically thick

clouds that are of particular interest in this study. Therefore, to better estimate the potential vertical distribution of CWC in deep optically thick clouds, a hybrid set of VDF's are derived by combining the information on ice clouds from CloudSat and CALIPSO in the upper troposphere (at altitude levels above the -20°C level) with information from cloud models in the lower troposphere. In the initial solution, $S(z^*)$ is developed from the RUC cloud analyses at 18 UTC between 1 January and 31 March, 2010. The RUC $S(z^*)$ climatology is than employed to derive CWC profiles from one month (April 2010) of nadir CERES MODIS cloud properties that are collocated with CALIPSO and CloudSat CWC retrievals. For optically thick clouds with COD > 10, the MODIS profiles are derived using Eqn. 17 after employing Eqns. 11-13 to estimate the TWP for each pixel. At cloud levels with temperatures below -20°C, the MODIS CWC values derived with the RUC climatology are replaced with the collocated CloudSat or CALIPSO retrieval (CALIPSO has precedence) to create a hybrid profile. The hybrid profiles are then renormalized and aggregated as a function of cloud type as before. Figure 23 shows the RUC/CloudSat/CALIPSO hybrid climatology for $S(z^*)$. For cloud types with lower CWP's below about 1000 gm^{-2}, the CWC-RVOD and the hybrid curves exhibit fairly similar behavior although the hybrid profiles are slightly less homogeneous and have Z_{max} values approximately 10% higher in the normalized altitude. Since optically thin cold clouds were excluded in the hybrid climatology, some of the cloud types with cold CTT values and low CWP are missing relative to the CWC-RVOD climatology shown in Figure 22. This is of no consequence in the actual application of the technique to imager cloud properties, since a separate set of $S(z^*)$ curves were developed for cirrus clouds (shown earlier). For cloud types with larger CWP, the hybrid climatology differs substantially from the CWC-RVOD climatology indicating more realistic values for Z_{max} at or below the mid-cloud level for most cold clouds. A transition in Z_{max} from

low to high values as the CTT increases is also evident and quite realistic as the cloud types transition from ice to liquid since LWC profiles are well known to increase with increasing altitude in a manner more typical of adiabatic ascent.

In the next section, the application of this technique is demonstrated with MODIS data and validated in the upper troposphere with CloudSat and CALIPSO data.

5.5 MODIS CWC Retrievals and Verification

In this section, the profiling method is evaluated with CloudSat and CALIPSO IWC retrievals in the upper troposphere. These retrievals also have uncertainties (e.g., Heymsfield et al., 2008). CWC profiles are derived from the MDCP by applying Eqn. 17 to the retrieved CWP and H, and applying the appropriate values of $S(z^*)$ from lookup tables. For ice-topped clouds with a MODIS-derived COD $<=10$, both the 2C-ICE and the CWC-RVOD cirrus $S(z^*)$ climatologies shown in Figure 19 and Figure 21 are tested. For all other ice-topped clouds, the hybrid climatology shown in Figure 23 is employed. For liquid-topped clouds, LWC profiles are also derived based on the RUC component of the hybrid climatology but these are not tested here since a suitable verification dataset has not been identified for those types of clouds. Thus, the validation presented here is focused on ice-topped clouds to take advantage of the CloudSat and CALIPSO profiles. The CERES C3M data product is used to validate the profiling method. C3M merges CloudSat, CALIPSO, CERES, and MODIS cloud and radiation parameters (Kato et al., 2010). A full-resolution (1-km) intermediate product that is available upon request from the CERES program at NASA LaRC is used to make an initial assessment of the profiling technique. This product includes the CERES MDCP, the CloudSat CWC-RO, and the CALIPSO CPro cloud properties. While other radar and lidar based IWC datasets are available (e.g., the CloudSat 2CICE product, or the ra**DAR**/li**DAR** (DARDAR) product by Delanoe and Hogan,

2008, 2010), the retrievals contained in the C3M intermediate dataset are particularly convenient since the data are already geo-located at full-resolution and packaged with the CERES MDCP.

Figure 24 shows a comparison of cirrus cloud IWC retrievals derived from MODIS and from the combination of the coincident CALIPSO and CloudSat retrievals contained in the April 2010 C3M dataset over the CONUS study area. Cirrus clouds are defined like before as having cloud base altitudes above the -20°C altitude level. The mean and relative frequency distribution of the retrieved IWC values are computed in 1-km altitude bins and aggregated in bins according to a range of MODIS derived COD as indicated in the figure. The plots on the left side show the mean IWC profiles derived from MODIS (red) and CALIPSO+CloudSat (black), along with the MODIS IWC frequency distribution. The plots on the right side show the same mean profiles but are plotted with the CALIPSO+CloudSat (hereafter CC) IWC frequency distributions. The frequencies are normalized to the maximum number of occurrences and therefore range from a value of 0 to 1 as indicated by the colorbar. Similar results are shown in Figure 25 - Figure 28. In Figure 24, the MODIS profiles are derived using the 2CICE climatology of $S(z^*)$ and the agreement with the CC profiles found to be somewhat mixed. Good agreement is found throughout the vertical column for the lowest COD bin but for higher COD's, the best agreement is found only at lower altitudes. The larger differences found at the higher altitudes, which are almost an order of magnitude at 12 km for the higher optical depth clouds, are most likely due to the much higher sensitivity that CALIOP has to the optically thinner clouds and poor cloud top height assignment in the MODIS retrievals (MODIS cloud top heights are too low). This is also apparent in the IWC frequency distributions shown in the comparisons. For example, in the plots shown for the COD bin ranging from 3 to 6, there is a much higher frequency of clouds with larger optical depths detected by CALIPSO than are derived with the MODIS profiling

technique. Only slightly better agreement is found in Figure 25 and in the statistics shown in Table 3a for the cirrus profiles derived from MODIS using the CWC-RVOD $S(z^*)$ climatology. While the 2CICE climatology may be more accurate since it includes the CALIOP data, the slightly better agreement found using the CloudSat climatology might simply be due to the fact that MODIS and CloudSat have more similar sensitivities near cloud top. To explore this further, the MODIS profiles were derived again using the CWC-RVOD climatology but this time they were constrained with the CloudSat cloud boundaries (rather than those derived from MODIS) and compared only with the CloudSat CWC-RO IWC retrieval. These results are depicted in Figure 26, which shows much better agreement in the mean IWC profiles derived from MODIS and CloudSat over a wide range of COD, and particularly at high altitudes where the differences are much less than an order of magnitude as found before. Thus, the IWC differences found for the passive satellite cloud profiling technique applied to cirrus and compared to the active sensor retrievals are due largely to errors in the imager cloud boundary estimates, particularly CTH, and to the much higher sensitivity to thin cirrus by the CALIOP. MODIS and the CPR have similar sensitivities as indicated by the mean IWC and IWP comparisons summarized in Table 3a and Table 3b. Despite the fact that there are large differences in IWC found at higher levels in the profile comparisons that include CALIPSO data, there are fewer clouds at these levels and the overall mean cirrus IWC and IWP values calculated from the passive and active sensor retrievals (see Tables 3a and 3b) are found to differ by less than 30%. In addition, the MODIS IWP is found to compare much better with CloudSat than with the combined CC IWP estimates, which tend to have higher values, particularly for the optically thicker clouds. This suggests that, for cirrus clouds, any IWP underestimates in the CERES MODIS Ed4 cloud properties are more likely due to instrument sensitivity issues rather than retrieval errors due to the vertical

homogeneity assumption. The mean cloud top height comparison shown in Table 3c further supports this possibility since the MODIS values tend to agree more closely with CloudSat than with CALIPSO.

For the same time period and over the same study area, the profiling technique was evaluated for optically thick clouds (COD>10) in a similar manner. The results of these comparisons are shown in Figure 27 and Figure 28. While a full range of optically thick clouds are assessed in these comparisons, including deep convective clouds, only IWC retrievals at altitudes above the -20°C altitude level are considered here, due to the cloud phase uncertainty at warmer temperatures and the CPR attenuation problem. The IWP computed above this level is hereafter referred to as IWP253. Good agreement is found between the passive and active sensor profiles over a wide range of COD demonstrating the potential for accurately characterizing the vertical distribution of cloud IWC from passive satellite data using the methods developed in this study. In particular, note the high level of agreement in the mean values of the IWP253 and IWC denoted in the plots and also tabulated in Table 4a and Table 4b. The mean IWC derived from MODIS is within 5-10% of the mean CC values in each COD bin, and the agreement on average for all clouds is 1.5%. Good agreement is also found in the mean IWP253 inferred from the CC data and from the MODIS profiles, both of which increase in a similar manner with increasing COD. Thus, the variability in the mean upper tropospheric IWC retrieved from MODIS appears to track the observations from the CPR over a wide range of COD quite well. This can be seen in the IWP comparison shown in Table 4b, which also compares the values derived in the profiling technique, with and without the SLIOW CWP parameterization, to those derived from the CC profiles. Without the parameterization, the mean values of the IWP253 retrieved from MODIS (Hybrid0 in Table 4b) are significantly less than those found for the CC retrievals. Two

important factors that appear to work well together in the profiling technique for optically thick clouds, are the RUC model CWC VDF's ($S(z^*)$) and the SLIOW TWP parameterization. In other words, the climatological characterization of the cloud analyses found in the RUC model, appears to partition the upper tropospheric IWP from the total mass quite well provided that the traditional MODIS cloud property retrievals are adjusted using the TWP parameterization for SLIOW clouds.

Some discrepancies are apparent in the mean vertical profiles shown in Figure 27 and Figure 28. For example, it appears that for clouds with COD less than about 40, the current method tends to overestimate the IWC at high altitudes and underestimate at lower altitudes relative to CloudSat and CALIPSO retrievals. For clouds with COD greater than 80, the opposite behavior is found. While the $S(z^*)$ climatology employed here is the hybrid developed from the RUC and tuned with CC data, it does not appear that the tuning approach made a significant impact on the derived vertical structure. While the current method is producing good results, better agreement between the average vertical profile of IWC derived from passive and active sensors may be possible with additional tuning. This will be revisited in a future study.

Figure 29 and Figure 30 show a comparison between the IWC retrieved from the GDCP (GOES-13) using the profiling method and that obtained from in-situ measurements collected by a sampling probe mounted on a research aircraft. These data were collected on 13 and 21 September 2013 using a 2D-S (stereo) optical array cloud particle imaging probe deployed from the wing tip of a DC-8 aircraft during the (SEAC4RS) field campaign. The measurement range for the 2D-S is from 10 μm to 3 mm and the detrimental effects of ice crystal shattering on the measurements are minimized with an anti-shattering tips and particle inter-arrival time algorithms. The mean values used in the comparison were computed by averaging the aircraft

measurements over distances of 5 km. The IWC profiles were derived from mean values of the GDCP, which were computed by distance weighting the retrievals for the 4 nearest 4-km GOES pixels to the central location of the aircraft average. Since the GDCP were generally available every 15 minutes during the experiment, the matched satellite and aircraft estimates are within +/- 8.5 minutes. Also shown here is the VIS satellite imagery taken during the middle of the flights with a flight track overlay and the corresponding altitude trace color coded according to the measurement time. The level of agreement in the IWC values is remarkably good overall, particularly in the areas that appear to be the most homogeneous in the satellite imagery. The satellite retrievals and the aircraft data also track each other well over a wide range of values at times in which the aircraft is ascending and descending (profiling). This can be seen, for example, near 1700 and 1900 UTC on 19 September (Figure 29) and near 1715 UTC on 21 September (Figure 30). The largest discrepancies between the satellite and aircraft IWC values appear to be in the most heterogeneous areas seen in the VIS imagery (e.g., near 21-22 UTC on 13 September), and found in the satellite CWP field not shown here (e.g., near 22 UTC on 21 September).

Considering the uncertainties in all of the retrieval techniques, the different instrument sensitivities, and the potential sampling mismatches, the level of agreement found for the IWC estimates derived using the passive satellite profiling technique is very encouraging. In the next section, the focus for the profiling technique, and its verification, shifts to the lower troposphere and the potential to estimate the flight icing threat to aircraft within SLIOW clouds.

6 The Flight Icing Threat to Aircraft

6.1 Background

The existence of liquid water at sub-freezing atmospheric temperatures is a natural phenomenon that poses a significant threat to aviation. In-flight icing (IFI) occurs when super-cooled liquid water (SLW) freezes on the airframe and alters the airflow, which can increase drag, reduce lift and induce control problems. High concentrations of SLW and/or the presence of super-cooled large droplets (SLD), freezing drizzle or freezing rain are particularly dangerous to aircraft. According to the European Aviation Safety Agency, icing was the primary cause of 80 accidents, 263 fatalities, and was a contributing factor in many more events worldwide over the last ten years (http://www.ainonline.com/aviation-news/aviation-international-news/2013-12-04/icing-research-struggling-physics). While no aspect of aircraft operations is immune to the icing threat, the greatest impacts are on General Aviation (GA) operations and smaller aircraft, as ~80% of IFI related accidents between 2006-2010 involved GA aircraft (Appiah-Kubi, 2011). Despite improvements in ice protection systems, even the most advanced aircraft system can perform inadequately in heavy icing conditions. In Alaska, many of the commercial airlines that operate in the state are not equipped with the same deicing capability available on many of the major airliners. IFI can also impact efficient flow within the National Airspace System (NAS) since portions of a busy airspace may be rendered unusable due to IFI conditions. Thus, aviation weather forecasters, traffic flow managers, pilots, and others need to know where and when icing can occur.

Accurate diagnoses and forecasts of the meteorological conditions associated with aircraft icing requires identifying the location and vertical distribution of clouds with super-cooled liquid water droplets, as well as the characteristics of the droplet size distribution. Forecasters use NWP

model output, pilot reports (PIREPS), and rules of thumb based on experience, to estimate the potential for icing conditions. The Aviation Weather Center (AWC) in Kansas City, for example, provides icing forecasts for the contiguous United States in the form of airmen's meteorological information (AIRMETs) and significant meteorological information (SIGMETs). These constitute a primary decision-making tool used by pilots and weather briefers to avoid hazardous weather. Textual and graphical AIRMET advisories are issued every 6 h by AWC that forecast areas with the potential for moderate icing at 3-hourly intervals for the following 12 hours unless amended by an unscheduled AIRMET. Icing AIRMETs are created using many weather data sources including temperature and humidity fields from numerical weather prediction (NWP) models, satellite imagery, and existing pilot reports of icing. SIGMETs are warnings issued as necessary for known severe icing based solely on current pilot reports. Both AIRMETs and SIGMETs are polygon in shape and widespread in the horizontal, covering areas of at least 3,000 square miles and encompassing a vertical range, usually from the freezing level to a specified altitude. Forecasting approaches based on NWP model diagnosed atmospheric temperature and moisture structure (Schultz et al., 1992; Thompson et al., 1997a) are widely used by AWC and other aviation weather forecasters because they do a reasonably good job of identifying the potential for icing conditions over the broad areas characteristic of AIRMETs (Brown et al., 1997). While these methods capture a large percentage of icing PIREPS, they also tend to over-warn, even indicating icing conditions in cloud-free areas (Brown et al., 1997, Thompson et al., 1997a,b). Furthermore, cloud microphysical properties that contribute to the potential intensity of aircraft icing are often highly variable over small scales and more difficult to accurately diagnose and forecast with model-based approaches alone. Since aircraft operations could benefit from improved resolution of icing conditions, PIREPS and other observational information, including

satellite data, are needed to improve diagnoses and forecasts of the flight icing threat. PIREPS are valuable because they provide direct evidence for airframe icing and its severity. However, PIREPS are rare or non-existent over the oceans and other parts of the world where accurate icing diagnoses and forecasts are also needed. Even over the relatively data rich contiguous United States (CONUS), PIREPS have certain characteristics that limit both their operational utility and their utility for icing algorithm verification. These limitations include spatial and temporal biases related to commercial flight schedules and proximity to major airports, as well as subjectivity and haphazardness (Brown et al., 1997; Brown and Young, 2000).

Operational satellite imager data have been used to improve icing diagnoses since they provide frequent observations of clouds at high spatial resolution. The early model-based approaches were improved by using satellite data to eliminate cloud-free areas and areas with warm cloud tops (Thompson et al., 1997b). Ellrod and Nelson (1996) developed a stepwise screening technique to infer the presence of cloud top SLW directly from the satellite radiances provided that the clouds are not obscured from view by higher altitude ice clouds. Bernstein et al. (2005) describe the Current Icing Potential (CIP), an advanced icing diagnosis method that blends relevant data from multiple sources, such as satellite, surface, radar, lightning, and routine Pilot Reports (PIREPs), with temperature, relative humidity, SLW, and vertical velocity fields produced by numerical models. The CIP is operational at the AWC and available via the NWS Aviation Digital Data Service. The NOAA RUC, and more recently the RAP, provides the model inputs used in the CIP. The RUC and RAP utilize an advanced assimilation system that incorporates a variety of cloud observations, and employs an explicit cloud microphysics scheme developed to improve forecasts of SLW (Reisner et al., 1998; Thompson et al., 2004). As discussed earlier, clouds remain relatively poorly diagnosed by models and often don't

characterize accurately the vertical distribution of cloud water with respect to observations at the smaller scales needed for pilots to avoid adverse weather. With respect to SLW, explicit cloud analyses in models have been found to capture less than 50% of pilot-observed icing (e.g., Brown et al., 2001). In the CIP, satellite data are used to identify the location of clouds (Thompson et al., 1997b). However, more quantitative information on icing conditions available from satellite data are not exploited in CIP or any other operational approach, despite the capability to retrieve cloud physical properties (e.g., Nakajima and King, 1990; Minnis and Smith, 1998; King et al., 2003; Minnis et al., 2011a) with significant accuracy, including cloud boundaries (Smith et al., 2008; Minnis et al., 2008; Sun-Mack et al., 2013), water path (Mace et al., 1998, 2005; Painemal et al., 2012), particle size (Mace et al., 2005; Painemal and Zuidema, 2011), and the dominant hydrometeor phase near cloud top. Thus, satellites offer a unique and critical vantage point to observe the physical characteristics of clouds associated with weather hazards, such as icing conditions, with accuracies not currently realized in model based approaches. To illustrate, consider the cloud products derived from GOES-13 and GOES-15 shown in Figure 31, which depicts the retrieved cloud top phase, CET, COD, H, CER and LWP. These parameters provide unique information about clouds that can be used to infer the potential for aircraft icing at the pixel resolution of the satellite imager, typically 1 to 4 km. For example, the cloud top phase, combined with CET, diagnose the presence of SLW directly from the satellite data. In this example, a wide range of cloud conditions is found to be associated with a broad area of low pressure centered over southeastern Missouri and southern Illinois. A large area of SLW (denoted by the cyan color in Figure 31a) is detected over parts of the Midwest and southeastern states. The corresponding SLW droplet sizes and their densities can be inferred from the CER and LWP images shown in Figure 31e and Figure 31f, while the cloud top height,

CTH (not shown) derived from CET, the cloud thickness, and knowledge of the freezing level provide information on the upper and lower altitude boundaries for the potential icing layers. Thus, geophysical cloud parameters derived from satellite data are useful for accurately diagnosing potential icing conditions because (1) they provide information on the likely location for SLW, (2) their 'parameter space' is closely related to the meteorological factors associated with aircraft icing – namely, the cloud temperature, the super-cooled liquid water content and the droplet size distribution (Rasmussen et al., 1992), and (3) they constitute the only observations available at the scales needed to resolve dangerous icing conditions over wide areas for the aviation community.

6.2 Satellite Algorithms

6.2.1 Version 1: Solution for low clouds

The initial method to determine the potential flight icing threat to aircraft, hereafter S-FITv1.0 (Smith et al., 2012, attached here in Appendix A.1), was developed for clouds with which the presence of SLW can be inferred directly from the satellite products using the combination of the retrieved cloud top phase and CET. These are typically lower level clouds with SLW tops and CTH less than about 4 km. The satellite-derived cloud properties derived for these types of clouds were matched with icing PIREPS using data collected over several years to determine relationships between the satellite data and icing conditions reported by pilots. While there are eight possible intensity categories available for pilots to characterize icing intensity, most reports fall into just a few categories. Therefore, the icing PIREPS were reclassified into two intensity categories, either light or MOG. The light category contained any icing intensities reported with trace to light icing conditions, while the MOG category contained all reports with light-moderate or greater conditions.

Relationships to determine the probability for icing based on the retrieved super-cooled LWP (SLWP) and CER, and intensity thresholds based on the retrieved SLWP, were developed over snow and snow-free surfaces. Larger values of SLWP and CER were found to be associated with a higher probability for encountering icing conditions and with greater intensities. Optically thin clouds are eliminated from the icing threat based on the retrieved COD, which helps to reduce over-warning.

An example of the SFITv1.0 product derived from the data shown in Figure 31 is provided in Figure 32. The FIT is color-coded for display purposes as indicated. Figure 33a-c depicts the satellite product output at three different times during the course of the day (1415, 1745, and 2045 UTC, respectively). Also shown in Figure 33d-f are the icing PIREPS that were filed near the same time as the satellite analyses. Figure 33g and Figure 33h show the g-AIRMET icing advisories valid at 1800 and 2100 UTC. Smith et al. (2012) found that the S-FITv1.0 algorithm has considerable skill in detecting and discerning light from MOG icing conditions provided there are no overlapping high clouds. In the satellite icing analyses shown here, the red colors indicate areas where moderate or greater icing conditions are possible. The purple and blue colors indicate lower probabilities for trace to light icing conditions. The satellite analysis clearly depicts icing conditions early in the day across the southern states extending from eastern Texas into Missouri, Arkansas and Mississipi. Only a few light icing PIREPS are evident in these regions in the early hours. As the day progressed, the MOG icing areas found in the satellite analyses expand and advect eastward and a number of MOG PIREPS occur that confirm the satellite analyses. The traditional forecast methods at AWC, however, completely miss the significant icing that is occurring in the southern states. In fact, it isn't until a number of MOG icing reports have occurred that AWC issues an updated advisory to include these areas at 2100

UTC. Clearly, in this case, the satellite analysis provides advanced and accurate warning of the icing conditions associated with the low-level SLW clouds that were later experienced and reported by aircraft pilots. An interesting aspect of this case is that the warnings that were issued by the AWC earlier in the day are in areas that appear in the satellite analyses to be influenced by deep ice over water clouds associated with the winter storm system. The SFITv1.0 algorithm does not provide an icing estimate in these areas because the lower level SLW is obscured from direct view by the satellite imager by high-level ice clouds. These areas are designated as unknown or indeterminate in the SFITv1.0 analyses (white areas in Figure 32 and in Figure 33a-c). Based on correlations between the satellite-derived cloud properties and thousands of icing PIREPS, it appears that these ice over water cloud conditions contain some 30-50% of the icing reported by pilots, which are not captured by the SFITv1.0 method. Thus, the traditional forecast methods, which tend to capture some of the icing associated with these deep cloud systems, and the SFITv1.0 analyses, which works well for low clouds, are complementary to each other. Nevertheless, based on the relatively poor resolution of cloud and icing conditions found in model analyses and forecasts, and in order to enhance the utility of the satellite icing products and provide a more complete solution to the problem under a wider variety of cloud conditions, a second-generation satellite algorithm is developed and described here. The primary goals are to further entice the aviation weather community to utilize satellite-based icing products by improving icing diagnoses in all cloud conditions, including ice over water cloud systems, and by improving the detection of the more severe conditions that are most dangerous to aircraft.

6.2.2 Version 2: New method with solutions for all clouds

To increase the satellite icing detection capability in all cloud conditions and to address the potential for detecting severe icing conditions, the legacy SFITv1.0 algorithm is enhanced in the following ways in the SFITv2.0 algorithm:

1. A 'Heavy' icing category is added to identify clouds that potentially contain SLD.

2. A multi-layer retrieval algorithm is employed to determine the icing threat in SLW clouds identified beneath overlapping high-level cirrus clouds.

3. A super-cooled liquid water content profiling technique is developed and employed to determine the icing threat embedded within deep ice over water clouds typically associated with storm systems.

The first two enhancements use existing satellite products, are simple to implement and impact a relatively small percentage of the clouds found to have the potential for icing. The third enhancement is more complex and has a much greater areal impact on the icing threat determined from satellite data. These enhancements are described briefly below.

6.2.2.1 Inferring Heavy To Severe Icing Conditions

In the SFITv1.0 algorithm, the icing threat estimate is most heavily dependent on the retrieved SLWP. Despite the fact that larger droplets are known to often be associated with higher icing intensities (Bernstein et al., 2007), only weak dependencies were found for CER when compared to thousands of icing intensity PIREPS in a wide range of cloud conditions. This may be due to the uncertainties associated with icing PIREPS (e.g., geo-location errors, subjectivity), the fact that the retrieved CER can be highly variable and occasionally contaminated with thin cirrus, or other factors. Detailed case studies of severe icing events, however, indicate that a stronger relationship exists and should be exploited. We have examined

a number of severe icing PIREPS and the corresponding CER values, as well as those retrieved in the vicinity of several recent aviation accident sites. The results suggest that larger values of CER are indeed often associated with the more severe icing found in lower level clouds and thus perhaps indicative of SLD. Based on these case studies, several of which are presented in the validation section, the flight icing threat is classified as 'Heavy' in the SFITv2.0 algorithm for SLW-topped clouds with CER values exceeding 13.5 μm. SLD is also known to be common in deep convective clouds, which aircraft typically try to avoid. Since avoidance is not always possible, particularly in areas void of weather radar coverage, the satellite retrievals indicating cold, optically thick, opaque cloud conditions with CET < -35°C, COD > 100, and 6.7-11 μm brightness temperature differences (BTD) greater than -1.0°, are also classified as 'Heavy' icing areas. These thresholds were chosen based on visual interpretations of the satellite retrievals in several case studies combined with visual correlations with radar imagery, which are used to identify the location of core convection.

6.2.2.2 Inferring The Flight Icing Threat In Overlapping Cloud Conditions

A unique feature found in the LaRC cloud property retrieval system is a multilayered (ML) cloud retrieval capability. This ML retrieval uses multiple imager channels to retrieve properties for thin-cirrus-over-thick-water cloud systems (e.g., Chang et al., 2005; Watts et al., 2011) and is based on the 2-channel Modified CO_2 Absorption Technique (MCAT) developed by Chang et al. (2010a, 2010b). It provides estimates of CET and emissivity ε for the upper cloud and a radiating temperature for the background. The MCAT ε retrieval is compared with that corresponding to the COD retrieved with the single-layer (SL) method (Chang et al., 2010b). If significantly different, the pixel is classified as ML and the lower and upper cloud properties are retrieved iteratively. In the SFITv2.0 algorithm, the icing threat is determined by applying the SFITv1.0

relationships to the cloud property retrievals for the underlying cloud, if CET < 273K. Thus, the temperature and LWP retrieved for the lower layer cloud largely determines the flight icing threat in these cloud conditions. The MCAT also returns a confidence factor pertaining to the accuracy of the cloud overlap detection. Reasonably good agreement has been found in the tropics between the ML retrievals from MODIS and multi-layered cloud systems characterized by the combination of CloudSat and CALIPSO active sensor data. The algorithm is being validated and refined for application to GEOsat. The algorithm is currently only applied to the most confident ML clouds detected by the MCAT, which is a relatively small percentage of ice cloud pixels. In a future version of the SFIT algorithm, it is expected that the refined version of the MCAT will provide a larger percentage of confident ML retrievals and thus improved detection of icing conditions beneath thin cirrus.

6.2.2.3   Inferring The Flight Icing Threat in Single Layer Ice Over Water Clouds

Thus far, a SFIT capability has been described for lower level SLW-topped clouds in SL and some ML cloud conditions with confident ML signatures. All remaining clouds are assumed to be either warm (CET > 273K), optically thin, or cold optically thick ice over water clouds. Only the latter pose a potential icing threat. These types of clouds are assumed to be SL (i.e. SLIOW clouds) and are generally identified by the red areas which indicate ice phase tops shown in Figure 31a, and from the corresponding COD retrievals shown in Figure 31c. In order to determine the potential for icing conditions within SLIOW clouds, a new methodology is developed that fuses a variety of relevant information available from multiple sources. Cloud properties derived from satellite imager data provide the near real-time (NRT) observations needed to constrain the method over large areas with the high horizontal and temporal resolution

desired by the aviation community. Vertical resolution is also desired since SLIOW clouds have significant vertical extent. This is achieved by applying the CWC profiling technique, developed above, that employs cloud vertical structure information predicted by cloud models and derived from active sensor observations and constrains it with NRT satellite retrievals of CWP and cloud boundaries. While the profiling method described thus far provides estimates of total CWC profiles, knowledge of the potential for SLW and of the SLWC is needed in order to infer the potential FIT. In this study, that information is also acquired in a climatological fashion from the RUC and RAP cloud analyses, since ice and liquid hydrometeors are explicitly resolved separately. The primary objectives for this approach are to estimate the potential for icing conditions in the vertical profile and the most likely maximum icing intensity.

In order to accomplish this, three additional sets of vertical distribution functions (VDF's) are derived from the satellite data and the cloud model output a-priori, and binned as a function of cloud type in a manner similar to the approach used to develop $S(z^*)$. These VDF's provide climatological cloud-type dependent information that are used to estimate; (1) the probability for cloud, PCLD(z), (2) the probability for SLW, PSLW(z), and (3) the LWC, LWC(z). The information is stored in lookup tables and applied in a NRT retrieval system designed to estimate the potential for icing conditions embedded within SLIOW cloud systems, and to estimate the icing altitude boundaries and a composite or maximum icing intensity for the layer.

Figure 34 shows the first set of VDF's that describe the probability of occurrence for cloud (PCLD) as a function of altitude relative to the cloud boundaries derived from MODIS imager data, and as a function of cloud type, which is defined by the CET and COD retrieved from MODIS. These are derived with the intermediate, full-resolution C3M dataset by matching one month (April 2010) of the CERES MODIS SL cloud property retrievals with coincident cloud

boundaries derived from CloudSat Cloud Profiling Radar (CPR) data taken over the study area. The level 2 Cloud Scenario Classification Product (2B-CLDCLASS) available from the CloudSat Data Processing Center is used here and assumed to provide accurate ground truth for the occurrence of cloud in up to 10 layers in the vertical column. For each coincidence that MODIS and CloudSat both detect cloud, PCLD is computed separately on a fixed grid for three regions in the vertical column as a function of distance: (1) above the MODIS cloud top, (2) below the MODIS cloud base, and (3) within the MODIS SL cloud top and base. Thus, the vertical grid is defined with reference to the MODIS cloud boundaries. For the MODIS cloud free regions in the vertical profile, the vertical grid is defined in 100-meter altitude increments above and below the MODIS cloud boundaries. For the cloudy region, the vertical grid is defined for 100 levels as a function of distance below cloud top and normalized by the cloud thickness so that the probabilities can be computed as a function of the relative position within the cloud and properly aggregated. The PCLD VDF's are constructed from the CloudSat data by computing the frequency of occurrence for cloud at each level of the vertical grid. The results shown in Figure 34 indicate that the imager-based accuracies for defining the vertical profile of cloud occurrence, increases for optically thicker and colder clouds. Perfect imager retrievals relative to CloudSat would yield PCLD values of 100% between the indicated top and base altitudes and values of zero at all other levels in the vertical profile. Uncertainties between the MODIS cloud boundaries for the warmest CET bin (not relevant for icing) appear to be largest (lowest probabilities) in this approach because the altitude values are relatively small numbers (i.e., a 0.5-km cloud height retrieval error translates to a 50% uncertainty for a cloud at 1 km, but only a 5% uncertainty for a cloud at 10 km). Mid-level clouds are found to be more uncertain than high cold clouds, as expected, since these data often include overlapping cloud systems and

the cloud top height retrieved with a SL assumption tends to lie between the two layers. Thus, the occurrence of mid-level clouds is overestimated in the imager retrievals based on a SL assumption, which results in relatively large values of PCLD above the CTH. The information shown in Figure 34 is stored in lookup tables and provides an initial method to estimate the vertically resolved probability for cloud from the imager-based cloud parameters. Additional improvements are possible but remain as work planned for a future upgrade. For example, the ML technique described earlier could help reduce the mid-level cloud bias but validation studies for the current ML method implemented in the LaRC NRT system have just begun. Model analyses of temperature and relative humidity profiles have also been shown to be useful for characterizing cloud vertical structure (Minnis et al., 2005). Methods to merge that information with the imager cloud properties and perhaps cloud ceiling observation over the CONUS could be developed and validated with CALIPSO and CloudSat data to further improve icing diagnoses in overlapping cloud conditions. This concept of a vertically resolved cloud probability field from operational satellite data could also be useful for other applications such as the 4D weather cube, and to improve cloud building and clearing in numerical cloud analyses.

Figure 35 depicts the probability for SLW (PSLW) and the median SLW mass fraction (FSLW) as a function of temperature for clouds with CTT < -40°C, and over a wide range of CWP values. These VDF's were derived from the five cloud water mixing ratios (liquid, ice, rain, snow and graupel) produced and cycled in the RAP cloud analysis system during the period between 1 January and 31 March, 2010. Here, CTT is the cloud top temperature defined as the highest model level with a non-negligible cloud mixing ratio. A non-negligible mixing ratio for either liquid or rain at model levels with temperatures below freezing indicates the existence of SLW. FSLW is computed as the ratio of the SLWC computed from the liquid hydrometeor

mixing ratios (liquid + rain) to the total CWC. The total CWC is computed from the sum of all five species mixing ratios and the CWP is the vertically integrated CWC over all cloudy levels. FSLW and PSLW are computed in 5-degree temperature bins for 28 cloud types defined by the model CTT and CWP and stored in lookup tables. Results for the other four CTT bins which range from -40°C to 0°C in increments of 10°C are not shown but exhibit similar behavior over shallower depths. As shown in Figure 35, the model analyses indicate that the probability for SLW increases with increasing temperature and increasing CWP. This is generally consistent with basic cloud physics concepts and relationships to atmospheric temperature and dynamic air motions. For example, upward vertical velocities found in developing clouds contribute to a greater production of liquid water and larger values of CWP, whereas downward air velocity is more likely associated with lower values of CWP and decreasing amounts of liquid in dissipating SLIOW clouds. In the S-FITv2.0 algorithm, PCLD(z) and PSLW(z) are estimated for each cloudy pixel by linearly interpolating the appropriate values retrieved from the lookup tables that correspond to the cloud type defined by the retrieved cloud properties, and by using a temperature profile obtained from a model analysis or short-range forecast valid at the time and location of the satellite data. In the LaRC NRT system these are usually acquired from the operational RAP obtained from NCEP over the GOES domain. The probability for icing as a function of altitude below ice-phase topped clouds is computed from PCLD(z) and PSLW(z) as

$$PICING(z) = PSLW(z) * PCLD(z). \qquad (18)$$

The relationship between the mean FSLW (Figure 35b), temperature, and CWP is more complex than that found for PSLW. Generally, the mean FSLW decreases with increasing values of CWP and there is a pronounced maxima that varies from about -15°C to -30°C as the CWP increases. The mean SLWC values corresponding to FSLW (not shown) indicate that while FSLW

decreases with increasing CWP, higher values of SLWC are associated with larger CWP values as expected.

Now that a strategy has been developed to estimate the vertical profiles of the probability for icing and the SLWC embedded within SLIOW clouds in a manner that is constrained by NRT satellite cloud retrievals, the next step is to map that information to the FIT in a way that is most useful to the aviation weather community. Until further guidance can be obtained from that community, the strategy employed here is to provide a product that is consistent with the SFITv1.0 output, and therefore includes estimates of the upper and lower altitude boundaries for the icing layer, and the maximum likely intensity for the icing layer embedded within SLIOW clouds. In order to estimate the icing intensity, it is assumed that the meteorological parameter with the greatest potential impact on intensity is the SLWC. Guidance derived from an airfoil modeling study (Politovitch, 2003) is used to map the SLWC values in the derived vertical profile to icing intensity. One adjustment to this table was made for application to the satellite algorithm. Since the light-moderate intensity index (value of 4) is grouped into the MOG side of two-category satellite intensity index, the SLWC range for this category was split so that values less than 0.093 are considered 'light' while larger values are considered 'MOG'. That mapping is shown in Table 5 and indicates the degree to which the potential icing intensity is expected to increase with increasing SLWC. The expected upper and lower altitude boundaries for the icing layer are determined from the icing probability profile, the derived CBH and knowledge of the freezing level. For SLIOW clouds, the icing base altitude is determined to be either the derived CBH or the freezing level whichever is higher. The icing top altitude is set to the level found for pre-determined PICING thresholds that best capture the icing layers reported by pilots. The thresholds, which were found to vary from 5% to 30% with increasing CTT and COD, were

empirically derived by matching the satellite-based PICING profiles with the altitude information contained in icing PIREPS over a 3-month period. Thus, the icing top altitude estimates for SLIOW clouds varies over a wide range of atmospheric conditions as a function of the satellite-derived cloud properties, and is tuned to icing PIREPS.

To better illustrate the SFITv2.0 process for SLIOW clouds, the method is demonstrated for two hypothetical clouds (cloud1 and cloud2) with VISST cloud properties similar to those found near Davenport, Iowa at 1745 UTC on 26 Feb 2013 as seen in Figure 31. The CTH was assumed to be the same for both clouds (10.8 km) and the COD was set to 50 (100) for cloud1 (cloud2), respectively. The IWP was computed from the COD by assuming a CER value of 50 for both clouds. H is determined from the CET, COD and IWP as in Minnis et al. (2010) and subtracted from the CTH in order to estimate the CBH. The TWP is estimated from the COD and IWP with equations 11 and 12.   The CTH, CBH, and TWP are then used to constrain the various climatological VDF's in order to derive vertical profiles of PCLD and PSLW (Figure 36a), TWC (Figure 36b), SLWC (Figure 36c) and icing intensity (Figure 36d) for cloud1 and cloud 2. The icing altitude boundaries, maximum probabilities and intensities, and other bulk cloud properties are tabulated for cloud1 and cloud2 in Table 6. In these examples, the temperature profile obtained from the 12 UTC Davenport radiosonde launch was used to identify the freezing level and for converting between temperature and height. While the results shown here may not capture the more complex vertical structures associated with SLW and icing conditions in SLIOW clouds, they appear to be quite reasonable. For example, higher values of SLWC, icing probability and intensity are found for the optically thicker cloud2 when compared to the values found for cloud1. Finally, the key elements and decisions for the SFITv2.0 algorithm are summarized in a high-level flowchart shown in Figure 37.

In the next section, the SFITv2.0 is applied to GOES data and demonstrated with a series of case studies. The results of an initial statistical analysis conducted to validate the SLIOW FIT estimates are also presented.

6.3 SFITv2.0 Examples and Initial Verification

An example of the SFITv2.0 product is shown in Figure 38 and corresponds to the same time period analyzed with the SFITv1.0 output that is shown in Figure 33. Unlike the SFITv1.0 estimates shown in Figure 33, the SFITv2.0 provides a solution for all cloud conditions, including areas with overlapping high ice clouds. In this case, the significant icing conditions captured in the g-airmet warnings issued by the AWC and also reported by pilots within the large area of SLIOW clouds, appear to be adequately captured in the satellite analyses. In addition, the satellite analyses provide improved spatial and temporal resolution of icing conditions relative to the conventional observations and model based forecasts. Note also the additional intensity category for heavy icing, which is denoted by the magenta pixels in the satellite icing analyses. The most significant area of heavy icing found for this case appears to be associated with the large water droplets retrieved in the SLW clouds over the Appalachians (see Figure 31e). Heavy icing was also identified with the SFITv2.0 algorithm in an area to the east of North Carolina over the Gulf Stream (Figure 39). These were triggered by high values of 6.7-11 μm BTD found in very opaque, deep, cold, optically thick clouds which are typically associated with convection and significant upward vertical velocities. These clouds are assumed to contain heavy icing conditions in the SFITv2.0 algorithm, although pilots are often able to avoid these using weather radar guidance, so encounters with icing in these cloud types are more rare.

To determine how well the SFITv2.0 is able to resolve icing conditions, the satellite estimates are matched and compared with icing PIREPS in a statistical manner similar to that described by Smith et al. (2012). The FIT derived from GOES-13 was compared to icing PIREPS over the eastern CONUS between January 1 and March 31, 2013. All satellite pixels within 20 km and 15 minutes of each icing PIREP were matched under the condition that the 20-km radius region was completely overcast. Regions containing any icing are considered to be positive detections from GOES. This strategy resulted in 11,851 matches during the daytime, of which 5,759 (2,713) of the matches were completely overcast liquid (ice) topped cloud regions, respectively. Two-by-two contingency tables are constructed to help quantify the intercomparisons with standard skill scores. The skill in detecting icing conditions is shown in Table 7. The probability of detecting icing (PODY) is 99% for all clouds, 99% for liquid clouds and 98% for ice clouds. The accuracies (percentage of correct detections) are 88%, 90% and 83% for all clouds, liquid clouds and ice clouds, respectively. False detections are common, but comprise only a small percentage of the total (false alarm rate, FAR~10%). Adequately quantifying false alarms using icing PIREPS appears to be impossible due to the low bias in 'no icing' observations (Brown and Young, 2000). The probability of detecting 'no icing' conditions (PODN) is also highly uncertain and misleading for the same reason. The high values of PODY and accuracy found for the daytime data indicate that the satellite technique has an excellent detection capability relative to positive icing PIREPS, even for overlapping clouds. These results are considerably better than those found by Ellrod and Bailey (2007) and by Smith et al. (2012) since those algorithms only applied to SLW clouds.

Statistics were computed from contingency tables that were formed to test the two-category intensity component of the FIT algorithm during daytime. The results are shown in Table 8 for

overcast SLW regions (N=5,711) and for overcast ice cloud regions (N=2,236). As in Smith et al. (2012), the PIREPS light-moderate reports (categorical index=4) were conservatively classified as MOG icing for matching with the two-category satellite icing intensity index. In other words, PIREPS icing intensity indices 1-3 are considered 'light', while indices with values greater than 3 are considered 'MOG'. Since there are only two intensity categories in the satellite technique, the SLWC range for 'light-moderate' found in Politovitch (2003) was redistributed so that the lower half of that range (SLWC=0.066-0.093) are considered to be 'light' and the upper half is considered to be 'MOG'. Two sets of statistics are shown in Table 8. Table 8a lists the results found by comparing the dominant icing intensity retrieved from GOES-13 in the 25 km radius area surrounding each PIREP. The accuracy of the satellite method for separating light from MOG icing conditions as reported by pilots is 60% and 57% for liquid and ice clouds, respectively. PODL and PODM are found to be 60% and 61% for liquid clouds. These results are similar to those found by Smith et al. (2012) for the SFITV1.0, which was tuned to produce similar values of PODL and PODM. The SLIOW algorithm is not tuned since it relies on a physical retrieval of SLWC that is subsequently is mapped to icing intensity. For ice clouds, PODL and PODM are found to be 61% and 45%, respectively. There is some ambiguity in these comparisons since at times the 25 km radius area assessed from satellite contains significant amounts of both intensities. To try and account for this more fairly, the contingency tables were formed again, but in this case, satellite regions covered with at least 30% of both 'light' and 'MOG' icing conditions were counted as hits in both categories. The performance statistics are somewhat better and are shown in Table 8b. In these cases, the intensity accuracies are 73% (72%), PODL is 76% (66%), and PODM is 80% (47%) for liquid (ice) clouds, respectively. While these comparisons indicate somewhat modest skill for

differentiating light from MOG icing conditions from satellite, the uncertainties associated with icing PIREPS and in the verification methods may mask the true utility of the method. For example, PIREPS are known to suffer from temporal and spatial reporting errors. When superimposed on the high natural variability of icing conditions often encountered in clouds, and the high spatial variability found in the satellite cloud property retrievals, sampling mismatches with PIREPS probably confound the comparisons. Smith et al. (2012) found higher accuracies when applying filters to help minimize the impact of sampling issues, and also found higher accuracies when comparing to ground-based icing remote sensing datasets, which are accurately time stamped and geo-located. Other complicating characteristics with respect to interpreting PIREPS include the fact that icing intensity reports are subjective, depending on the experience of the pilots. In addition, the severity to the airframe depends not only on the meteorological conditions, but also on flight and airframe characteristics, which are currently impossible to account for. Despite all of these potential issues, the comparisons shown here appear to be reasonably good. Another test for the veracity of the satellite method is to determine whether it produces the same relative frequency of light and MOG icing conditions as observed and reported by pilots. Those values are shown in the far right columns of Table 8. In fact, this test may be a better accuracy gauge than the relative values found for PODL and PODM. The fact that the frequency of 'light' icing PIREPS are typically found to be 2.5 to 3 times greater than the frequency of 'MOG' icing PIREPS may in fact yield misleading values of PODL and PODM, when considering the sampling errors that likely exist. It is interesting to note from the results in Table 8 that for the case of SLW clouds, the satellite method overestimates the frequency of MOG icing by 10-20%, despite the fact that the SLW algorithm was tuned to maximize the agreement in PODL and PODM. On the other hand, the ice cloud algorithm was

not tuned in this way. While the values of PODL found for ice clouds are much higher than the values found for PODM, the level of agreement with PIREPS found for the frequency of MOG icing conditions is better than the level of agreement found for SLW clouds. Thus, it appears that any algorithm tuning designed to maximize the values of both PODL and PODM, may lead to overestimates in the frequency of occurrence of MOG icing. Some future work is probably needed to reassess the low cloud SLW algorithm with respect to these issues. For ice clouds, the SFITv2.0 algorithm appears to be producing results that overall have accuracies that are comparable to those found for SLW clouds. While the values found for PODM are low, the algorithm does seem to produce the right amount of MOG icing embedded beneath ice topped clouds, relative to the frequencies reported by pilots.

In Figure 40, the icing top altitudes derived from GOES-13 data using the SFITv2.0 algorithm are shown. Pilots typically report the altitude that the icing was encountered rather than a top and base altitude, so validating the satellite icing layer boundaries is currently impossible. Nevertheless, an assessment is made as to how well the satellite estimates capture the altitudes reported by pilots. For the case on 26 February 2013 that is shown in Figure 40, the PIREPS altitudes are plotted on top of the satellite analysis and good correspondence is found in general. Figure 41 summarizes the altitude comparison found for the 3-month period analyzed from January-March, 2013. The frequency distribution of the distance from the PIREPS icing altitudes to the icing altitude boundaries derived from GOES with the SFITv2.0 algorithm is plotted here. The frequencies indicated for the distance value of zero indicate the percentage of the time that the satellite icing layers captured the PIREP altitudes. Negative (positive) distance values indicate that the PIREPS altitudes were found below (above) the satellite icing base (top) altitude estimates, respectively. The results indicate that for both ice and liquid topped clouds,

the satellite analyses capture the PIREPS altitudes about 65% of the time. Furthermore, the satellite-derived icing boundaries are within about 1000 feet of the reported altitudes over 90% of the time. The fact that this level of agreement is found is perhaps more remarkable for the ice clouds since they span much greater vertical depths than the shallower low-level SLW clouds.

Several case studies are conducted with the SFITv2.0 output to examine the icing conditions as determined from satellite at the time of several serious icing-related aviation incidents. The first case occurred on 20 December 2011. A single engine turboprop crashed near Morristown, New Jersey, narrowly missing a crowded Interstate highway, after departing nearby Tetersboro airport. All five passengers were killed. Numerous encounters of severe icing were reported near the time and location of the crash at altitudes near 17 kft that had commercial air traffic in and out of New York City airports scrambling to acquire altitude clearances to exit and avoid the dangerous conditions. The satellite cloud top phase analysis using GOES data taken at the time of the incident indicated that a large area of SLW clouds covered the region from Pennsylvania, across New Jersey, and extended eastward over the Atlantic Ocean. The icing analysis shown in Figure 42a indicates that while a wide range of icing conditions were present, the possibility for severe icing was significant across New Jersey, particularly in a wide area just south and west of the crash site. Large water droplets inferred from the GOES 3.9 μm channel (Figure 42b) triggered the severe condition in the SFITv2.0 algorithm. The severe condition was not detected from GOES along the route of the ill-fated turboprop. The 12 UTC radiosonde profile from Upton, New York may have sufficiently captured the meteorological conditions, although these data were taken several hours earlier and in an area downstream of the crash site. Nevertheless, the sounding shown in Figure 43a indicates that the conditions were ripe for SLD (super-cooled large droplets) due to the saturated air column above a significant capping inversion that

occurred at about 800 hPa. The capping inversion has the potential to impact icing conditions aloft by confining pollution to lower levels beneath the cloud. Cleaner clouds contain fewer cloud condensation nuclei and tend to produce larger water droplets since there is less competition for the available water vapor. The sounding also indicates that a second thinner cloud level may have obscured the satellite view to the more dangerous icing conditions below that were encountered by the aircraft before it crashed. An overlapping cloud with smaller water droplets could explain why smaller values of CER were retrieved, which subsequently led to a lower flight icing threat estimate in this area. The NEXRAD imagery from nearby Binghamton, New York shown in Figure 43b indicates that the clouds across northern New Jersey were producing low values of radar reflectivity, which are usually suggestive of large drizzle size water droplets or ice crystals. The radar echoes appear to occur in areas that the larger values of CER are found but also occur over the crash site area. Considering the severity of the icing conditions that were reported in the area, these clouds probably did contain SLD. While it is disappointing that this condition was not detected from satellite in the area of the plane crash, it may be possible to better diagnose these types of conditions in the future by combining information from satellite and radar data. More advanced satellite sensors, such as the MODIS, have additional spectral channels that provide some information on the vertical profile of CER (e.g., Platnick (2000), Chang and Li (2002)), but these data are difficult to evaluate with respect to icing conditions since they are only available over a given area a few times per day, and thus they rarely correspond with the more significant known icing events such as this. In the near future, the 16-channel ABI planned for the next generation GOES-R satellite will provide the high frequency multi-spectral observations needed to further improve icing diagnoses.

Another interesting severe icing case occurred on 22 February 2013. On this day, a wide area of SLW blanketed the upper Midwest. The satellite icing analysis at 20 UTC shown in Figure 44a indicated that a wide are of MOG icing conditions could be expected across much of southern Wisconsin, northern Illinois and Indiana and most of Michigan. An area of potentially severe icing was also identified over Lake Michigan. As in the previous case, large CER retrievals triggered the severe condition determined with the SFITv2.0 algorithm. Near the same time, two severe icing PIREPS were filed, one over northern Illinois and one over Lake Michigan. No signal in the satellite data was found to discern the severe condition over Illinois, but the severe icing PIREP corroborates the severe condition found over the lake in the satellite analysis. The severe condition identified from satellite persisted throughout the afternoon and early evening and pushed eastward into southeastern Michigan. It was not until 2355 UTC after several more severe icing PIREPS had been filed, that the AWC issued the icing SIGMET (severe icing warning) over the area shown in Figure 44b. Clearly, in this case, the severe icing threat was accurately diagnosed many hours earlier in the satellite analyses, which could have been useful to AWC forecasters and aviators had the information been made available to them.

On 5 September 2012, a commercial Bombadier DHC-8-103 aircraft with 15 people on board experienced a 5 kft altitude loss due to icing conditions encountered shortly after takeoff from Anchorage while on its planned route to Homer, Alaska (Figure 45a). The corresponding GOES-15 cloud top phase analysis (not shown) indicated that SLW clouds were present along the route. The satellite icing analysis shown in Figure 45b appears to have correctly diagnosed the severe conditions over the same area of the Alaska Kenai peninsula where the aircraft lost altitude. In this case, the aircraft was able to maintain flight and return safely to Anchorage. This

case is of particular interest to the NWS Alaska Aviation Weather Unit (AAWU) since the dangerous conditions that occurred on this day were not forecasted.

7 Summary and Discussion

This research is motivated by the realization that despite the considerable amount of work and resources spent to develop and improve cloud observing systems, quantitative real-time retrievals of cloud properties, particularly those with high spatial and temporal resolution from passive geostationary satellite imagers, remain underutilized in weather applications and decision support systems (DSS). In this study, new techniques are developed for interpreting cloud products derived from satellite imager data in order to (1) better account for uncertainties and improve their absolute accuracies, (2) improve the definition of cloud vertical structure, and (3) demonstrate NRT weather applications for their use. The methods are developed using datasets taken over the CONUS and adjacent ocean areas with the majority of the data taken over land areas. No attempt has yet been made to stratify the techniques for separate application over land and ocean. Thus the current profiling method, and particularly the icing technique which is tuned to icing PIREPS over the CONUS, are most applicable to mid–latitude land areas.

A significant outcome of this study is the development of a method to derive 4-D cloud properties that improves the resolution of cloud vertical structure, including the potential mass partitioning of cloud liquid and ice in deep ice cloud over water cloud systems, which are generally poorly observed in their entirety. This study demonstrates that while these clouds are relatively rare (see Figure 11), they are important because of their association with large synoptic scale storm systems, convection, precipitation and adverse weather conditions, including dangerous icing conditions, and because they comprise a significant fraction of the total cloud

water budget found over large areas of the Earth (see Figure 12). Therefore, accurate characterizations of these types of clouds are important for both weather and climate applications and studies. Since no single observing system provides the comprehensive information needed to solve this complex problem alone, a synergistic approach is taken that combines information from multiple sources including satellite and ground-based active sensor data, cloud model output, passive satellite imager data, and aircraft observations. Verification studies indicate that the cloud profiling technique produces reasonably good estimates of upper tropospheric IWC compared to active sensor retrievals when the technique is applied to CERES MODIS cloud property retrievals. For cirrus clouds, the satellite imager and active sensor retrievals of IWC and IWP agree on average to within 30%. The effect of the MODIS cloud boundary errors on the differences was examined by constraining the MODIS profiles with the CloudSat cloud boundaries. In those cases, the mean cirrus IWC values derived from MODIS are found to agree to with CloudSat retrievals to within 10%. For optically thick clouds, the mean IWC and IWP retrievals are found to agree to a level of 10% over a wide range of COD values.

When applied to high frequency cloud products derived from GOES data, the profiling method also produces cloud LWC estimates beneath overlapping ice clouds that correspond well with pilot reports of icing intensity. Taken together, an unprecedented level of closure is obtained for characterizing the cloud water budget in SLIOW cloud systems using NRT satellite observations. This level of closure is only possible by developing and employing empirical methods to help account for systematic errors found in the retrieval of CWP due to the simplifying assumptions regarding cloud phase and vertical homogeneity that are common in passive satellite retrieval methods. Thus, an additional outcome of this research is more accurate CWP retrievals from satellite imager data.

Two different methods are developed in this study for estimating the potential LWP embedded in SLIOW clouds. The first method is developed based on comparisons of the GOES-derived COD with MWR data taken from the ARM SGP site, which are included in the ARM MICROBASE dataset. These data were used to develop parameterizations to estimate the TWP in SLIOW clouds from the satellite imager cloud products. The second method is employed in the profiling technique, which incorporates the TWP parameterization but also uses information derived from the cloud analysis scheme in the RUC model to partition the liquid and ice mass fractions from the total mass. A comparison of the LWP derived from the two methods reveals surprisingly good agreement on average over a wide range of cloud optical thicknesses (COD). The absolute values derived from the MICROBASE parameterization (Equation 12) are about 10-20% higher for clouds with COD values less than about 20 and about 10-20% higher for clouds with COD values greater than about 110. However, for COD values between 20 and 100, the LWP values are remarkably consistent between the two methods, which indicates in a rather indirect way that the partitioning of liquid and ice in the model cloud analyses is quite consistent with the ARM observations. Figure 46 shows the comparison of the two SLIOW cloud LWP retrieval estimates expressed as the ratio (in percent) of the LWP difference to the TWP, which is binned and plotted as a function of the COD retrieved from the GOES-13 imager. With respect to the TWP estimated for these clouds, the level of agreement is found to be within a few percent. This is a rather unique and unexpected outcome that supports the idea and approach developed as part of this thesis to integrate information from multiple observing systems along with information captured in cloud models to more accurately determine the geographic and vertical distribution of cloud water. Since the profiling method developed here, which incorporates climatological information on cloud vertical structure and water phase derived from

models, is found to produce relatively accurate IWC and LWC retrievals when constrained with satellite imager data, this study also demonstrates that for these types of clouds, the models do in fact have notable skill in characterizing the vertical distribution of cloud water. The most basic problem that remains with models is that they do not diagnose clouds at the right time and in the right place except on very large scales.

With respect to NWP and its utility in DSS, the need to improve cloud diagnoses and forecasts is well recognized, but many challenges exist. A significant deficiency in models is that clouds and their key characteristics are poorly initialized. Thus, it seems unlikely that improvements in model resolution and physics, which garner a lopsided amount of attention and resources in weather programs, will have much impact until this most fundamental initialization problem is more adequately addressed with observations, particularly with respect to SLIOW clouds. The results of this research suggest that a potential avenue for future research is to develop methods to improve cloud initializations in models that better incorporate satellite-derived cloud properties, such as the 4-D cloud profiles developed in this study.

Applications are also developed here to infer the flight icing threat to aircraft from the NRT cloud properties and profiles that are now routinely derived from geostationary satellite imager data. These methods are found to significantly improve the early warning and resolution of icing conditions that are often not adequately captured in current forecasting techniques. Compared to PIREPS and ground-based icing remote sensing datasets, the satellite icing detection and intensity accuracies are approximately 90% and 70%, respectively. The satellite-derived icing boundaries capture the reported altitudes over 90% of the time.

These results demonstrate improved accuracies and new utilities for operational satellite-derived cloud products; however, more work is needed to further validate and improve the

methods. For example, there are several other active sensor based IWC datasets available for verification other than the datasets employed here. These include the CloudSat 2CICE product and the ICARE (Cloud-Aerosol-Water-Radiation Interactions) DARDAR datasets. 2CICE and DARDAR employ optimal estimation techniques that combine the CPR and CALIOP data in IWC retrieval schemes. While the upper level IWC and IWP retrievals derived from the passive sensor profiling method agree well with CloudSat in the initial comparisons presented here, further improvements may be realized through comparison with additional observations. In addition, the climatological approach and the verification studies presented here were only developed and performed over the CONUS. The method could be expanded for global application and additional studies should be conducted to determine how well these new passive satellite retrievals capture the global distribution of cloud ice and liquid water.

With respect to the icing algorithms contained in the SFITv2.0, more work is needed to ready these datasets for operational use. A significant issue in icing verification studies is the inherent difficulty associated with validating false alarms since 'no icing' PIREPS are relatively rare. Some false alarms are already known but these occur relatively infrequently and it should be possible to reduce these with additional work. For example, CER has proven to be a potentially effective retrieval parameter for diagnosing severe icing conditions but CER overestimates are known to occur in close proximity to ice clouds and along cloud edges. New methods are needed to properly screen these contaminated retrievals to eliminate 'severe' icing false alarms. Another significant potential source of error is associated with our inability to properly account for the bright background in some cloud retrievals over snow. The development of more accurate cloud property retrievals over snow surfaces is underway. These could be applicable to GOES-R data but have not yet been tested in satellite icing applications.

Ultimately, the end users, including aviation weather forecasters and pilots, should provide the best test for the utility of the satellite icing products. Plans are being developed to deliver these exciting new products to the GOES-R Proving Ground in the near future so that they can be evaluated in operational applications.

Bibliography

Ackerman, S. A., K. I. Strabala, W. P. Menzel, R. A. Frey, C. C. Moeller, and L. E. Gumley, 1998: Discriminating clear sky from clouds with MODIS. *J. Geophys. Res.,* **103**, 32141–32157.

Ackerman, S. A., R. E. Holz, R. Frey, E. W. Eloranta, B. C. Maddux, M. McGill, 2008: Cloud Detection with MODIS. Part II: Validation. J. *Atmos. Oceanic Technol*., **25**, 1073–1086.

Ahlgrimm, M., R. Forbes, 2012: The Impact of Low Clouds on Surface Shortwave Radiation in the ECMWF Model. *Mon. Wea. Rev*., **140**, 3783–3794.

Andersson, E., J. Pailleux, J-N. Thepaut, J. R. Eyre, A. P. McNally, G. A. Kell, P. Courtier, 1994: Use of cloud-cleared radiances in three/four- dimensional variational data assimilation. *Q. J. R. Meteorol. Soc.,* **120**, 627–653.

Appiah-Kubi, P., 2011: U.S Inflight Icing Accidents and Incidents, 2006 to 2010, Master's Thesis, University of Tennessee. http://trace.tennessee.edu/utk_gradthes/1055

Austin, R. T., A. J. Heymsfield, and G. L. Stephens, 2009: Retrieval of ice cloud microphysical parameters using the CloudSat millimeter-wave radar and temperature*, J. Geophys. Res.*, **114**, D00A23, doi:10.1029/2008JD010049.

Bureau of Transportation Statistics, "Airline On-Time Statistics and Delay Causes", http://www/transtats.bts.gov.

Baker, B. A., and R. P. Lawson, 2006: In situ observations of the microphysical properties of wave, cirrus and anvil clouds. part I: Wave clouds, *J. Atmos. Sci.,* **63**, 3160–3185.

Barnes W. L., T. S. Pagano, V. V. Salomonson, 1998: Prelaunch characteristics of the moderate resolution imaging spectroradiometer (MODIS) on EOS-AM1. *IEEE Trans Geosci Remote Sens,* **36**, 1088–1100

Baumgardner, D., 1983: An analysis and comparison of five water droplet measuring instruments, *J. Appl. Meteorol.*, **522**, 891–910.

Baumgardner, D., H. Jonsson, W. Dawson, D. O'Connor, and R. Newton, 2002: The cloud, aerosol and precipitation spectrometer (CAPS): A new instrument for cloud investigations, *Atmos. Res*., **59–60**, 251– 264.

Baylor, G. M., R. M. Aune, and W. H. Raymond, 2000: NWP cloud initialization using GOES sounder data and improved modeling of nonprecipitating clouds, *Mon. Weather Rev.*, **128**, 3911 – 3920.

Benedetti, A, M. Janiskova, 2008: Assimilation of MODIS cloud optical depths in the ECMWF model. *Mon. Weather Rev*, **136**, 1727-1746.

Bennartz, R., 2007: Global assessment of marine boundary layer cloud droplet number concentration from satellite, *J. Geophys. Res.*, **112** , D02201, doi:10.1029/2006JD007547.

Bennartz R, T. Greenwald, 2011: Current problems in scattering radiative transfer modelling for data assimilation. *Q. J. R. Meteorol. Soc.* **137**: 1952–1962.

Benjamin, S. G., G. A. Grell, J. M. Brown, and T. G. Smirnova, 2004a: Mesoscale weather prediction with the RUC hybrid isentropic--terra-following coordinate model. *Mon. Wea. Rev.*, **132**, 473-494.

Benjamin, S. G., D. Dévényi, S. S. Weygandt, K. J. Brundage, J. M. Brown, G. A. Grell, D. Kim, B. E. Schwartz, T. G. Smirnova, and T. L. Smith, and G. S. Manikin, 2004b: An hourly assimilation-forecast cycle the RUC. *Mon. Wea. Rev.*, **132**, 495-518.

Bernstein, B., F. McDonough, M. Politovich, B. Brown, T. Ratvasky, D. Miller, C. Wolff, and G. Cunning, 2005: Current icing potential (CIP): Algorithm description and comparison with aircraft observations. *J. Appl. Meteor.*, **44**, 969–986.

Bernstein, B. C., C. A. Wolff and F. McDonough, 2007; An Inferred climatology of icing conditions aloft, including supercooled large drops. Part I: Canada and the Continental United States. *J. Appl. Meteor. Clim.*, **46**, 1857-1878.

Bleck, R., and S. G. Benjamin, 1993: Regional weather prediction with a model combining terrain-following and isentropic coordinates. Part I: model description. *Mon. Wea. Rev.*, **121**, 1770-1785.

Bodas-Salcedo, A., M. J. Webb, M. E. Brooks, M. A. Ringer, K. D. William, S. F. Milton, and D. R. Wilson, 2008: Evaluating cloud systems in the Met Office global forecast model using simulated CloudSat radar reflectivities, *J. Geophys. Res.*, **113**, D00A13, doi:10.1029/2007JD009620.

Brown, B. G., G. Thompson, R. T. Bruintjes, R. Bullock, and T. Kane, 1997: Intercomparison of in-flight icing algorithms. Part II: Statistical verification results. *Wea. Forecasting*, **12**, 890–914.

Brown, B. G., and G. S. Young, 2000: Verification of icing and turbulence forecasts: Why some verification statistics can't be computed using PIREPs. Preprints, Ninth Conf. on Aviation, Range, and Aerospace Meteorology, Orlando, FL, Amer. Meteor. Soc., 393–398.

Brown, B., J. L. Mahoney, R. Bullock, T. L. Fowler, J. Henderson, and A. Loughe, 2001: Quality assessment report: Integrated Icing Diagnostic Algorithm (IIDA). AWIT Technology Review Panel Internal Report, 35 pp. [Available from B. Brown, Re- search Applications Program, National Center for Atmo- spheric Research, P.O. Box 3000, Boulder, CO 80307-3000.]

Cess, R. D., and co-authors, 1989: Interpretation of cloud-climate feedback as produced by 14 atmospheric general circulation models, *Science*, **245**, 513-515.

Chang, F. L., and Z. Li, 2002: Estimating the vertical variation of cloud droplet effective radius using multispectral near-infrared satellite measurements, *J. Geophys. Res.*, **107**, 4257, doi:10.1029/2001JD000766.

Chang, F-L., and Z. Li, 2005: A near-global climatology of single-layer and overlapped clouds and their optical properties retrieved from Terra/ MODIS data using a new algorithm. *J. Climate*, **18**, 4752–4771, doi:10.1175/JCLI3553.1.

Chang, F.-L., P. Minnis, J. K. Ayers, M. J. McGill, R. Palikonda, D. A. Spangenberg, W. L. Smith Jr., and C. R. Yost, 2010: Evaluation of satellite-based upper troposphere cloud top height retrievals in multilayer cloud conditions during TC4, *J. Geophys. Res.*, **115**, D00J05, doi:10.1029/2009JD013305.

Chang, F.-L., P. Minnis, B. Lin, M. M. Khaiyer, R. Palikonda, and D. A. Spangenberg, 2010b: A modified method for inferring upper troposphere cloud top height using the GOES 12 imager 10.7 and 13.3 μm data. *J. Geophys. Res.*, **115**, D06208, doi:10.1029/2009JD012304.

Clothiaux E. E. , M. A. Miller, B. A. Albrecht, T. P. Ackerman, J. Verlinde, D. M. Babb, R. M. Peters, and W. J. Syrett. 1995: An Evaluation of a 94-GHz Radar for Remote Sensing of Cloud Properties. *J. Atmos. Oceanic Technol.*, **12**, 201-229.

Clothiaux E. E., T. P. Ackerman, G. G. Mace, K. P. Moran, R. T. Marchand, M. Miller, and B. E. Martner, 2000: Objective determination of cloud heights and radar reflectivities using a combination of active remote sensors at the ARM CART sites. *J. Appl. Meteor. Climatol*, **39**, 645-665.

Delanoe, J., and R. J. Hogan, 2008: A variational scheme for re-trieving ice cloud properties from combined radar, lidar and infrared radiometer. *J. Geophys. Res.*, **113**, D07204, doi:10.1029/2007JD009000.

Delanoe, J., and R. J. Hogan, 2010: Combined CloudSat-CALIPSO-MODIS retrievals of the properties of ice clouds. *J. Geophys. Res.*, **115**, D00H29, doi:10.1029/2009JD012346.

Deng, M., G. G. Mace, Z. Wang, and H. Okamoto, 2010: Tropical Composition, Cloud and Climate Coupling Experiment validation for cirrus cloud profiling retrieval using CloudSat radar and CALIPSO lidar. *J. Geophys. Res.*, **115**, D00J15, doi:10.1029/2009JD013104.

Deng, M, G. G. Mace, Z. Wang, R., P. Lawson, 2013: Evaluation of Several A-Train Ice Cloud Retrieval Products with In Situ Measurements Collected during the SPARTICUS Campaign. *J. Appl. Meteor. Climatol.*, **52**, 1014–1030.

Derber J. C., W-S. Wu, 1998: The use of TOVS cloud-cleared radiances in the NCEP SSI analysis system. *Mon. Weather Rev.* **126**: 2287–2299.

Dong, X., P. Minnis, B. Xi, S. Sun-Mack, and Y. Chen, 2008: Comparison of CERES-MODIS stratus cloud properties with ground-based measurements at the DOE ARM Southern Great Plains site, *J. Geophys. Res*., **113**, D03204, doi:10.1029/2007JD008438.

Dunn, M., Johnson, K. L., and Jensen, M. P.: The Microbase value-added product: A baseline retrieval of cloud microphysical properties, DOE/SC-ARM/TR-095, available at: http://www.arm.gov/publications/tech reports/doe-sc-arm-tr-095.pdf, 2011.

Ellrod, G. and J. P. Nelson, 1996: Remote Sensing of Aircraft Icing Regions Using GOES Multispectral Imager Data, *Proc. AMS 15th Conf. Weather Anal. & Forecasting*, 19-23 August, Norfolk, VA, 9-12.

Ellrod, G. and A. P. Bailey, 2007: Assessment of aircraft icing potential and maximum icing altitude from geostationary meteorological satellite data. *Wea. Forecasting*, **22**, 160–174.

Errico, R. M., P. Bauer, J-F. Mahfouf, 2007: Issues Regarding the Assimilation of Cloud and Precipitation Data. *J. Atmos. Sci*., **64**, 3785–3798.

FAA National Aviation Safety Data Analysis Center, "NTSB Weather related Accident Study", http://www.asias.faa.gov/aviation_studies/weather_study/summary.html.

Gardiner, B. A. and J. Hallett, 1985: Degradation of in-cloud forward scattering spectrometer probe measurements in the presence of ice particles. *J. Atmos. Oceanic Technol*., **2**,171–180.

Greenwald, T. J., R. Hertenstein, and T. Vukic´evic´, 2002: An all weather observational operator for radiance data assimilation with mesoscale forecast models. *Mon. Wea. Rev*., **130**, 1882–1897.

Greenwald, T. J., 2009: A 2 year comparison of AMSR-E and MODIS cloud liquid water path observations, *Geophys. Res. Lett*., **36**, L20805, doi:10.1029/2009GL040394.

Ham, S.-H., S. Kato, H. Barker, F. Rose and S. Sun-Mack, 2014: Improving the modeling of shortwave radiation through the use of 3D scene construction algorithm. Submitted to Q. J. R. Meteorol. Soc.

Han, Q., W. Rossow, J. Chou, and R. Welch, 1998: Global survey of the relationships of cloud albedo and liquid water path with droplet size using ISCCP, *J. Clim*., **11**, 1516–1528.

Hashino, T., G. J. Tripoli, 2007: The Spectral Ice Habit Prediction System (SHIPS). Part I: Model Description and Simulation of the Vapor Deposition Process. *J. Atmos. Sci*., **64**, 2210–2237.

Heymsfield, A. J., L. J. Donner, 1990: A scheme for parameterizing ice-cloud water content in general circulation models, *J. Atmos. Sci*., **47**, 1865–1877.

Heymsfield, A. J., D. Winker and G.-J. van Zadelhoff, 2005: Extinction-ice water content-effective radius algorithms for CALIPSO, *Geophys. Res. Lett*, **32**, L10807, 1-4.

Heymsfield, Andrew J., Aaron Bansemer, Cynthia H. Twohy, 2007: Refinements to Ice Particle Mass Dimensional and Terminal Velocity Relationships for Ice Clouds. Part I: Temperature Dependence. *J. Atmos. Sci*., **64**, 1047–1067.

Heymsfield, Andrew J., and Coauthors, 2008: Testing IWC Retrieval Methods Using Radar and Ancillary Measurements with In Situ Data. *J. Appl. Meteor. Climatol*., **47**, 135–163.

Holz, R. E., S. A. Ackerman, F. W. Nagle, R. Frey, S. Dutcher, R. E. Kuehn, M. A. Vaughan, and B. Baum, 2008: Global Moderate Resolution Imaging Spectroradiometer (MODIS) cloud detection and height evaluation using CALIOP, *J. Geophys. Res*., **113**, D00A19, doi:10.1029/2008JD009837.

Jones, T. A., D. J. Stensrud, P. Minnis, R. Palikonda, 2013: Evaluation of a Forward Operator to Assimilate Cloud Water Path into WRF-DART. *Mon. Wea. Rev*., **141**, 2272–2289.

Kato S., S.Sun-Mac, W. F. Miller, F. G. Rose, Y. Chen, P. Minnis, B. A. Wielicki, 2010: Relationships among cloud occurrence frequency, overlap, and effective thickness derived from CALIPSO and CloudSat merged cloud vertical profiles. *J. Geophys. Res*. **115**: D00H28. DOI:10.1029/2009JD012277.

Khain, A., M. Otchinnikov, M. Pinsky, A. Pokrovsky, H. Krugliak, 2000: Notes on the state-of-the-art numerical modeling of cloud microphysics. *Atmos. Res.*, **55**, 159-224.

King, M. D., S. C. Tsay, S. E. Platnick, M. Wang, and K. N. Liou, "Cloud retrieval algorithms for MODIS: Optical thickness, effective particle radius, and thermodynamic phase," *MODIS Algorithm Theoretical Basis Document No. ATBD-MOD-05*, 79 pp., 1997. [Online]. Available: modis-atmos.gsfc.nasa.gov/_docs/atbd_mod05.pdf

King, M., W. Menzel, Y. Kaufman, D. Tanre, B. Gao, S. Platnick, S. Ackerman, L. Remer, R. Pincus, and P. Hubanks, 2003: Cloud and aerosol properties, precipitable water, and profiles of temperature and water vapor from MODIS, *IEEE Trans. Geosci. Remote Sens.*, **41**, 442–458.

Le Marshall, J. and Coauthors, 2006: Improving global analysis and forecasting with AIRS. *Bull. Amer. Meteor. Soc.*, **87**, 891 – 894.

Li, J.-L. F., D. Waliser, C. Woods, J. Teixeira, J. Bacmeister, J. Chern, B.-W. Shen, A. Tompkins, W.-K. Tao, and M. Köhler (2008), Comparisons of satellites liquid water estimates to ECMWF and GMAO analyses, 20th century IPCC AR4 climate simulations, and GCM simulations, *Geophys. Res. Lett*., **35**, L19710, doi:10.1029/2008GL035427.

Lin, W. Y., M. H. Zhang, 2004: Evaluation of Clouds and Their Radiative Effects Simulated by the NCAR Community Atmospheric Model Against Satellite Observations. *J. Climate*, **17**, 3302–3318.

Lipton, A. E., and G. D. Modica, 1999: Assimilation of visible band satellite data for mesoscale forecasting in cloudy conditions. *Mon. Wea. Rev.*, **127**, 265–278.

Mace G. G., T. P. Ackerman, P. Minnis, and D. F. Young. 1998: Cirrus Layer Microphysical Properties Derived from Surface-Based Millimeter Radar and Infrared Interferometer Data. *J. Geophys. Res.*, **103**, 23207-16.

Mace, G. G., Y. Zhang, S. Platnick, M. D. King, P. Minnis, P. Yang, 2005: Evaluation of Cirrus Cloud Properties Derived from MODIS Data Using Cloud Properties Derived from Ground-Based Observations Collected at the ARM SGP Site. *J. Appl. Meteor.*, **44**, 221–240.

Mace, G. G., Q. Zhang, M. Vaughan, R. Marchand, G. Stephens, C. Trepte, and D. Winker, 2009: A description of hydrometeor layer occurrence statistics derived from the first year of merged Cloudsat and CALIPSO data, *J. Geophys. Res.*, **114**, D00A26, doi:10.1029/2007JD009755.

Matrosov S. Y., T. Uttal, J. B. Snider, and R. A. Kropfli. 1992: Estimation of Ice Cloud Parameters from Ground-Based Infrared Radiometer and Radar Measurements. *J. Geophys. Res.*, **97**, 11567-11574.

Menzel, W. Paul, Purdom, James F.W. Introducing GOES-I, 1994: The First of a New Generation of Geostationary Operational Environmental Satellites. *Bull. Amer. Meteor. Soc.*, **75**, 757–782.

Meyers, M.P., R. L. Walko, J. Y. Harrington, and W. R. Cotton, 1997: New RAMS cloud microphysics parameterization. Part II: The two-moment scheme. *Atmos. Res.*, **45**, 3-39.

Miller, Steven D., and Coauthors, 2014: Estimating Three-Dimensional Cloud Structure via Statistically Blended Satellite Observations. *J. Appl. Meteor. Climatol.*, **53**, 437–455.

Minnis, P., P. W. Heck, and E. F. Harrison (1990a), The 27– 28 October 1986 Fire IFO Cirrus Case-Study: Cloud parameter fields derived from satellite data, *Mon. Weather Rev.*, **118**, 2426–2446.

Minnis, P., D. F. Young, K. Sassen, J. M. Alvarez, and C. J. Grund (1990b), The 27 – 28 October 1986 FIRE IFO Case Study: Cirrus parameter relationships derived from satellite and lidar data, *Mon. Weather Rev.*, **118**, 2402– 2425.

Minnis, P., P. W. Heck, D. F. Young, C. W. Fairall, and J. B. Snider (1992), Stratocumulus cloud properties derived from simultaneous satellite and island-based instrumentation during FIRE, *J. Appl. Meteorol.*, **31**, 317– 339.

Minnis, P.; Kratz, D. P.; Coakley, J. A., Jr.; King, M. D.; Garber, D.; Heck, P.; Mayor, S.; Young, D. F. and Arduini, R.: Cloud Optical Property Retrieval (Subsystem 4.3). "Clouds and the Earth's Radiant Energy System (CERES) Algorithm Theoretical Basis Document, Volume

III: Cloud Analyses and and Determination of Improved Top of Atmosphere Fluxes (Subsystem 4)", *NASA RP 1376 Vol. 3, edited by CERES Science Team, December, 1995, pp. 135-176.*

Minnis, P.; Garber, D. P.; Young, D. F.; Arduini, R. F.; and Takano, Y., 1998: Parameterization of reflectance and effective emittance for satellite remote sensing of cloud properties. *J. Atmos. Sci.*, **55**, 3313-3339.

Minnis, P. and W. L. Smith,,Jr., 1998: Cloud and Radiative Fields Derived from GOES-8 During SUCCESS and the ARM-UAV Spring 1996 Flight Series. *Geophys. Res. Ltrs.,* **25***, 1113-1116.*

Minnis, P., L. Nguyen, D. R. Doelling, D. F. Young, W. F. Miller, and D. P. Kratz, 2002: Rapid calibration of operational and research meteorological satellite imagers, Part I: Evaluation of research satellite visible channels as references. *J. Atmos. Oceanic Technol.*, **19**, 1233-1249.

Minnis, P., W. L. Smith, Jr., L. Nguyen, D. A. Spangenberg, P. W. Heck, R. Palikonda, J. K. Ayers, C. Wolff, and J. J. Murray, 2004: Near-real time cloud properties and aircraft icing indices from GEO and LEO satellites. Proc. SPIE 49th Ann. Mtg., Weather and Environ. Satellites Conf., Denver, CO, August 2-3 5549, 145-155.

Minnis, P., Y. Yi, J. Huang, and K. Ayers (2005), Relationships between radiosonde and RUC-2 meteorological conditions and cloud occurrence determined from ARM data, *J. Geophys. Res.*, **110**, D23204, doi:10.1029/2005JD006005.

Minnis, P., J. Huang, B. Lin, Y. Yi, R. F. Arduini, T.-F. Fan, J. K. Ayers, and G. G. Mace, 2007: Ice cloud properties in ice-over-water cloud systems using TRMM VIRS and TMI data. *J. Geophys. Res.*, **112**, D06206, doi:10.1029/2006JD007626.

Minnis, P., Q. Z. Trepte, S. Sun-Mack, Y. Chen, D. R. Doelling, D. F. Young, D. A. Spangenberg, W. F. Miller, B. A. Wielicki, R. R. Brown, S. C. Gibson, and E. B. Geier, 2008a: Cloud detection in non-polar regions for CERES using TRMM VIRS and Terra and Aqua MODIS data. *IEEE Trans. Geosci. Remote Sens.*, **46**, 3857-3884.

Minnis, P., D. R. Doelling, L. Nguyen, W. F. Miller, and V. Chakrapani, 2008b: Assessment of the visible channel calibrations of the TRMM VIRS and MODIS on Aqua and Terra. *J. Atmos. Oceanic Technol.*, **25**, 385-400.

Minnis, P., C. R. Yost, S. Sun-Mack, and Y. Chen 2008c: Estimating the top altitude of optically thick ice clouds from thermal infrared satellite observations using CALIPSO data. *Geophys. Res. Lett.,* L12801, doi:10.1029/2008GL033947.

Minnis, P., and coauthors, 2010: CERES Edition 3 cloud retrievals, AMS 13th Conf. Atmos. Rad., Portland, OR, June 27 – July 2, http://ams.confex.com/ams/13CldPhy13AtRad/techprogram/paper_171366.htm

Minnis, P., S. Sun-Mack, D. F. Young, P. W. Heck, D. P. Garber, Y. Chen, D. A. Spangenberg, R. F. Arduini, Q. Z. Trepte, W. L. Smith, Jr., J. K. Ayers, S. C. Gibson, W. F. Miller, V.

Chakrapani, Y. Takano, K.-N. Liou, Y. Xie, and P. Yang, 2011a: CERES Edition-2 cloud property retrievals using TRMM VIRS and Terra and Aqua MODIS data, Part I: Algorithms. *IEEE Trans. Geosci. Remote Sens.*, **49**, 4374-4400.

Minnis, P., S. Sun-Mack, Y. Chen, M. M. Khaiyer, Y. Yi, J. K. Ayers, R. R. Brown, X. Dong, S. C. Gibson, P. W. Heck, B. Lin, M. L. Nordeen, L. Nguyen, R. Palikonda, W. L. Smith, Jr., D. A. Spangenberg, Q. Z. Trepte, and B. Xi, 2011b: CERES Edition-2 cloud property retrievals using TRMM VIRS and Terra and Aqua MODIS data, Part II: Examples of average results and comparisons with other data. *IEEE Trans. Geosci. Remote Sens.*, **49**, 4401-4430.

Nakajima, T., and M. D. King, 1990: Determination of the optical thickness and effective particle radius of clouds from reflected solar radiation measurements. Part I: Theory. *J. Atmos. Sci.*, **47**, 1878-1893.

Painemal, D., and P. Zuidema (2011), Assessment of MODIS cloud effective radius and optical thickness retrievals over the Southeast Pacific with VOCALS-REx in situ measurements, *J. Geophys. Res.*, **116**, D24206, doi:10.1029/2011JD016155.

Painemal, D., P. Minnis, J. K. Ayers, and L. O'Neill (2012), GOES-10 microphysical retrievals in marine warm clouds: Multi-instrument validation and daytime cycle over the southeast Pacific, *J. Geophys. Res.*, **117**, D19212, doi:10.1029/2012JD017822.

Platnick, S., 2000: Vertical photon transport in cloud remote sensing problems, *J. Geophys. Res.,* **105**(D18), 22,919–22,935, doi:10.1029/ 2000JD900333.

Politovich, M.K., 2003: Predicting inflight aircraft icing intensity. *J. Aircraft*, **40**, 639-644.

Ramanathan, V., B. R. Barkstrom, and E. F. Harrison, 1989: Climate and the Earth's Radiation Budget. *Physics Today*, **42**(5), 22-33.

Rasmussen, R., and Coauthors, 1992: Winter Icing and Storms Project (WISP). *Bull. Amer. Meteor. Soc.*, **73**, 951-974.

Reisner, J., R. M. Rasmussen, and R. T. Bruintjes, 1998: Explicit forecasting of supercooled liquid water in winter storms using the MM5 mesoscale model. *Quart. J. Roy. Meteor. Soc.*, **124**,1071–1107.

Reisner, J., Rasmussen, R.M., Bruintjes, R.T., 1998. Explicit forecasting of supercooled liquid water in winter storms using the MM5 mesoscale model. *Q. J. R. Meteorol. Soc.,* **124**, 1071–1107.

Rossow, W. B. and R. A. Schiffer, 1991: ISCCP cloud data products. *Bull. Amer. Meteor. Soc.*, **72**, 2–20.

Sassen K. 1991: The Polarization Lidar Technique for Cloud Research: A Review and Current Assessment. *Bull. Amer. Meteor. Soc.*, **72**, 1848-1866.

Schreiner, A. J., T. J. Schmit, and W. P. Menzel, 2001: Observations and trends of clouds based on GOES sounder data. *J. Geophys. Res.*, **106**, 20349–20363.

Schultz, P., M. K. Politovich, 1992: Toward the Improvement of Aircraft-Icing Forecasts for the Continental United States. *Wea. Forecasting*, **7**, 491–500.

Seethala, C., and Á. Horváth, 2010: Global assessment of AMSR-E and MODIS cloud liquid water path retrievals in warm oceanic clouds, *J. Geophys. Res.*, **115**, D13202, doi:10.1029/2009JD012662.

Sengupta, M., E. E. Clothiaux, T. P. Ackerman, 2004: Climatology of Warm Boundary Layer Clouds at the ARM SGP Site and Their Comparison to Models. *J. Climate*, **17**, 4760–4782.

Smith, W. L., C. M. R. Platt, 1978: Comparison of Satellite-Deduced Cloud Heights with Indications from Radiosonde and Ground-Based Laser Measurements. *J. Appl. Meteor.*, **17**, 1796–1802.

Smith, W. L., Jr., P. Minnis, S. G. Benjamin, 2006: Comparison of RUC condensate analyses and forecasts with satellite-derived cloud properties. Proc of the AMS 14th Conference on Satellite Meteorology and Oceanography, Atlanta, GA, 29 Jan. – 2 Feb, 2006.

Smith W. L., Jr., P. Minnis, H. Finney, R. Palikonda, and M. M. Khaiyer, 2008: An evaluation of operational GOES derived single-layer cloud top heights with ARSCL over the ARM Southern Great Plains site, *Geophys. Res. Lett.*, **35**, L13820, doi:10.1029/2008GL034275.

Smith, W.L., Jr., P. Minnis, S. G. Benjamin, S. S. Weygandt, 2010: 4-D cloud water content fields derived from operational satellite data. Proc. of the 2010 IGARSS, Honolulu, HI, July 25-30, 2010, 4pp.

Smith, W. L., P. Minnis, C. Fleeger, D. Spangenberg, R. Palikonda, L. Nguyen, 2012: Determining the Flight Icing Threat to Aircraft with Single-Layer Cloud Parameters Derived from Operational Satellite Data. *J. Appl. Meteor. Climatol.*, **51**, 1794–1810.

Stephens, G. L., Coauthors 2002: The Cloudsat Mission and the A-Train. *Bull. Amer. Meteor. Soc.*, **83**, 1771–1790.

Stephens, G. L., 2005: Cloud Feedbacks in the Climate System: A Critical Review. *J. Clim.*, **18**, 237-273.

Stephens, G. 2006: The Role of Water Vapor and Clouds in the Climate System. *Encyclopedia of Hydrological Sciences.*

Stephens, G. L., et al.. 2008: CloudSat mission: Performance and early science after the first year of operation, *J. Geophys. Res.*, **113**, D00A18, doi:10.1029/2008JD009982.

Sun-Mack, S., P. Minnis, Y. Chen, S. Kato, Y. Yi, S. Gibson, P. W. Heck, and D. Winker, 2013: Global cloudy boundary layer apparent lapse rates determined from CALIPSO and MODIS data. Accepted, *J. Appl. Meteorol. Climatol.*

Thompson, G., R. T. Bruintjes, B. G. Brown, F. Hage, 1997a: Intercomparison of In-Flight Icing Algorithms. Part I: WISP94 Real-Time Icing Prediction and Evaluation Program. *Wea. Forecasting*, **12**, 878–889.

Thompson, G., R. Bullock, and T. F. Lee, 1997b: Using satellite data to reduce spatial extent of diagnosed icing. *Wea. Forecasting*, **12**, 185–190.

Thompson, G., R. M. Rasmussen, K. Manning, 2004: Explicit Forecasts of Winter Precipitation Using an Improved Bulk Microphysics Scheme. Part I: Description and Sensitivity Analysis. *Mon. Wea. Rev.*, **132**, 519–542.

Tripoli, G. J., and W. R. Cotton, 1982: The Colorado State University three-dimensional cloud/mesoscale model-1982. Part 1: General theoretical framework and sensitivity experiments. *J. Rech. Atmos.*, **16**, 185-220.

Twohy, C. H., A. J. Schanot, and W. A. Cooper, 1997: Measurement of condensed water content in liquid and ice clouds using an airborne counterflow virtual impactor, *J. Atmos. Ocean. Technol.*, **14**, 197– 202.

Vukic´evic´ , T., T. Greenwald, M. Županski, D. Županski, T. Vonder Haar, and A. S. Jones, 2004: Mesoscale cloud state estimation from visible and infrared satellite radiances. *Mon. Wea. Rev.*, **132**, 3066–3077.

Vukicevic, T., M. Sengupta, A. Jones and T. Vonder Haar, 2006: Cloud Resolving Data Assimilation: Information content of IR window observations and uncertainties in estimation. *J. Atmos. Sci.*, **63**, 901-919.

Watts, P., R. Bennartz, and F. Fell, 2011: "Retrieval of two-layer cloud properties from multi-spectral observations using optimal estimation", *J. Geophys. Res.,* **116,** D16203, doi:10.1029/2011JD015883.

Wielicki, B. A., B. R. Barkstrom, E. F. Harrison, R. B. Lee, G. L. Smith, and J. E. Cooper, 1996: Clouds and the Earth's Radiant Energy System(CERES): An Earth Observing System experiment. *Bull. Amer. Meteor. Soc.*, **77**, 853–868.

Winker, D.M., M.A.Vaughan, A.H.Omar, Y.Hu, K.A.Powell, Z. Liu, W. H. Hunt, and S. A. Young, 2009: Overview of the CALIPSO mission and CALIOP data processing algorithms. *J. Atmos. Oceanic Technol.*, **26**, 2310–2323.

Wood, N., 2008: Level 2B Radar-Visible Optical Depth Cloud Water Content (2B-CWC-RVOD) process description document, Cooperative Inst. Res. Atmosphere (CIRA), Fort Collins, CO, Rep. Version 5.1, Oct. 2008.

Yoo H. L., Z. Li, 2012: Evaluation of cloud properties in the NOAA/NCEP global forecast system using multiple satellite products. *Clim Dyn*., doi:10.1007/s00382-012-1430-0

Yoo, H., Z. Li, Y.-T. You, S.Lord, F. Weng, and H. W. Barker, 2013:Diagnosis and testing of low-level cloud parameterizations for the NCEP/GFS model satellite and ground-based measurements, *Clim Dyn*., doi:10.1007/s00382-013-1884-8.

Young, S. A. and M. A. Vaughan, 2009: The retrieval of profiles of particulate extinction from Cloud Aerosol Lidar Infrared Pathfinder Satellite Observations (CALIPSO) data: Algorithm description, *J. Atmos. Oceanic Technol*., **26**, 1105-1119, doi:10.1175/2008JTECHA1221.1

Yucel, I., W. J. Shuttleworth, R. T. Pinker, L. Lu, and S. Sorooshian, 2002: Impact of ingesting satellite-derived cloud cover into the Regional Atmospheric Modeling System. *Mon. Wea. Rev.*, **130**, 610-628.

Yucel, I., W. J. Shuttleworth, X. Gao, and S. Sorooshian, 2003: Short-term performance of MM5 with cloud-cover assimilation from satellite observations. *Mon. Wea. Rev.*, **131**, 1797-1810.

Zhao C., S. Xie, S.A. Klein, A. Protat, M. D. Shupe, S. A. McFarlane, J. M. Comstock, J. Delanoë, M. Deng, M. Dunn, M. P. Jensen, G. G. Mace, R. McCoy, E. J. O'Connor, D.D. Turner, and Z. Wang. 2012a: Toward understanding of differences in current cloud retrievals of ARM ground-based measurements. *J. Geophys. Res*, **117**, D10206, doi:10.1029/2011JD016792.

Zhao C., S. Xie, R. McCoy, Y. Zhang, M. Dunn, M. P. Jensen, E. J. O'Connor. 2012b.: Uncertainty analysis of cloud properties retrieved from MICROBASE, presentation at the third Science Team Meeting of the Atmospheric System Research program, available at http://asr.science.energy.gov/meetings/stm/2012/presentations/zhaoquicr.pdf.
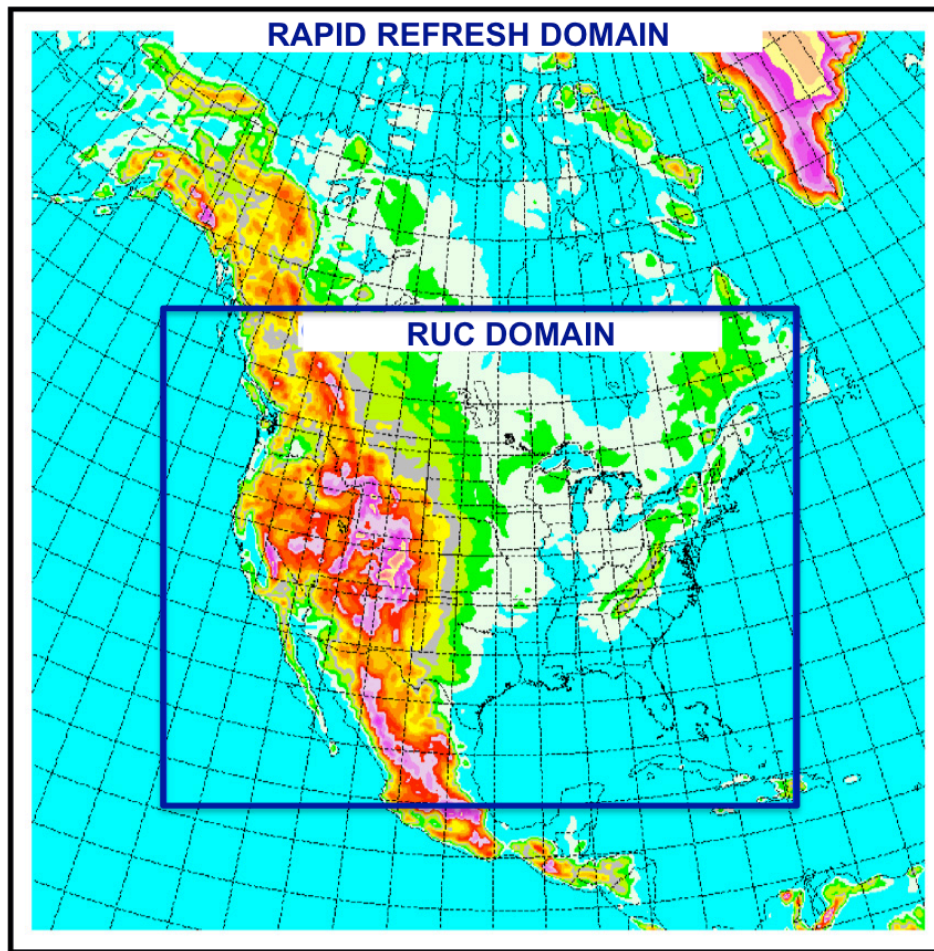
Figures

Figure 1. Illustration depicting the geographic domain for the RUC and Rapid Refresh numerical modeling systems at NOAA GSD and NCEP (courtesy of Stan Benjamin, NOAA ESRL/GSD).
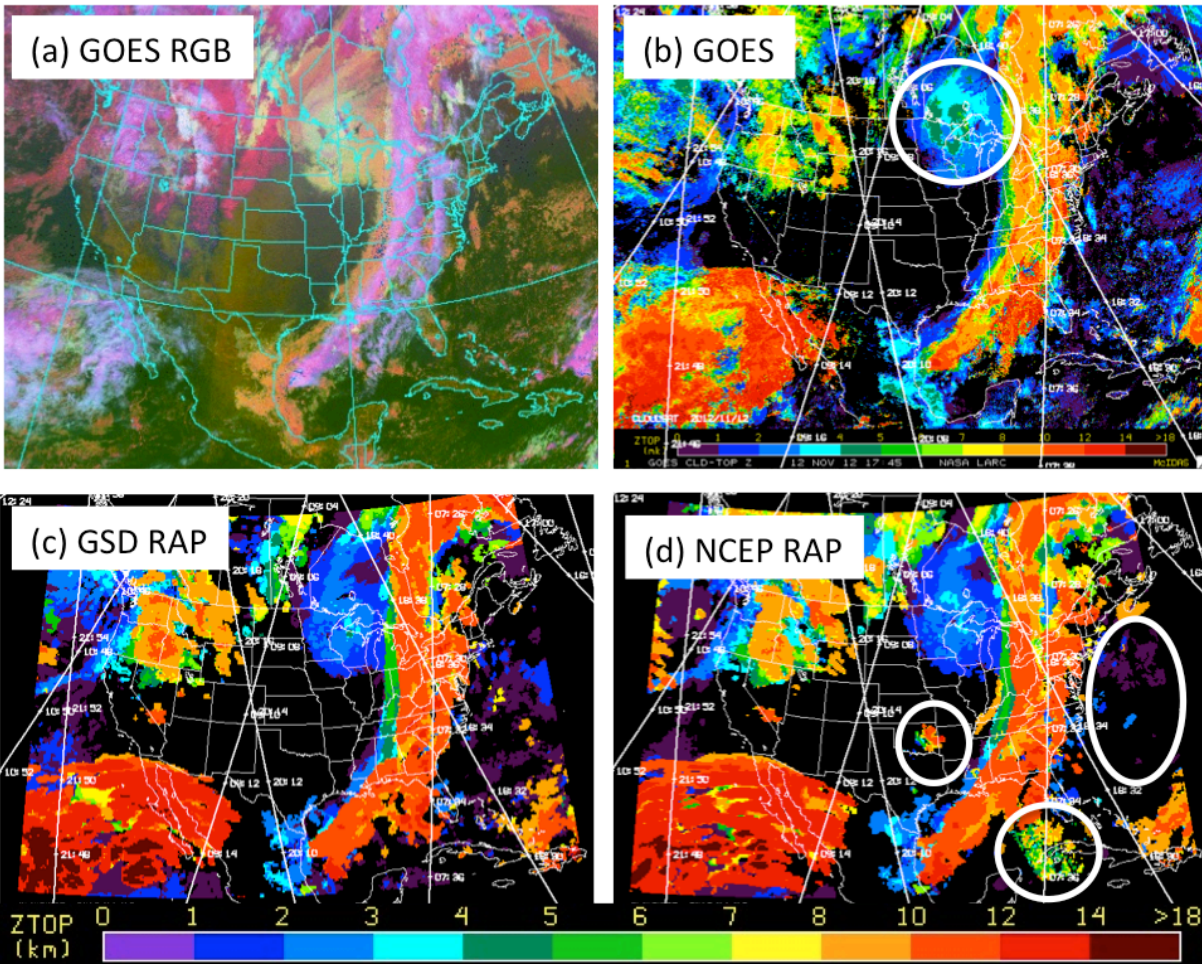
Figure 2. Satellite and NWP cloud top height comparison on 12 November 2012. (a) The 1745 UTC GOES RGB image (derived from the VIS, IR and SIR channels, (b) the corresponding cloud top height (km) analysis derived in the NASA LaRC operational cloud retrieval system using data taken from GOES-E and GOES-W, the 1800 UTC cloud top height analysis from the (c) GSD RAP, and (d) the NCEP RAP. Overall, cloud top height is well characterized in the model analyses. Some problem areas are noted with the white circles and described in the text.
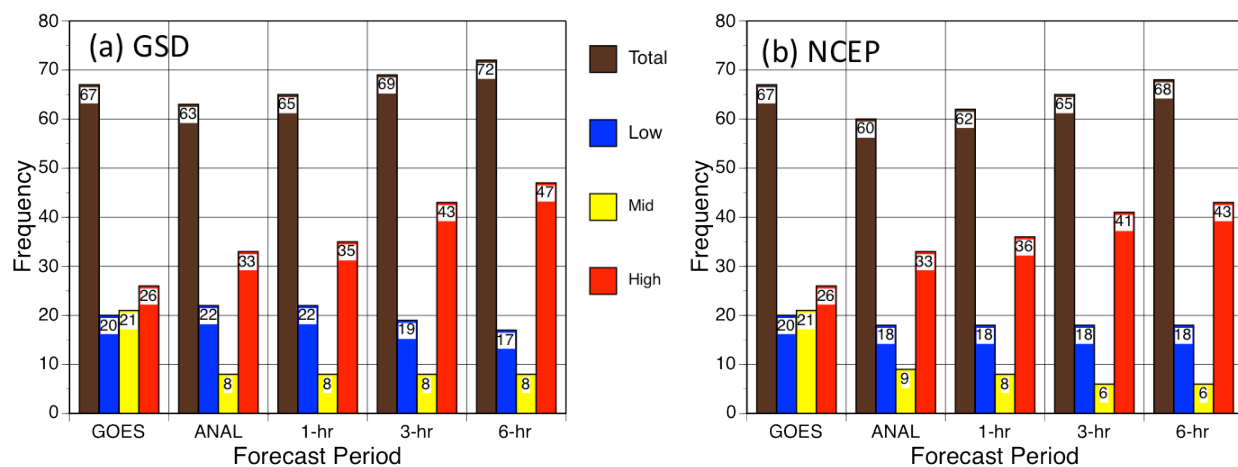
Figure 3. Cloud amount comparison between GOES (1745 UTC) and the model cloud analyses and forecasts (valid time at 18 UTC) from the (a) GSD and (b) NCEP RAP for low (0-3 km), middle (3-7 km), and high (> 7 km) clouds as defined by the cloud top height, and for the period 12-18 Nov 2012. The satellite data are used to clear clouds in the model analysis procedure but the impact of the satellite assimilation is only temporary as these results indicate that the cloud clearing procedure loses retention (for high clouds) as the forecast period increases.
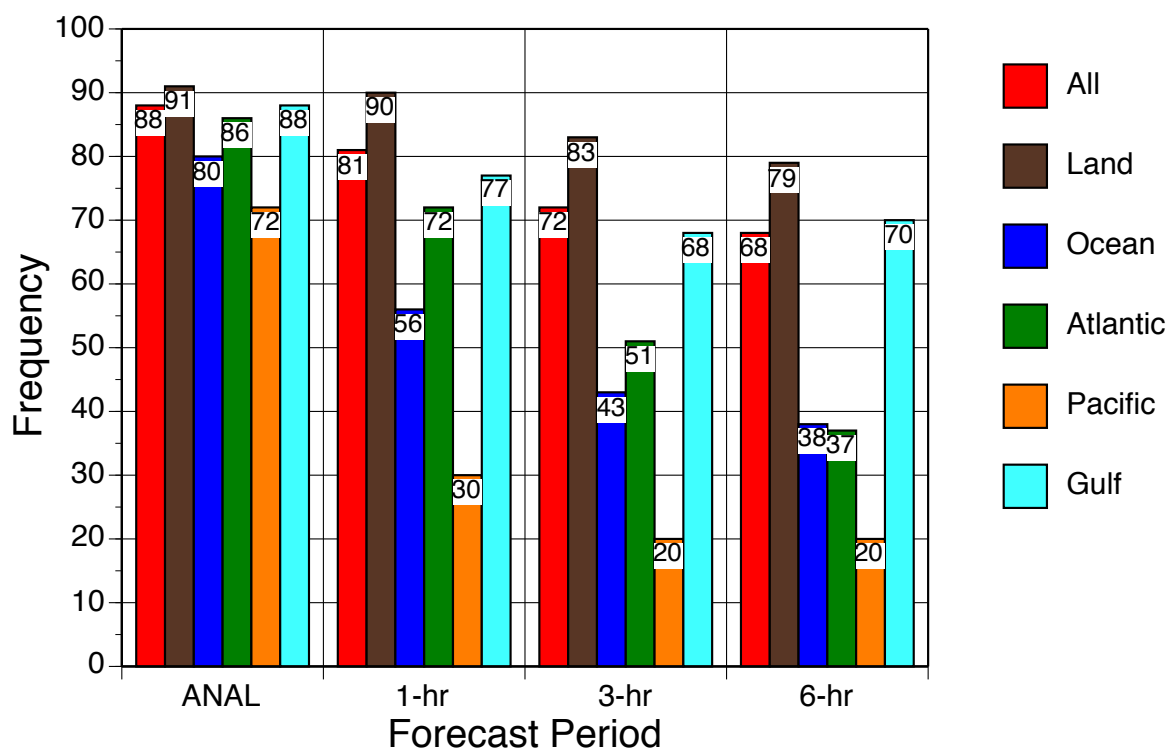
Figure 4. Frequency (%) of GSD RAP cloud free grid boxes corresponding with GOES clear areas as a function of forecast hour (valid time 18 UTC) over the period 12-18 Nov 2012. The level of agreement decreases with increasing forecast hour and is regionally dependent indicating problems with the forecast models ability to retain the satellite cloud information that is assimilated into the model analysis.
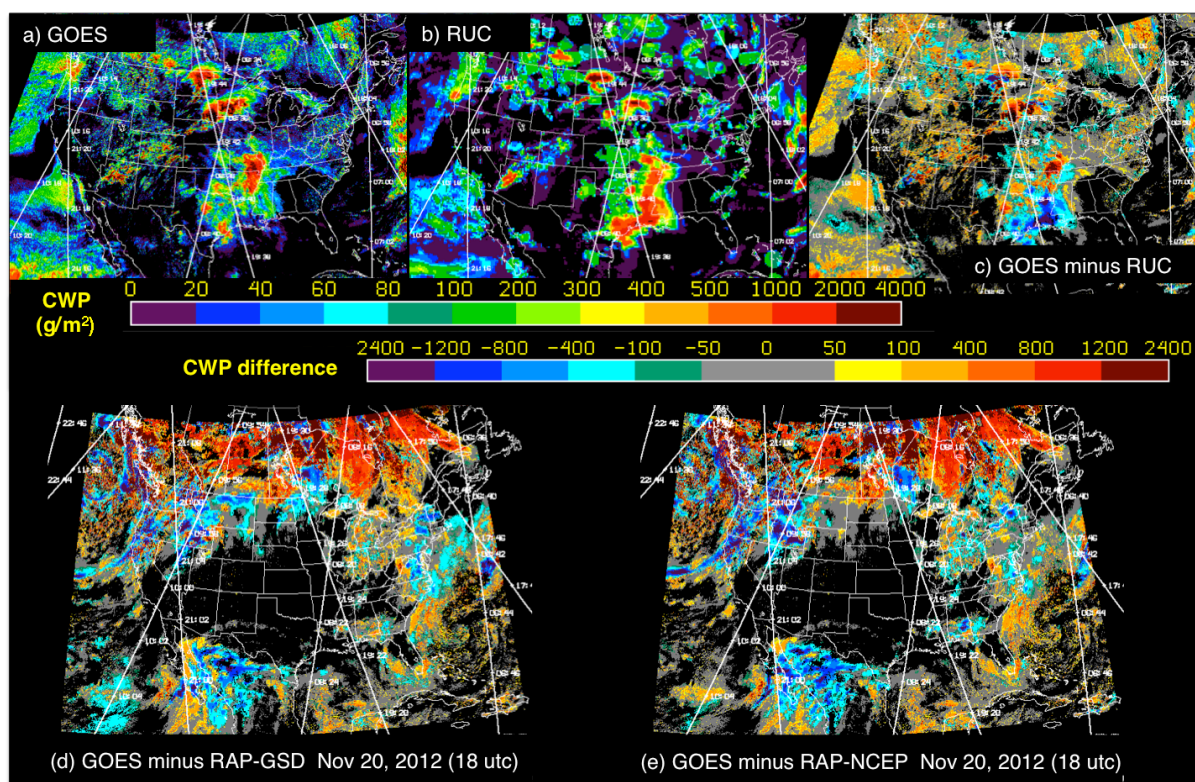
Figure 5. Cloud water path (gm^{-2}) derived from (a) GOES, (b) RUC and (c) their difference at 2000 UTC on 6 May 2008. The results indicate that while the two analyses appear to agree quite well overall at large scales, the instantaneous differences at smaller scale are quite large. The GOES comparisons with the RAP-GSD shown in (d) and with the RAP-NCEP shown in (e) valid at 1800 UTC on 20 November 2012 indicates that the relative differences between satellite retrievals and the model analyses have remained similar over time and in different implementations of the model.
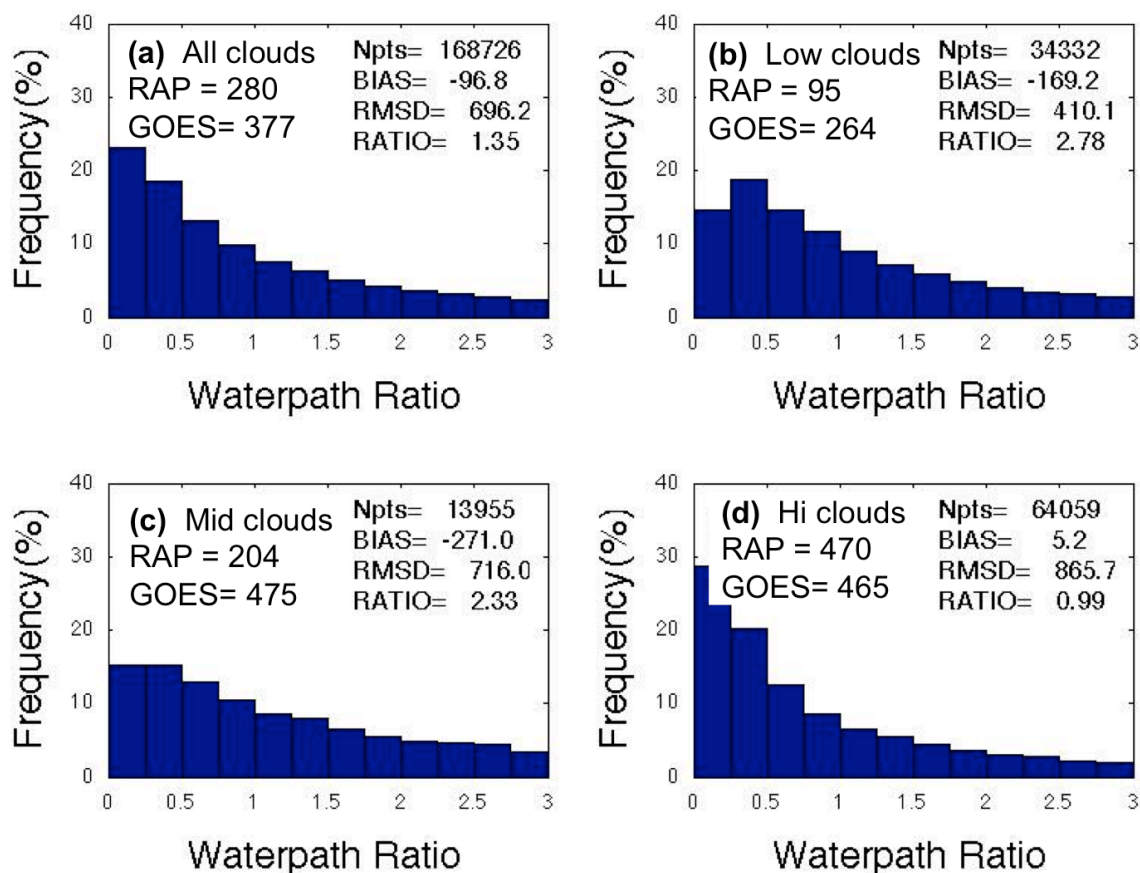
Figure 6. Cloud water path ratio for (a) all, (b) low, (c) mid, and (d) high level, coincident clouds observed from GOES and derived in the GSD RAP cloud analysis for the period 12-18 November 2012 and over the entire domain shown in Figure 5d. The results indicate that there is very little correlation between the cloud water path found in the model and the satellite retrievals at the gridbox level, and that the instantaneous differences can be very large.
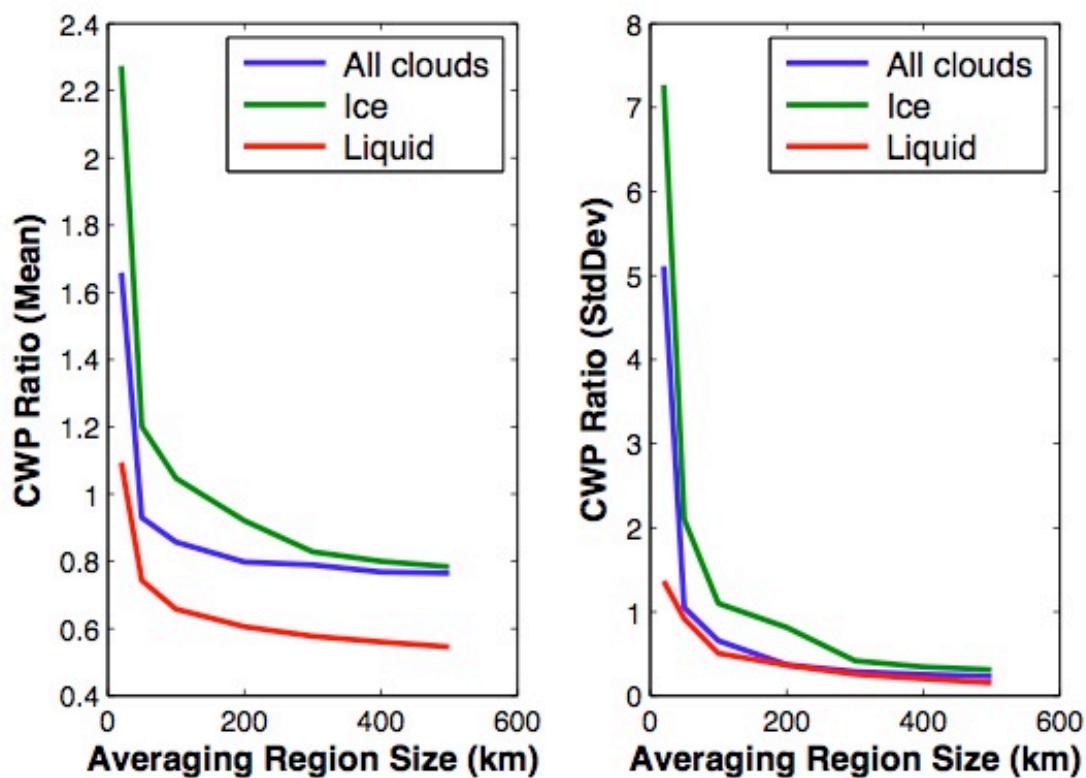
Figure 7. The mean (a), and standard deviation (b) of the ratio of the CWP derived from the model analyses and from satellite observations (computed as GSD RAP/GOES) as a function of the resolution of the averaging region. The results indicate that the model output does not agree well with observations at smaller spatial scales and must be averaged over scales of 100-300 km before it captures the natural variability in the CWP as observed from GOES.
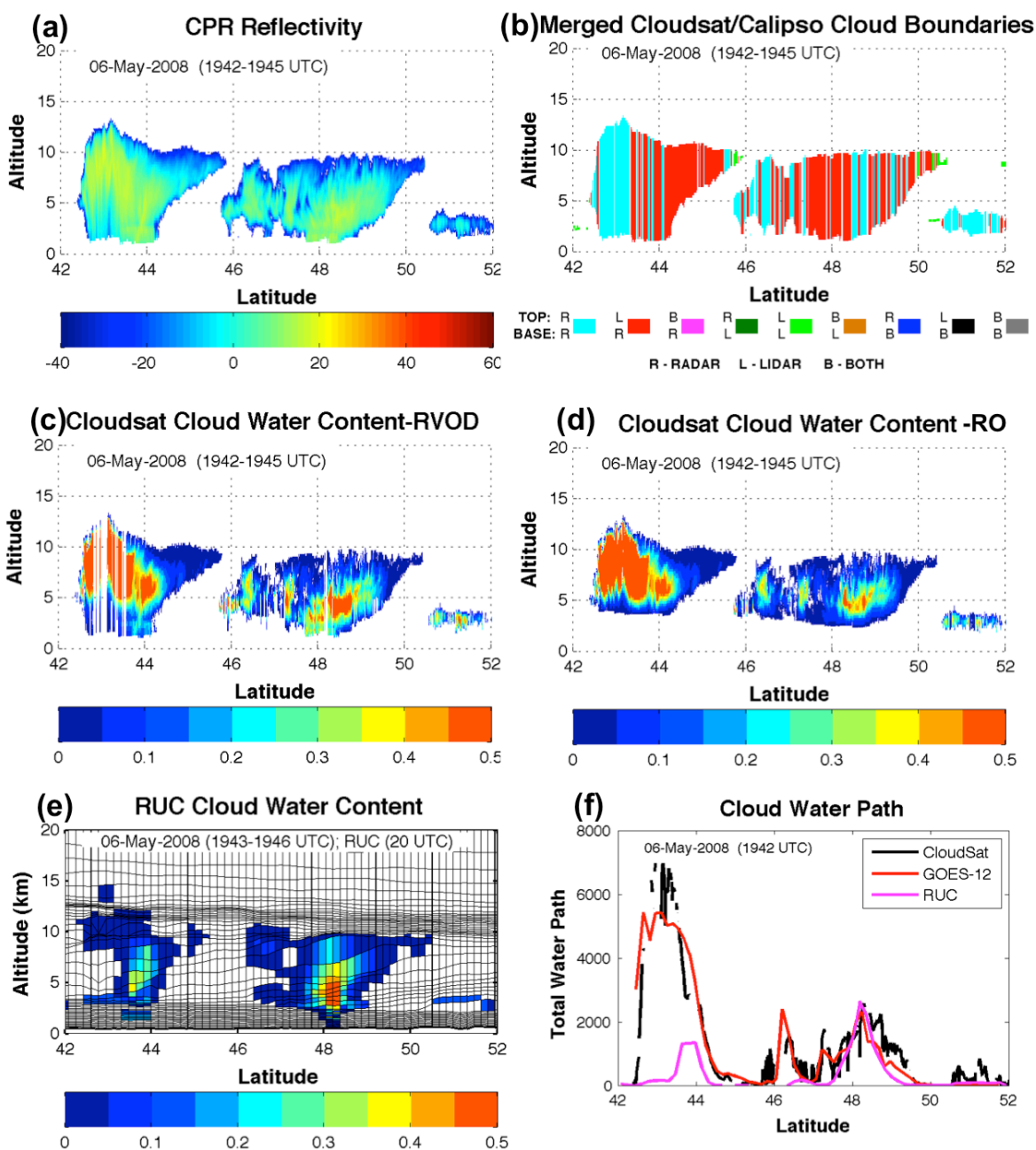
Figure 8. Cloud analyses along the CloudSat/CALIPSO orbit track over the eastern Dakotas (see figs. 5a-5c) near 20 UTC on May 6, 2008 depicting the (a) CPR reflectivity (dbZ), (b) cloud boundaries derived by combining the CPR and CALIOP signals, total CWC (g/m^3) profiles derived from the CPR in the CloudSat (c) CWC-RVOD product and the (d) CWC-RO product, (e) the total CWC (g/m^3) profiles derived in the RUC 0-hr forecast, and (f) the CWP derived from the RUC, GOES-12 and the CWC-RVOD product.
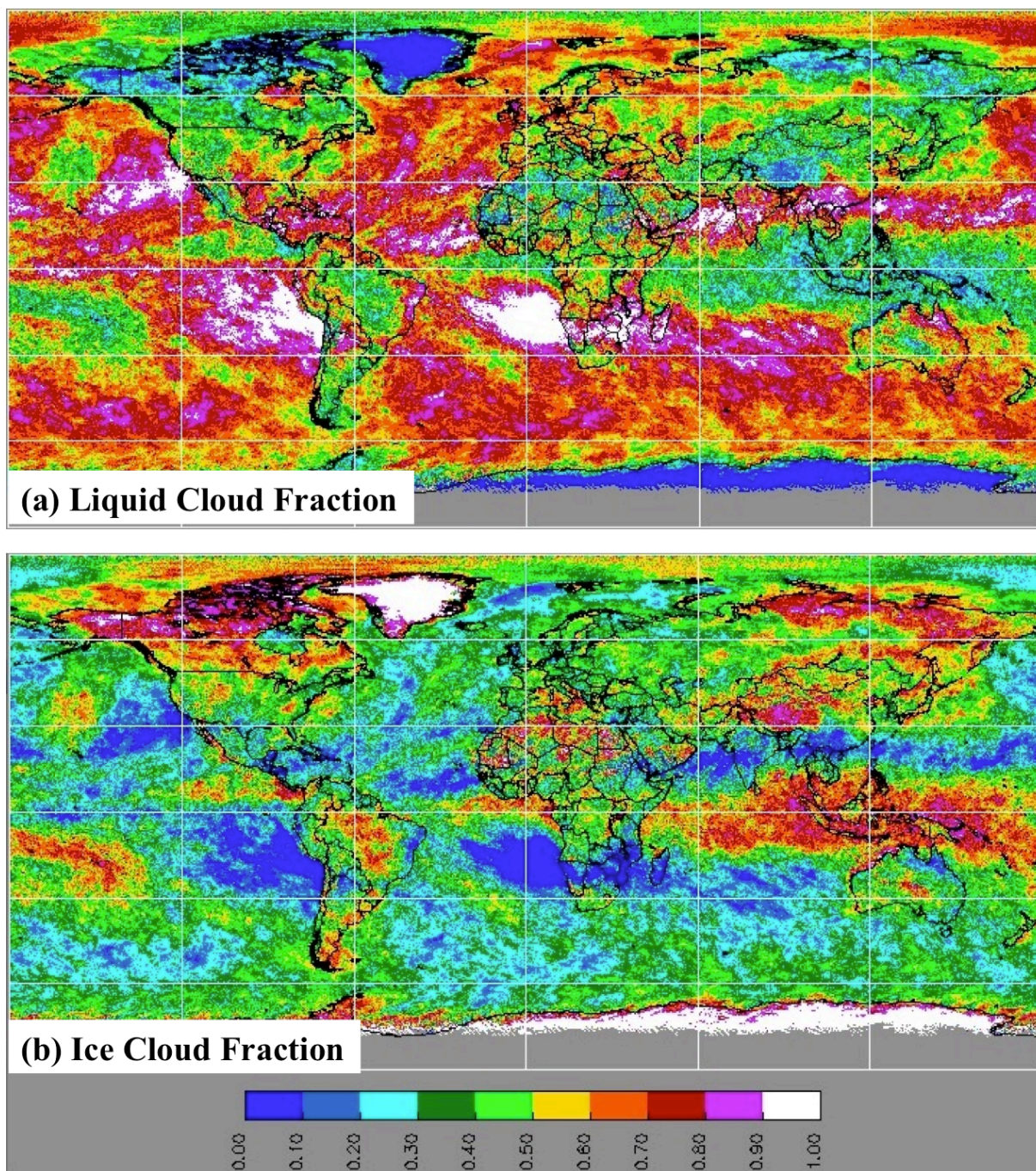
Figure 9. The monthly mean cloud fraction during April, 2013 for (a) clouds with liquid tops, and (b) clouds with ice phase tops, derived from the CERES MODIS Edition 4 cloud algorithm.
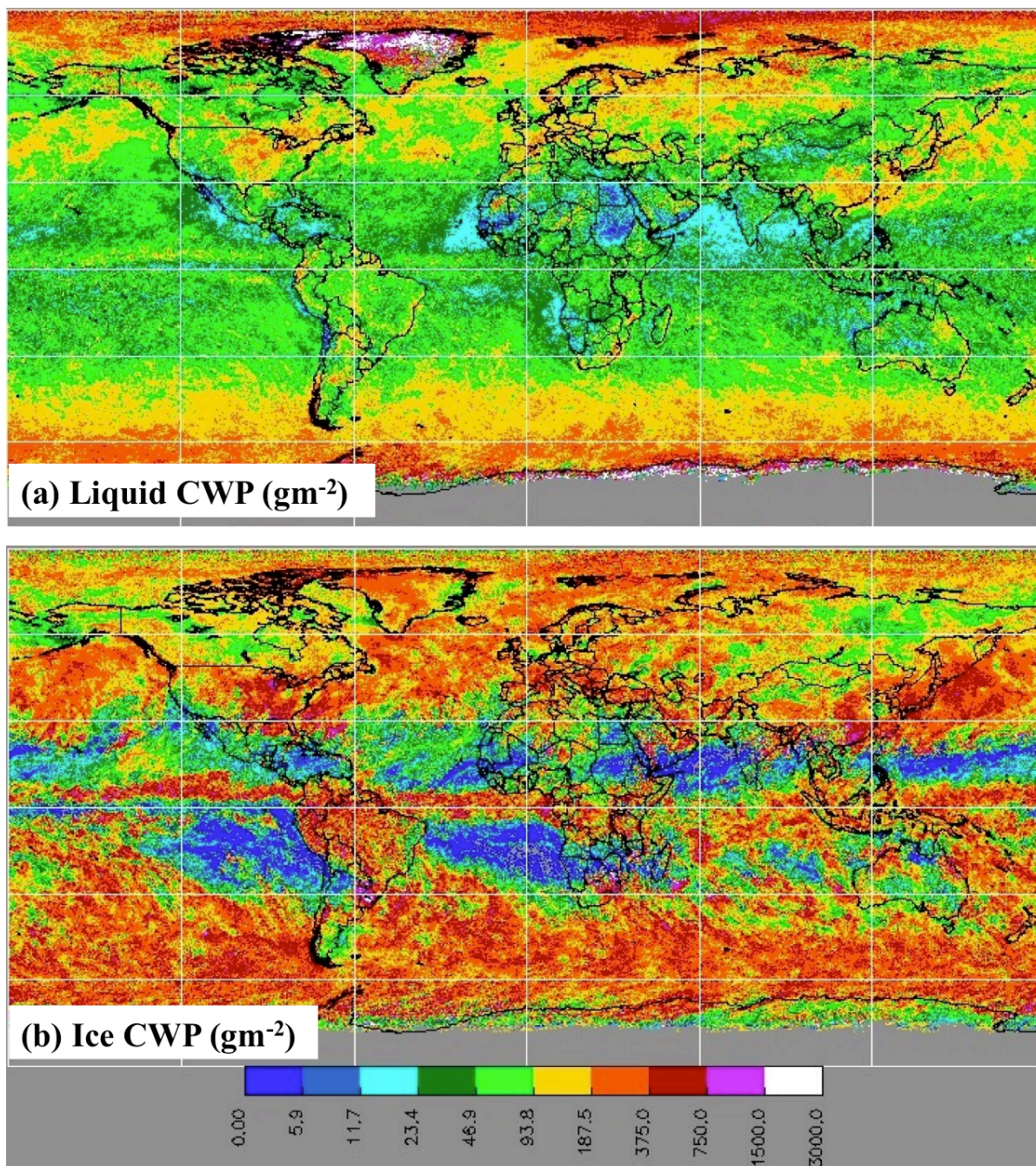
Figure 10. The monthly mean cloud water path during April, 2013 for (a) clouds with liquid tops, and (b) clouds with ice phase tops, derived from the CERES MODIS Edition 4 cloud algorithm.
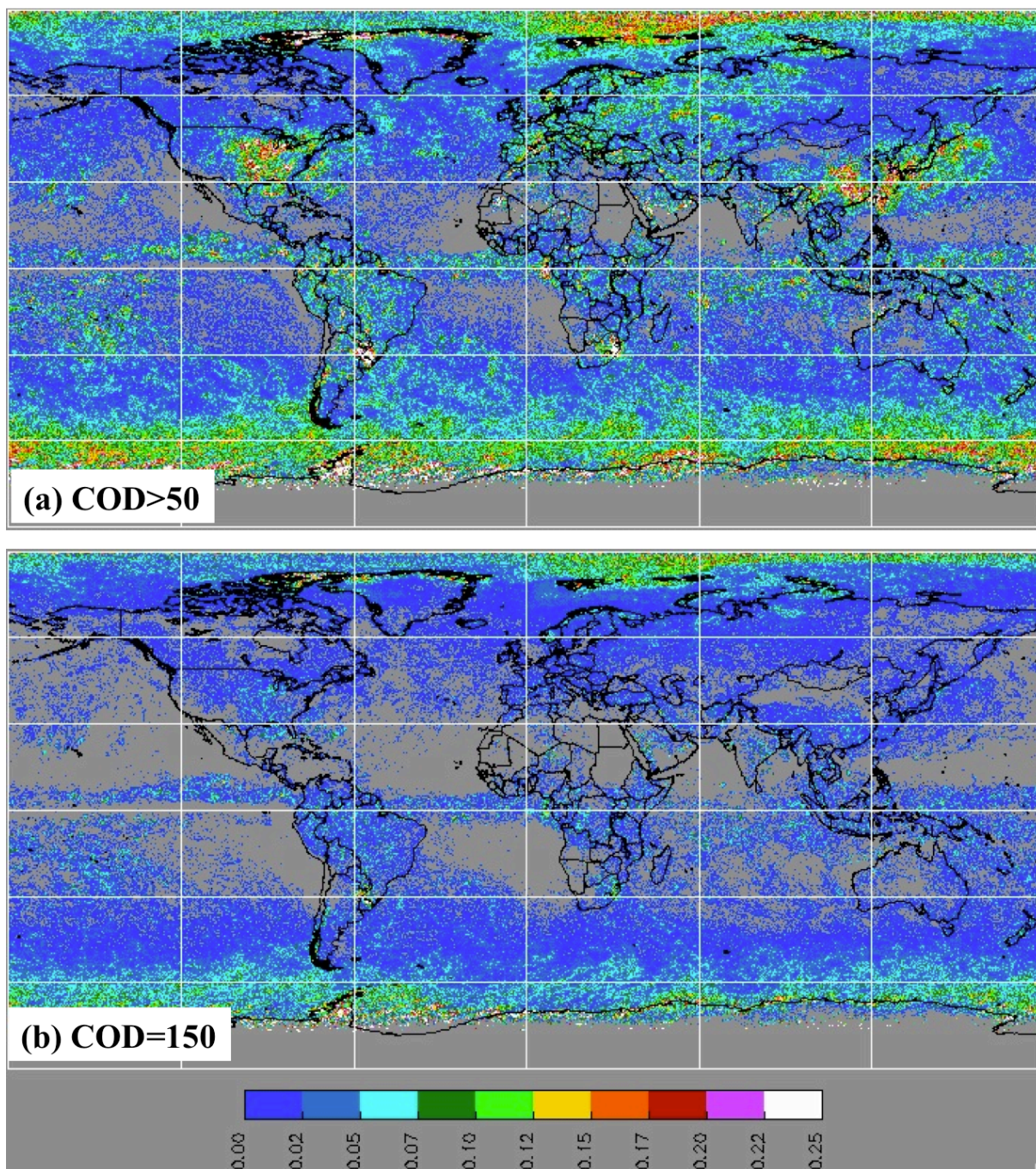
Figure 11. The fraction of all clouds during April, 2013 with (a) COD > 50 and (b) COD=150 (saturated) derived from the CERES MODIS Edition 4 cloud algorithm indicating that optically thick clouds are relatively rare.
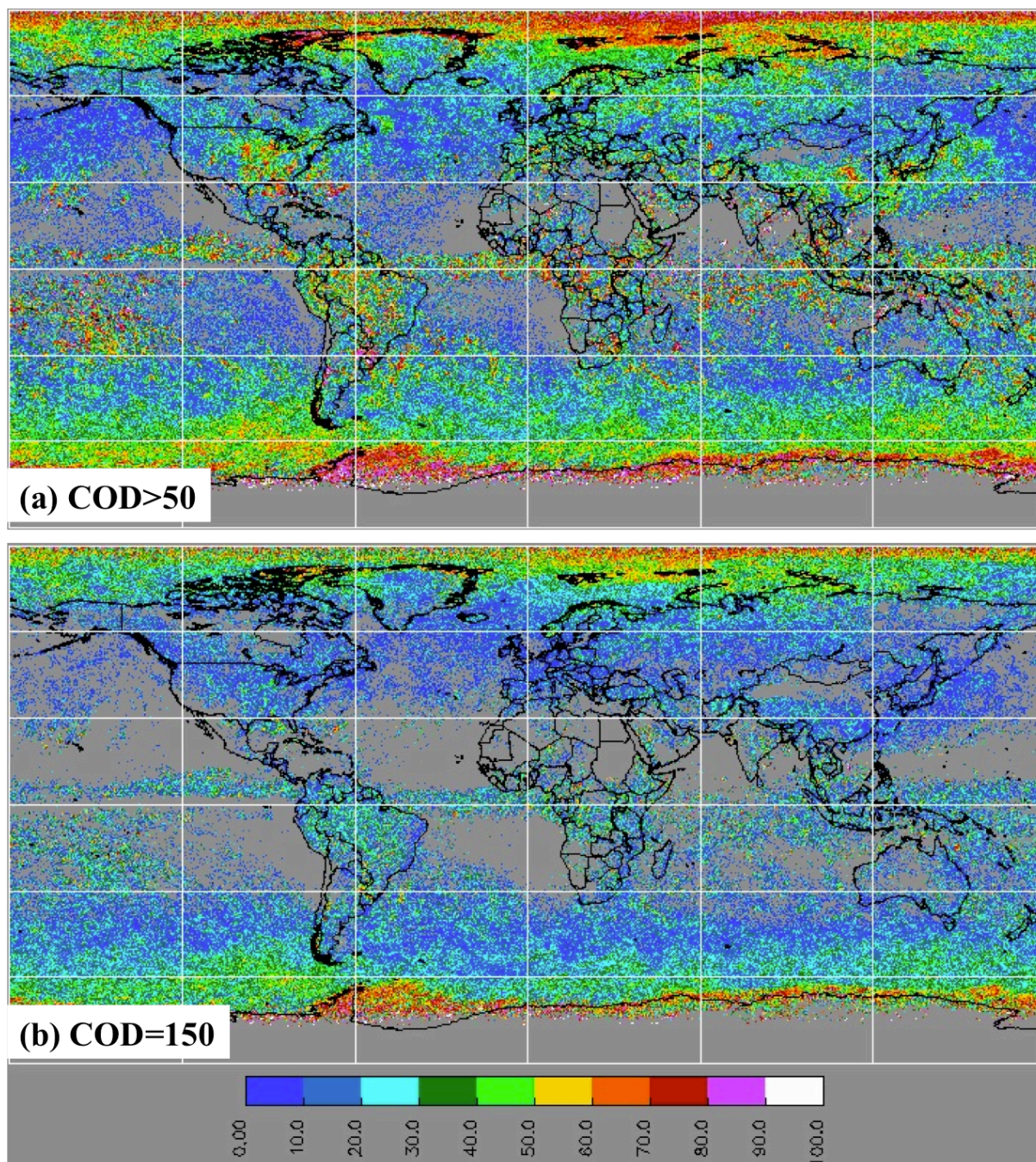
Figure 12. The relative contribution (%) of the cloud water path for optically thick clouds to the total mean CWP for (a) clouds with COD > 50, and (b) clouds with COD =150 (saturated clouds). Despite the fact that these clouds are relatively rare (as seen in Figure 11) their contribution to the total mean cloud water path is significant over large areas of the tropics and mid-latitudes, highlighting their importance in both weather and climate. These results were derived from the April 2013 CERES MODIS Edition 4 cloud properties.
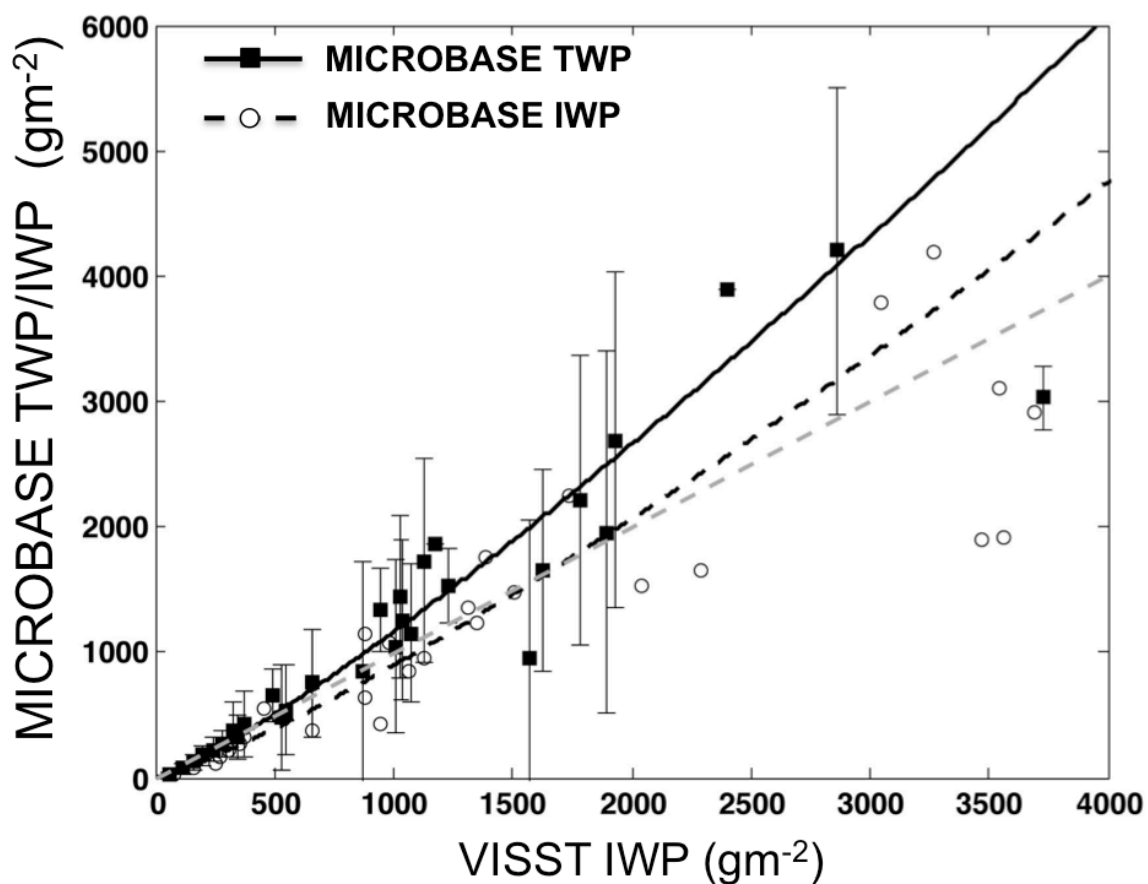
Figure 13. Bin-averaged relationship between the GOES VISST IWP and the MICROBASE TWP (squares) and MICROBASE IWP (circles) at the ARM SGP site over a 5-year study period. The solid and dashed lines are the power law best fits to the MICROBASE TWP and IWP data, respectively. The one-to-one line is also shown (dashed-grey).
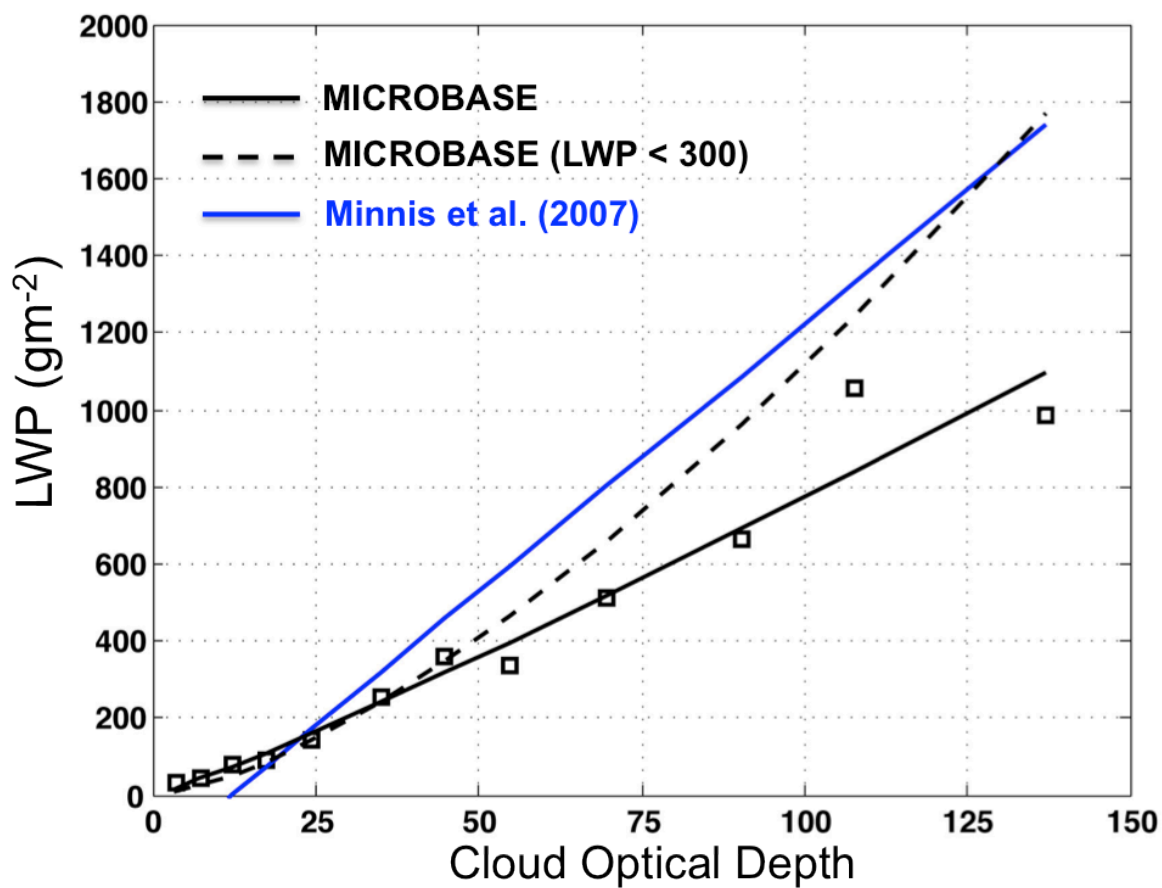
Figure 14. Bin-averaged relationship between the GOES VISST COD and the LWP derived from the microwave radiometer at the ARM SGP site over the 5-year study period (solid black line) and extrapolated from Minnis et al. (2007) using a linear (blue line) and a power law (black dashed line) fit.
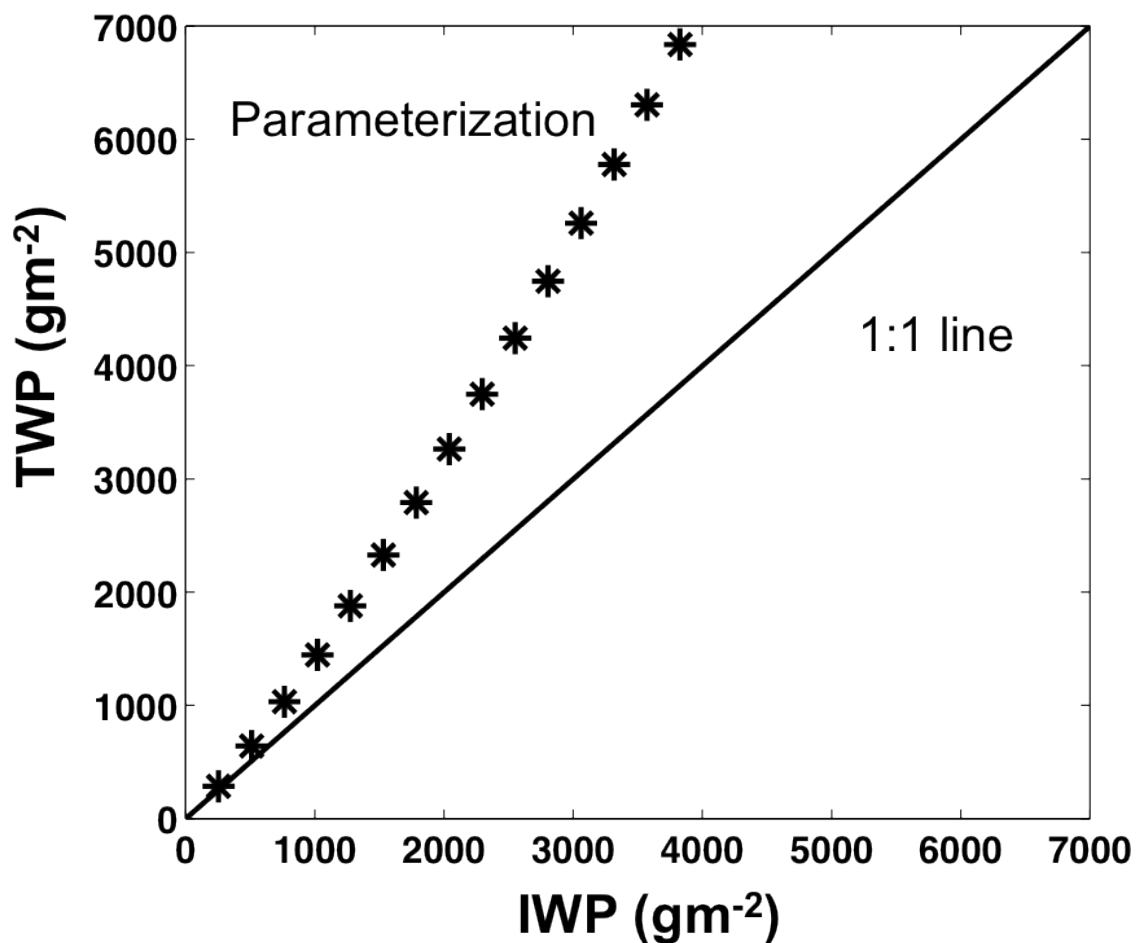
Figure 15. Example of the parameterized TWP computed for a full range of imager IWP retrievals assuming an ice cloud effective radius of 55 μm and using the relationships depicted with the black solid lines shown in Figures 13 and 14. The TWP estimated using the parameterization described in the text is nearly a factor of two larger than the retrieved IWP at the high end.
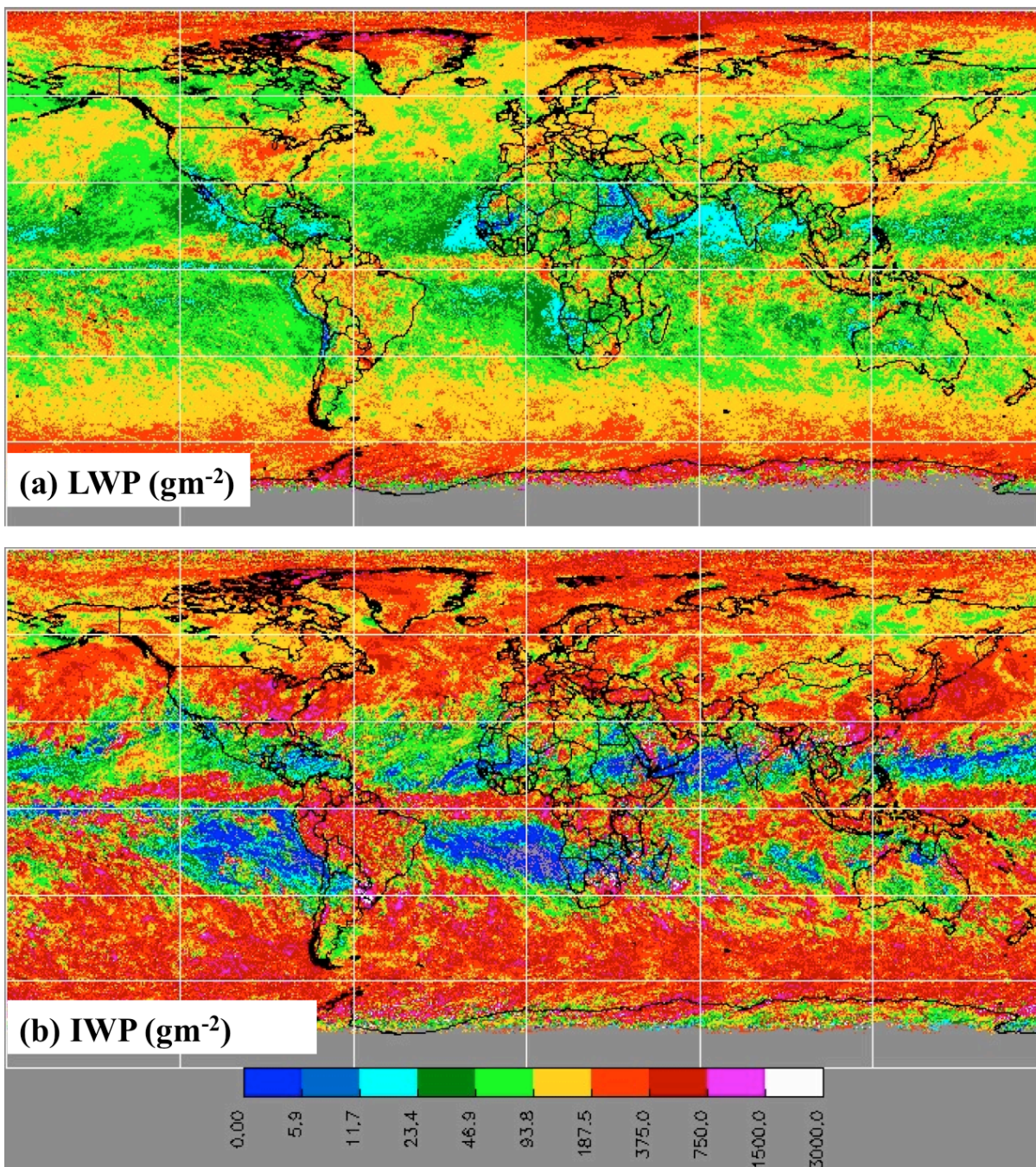
Figure 16 The monthly mean LWP and IWP during April, 2013 derived from the CERES MODIS Edition 4 cloud retrievals and by applying the optically thick cloud overlap parameterizations.
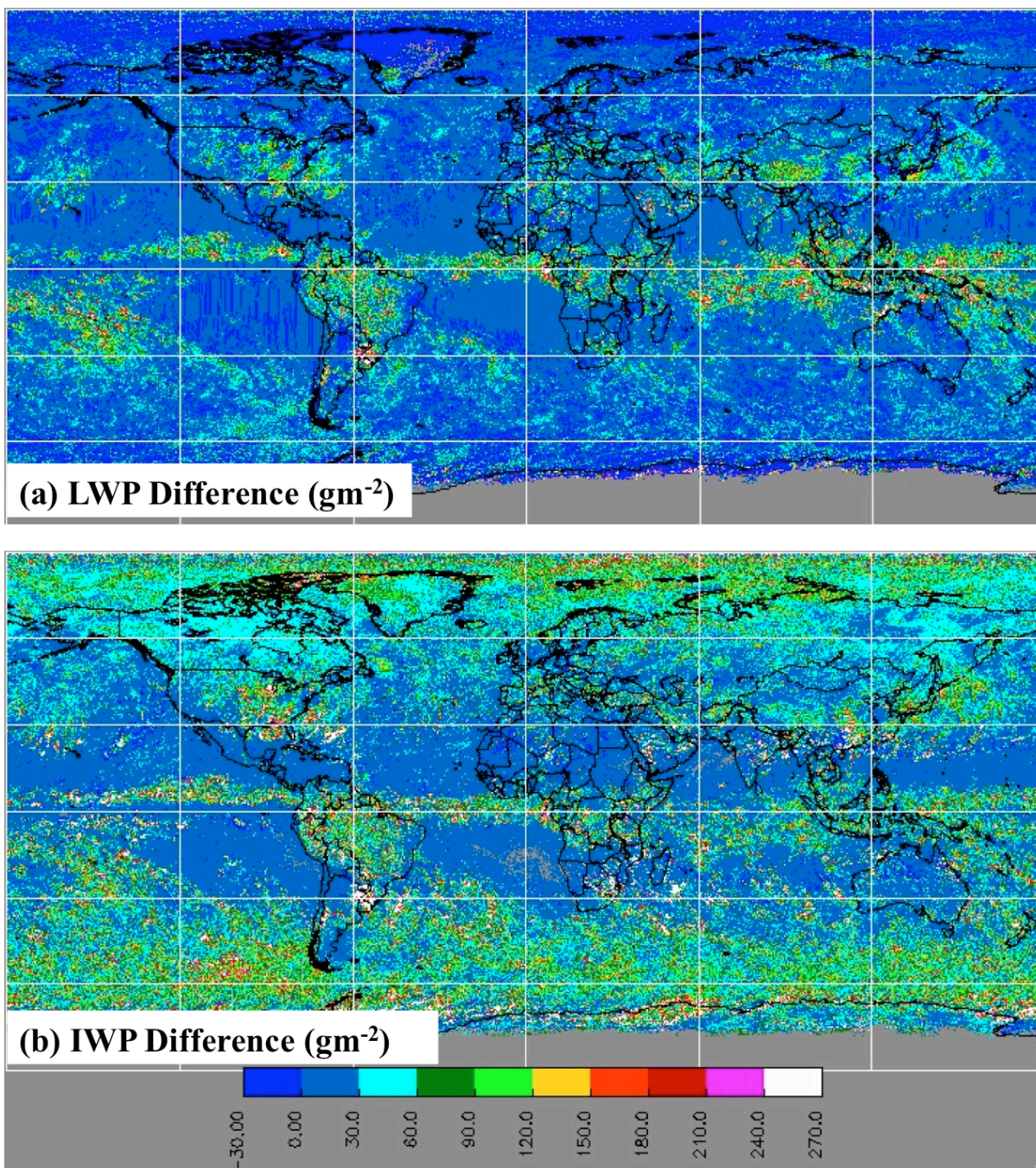
Figure 17. The difference in the monthly mean LWP and IWP during April, 2013 derived from the CERES MODIS Edition 4 cloud retrievals after applying the optically thick ice over water cloud overlap parameterizations vs. the standard retrieval assuming no overlap.
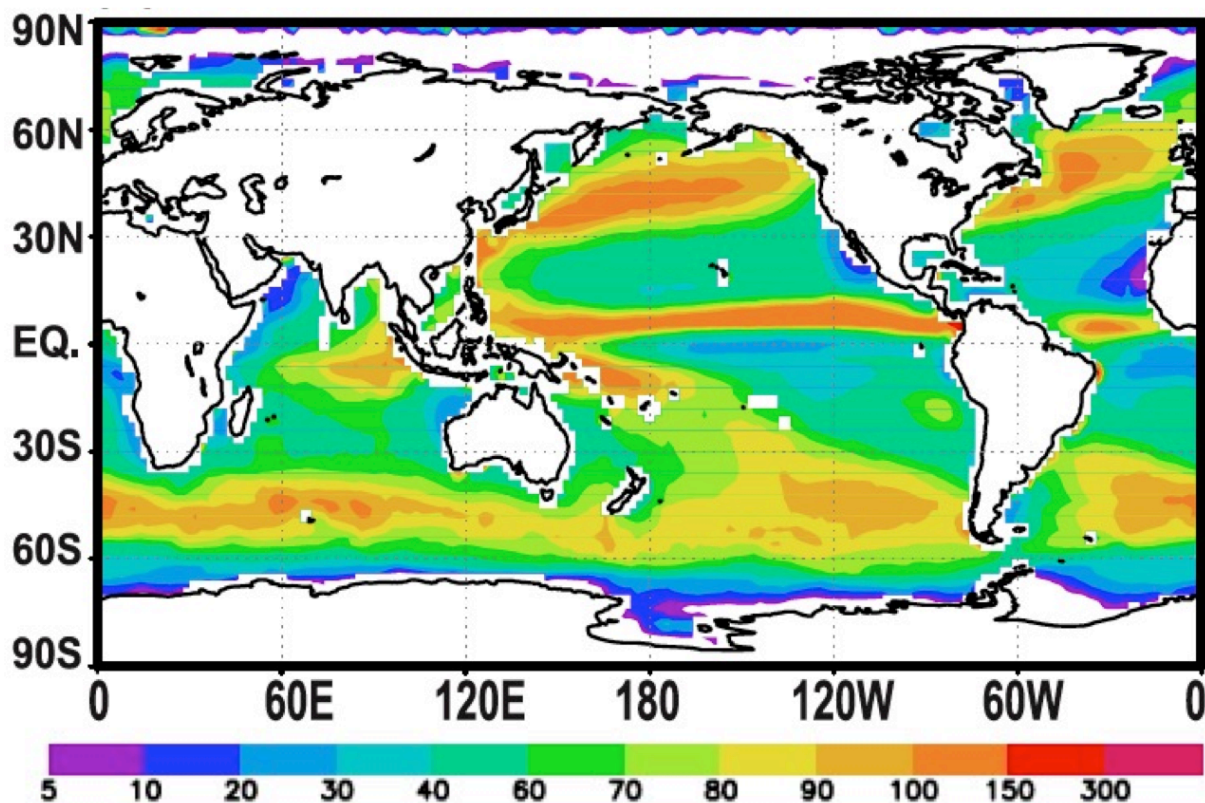
Figure 18. A 5-year (2002-2007) all sky LWP climatology constructed from Special Sensor Microwave/Imager (SSM/I) retrievals over ocean. Adapted from Li et al. (2008). These results help to corroborate the liquid portion of the TWP parameterization developed in this study for ice over water cloud systems that are applied to MODIS and GOES imager data.
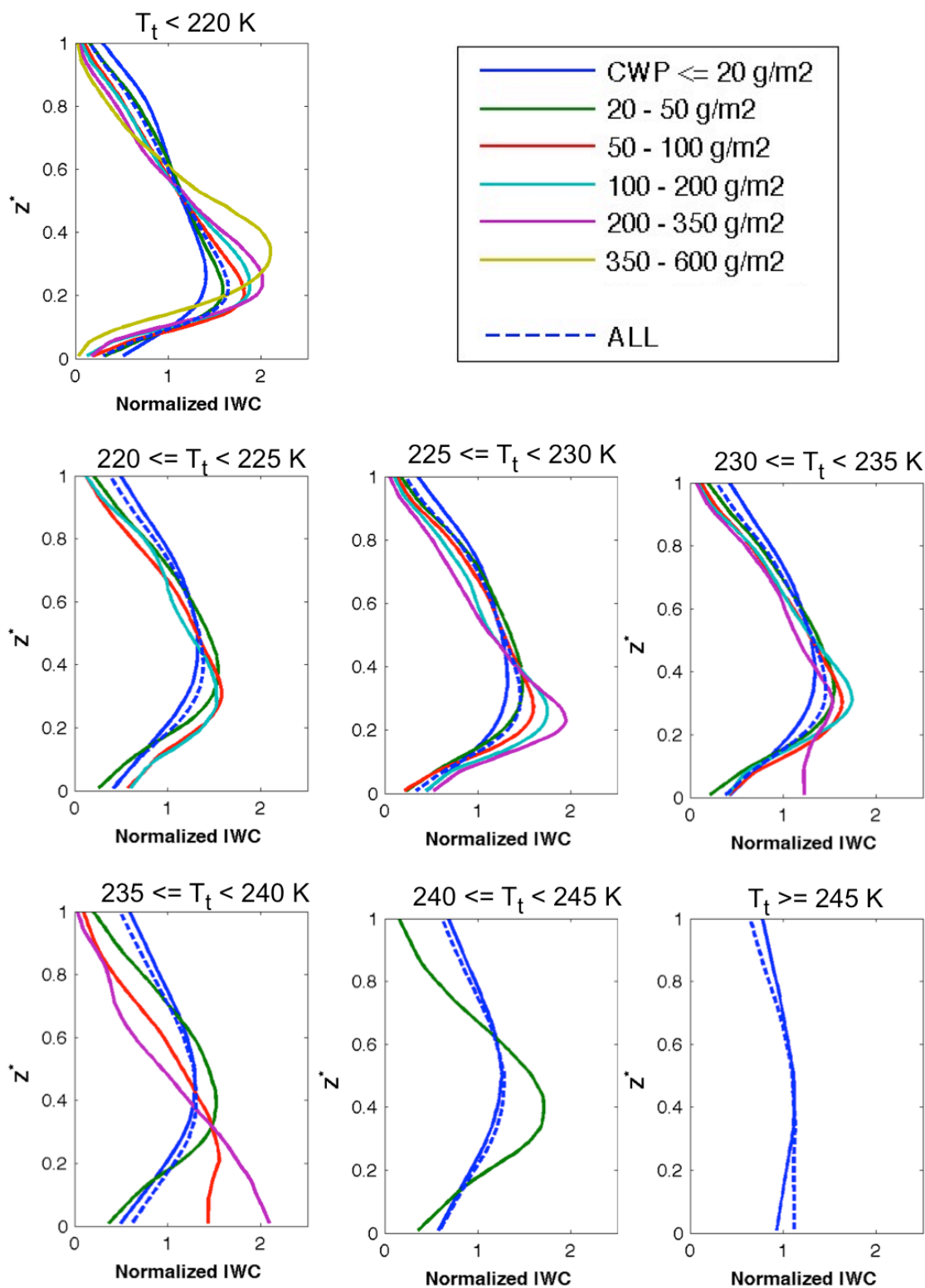
Figure 19. Mean normalized IWC profiles, *S(z*)*, depicting the typical vertical distribution of IWC from cloud top (*z**=1) to cloud base (*z**=0) derived from the CloudSat 2C-ICE product for single-layer cirrus clouds during Jan-March, 2007 and from 20-55°N and 65-150°W.
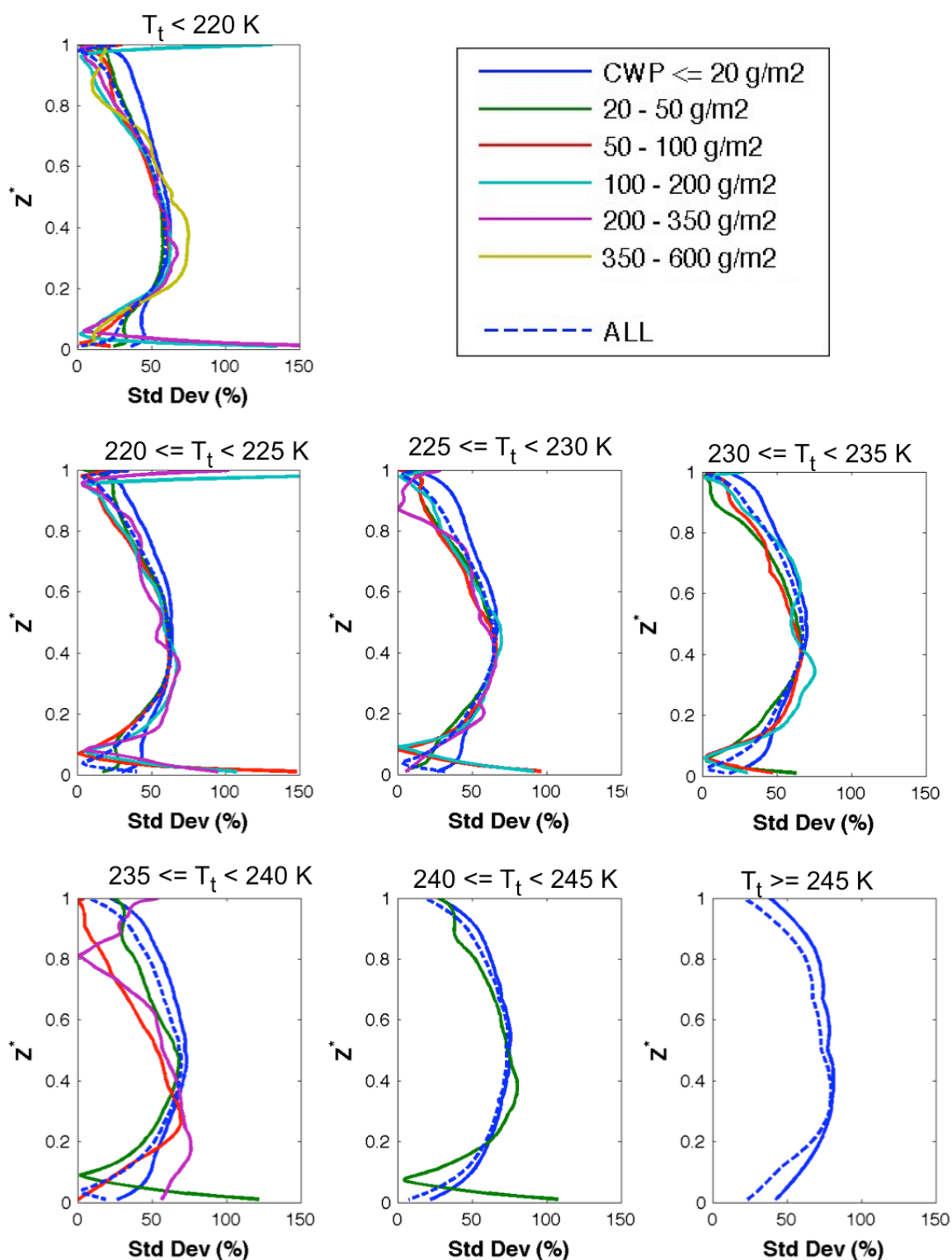
Figure 20. Same as **Figure 19** but showing the standard deviation in *S(z*)* expressed as the percentage of the mean. The relative uncertainty shown here is due to a combination of the natural variability found in cirrus cloud vertical profiles as well as retrieval uncertainties.
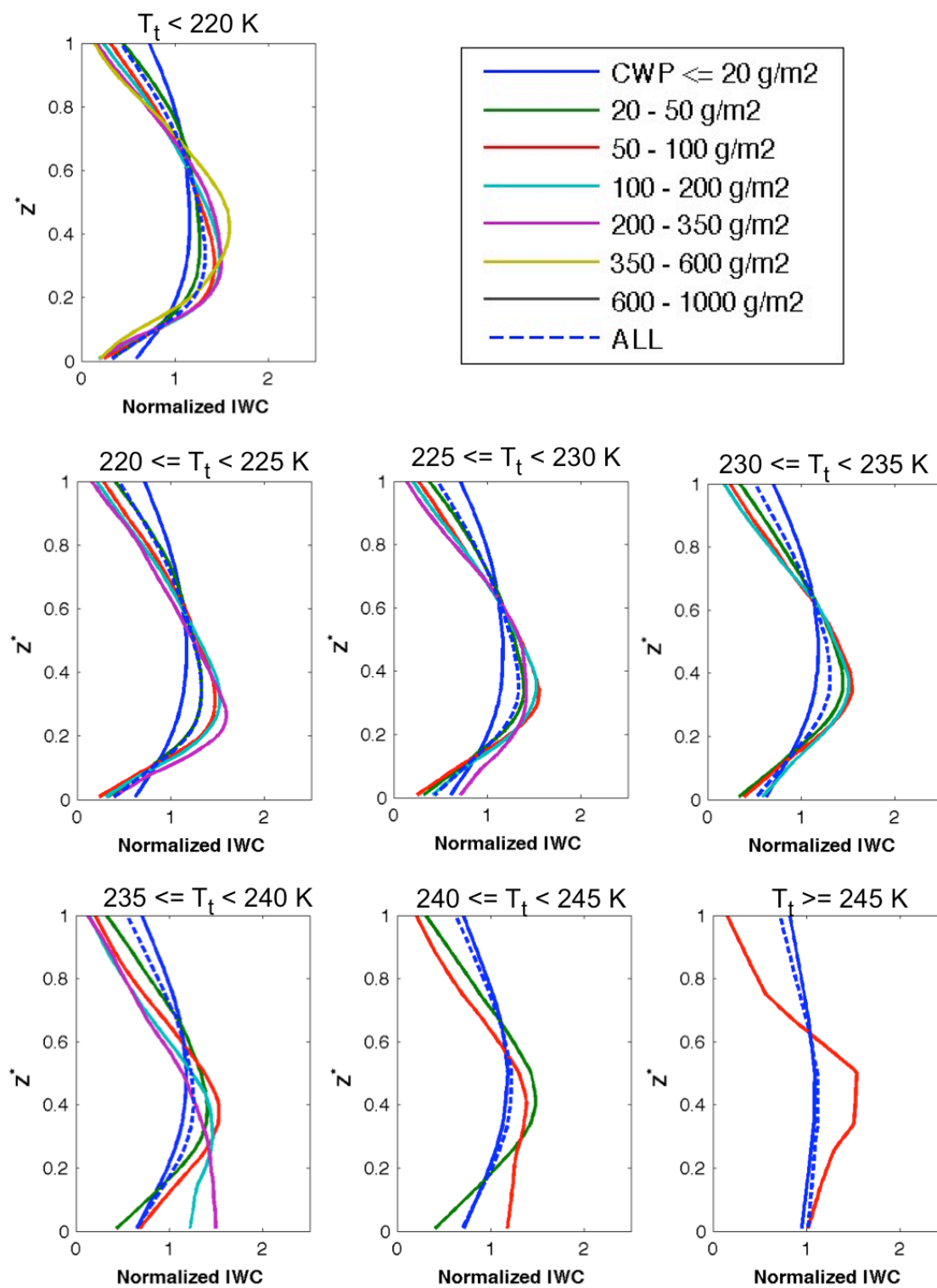
Figure 21. Same as **Figure 19** for cirrus clouds but constructed with the CloudSat CWC-RVOD product.
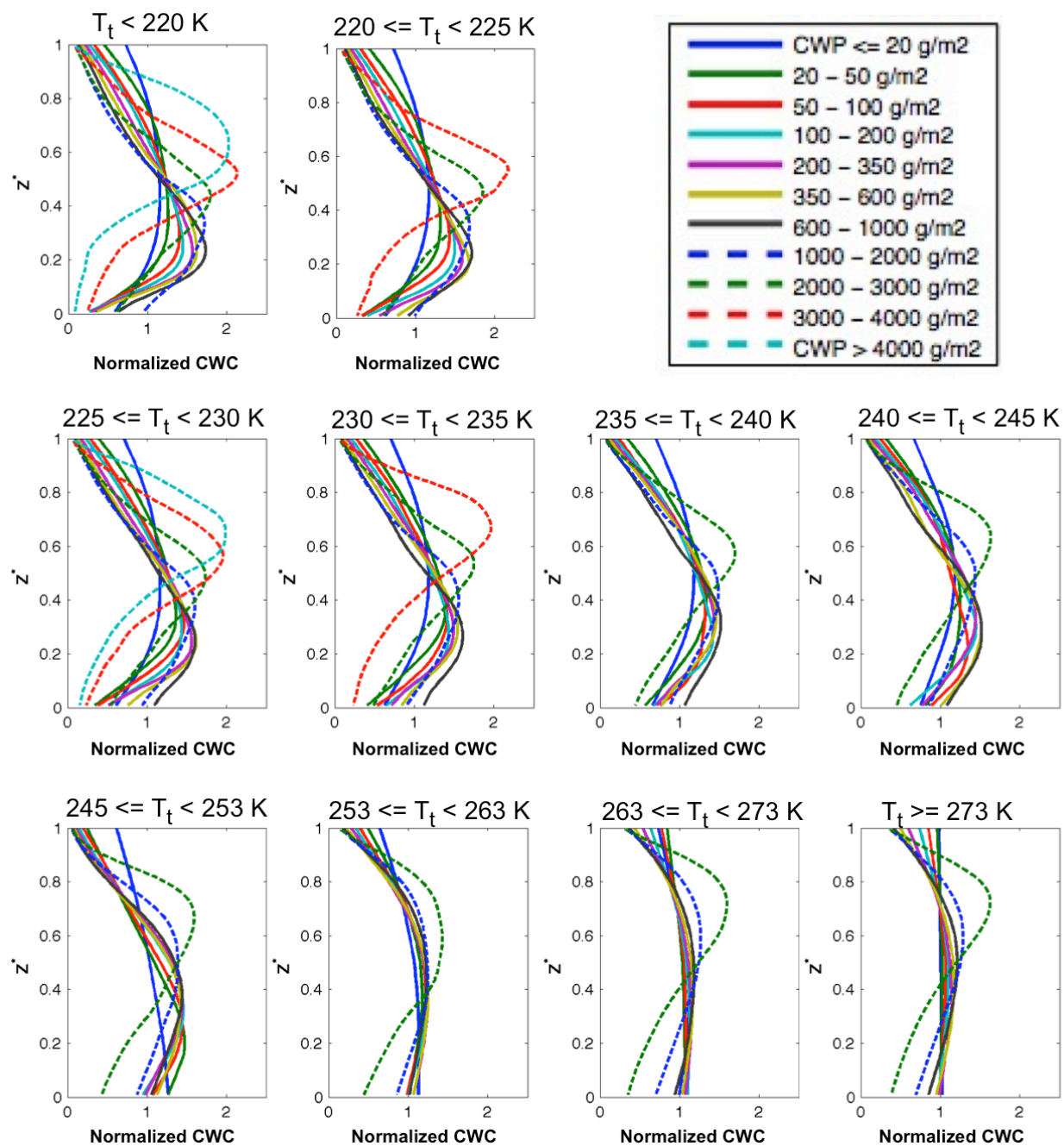
Figure 22. Normalized CWC profiles, *S(z*)*, derived from the CloudSat CWC-RVOD product for all single-layer clouds during Jan-March, 2007 and from 20-55°N and 65-150°W.
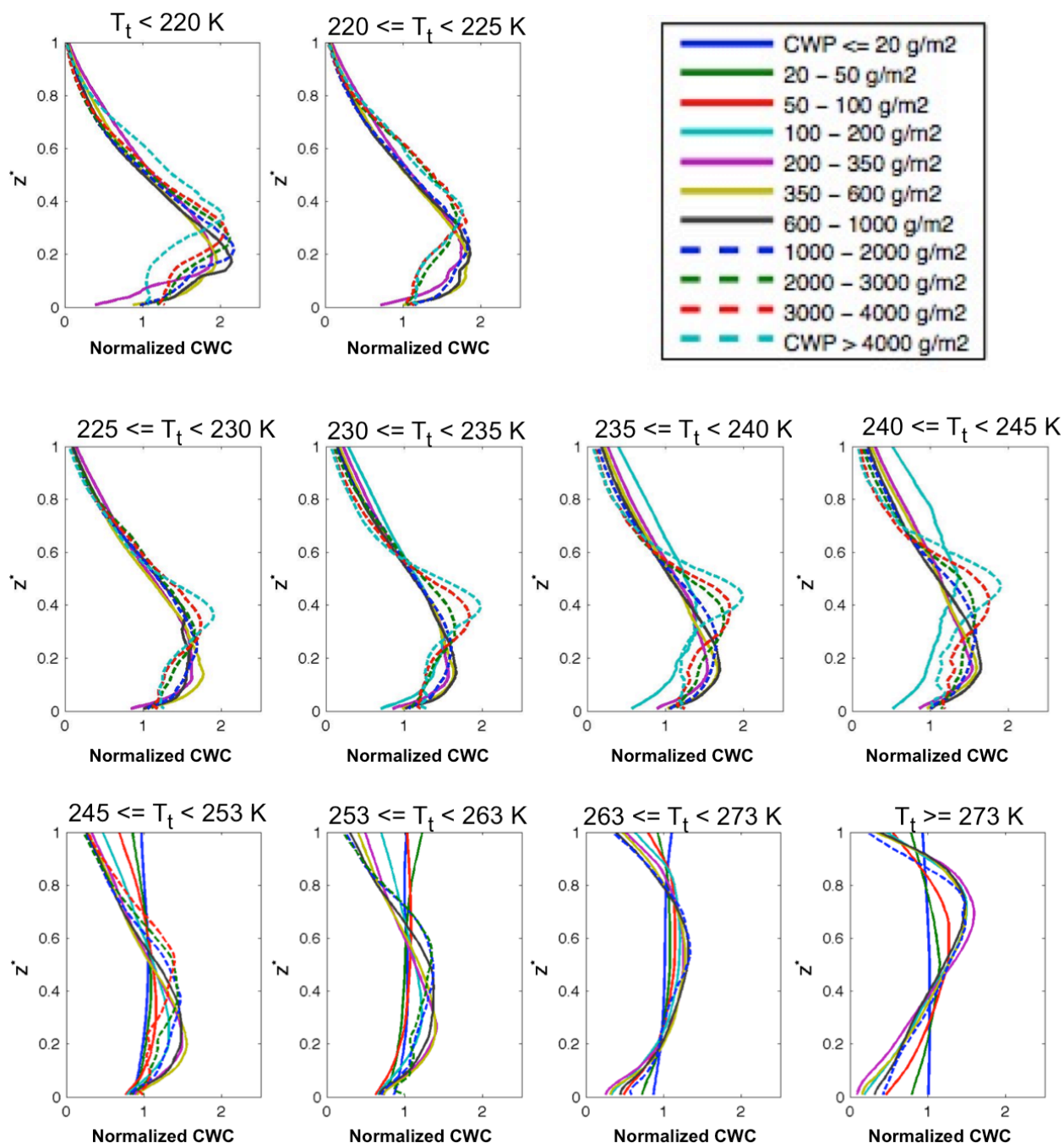
Figure 23. Normalized hybrid CWC profiles, *S(z*)*, derived from the RUC model and adjusted to better match CloudSat/CALIPSO IWC at temperatures below -20°C. The RUC data are from the 18 UTC cloud model analyses during Jan-March, 2010 from 20-55°N and 65-150°W. The CloudSat/CALIPSO adjustments were made using C3M data taken over the same area in April 2010.
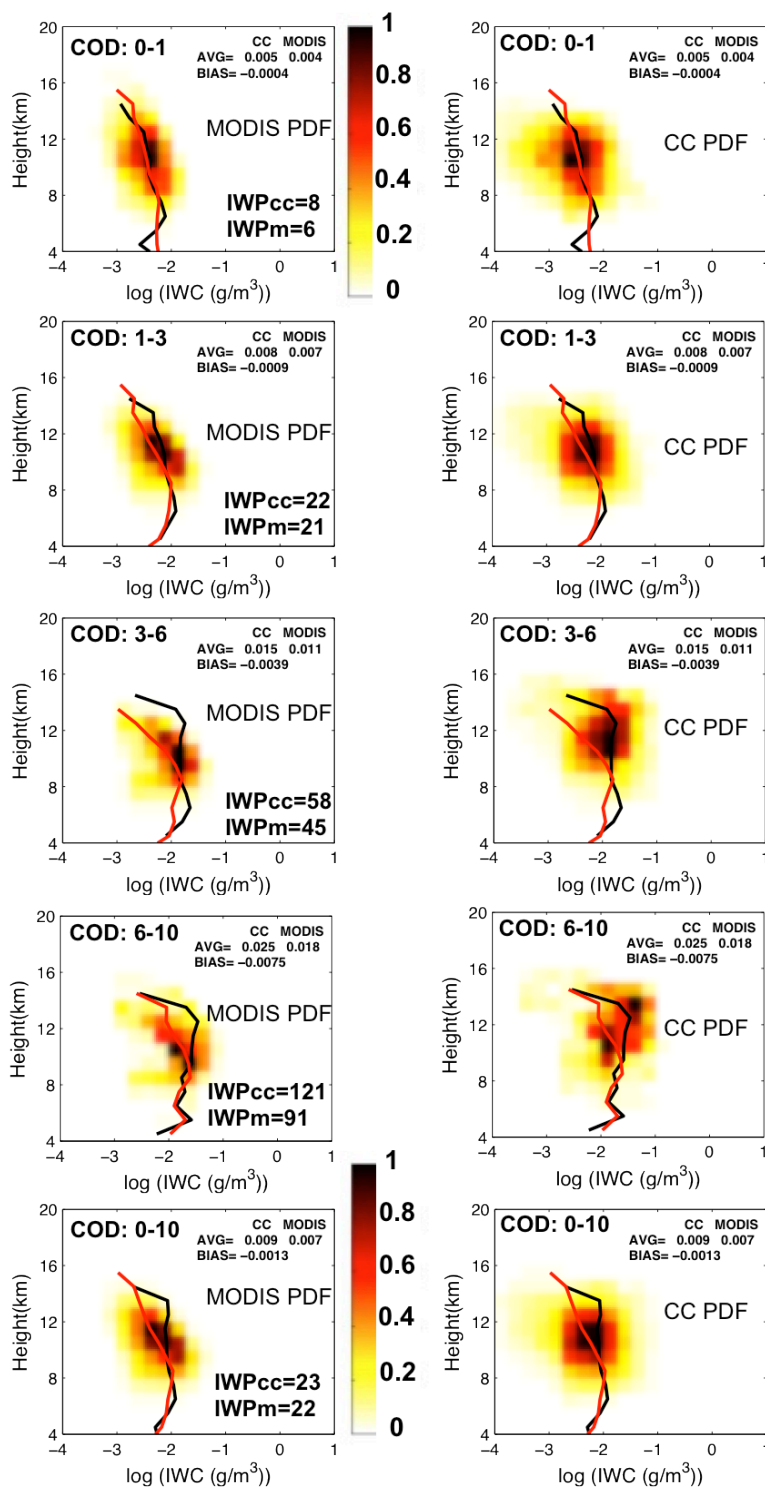
Figure 24. Cirrus IWC frequencies and average profiles derived from MODIS (red line) using the 2C-ICE climatology of *S(z*)* and from CALIPSO CPro + CloudSat RO retrievals (black line) using data taken over the CONUS in April 2010. The results are stratified into 5 COD bins and duplicated in the left and right panels. The images depict the IWC relative frequencies, which were normalized to the maximum number of occurrences, and are shown for the MODIS retrievals in the left panels and for the CloudSat+CALIPSO retrievals in the right panels.
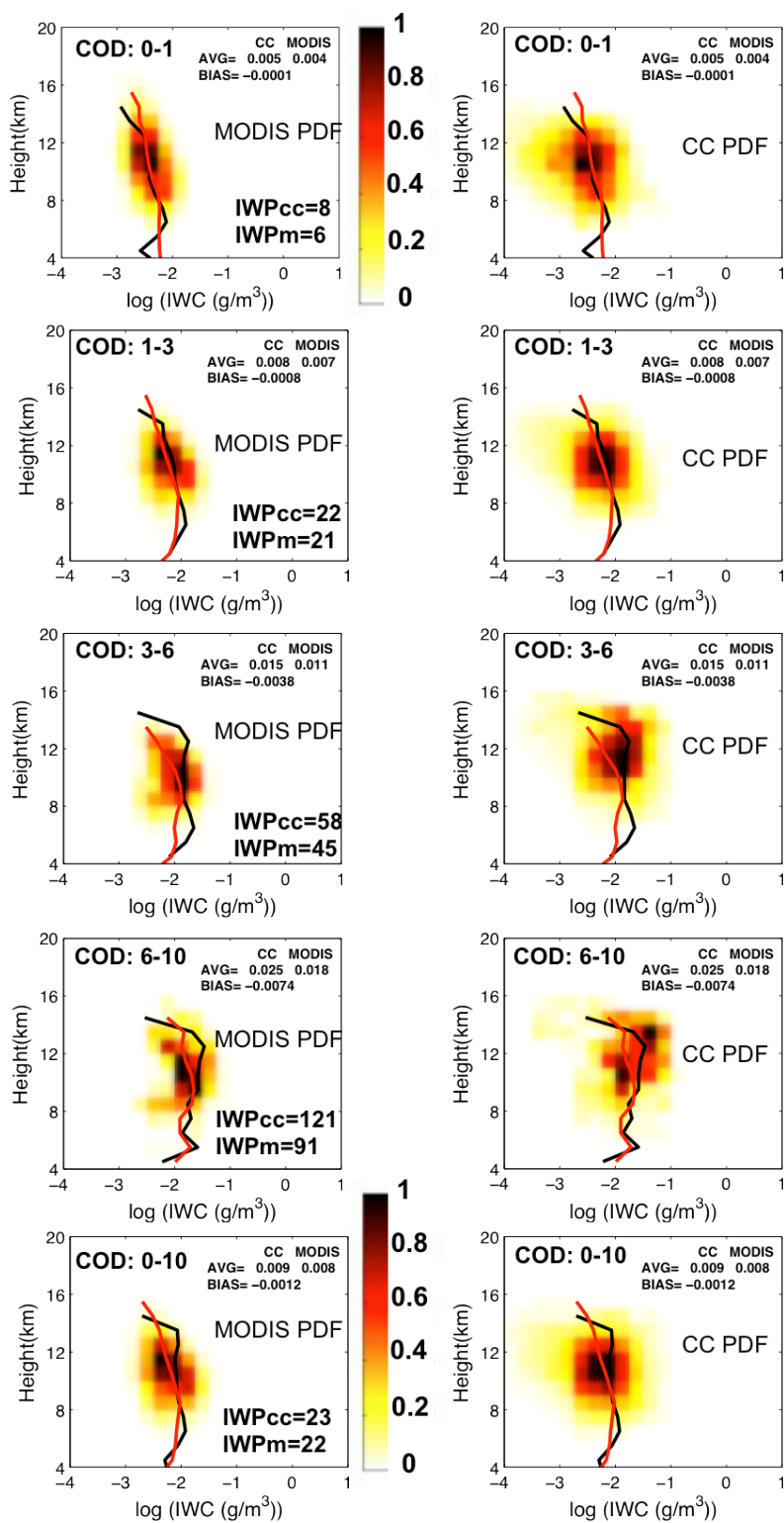
Figure 25. Same as **Figure 24** but using the CWC-RVOD climatology of *S(z*)* to derive the MODIS profiles.
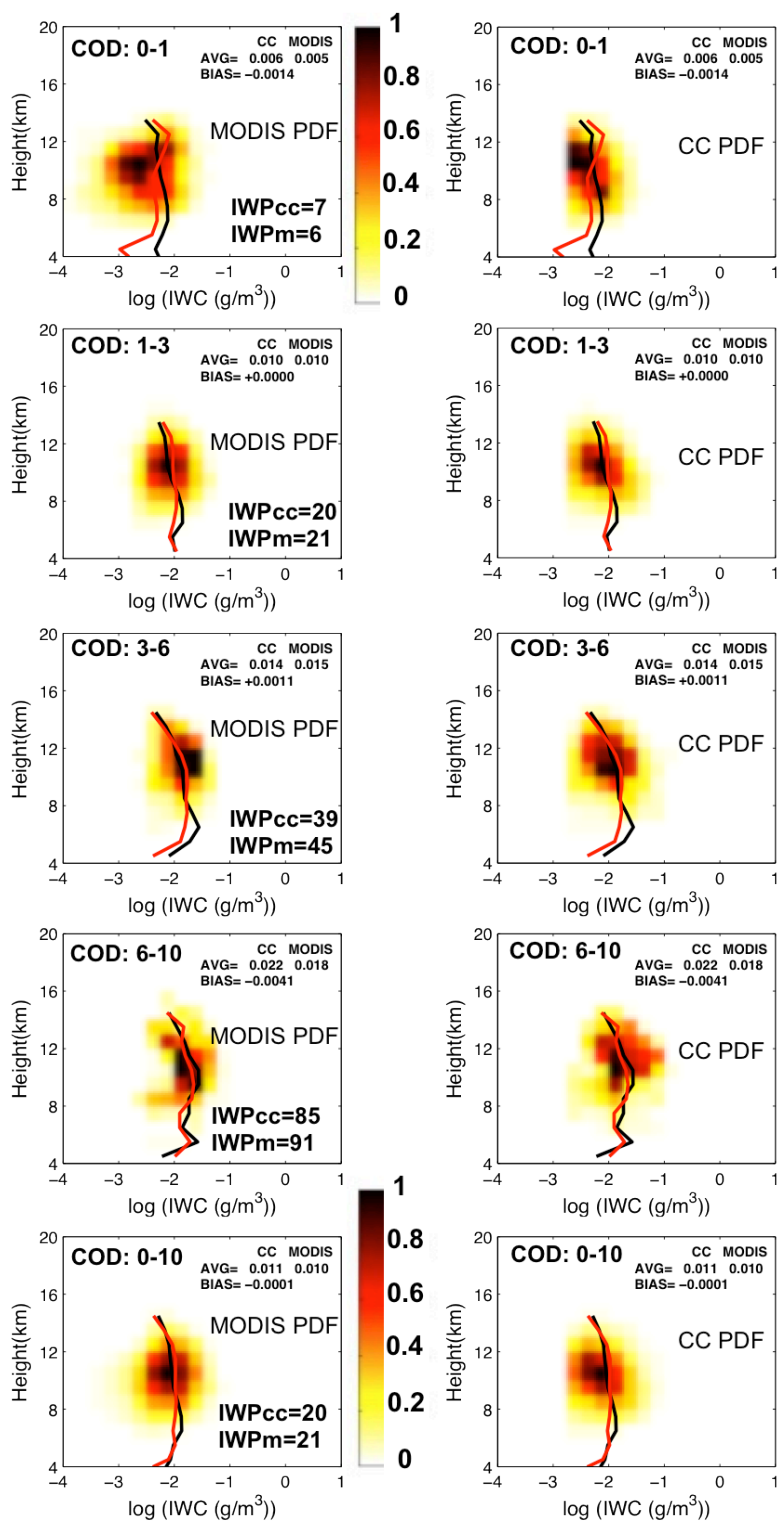
Figure 26. Same as **Figure 25** but for MODIS derived profiles constrained with the CloudSat cloud boundaries rather than the MODIS derived cloud boundaries and compared to the CloudSat CWC-RO IWC profiles.
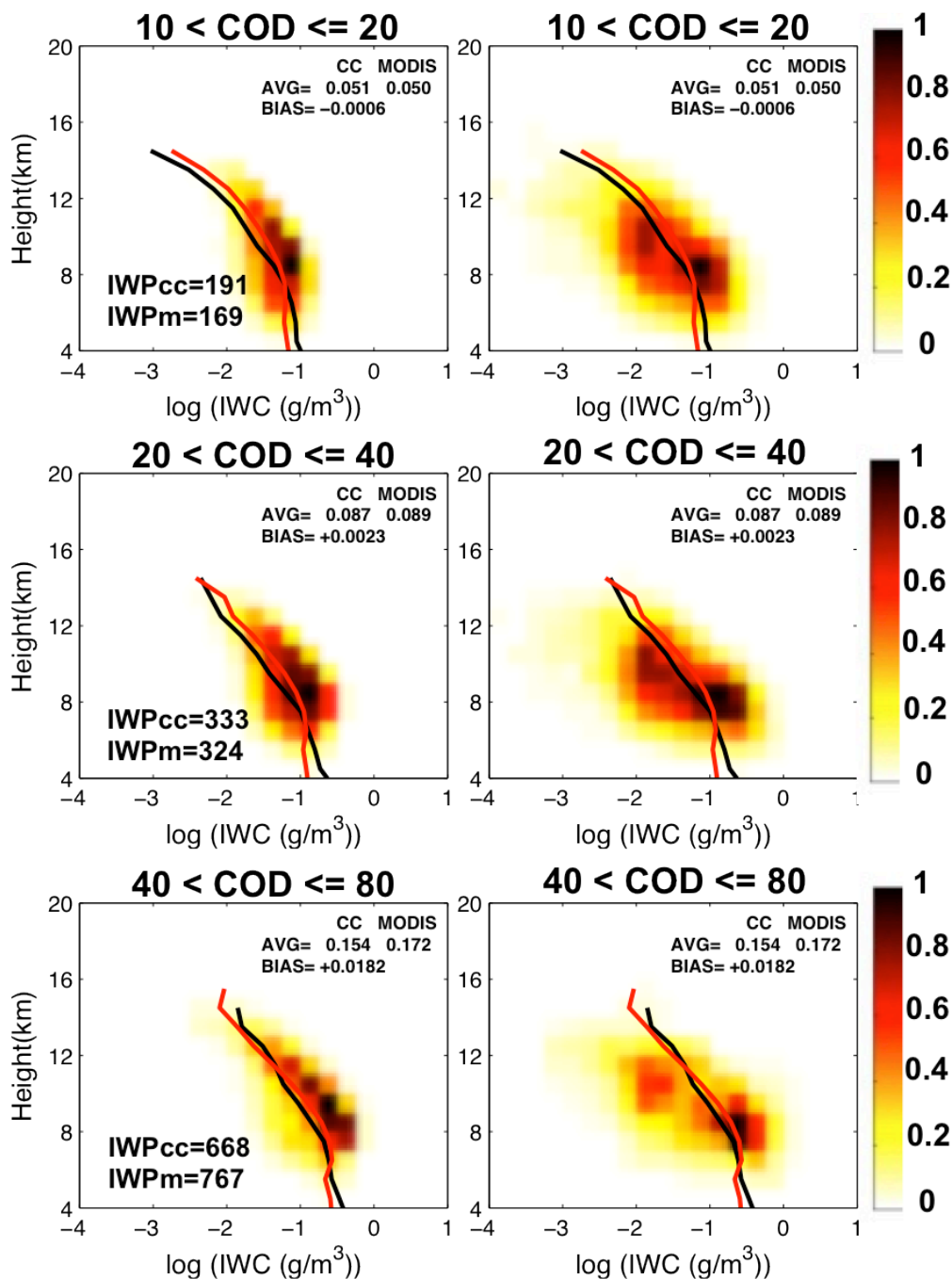
Figure 27. IWC profiles for cloud levels above the -20°C altitude level for optically thick clouds derived from MODIS (red line) using the hybrid climatology of *S(z*)* and from CALIPSO CPro + CloudSat RVOD retrievals (black line) using data taken over the CONUS in April 2010. Mean values of the IWC and the IWP computed above the -20°C altitude level (IWP253 in the text) are also shown. The results are stratified into 5 MODIS COD bins and duplicated in the left and right panels. The images depict the IWC relative frequencies, which were normalized to the maximum number of occurrences, and are shown for the MODIS retrievals in the left panels and for the CloudSat+CALIPSO retrievals in the right panels.
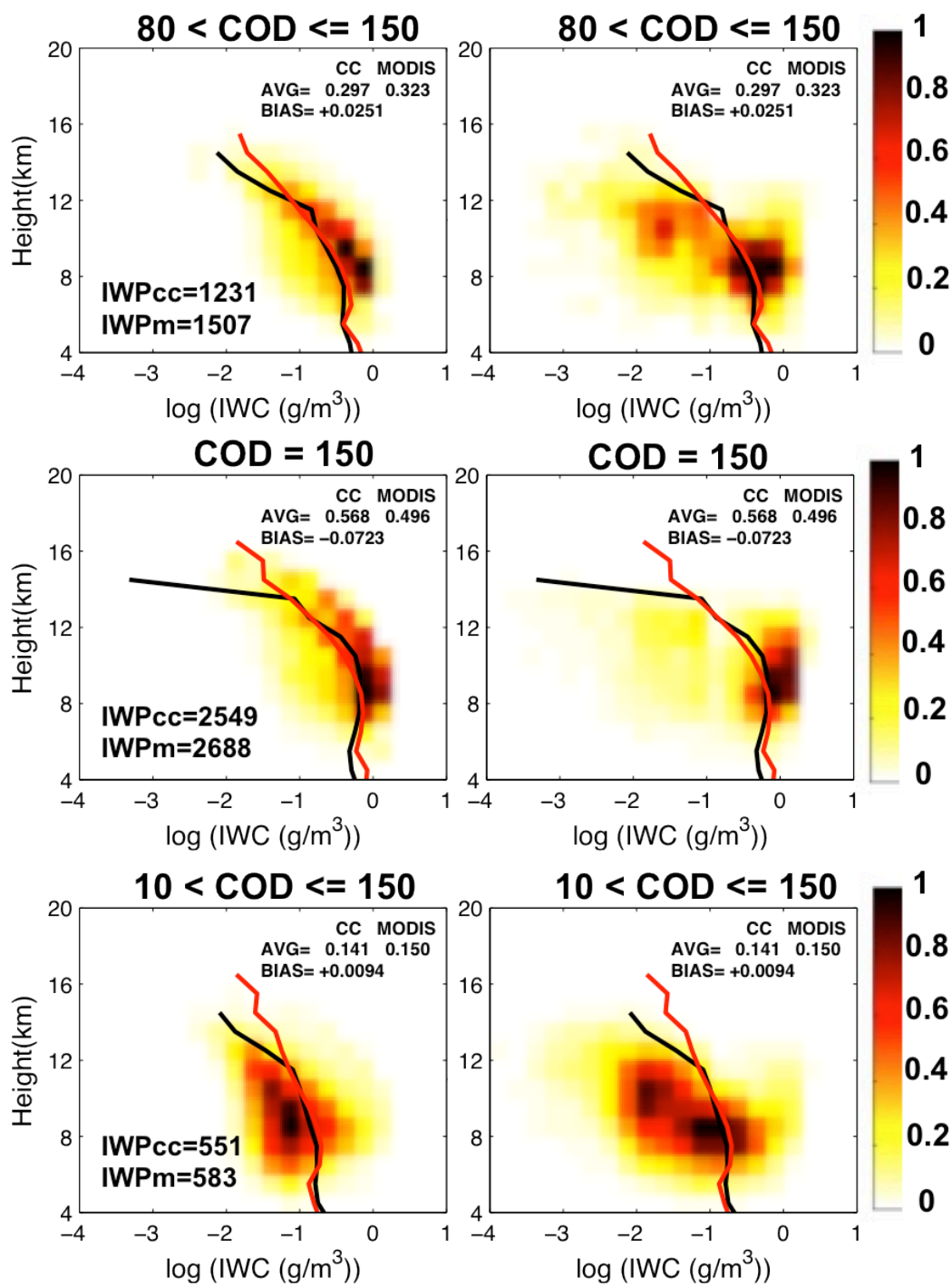
Figure 28. Same as **Figure 27** but for profiles binned in different ranges of COD
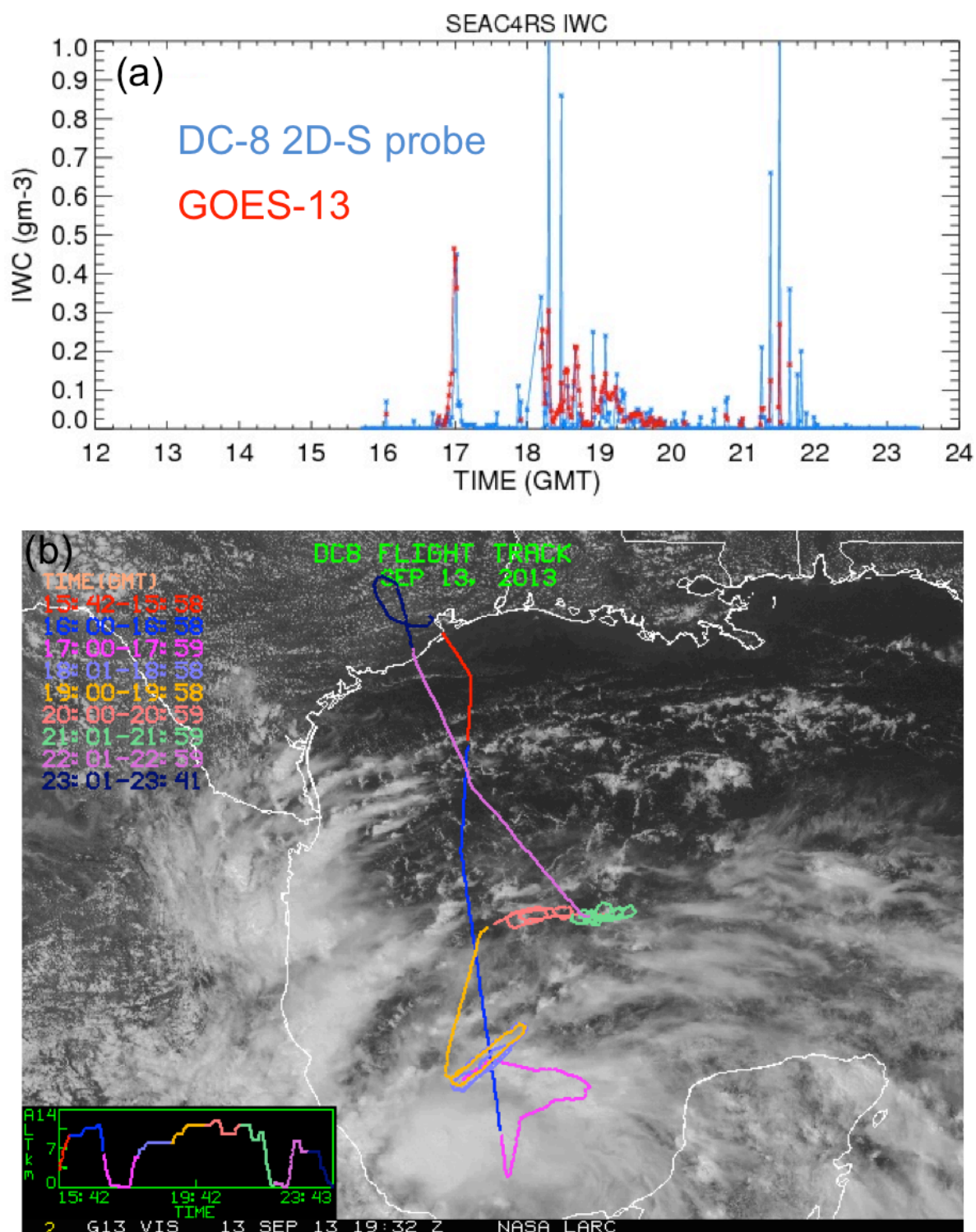
Figure 29. (a) IWC retrieval comparison between GOES-13 and the 2D-S probe deployed from the NASA DC-8 aircraft on 13 September 2013 during SEAC4RS and (b) corresponding flight track with altitude trace.
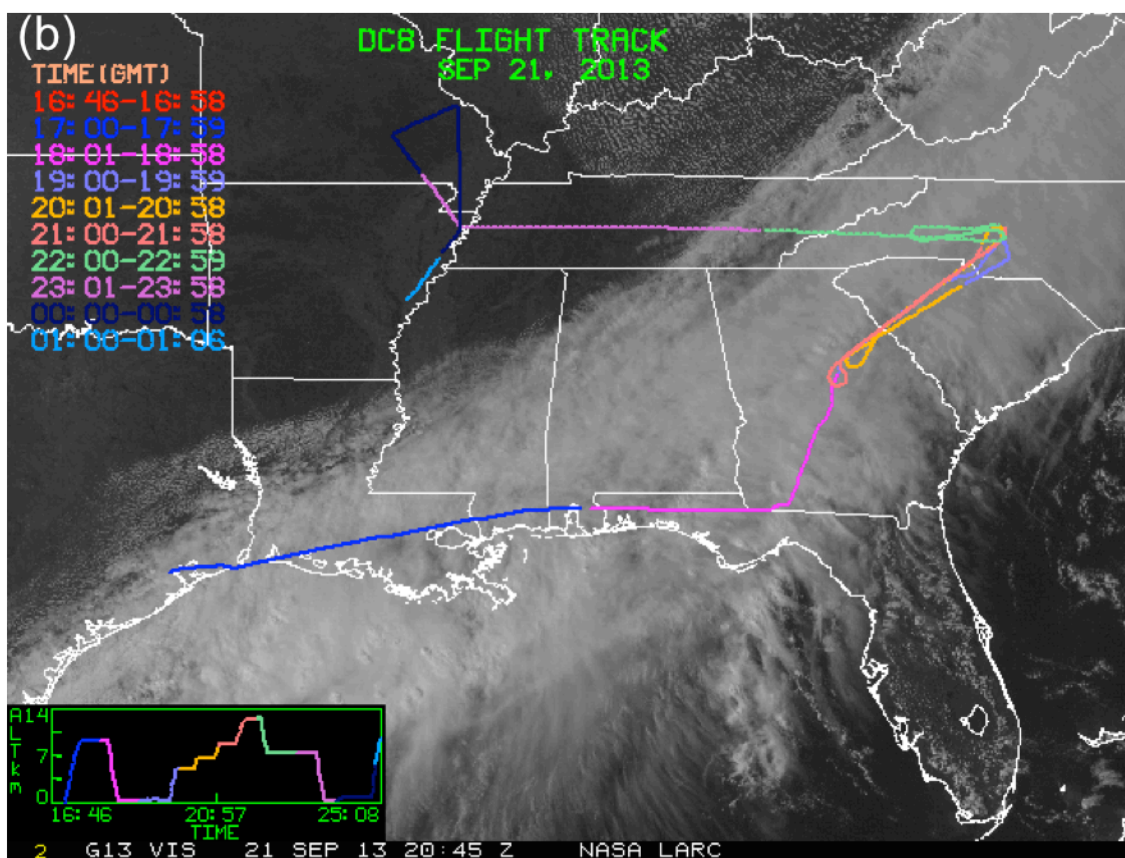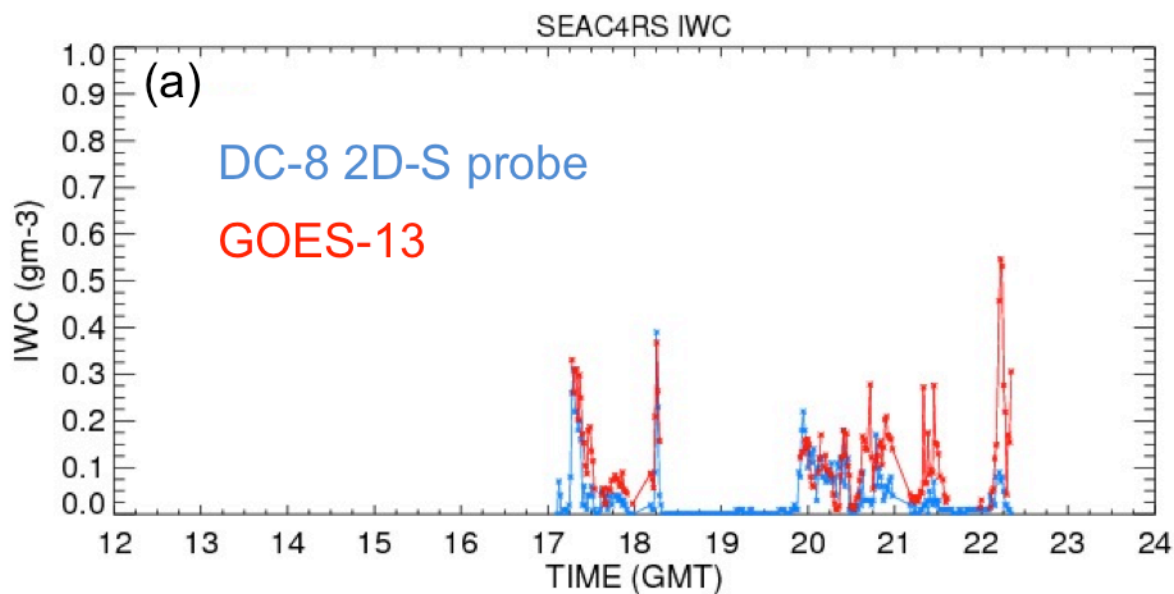
Figure 30. (a) WC retrieval comparison between GOES-13 and the 2D-S probe deployed from the NASA DC-8 aircraft on 21 September 2013 during SEAC4RS and (b) corresponding flight track with altitude trace.
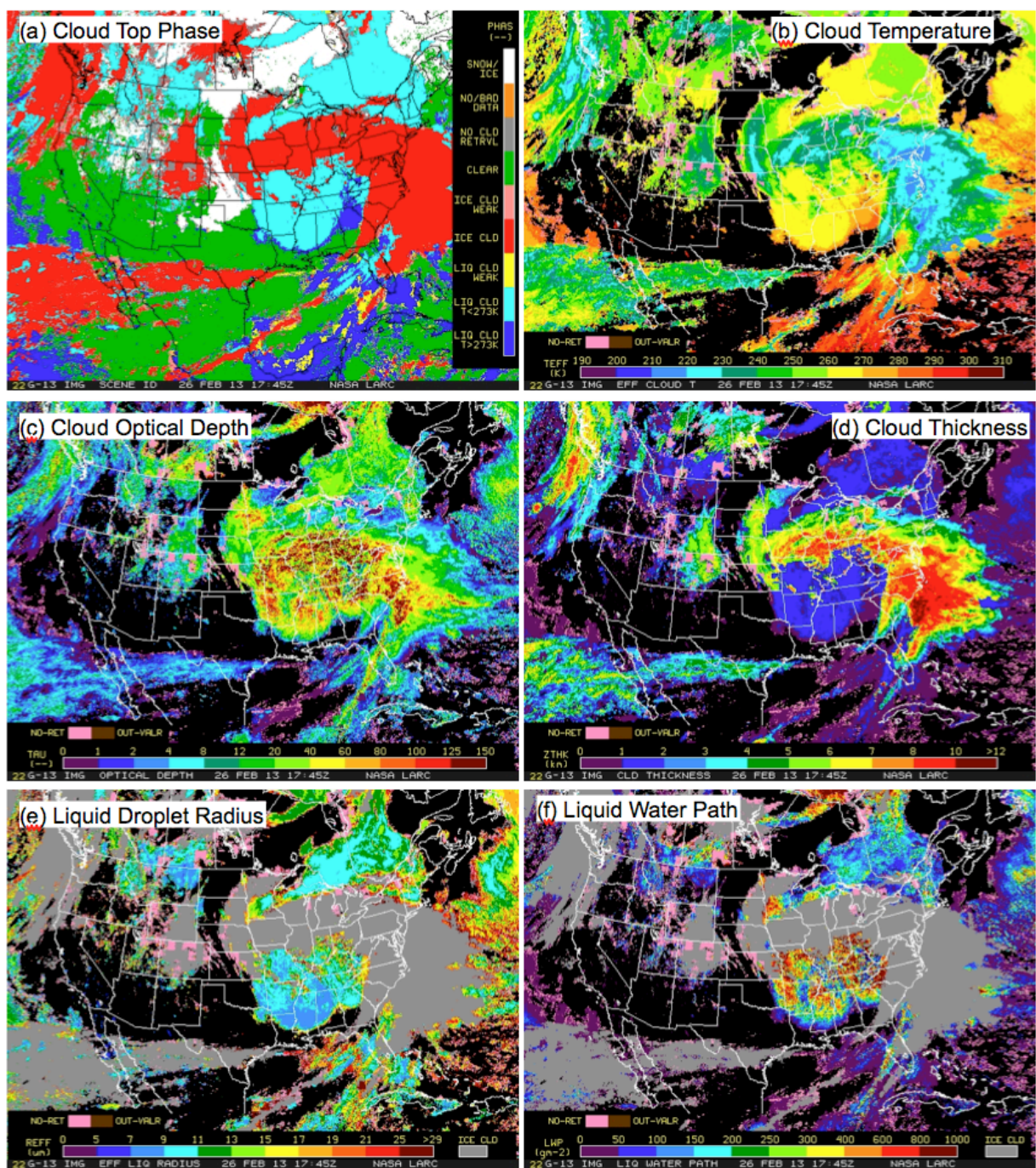
Figure 31. Select cloud parameters derived in the NASA LaRC operational cloud retrieval system using data taken from GOES-E and GOES-W at 1745 UTC, 26 February 2013: (a) cloud top phase, (b) effective temperature [K], (c) optical depth, (d) cloud thickness [km], (e) effective droplet size [μm] for liquid clouds, and (f) liquid water path [g m^{-2}].
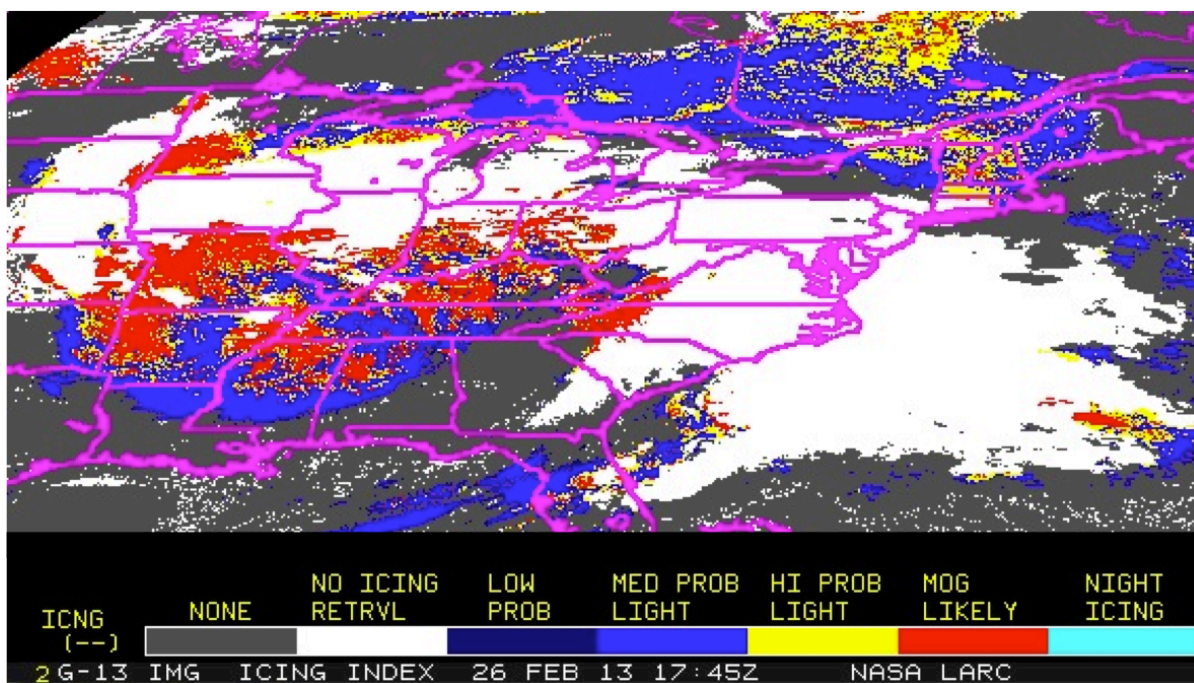
Figure 32. Flight icing threat derived from GOES-E data on 26 Feb 2013 using the SFITv1 algorithm for low clouds described in Smith et al. (2012).
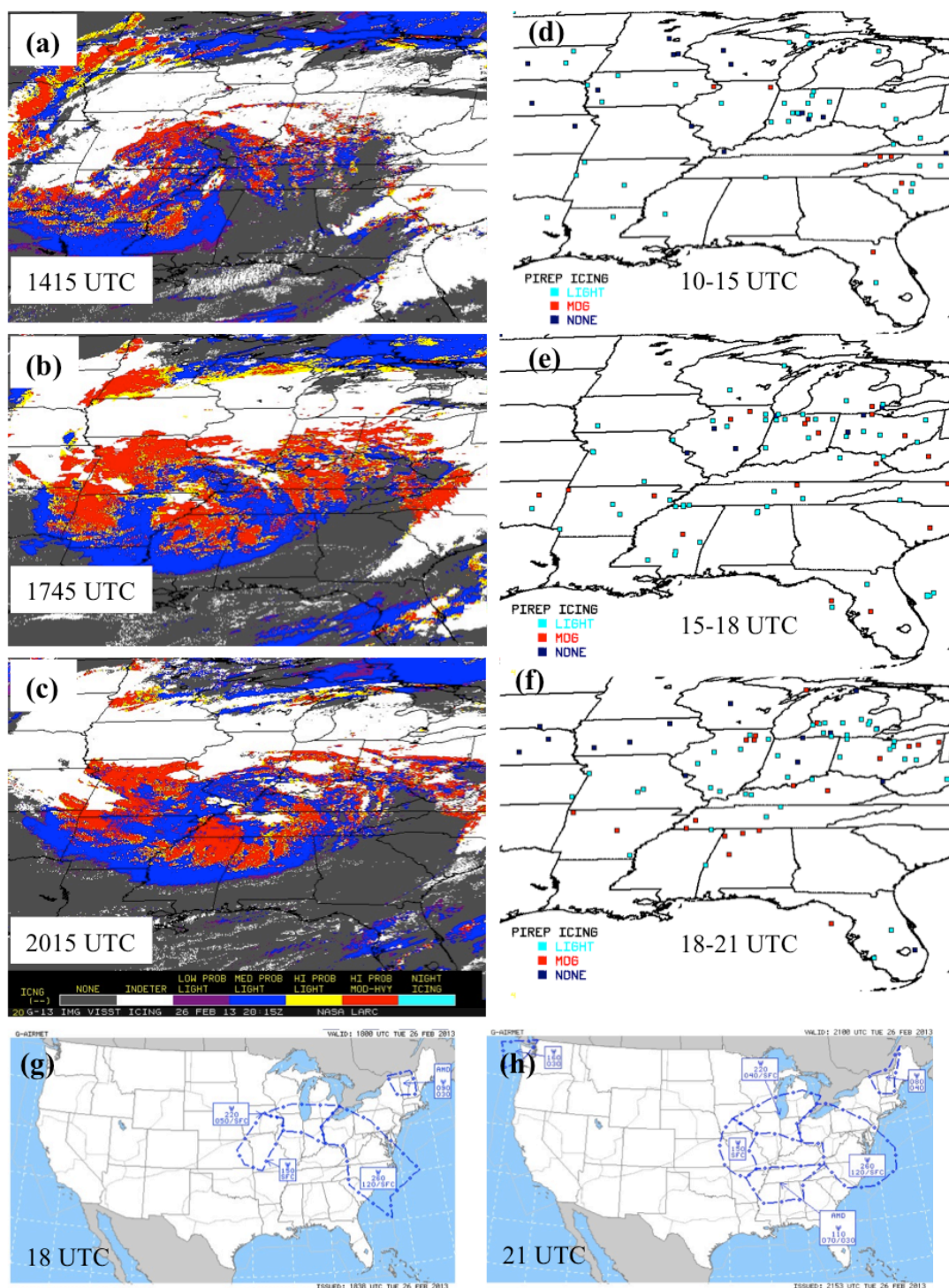
Figure 33. The flight icing threat derived from GOES data taken at 1415 UTC (a), 1745(b), and 2015 (c) and that observed and reported by pilots at different times during 26 Feb 2013 (d) - (f). Icing advisories issued by AWC shown at 1800 UTC (g) do not capture the low cloud threat identified from satellite until 2100 UTC (h) after numerous icing PIREPS were filed. The AWC advisories do capture the threat beneath overlapping clouds that the satellite low cloud method can not resolve.
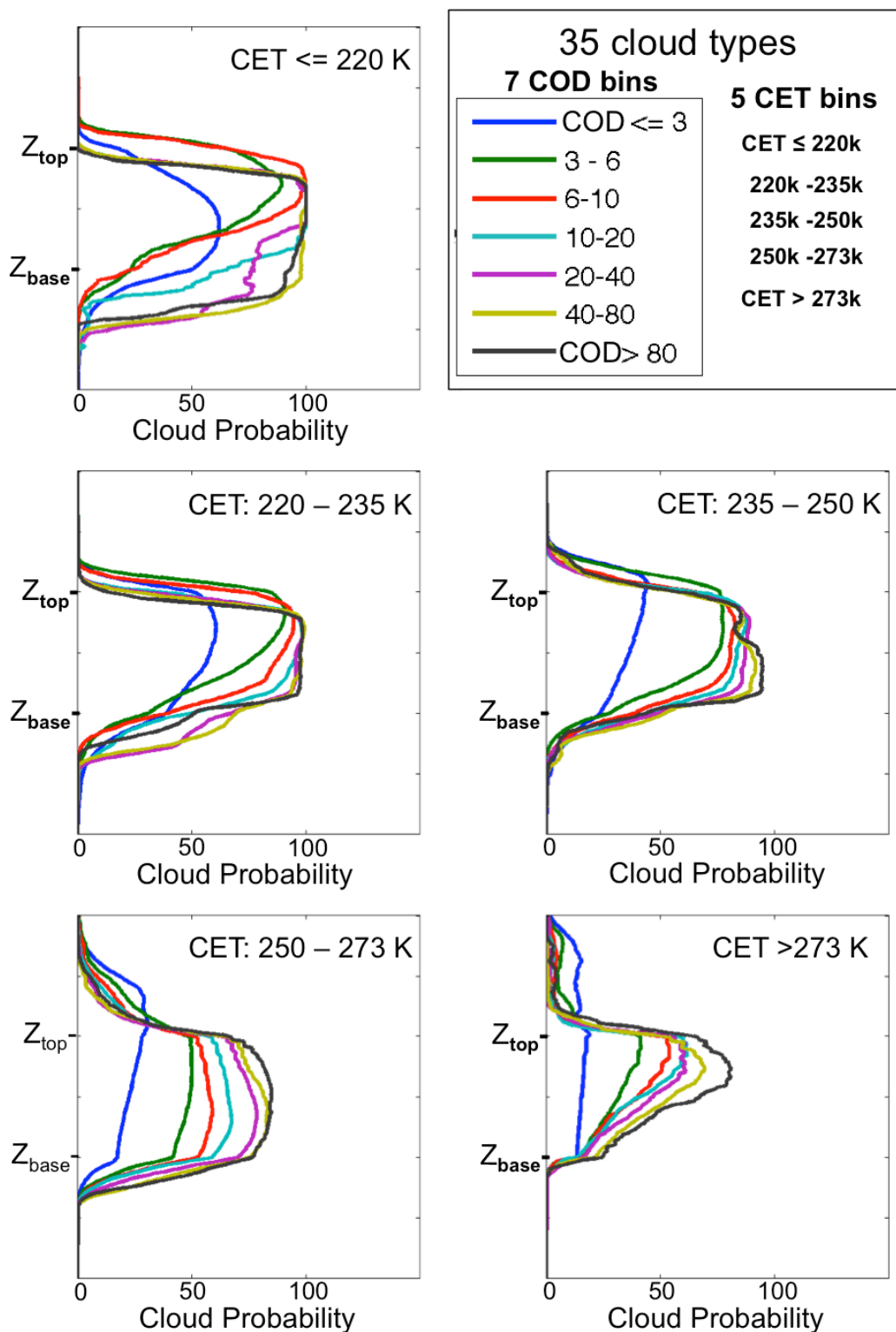
Figure 34. The probability for the existence of cloud relative to the single-layer cloud boundaries derived from CERES MODIS data during April 2010 for 35 cloud types defined by the MODIS cloud effective temperature and cloud optical depth. Coincident cloud profiles in the CloudSat 2B-CLOUDCLASS product are used as ground-truth.
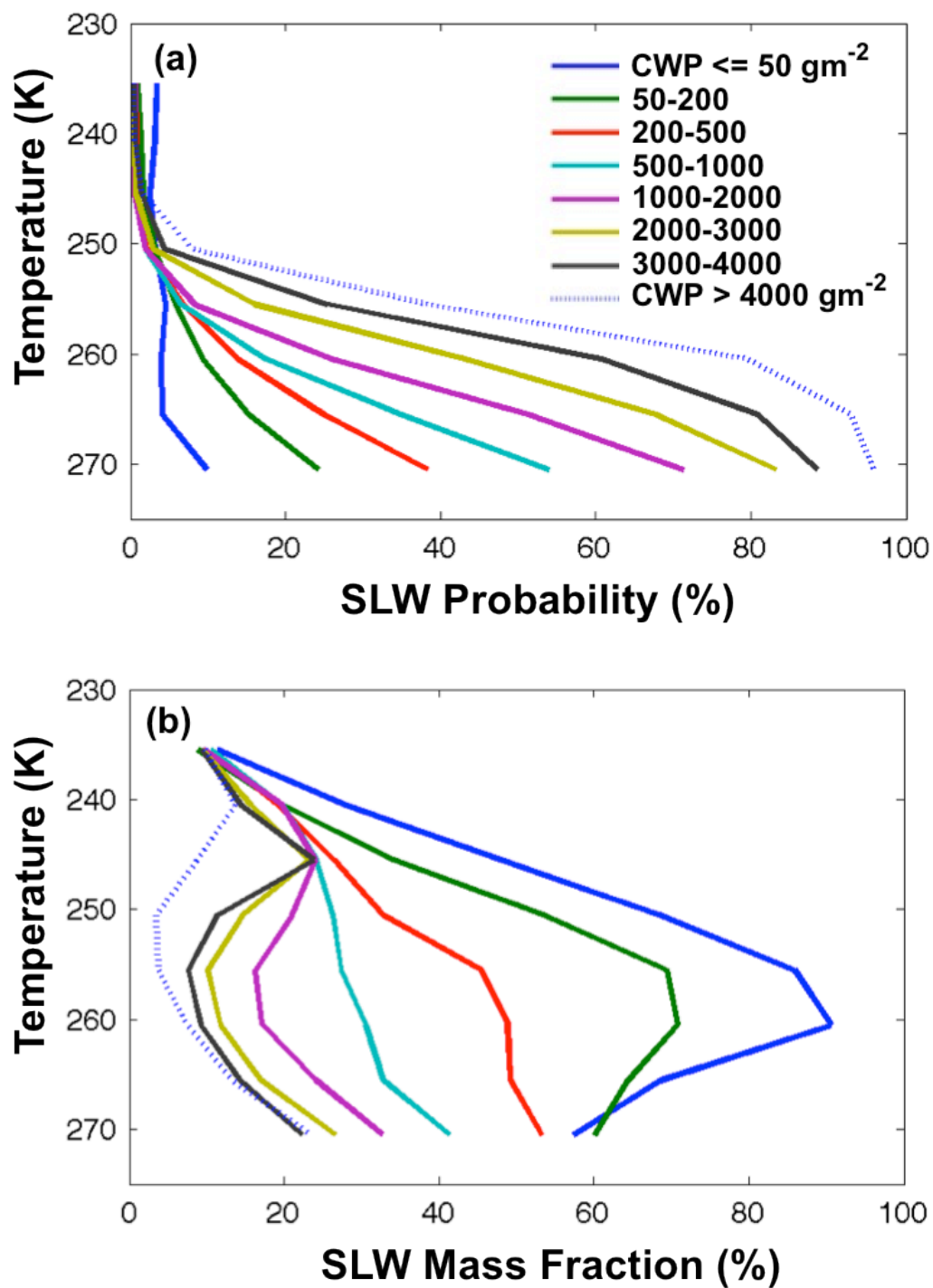
Figure 35. The relationship between the SLW probability and mass fraction with temperature for clouds with CTT < 233K derived from RUC cloud analyses at 18 UTC during Jan-Mar, 2010.
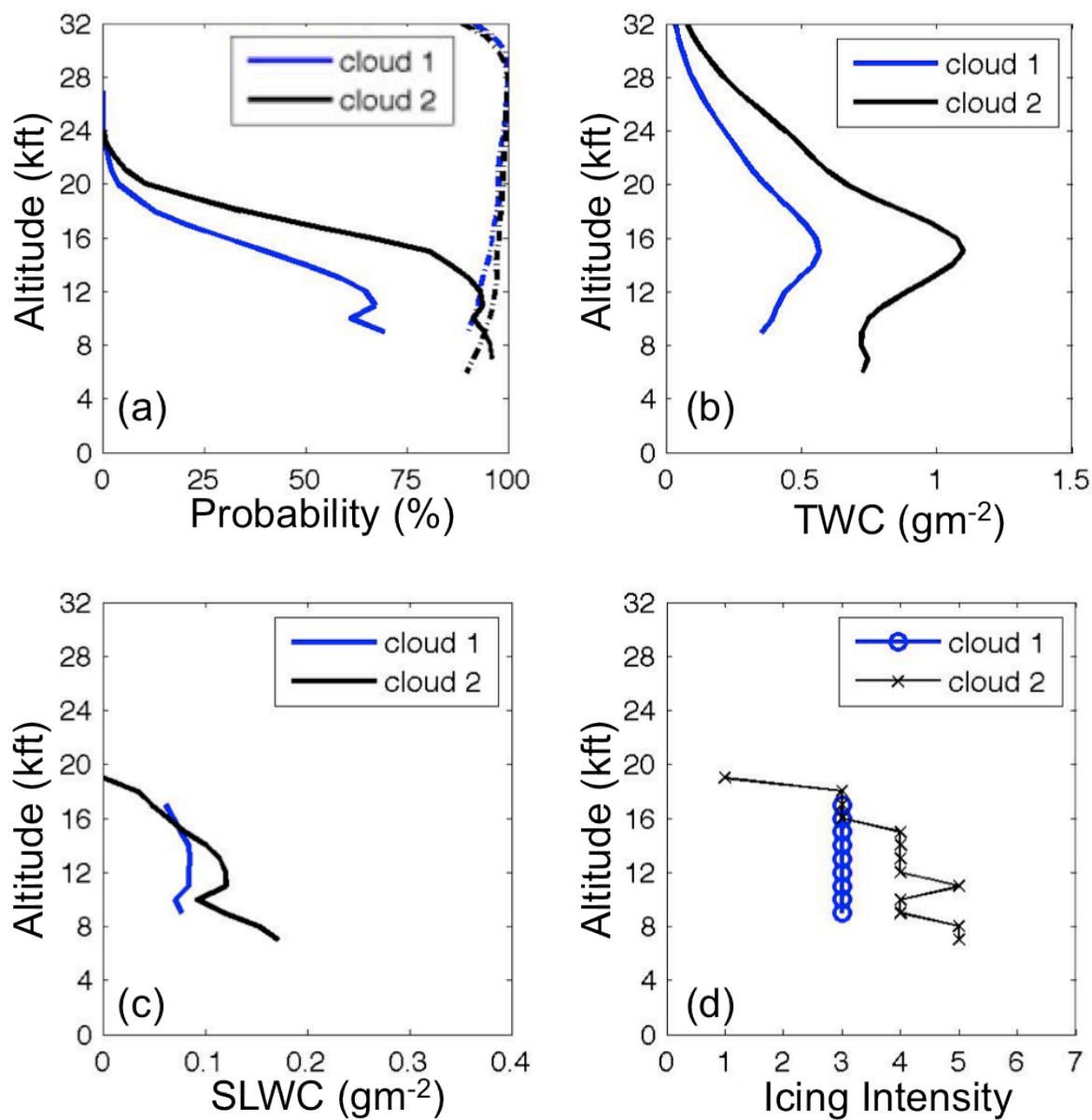
Figure 36. Cloud (solid) and SLW(dashed) probability profiles (a), TWC profiles (b), SLWC profiles (c), and icing intensity profiles (d) derived for the two single-layer ice over water clouds described in Table 6 with COD=50 (cloud 1) and COD=100 (cloud 2).
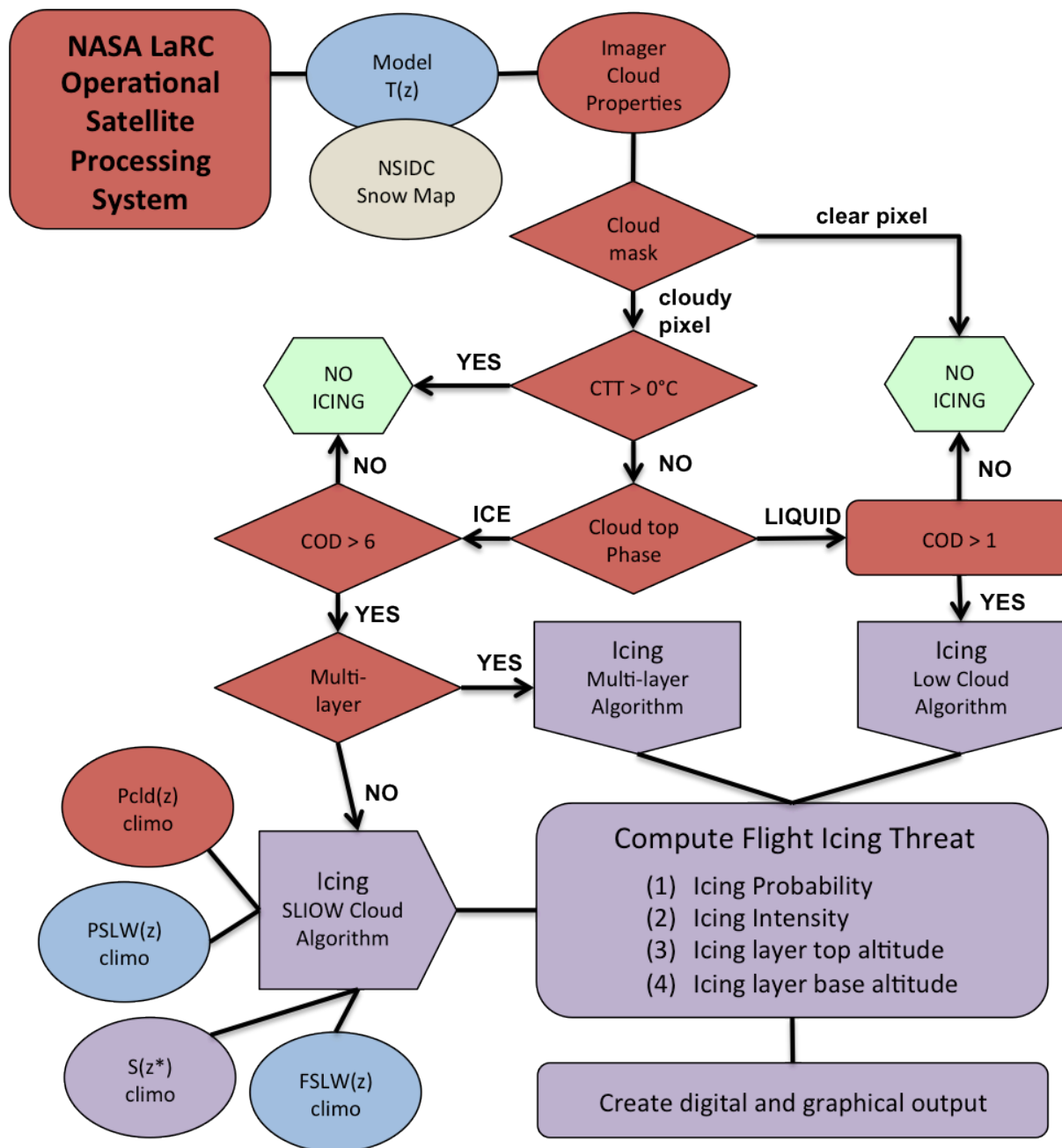
Figure 37. High level flowchart depicting the key elements and decision tree for the SFITv2.0 algorithm.
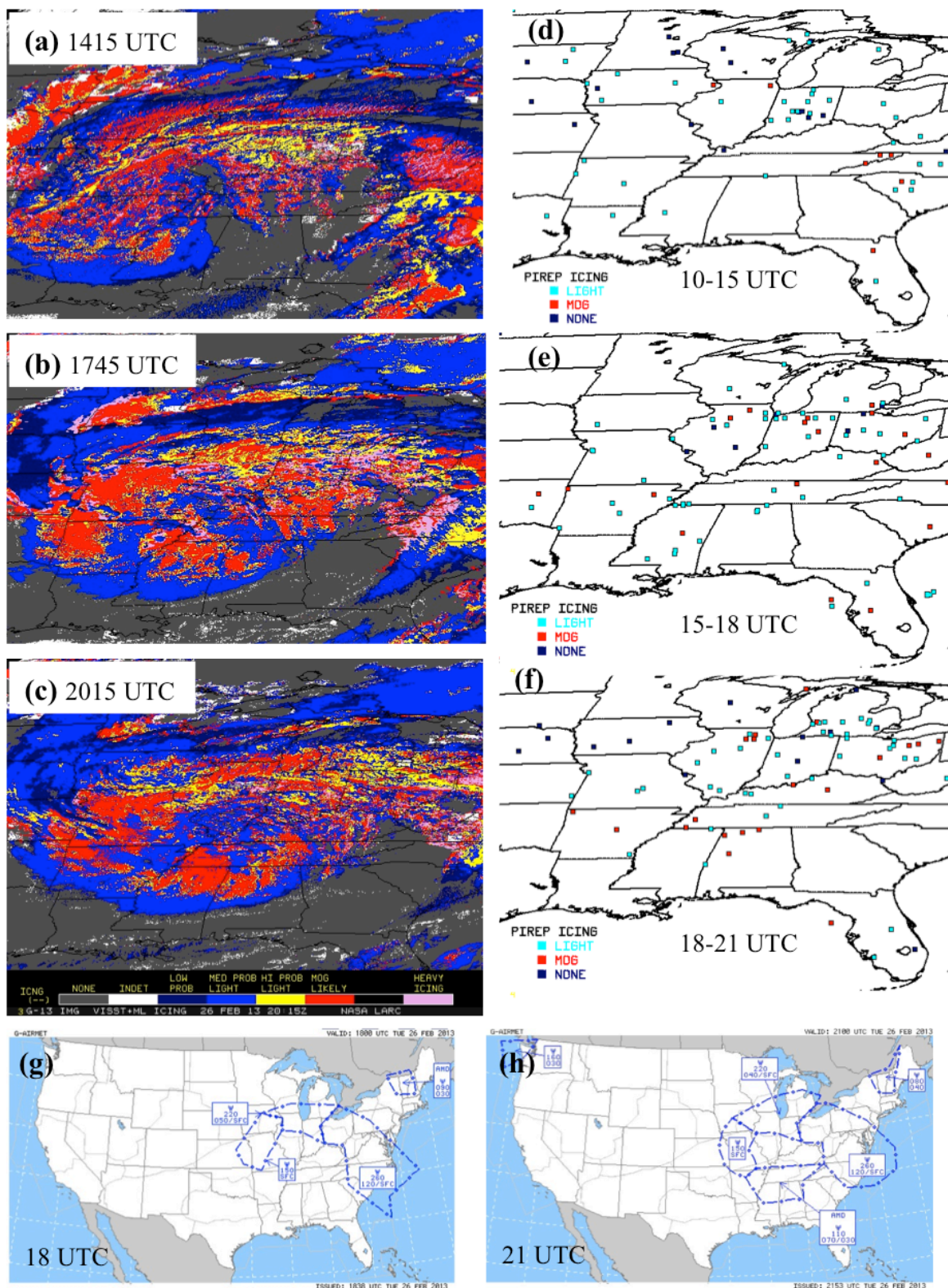
Figure 38. Same as Figure 31 but depicting results from the satellite version 2 icing algorithm (SFITv2.0) output which correctly captures the icing threat as verified by PIREPS in both low cloud and overlapping cloud conditions**.**
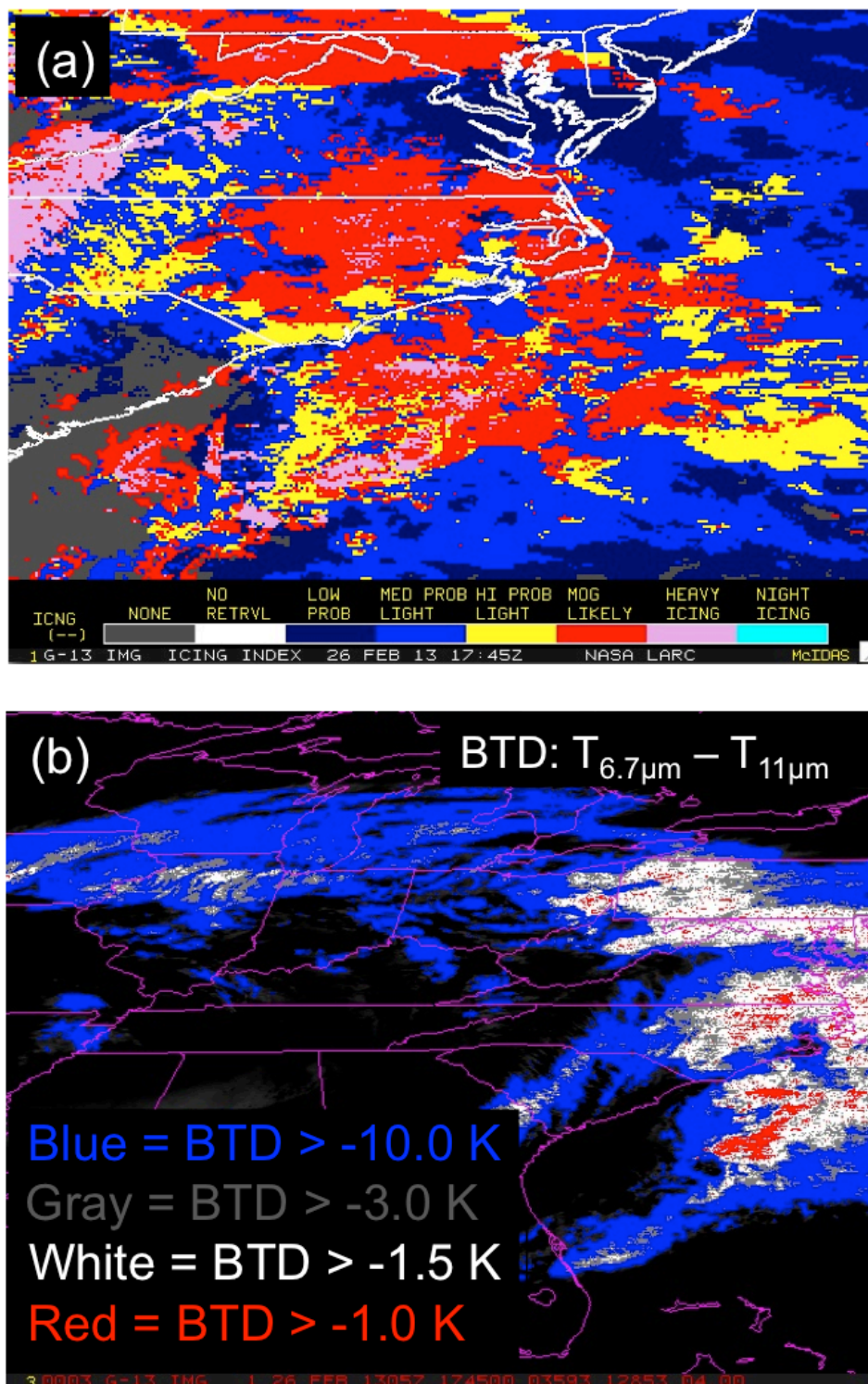
Figure 39. (a) The flight icing threat derived from GOES-13 over the southeastern seaboard on 26 Feb 2013 at 1745 UTC indicating heavy icing potential associated with convection over the Gulf Stream and (b) the corresponding 6.7-11 μm BTD image.
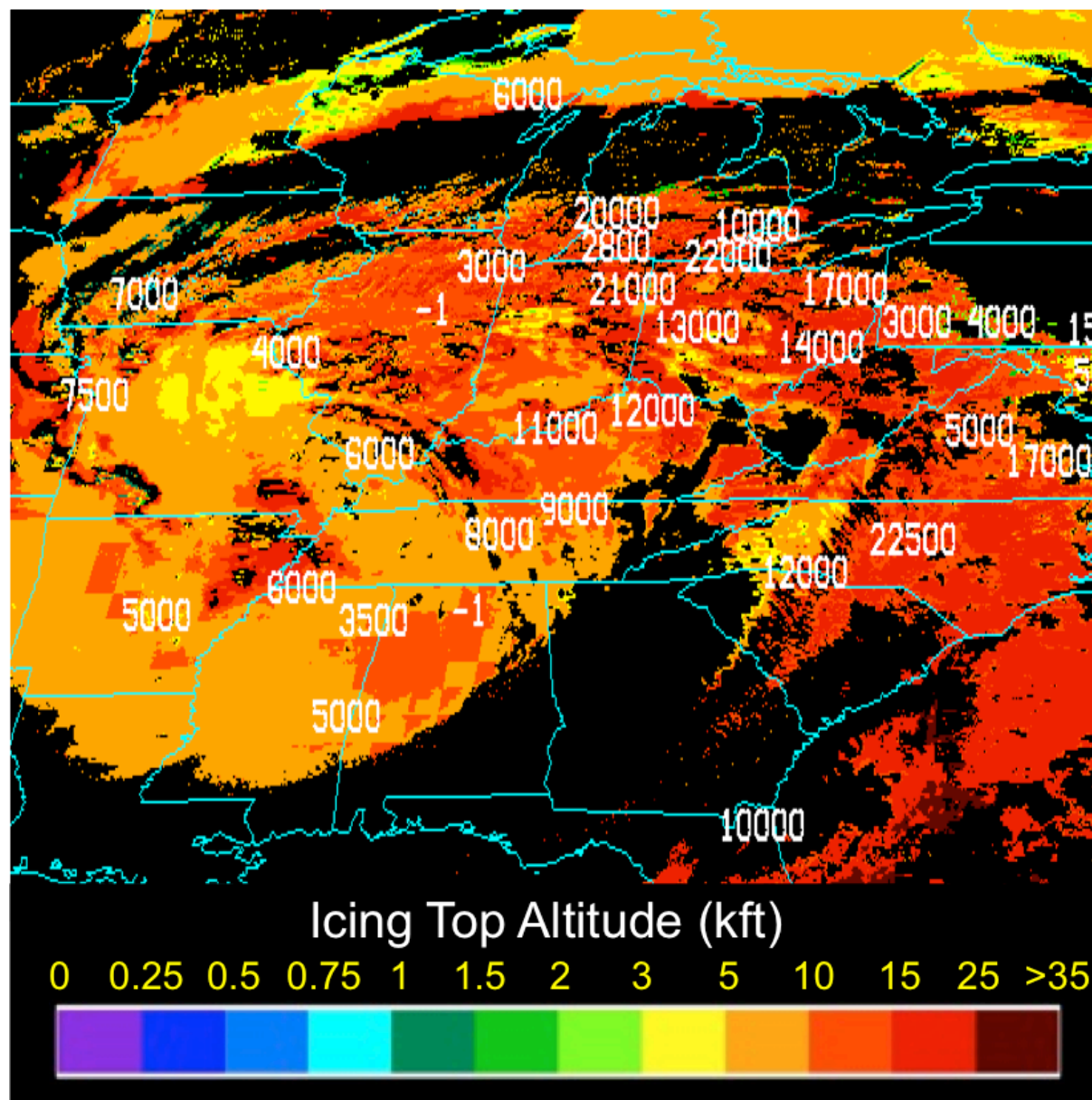
Figure 40. Icing top altitude image derived from the SFITv2.0 algorithm and the corresponding icing altitude reports from pilots (white) near 1745 UTC on 26 February 2013.
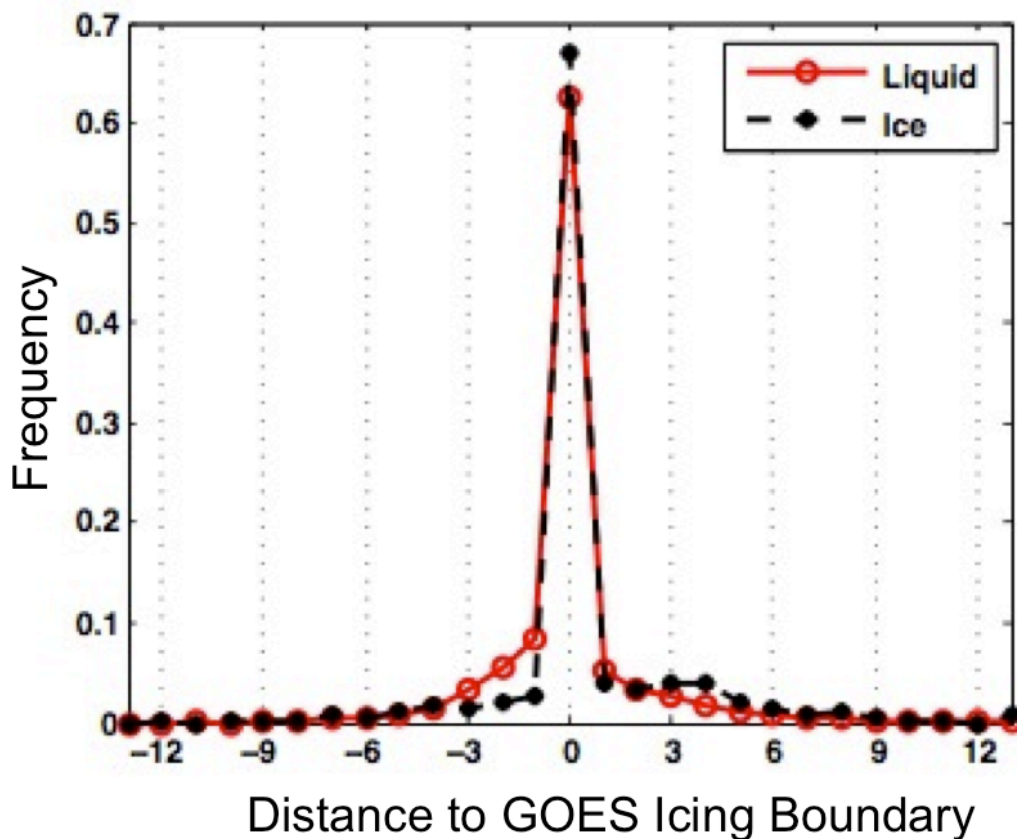
Figure 41. Frequency distribution of the distance between the PIREPS icing altitude to the icing altitude boundary derived from GOES with the SFITv2.0 algorithm. The frequency at the distance value of zero indicates how often the satellite icing layer estimates captured the PIREP altitudes. The frequency values at the negative (positive) distance values indicate how often the PIREPS altitudes were found below (above) the satellite icing base (top) altitude estimates, respectively.
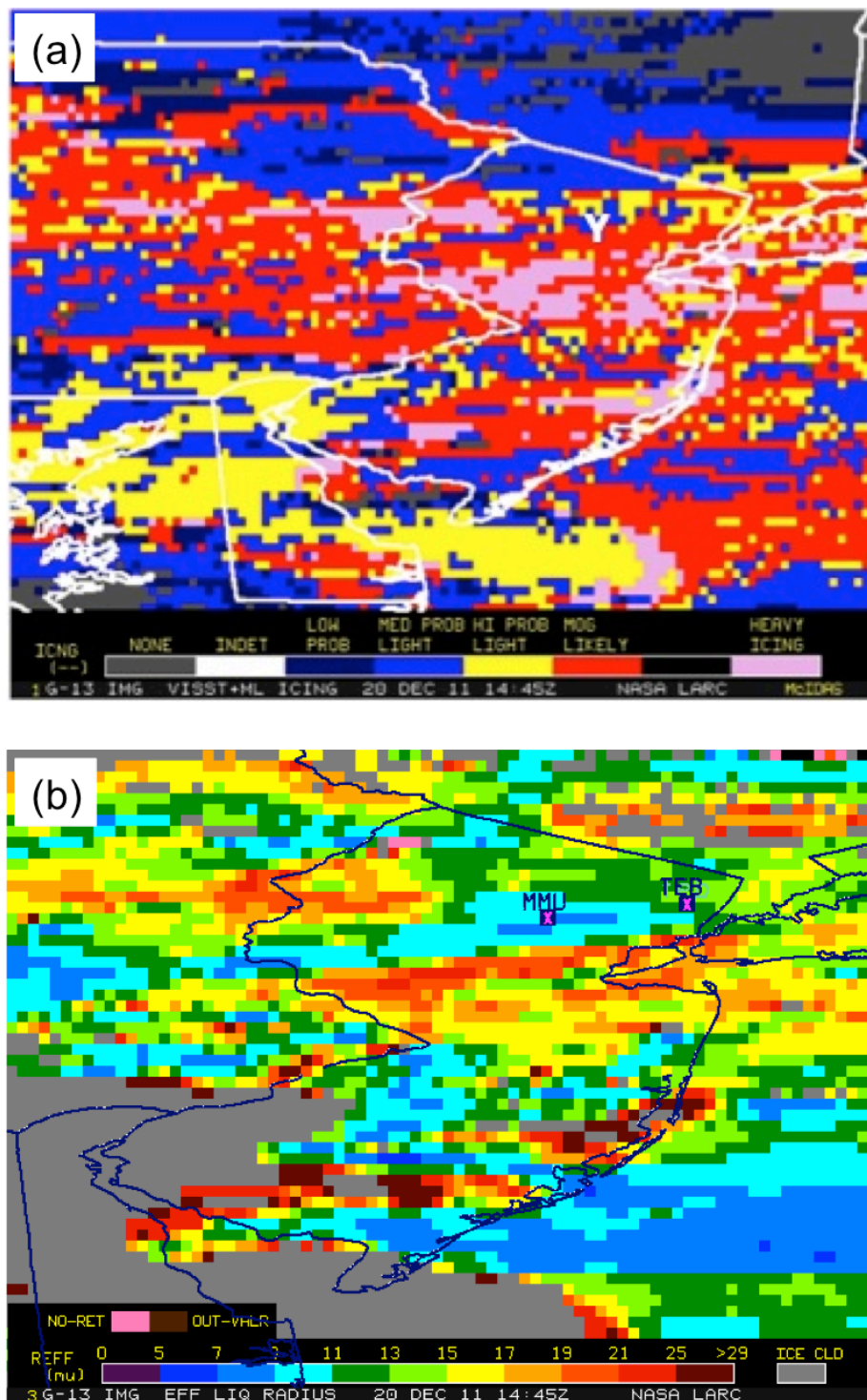
Figure 42. The (a) flight icing threat and (b) CER (μm) derived from GOES-13 data taken at 1445 UTC on 20 December 2011 near the time of a fatal plane crash near Morristown, NJ. The crash site is indicated by the white symbol 'Y' in the top panel.
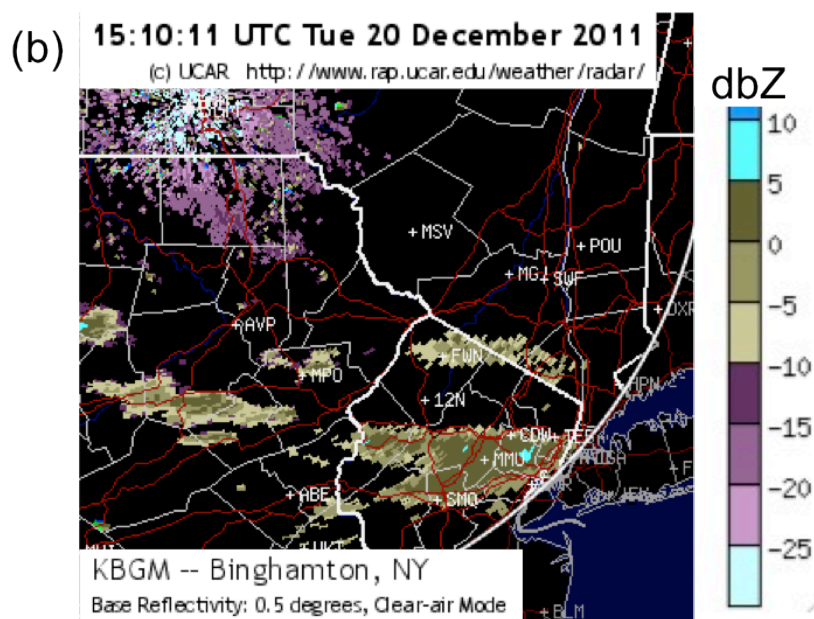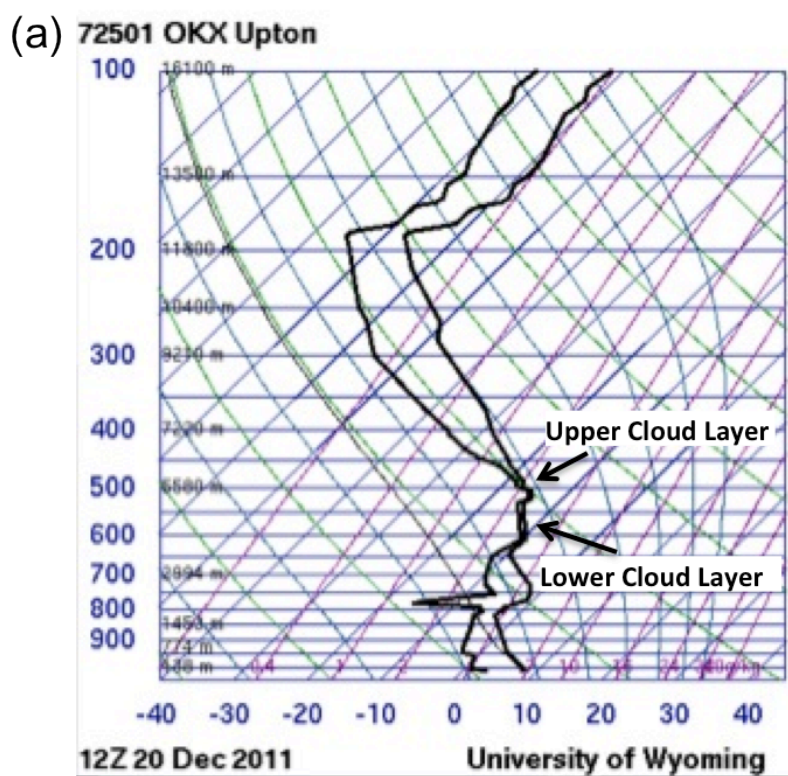
Figure 43. Radiosonde observations of the temperature and humidity profile (a) and weather radar observations (b) taken near the time of a severe icing outbreak over eastern Pennsylvania and New Jersey on 20 December 2011.
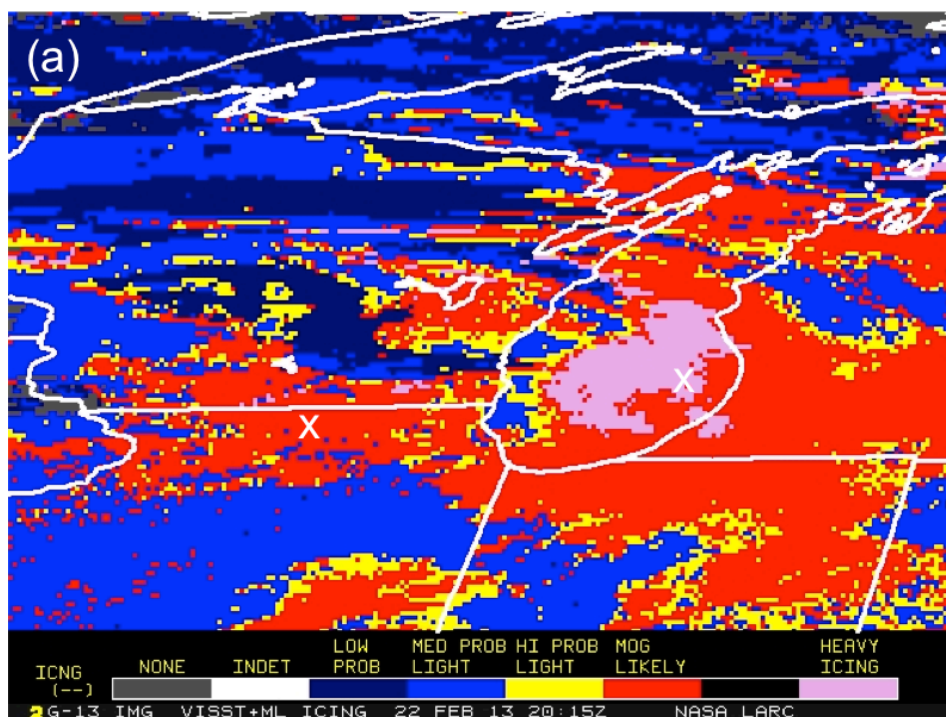
Figure 44. (a) Icing analysis derived from GOES-13 at 2015 UTC on 22 February 2013. The two 'x' symbols indicate the location of severe icing PIREPS filed near that time. (b) Map depicting the location of a SIGMET issued by AWC at 2355 UTC.
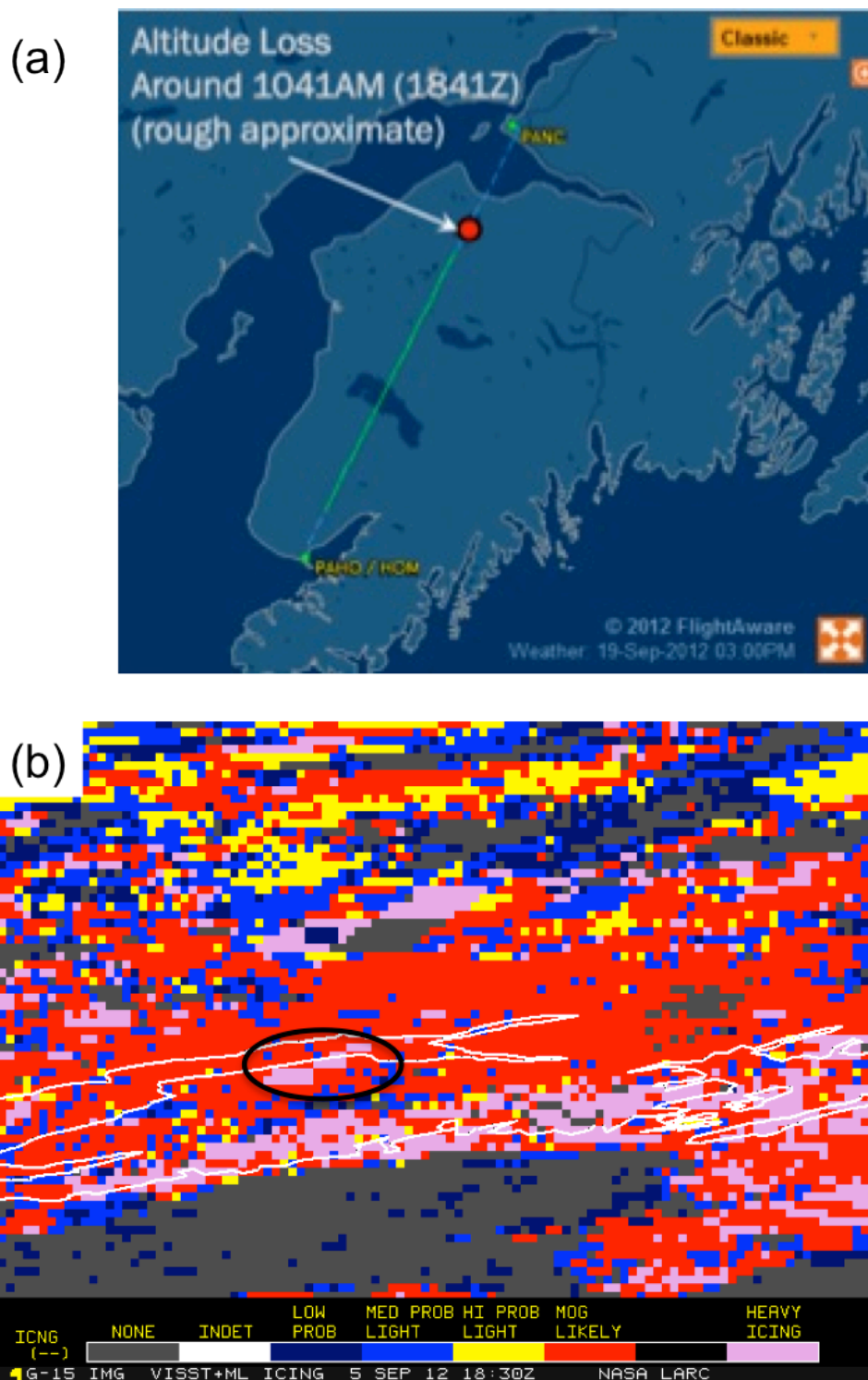
Figure 45. (a) Location that a Bombadier DHC-8 experienced a 5kft altitude loss during an icing encounter after takeoff from Anchorage on 5 September 2012 and (b) the corresponding GOES-15 icing analysis indicating potential severe conditions over the same area of the Alaska Kenai peninsula.
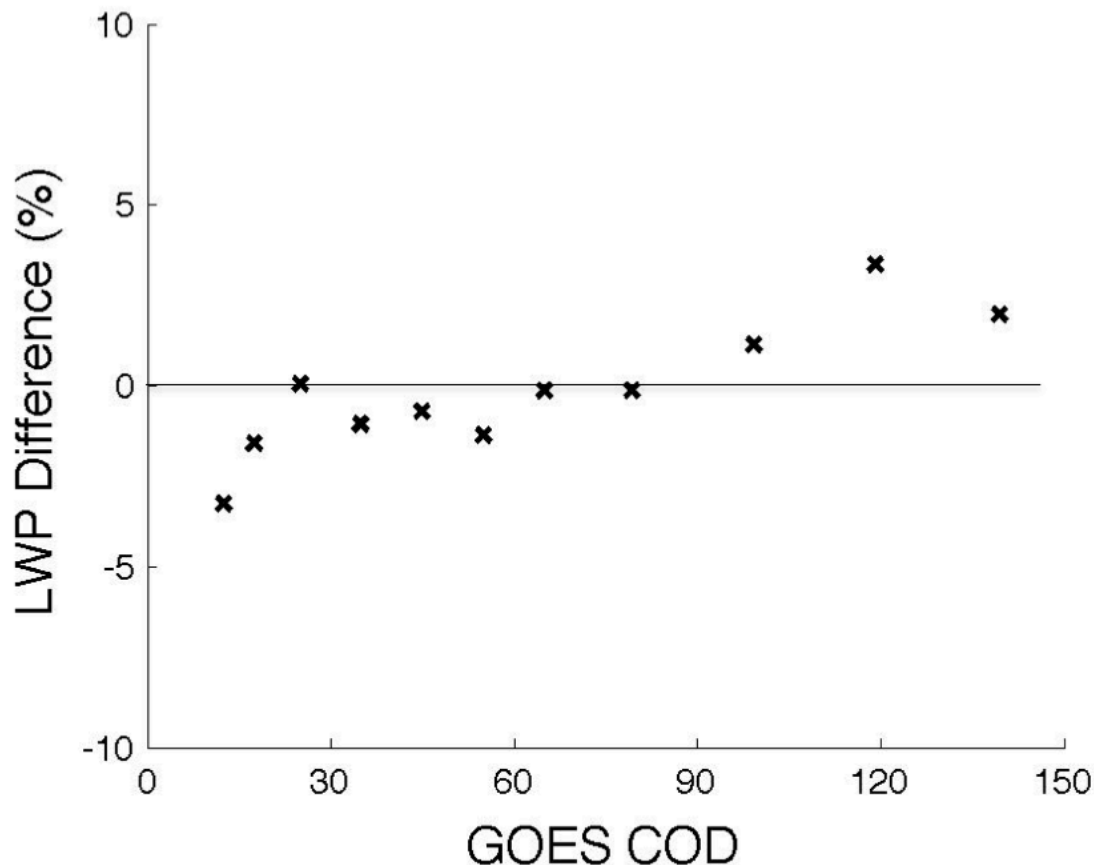
Figure 46. GOES LWP comparison for SLIOW clouds estimated in two different ways; (1) empirically with a parameterization developed from ARM MWR data co-located with GOES VISST COD at the ARM SGP using a 5-year dataset, and (2) from GOES VISST data co-located with icing PIREPS over a 3-month winter period in 2013 and inferred using the profiling technique and climatological guidance from the Thompson microphysics scheme embedded in the RUC cloud analysis system. The mean LWP differences between the values derived from the parameterization and the values estimated from the profiling technique are expressed here as the percentage of the corresponding mean TWP. While not a direct comparison, the relationship shown as a function of the retrieved COD indicates that the cloud phase partitioning in the RUC agrees well with MWR observations over a wide range COD.

Tables

Table 1a. Cloud frequency (%) derived from GOES data and from the GSD-ESRL RAP over the RUC domain shown in Figure 1 and for the period 12-18 November 2012

REGION	All		Low		Mid		High	
	GOES	**RAP**	**GOES**	**RAP**	**GOES**	**RAP**	**GOES**	**RAP**
ALL	67	63	20	22	21	8	26	33
LAND	56	52	13	14	21	8	23	30
OCEAN	75	73	27	28	19	7	30	38
Pacific	81	81	21	26	19	9	41	46
Atlantic	73	68	32	30	18	4	24	34
Gulf of Mex.	71	59	40	33	19	4	12	22

Table 1b. Cloud frequency (%) derived from GOES data and from the NCEP RAP over the RUC domain shown in Figure 1 and for the period 12-18 November 2012

REGION	All		Low		Mid		High	
	GOES	**RAP**	**GOES**	**RAP**	**GOES**	**RAP**	**GOES**	**RAP**
ALL	67	60	20	18	21	9	26	33
LAND	56	52	13	13	21	10	23	30
OCEAN	75	64	27	20	19	7	30	37
Pacific	81	72	21	18	19	9	41	45
Atlantic	73	60	32	23	18	4	24	33
Gulf of Mex.	71	39	40	17	19	5	12	17

Table 2a. CWP derived from GOES data for all clouds and from the GSD-ESRL and NCAR RAP over the RUC domain shown in Figure 1 and for the period 12-18 November 2012

REGION	CWP (gm^{-2})				CWP (gm^{-2})			
	GOES	GSD	Bias	Ratio	GOES	NCEP	Bias	Ratio
ALL	377	280	-97	1.4	396	318	-78	1.3
LAND	439	263	-175	1.7	443	333	-110	1.3
OCEAN	269	295	26	0.9	290	304	14	1.0
Pacific	196	366	169	.5	204	352	148	0.6
Atlantic	305	250	-55	1.2	332	254	-78	1.3
Gulf of Mex.	196	181	-15	1.1	249	197	-52	1.3

Table 2b. Same as 2a but for low clouds with cloud tops below 3 km.

REGION	CWP (gm^{-2})				CWP (gm^{-2})			
	GOES	GSD	Bias	Ratio	GOES	NCEP	Bias	Ratio
ALL	264	95	-169	2.8	307	105	-202	2.9
LAND	357	87	271	4.1	371	120	-251	3.1
OCEAN	162	105	-58	1.6	202	95	-107	2.1
Pacific	127	122	-5	1.0	148	107	-42	1.4
Atlantic	142	115	-26	1.2	167	83	-85	2.0
Gulf of Mex.	92	59	-23	1.4	108	98	-10	1.1

Table 2c. Same as 2a but for mid clouds with cloud tops between 3 and 7 km.

REGION	CWP (gm^{-2})				CWP (gm^{-2})			
	GOES	GSD	Bias	Ratio	GOES	NCEP	Bias	Ratio
ALL	475	204	-271	2.3	472	311	-162	1.5
LAND	436	141	-296	3.1	441	273	-168	1.6
OCEAN	450	310	-140	1.5	455	372	-83	1.2
Pacific	405	350	-55	1.2	424	391	-33	1.1
Atlantic	259	247	-12	1.1	297	297	-1	1.0
Gulf of Mex.	229	358	128	0.6	222	359	137	0.6

Table 2d. Same as 2a but for high clouds with cloud tops above 7 km.

REGION	CWP (gm^{-2})				CWP (gm^{-2})			
	GOES	GSD	Bias	Ratio	GOES	NCEP	Bias	Ratio
ALL	465	470	5	1.0	458	484	26	1.0
LAND	513	418	-95	1.2	507	484	-24	1.1
OCEAN	345	496	151	0.7	341	461	121	0.7
Pacific	235	554	319	0.4	229	490	260	0.5
Atlantic	565	475	-91	1.2	567	469	-98	1.2
Gulf of Mex.	477	362	-114	1.3	475	245	-230	1.9

Table 3a. Mean cirrus cloud IWC (gm^{-3}) during April 2010 derived from CALIPSO and CloudSat (CC), CloudSat only (CS), and from CERES MODIS data from 20-55°N and 65-150°W. The MODIS retrievals were derived with the profiling technique using the 2CICE and CWC-RVOD climatologies of $S(z^*)$ and constrained with the MODIS IWP and MODIS cloud boundaries. The RVOD* column lists the MODIS IWC retrievals when constrained with the MODIS IWP and the CloudSat cloud boundaries.

COD	N	Mean COD	CC-IWC C3M	MODIS-IWC 2CICE	MODIS-IWC RVOD	CS-IWC C3M	MODIS-IWC RVOD	MODIS-IWC RVOD*
0-1	2883	0.6	0.005	0.004	0.004	0.006	0.004	0.005
1-3	7878	1.9	0.008	0.007	0.008	0.010	0.007	0.010
3-6	934	3.9	0.015	0.011	0.015	0.014	0.011	0.015
6-10	171	7.3	0.025	0.018	0.025	0.022	0.018	0.023
0-10	11866	1.8	0.009	0.007	0.009	0.011	0.008	0.010

Table 3b. Similar to Table 3a but for the mean cirrus cloud IWP (gm^{-2}).

COD	N	Mean COD	CC-IWP C3M	MODIS-IWP 2CICE	MODIS-IWP RVOD	CS-IWP C3M	MODIS-IWP RVOD	MODIS-IWP RVOD*
0-1	2883	0.6	8	6	6	7	6	6
1-3	7878	1.9	22	21	21	20	21	21
3-6	934	3.9	58	45	45	39	45	45
6-10	171	7.3	129	91	91	85	91	91
0-10	11866	1.8	23	22	22	20	21	21

Table 3c. Mean cirrus cloud top altitude (km) during April 2010 derived from CALIPSO, CloudSat, and from the CERES MODIS Ed4 cloud properties between 20-55°N and 65-150°W.

COD	N	Mean COD	Cloud Top Height (km) CALIOP	CPR	MODIS
0-1	2883	0.6	10.9	10.1	10.3
1-3	7878	1.9	11.7	10.7	11.2
3-6	934	3.9	12.7	11.7	11.1
6-10	171	7.3	13.2	12.3	12.3
0-10	11866	1.8	11.6	10.6	11.0

Table 4a. Mean and bias values of cloud IWC (gm^{-3}) during April 2010 derived for optically thick clouds (MODIS COD>10) above the -20°C altitude level from CALIPSO and CloudSat (CC) and from CERES MODIS data from 20-55°N and 65-150°W. The MODIS retrievals were derived with the profiling technique using the RUC and the RUC+CC (Hybrid) climatologies of *S(z*)* and constrained with the parameterized MODIS TWP and MODIS-derived cloud boundaries.

COD	N	Mean COD	CC-IWC C3M	MODIS-IWC Hybrid	MODIS-IWC RUC	BIAS Hybrid	BIAS RUC
10-20	5083	14	0.051	0.047	0.050	0.004	0.001
20-40	4149	28	0.087	0.083	0.089	0.004	-0.002
40-80	2635	54	0.154	0.161	0.172	-0.007	-0.018
80-150	730	106	0.297	0.325	0.323	-0.028	-0.026
150	965	150	0.568	0.480	0.496	0.088	0.072
10-150	13562	41	0.141	0.143	0.150	-0.002	-0.009

Table 4b. Similar to Table 4a but showing the mean values of IWP (gm^{-2}) retrieved and computed above the -20°C altitude level (IWP253). The Hybrid0 column lists the MODIS IWP253 computed without employing the TWP parameterization (i.e. assuming that the retrieved IWP represents the TWP). For context, the traditional full column MODIS IWP and the parameterized TWP derived from MODIS are also shown in columns 4 and 5.

COD	N	Mean COD	MODIS IWP	MODIS TWP	CC-IWP253 C3M	MODIS-IWP253 RUC	MODIS-IWP253 Hybrid	MODIS-IWP253 Hybrid0
10-20	5083	14	310	405	191	157	169	132
20-40	4149	28	592	849	333	302	324	228
40-80	2635	54	1132	1754	668	718	767	486
80-150	730	106	2239	3815	1231	1522	1507	868
150	965	150	3006	5437	2549	2608	2688	1409
10-150	13562	41	860	1342	551	557	583	364

Table 5. Icing intensity mapping adapted from Politovitch (2003). The original value of 0.066 was adjusted to 0.093 to separate 'Light' from 'Moderate or Greater' icing in the satellite technique.

LWC (gm^{-2})	Icing Category
< 0.01	No icing
0.010 to 0.017	Trace
0.017 to 0.030	Trace-light
0.030 to 0.093*	Light
0.093* to 0.120	Light-moderate
0.120 to 0.200	Moderate
0.200 to 0.370	Moderate-heavy
> 0.370	Heavy

Table 6. Example cloud and icing parameters retrieved for two clouds with the same CTH but different values of COD.

Parameter	Source	Cloud 1	Cloud 2
COD	VISST	50	100
CER (μm)	VISST	50	50
IWP (gm^{-2})	VISST	1500	3000
TWP (gm^{-2})	parameterization	2212	5004
LWP (gm^{-2})	parameterization	321	679
LWP (gm^{-2})	Profile method	200	362
CTH (kft)	VISST	35.4	35.4
CBH (kft)	VISST	8.9	5.9
Zfrz (kft)	RAOB	3.9	3.9
ITH (kft)	Profile method	17.5	19.0
IBH (kft)	Profile method	8.9	5.9
Icing Intensity Index (max)	Profile method	3	5
Icing Probability (max)	Profile method	0.63	0.9
FIT Intensity Index	Profile method	Light	MOG
FIT Probability Index	Profile method	Medium	High

Table 7. GOES-13 SFITv2.0 icing detection statistics when compared to PIREPS over the eastern CONUS from 1 January - 31 March, 2013.

Cloud Conditions	N	PODY	Accuracy
OVC Liquid	5759	99%	90%
OVC Ice	2713	98%	83%
All OVC regions	11851	99%	88%

Table 8a. GOES-13 SFITv2.0 icing intensity detection statistics when compared to PIREPS over the eastern CONUS from 1 January - 31 March, 2013. The most dominant intensity found in the satellite region was used when constructing this comparison.

Cloud Top Conditions	N	PODL	PODM	Accuracy	MOG Icing %	
					PIREP	SAT
Liquid	5013	60%	61%	60%	27	46
Ice	2236	61%	45%	57%	26	40

Table 8b. GOES-13 SFITv2.0 icing intensity detection statistics when compared to PIREPS over the eastern CONUS from 1 January - 31 March, 2013. Regions found to contain both 'light' and 'MOG' conditions from satellite are considered as 'hits' in both categories if they both cover more than 30% of the 20-km radius area.

Cloud Top Conditions	N	PODL	PODM	Accuracy	MOG Icing %	
					PIREP	SAT
Liquid	5013	76%	66%	73%	27	36
Ice	2236	80%	47%	72%	26	27

List of Acronyms

AD   adding-doubling

AIRMET   airmen's meteorological information

ARM   Atmospheric Radiation Measurement

AWC   Aviation Weather Center

BTD   brightness temperature difference

C3M   CERES/CloudSat/Calipso/MODIS

CALIOP   Cloud-Aerosol Lidar with Orthogonal Polarization

CBH   cloud base height

CC   CloudSAT/CALIPSO

CER   cloud effective radius

CERES   Clouds and Earth's Radiant Energy System

CEH   cloud effective height

CET   cloud effective temperature

CIP   Current Icing Potential

COD   cloud optical depth

CONUS   contiguous United States

CPR   Cloud Profiling Radar

CTH   cloud top height

CTP   cloud top pressure

CTT   cloud top temperature

CWC   cloud water content

CWP   cloud water path

DARDAR ra**DAR**/li**DAR**

DOE   Department of Energy

DSS   decision support systems

ECMWF   European Center for Medium-Range Weather

ESRL   Earth Systems Research Laboratory

FAA   Federal Aviation Administration

FAR   false alarm rate

FIT   flight icing threat

FSLW   fraction of super-cooled liquid water

GA   general aviation

GDCP   GOES derived cloud properties

GEOsat   geostationary satellite

GFS   Global Forecast System

GSD   Global Systems Division

GOES   Geostationary Operational Environmental Satellite

H   cloud geometric thickness

ICARE   Cloud-Aerosol-Water-Radiation Interactions

IFI   in-flight icing

IR   infrared

ITCZ   intertropical convergence zone

ISCCP   International Satellite Cloud Climatology Project

IWC   ice water content

IWP   ice water path

IWP253   ice water path computed at altitudes above the 253K level

LaRC   NASA Langley Research Center

LWC   liquid water content

LWP   liquid water path

MCAT   modified co2 absorption technique

MDCP   MODIS derived cloud properties

METAR   Meteorological Terminal Aviation routine weather Report

MICROBASE   Continuous Baseline Microphysical Retrieval

ML   multi-layer

MMCR   millimeter-wavelength cloud radar

MODIS   Moderate Resolution Imaging Spectroradiometer

MOG   moderate or greater

MWR   microwave radiometer

NAS   National Airspace System

NASA   National Aeronautics and Space Administration

NCAR   National Center for Atmospheric Research

NCEP   National Centers for Environmental Prediction

NEXRAD Next Generation Weather Radar

NEXTGEN   Next Generation Transportation System

NOAA   National Oceanic and Atmospheric Administration

NRT   near real-time

NWP   numerical weather prediction

NWS   National Weather Service

PCLD   probability for the occurrence of cloud

PDF   probability distribution function

PICING   probability for icing

PIREP   pilot report

PODL   probability of detecting light icing conditions

PODM   probability of detecting MOG icing conditions

PODY   probability of detecting the occurrence of icing conditions

PODN   probability of detecting the 'no icing' conditions

PSLW   probability for the occurrence of super-cooled liquid water

RAP   Rapid Refresh model

RGB   Red Green Blue

RO   radar only

RUC   Rapid Update Cycle model

RVOD   radar constrained with visible optical depth

SEAC4RS   Studies of Emissions and Atmospheric Composition, Clouds and Climate Coupling by Regional Surveys

SFIT   satellite-derived flight icing threat

SIGMET   airmen's significant meteorological information

SIR   solar-infrared

SGP   southern great plains

SL   single-layer

SLD   super-cooled large droplets

SLIOW   single-layer ice over water clouds

SLW super-cooled liquid water

SLWC super-cooled liquid water content

SLWP super-cooled liquid water path

SSM/I Special Sensor Microwave/Imager

SZA solar zenith angle

TRMM Tropical Rainfall Measuring Mission

TWC total water content

TWP total water path

VDF vertical distribution function

VIRS Visible and Infrared Scanner

VIS visible

VISST visible infrared solar-infrared split-window technique

VZA viewing zenith angle

WRF Weather Research and Forecasting

Appendices

A.1 Version 1 icing algorithm paper published in the Journal of Applied Meteorology and Climatology

Smith, W. L., P. Minnis, C. Fleeger, D. Spangenberg, R. Palikonda, L. Nguyen, 2012: Determining the Flight Icing Threat to Aircraft with Single-Layer Cloud Parameters Derived from Operational Satellite Data. J. Appl. Meteor. Climatol., 51, 1794–1810.

Determining the Flight Icing Threat to Aircraft with Single-Layer Cloud Parameters Derived from Operational Satellite Data

WILLIAM L. SMITH JR. AND PATRICK MINNIS

NASA Langley Research Center, Hampton, Virginia

CECILIA FLEEGER, DOUGLAS SPANGENBERG, AND RABINDRA PALIKONDA

Science Systems and Applications, Inc., Hampton, Virginia

LOUIS NGUYEN

NASA Langley Research Center, Hampton, Virginia

ABSTRACT

An algorithm is developed to determine the flight icing threat to aircraft utilizing quantitative information on clouds derived from meteorological satellite data as input. Algorithm inputs include the satellite-derived cloud-top temperature, thermodynamic phase, water path, and effective droplet size. The icing-top and -base altitude boundaries are estimated from the satellite-derived cloud-top and -base altitudes using the freezing level obtained from numerical weather analyses or a lapse-rate approach. The product is available at the nominal resolution of the satellite pixel. Aircraft pilot reports (PIREPs) over the United States and southern Canada provide direct observations of icing and are used extensively in the algorithm development and validation on the basis of correlations with Geostationary Operational Environmental Satellite imager data. Verification studies using PIREPs, Tropospheric Airborne Meteorological Data Reporting, and NASA Icing Remote Sensing System data indicate that the satellite algorithm performs reasonably well, particularly during the daytime. The algorithm is currently being run routinely using data taken from a variety of satellites across the globe and is providing useful information on icing conditions at high spatial and temporal resolutions that are unavailable from any other source.

---

1. Introduction

It is natural for clouds to contain supercooled liquid water (SLW) droplets at altitudes where the air temperature is below freezing. When SLW comes in contact with a hard surface such as the frame of an aircraft, it freezes, thereby icing the airframe. As ice accumulates on an aircraft, it alters the airflow, which can increase drag and reduce the ability of the airframe to create lift, leading to control problems with potentially disastrous consequences. Over the last half-century, a significant percentage of weather-related aviation accidents have been attributed to icing (National Aviation Safety Data Analysis Center 2005). Typically, the flight icing threat

(FIT) to aircraft is reduced by avoidance or by protecting the aircraft with deicing and/or anti-icing equipment. Severe icing can overwhelm an aircraft's icing protection system, however. Model analyses, forecasts, and pilot reports (PIREPs) currently constitute much of the database available to pilots for assessing the icing conditions in a particular area. Such data may be uncertain or sparsely available. Icing conditions can be highly variable, often occurring in small areas that cannot be resolved with current icing diagnosis and forecasting methods, which tend to overestimate the areal coverage of the FIT. Thus, avoidance can be expensive, resulting in significant increases in flight time or delays on the ground. Although there have been improvements in systems to mitigate aircraft icing, no aspect of aircraft operations is immune to the threat.

The intensity of aircraft icing depends on meteorological factors, including the cloud temperature, liquid

water content, and droplet size (Rasmussen et al. 1992), and the level of severity depends on the intensity as well as on characteristics of the airframe and flight parameters. Because it is possible to infer these meteorological factors, or closely related cloud parameters, from satellite data (Minnis et al. 1995, 2004, 2011a), and because SLW is often found to reside in the top several hundred meters of cloud layers (Rauber and Tokay 1991), satellite data can be used advantageously to diagnose icing conditions. Curry and Liu (1992) developed an icing product that is based on cloud parameters derived for SLW clouds using microwave satellite remote sensing data. This technique is limited to the data with relatively low spatial and temporal resolution taken over oceanic regions from spaceborne meteorological microwave sensors, and this is perhaps most relevant for military applications. Ellrod and Nelson (1996) developed a multispectral thresholding technique using Geostationary Operational Environmental Satellite (GOES) imager data to discriminate clouds likely to be composed of SLW at cloud top. That product was later enhanced with estimates of cloud-top altitude to provide an upper altitude boundary for the icing layer (Ellrod and Bailey 2007), but no information on the base altitude or icing intensity was determined. Thompson et al. (1997) used satellite data to improve icing diagnoses on the basis of numerical weather analyses by eliminating areas with warm cloud tops.

Bernstein et al. (2005) describe methods to identify and forecast areas with potential aircraft icing conditions by blending relevant data from multiple sources such as satellite, surface, radar, lightning, and routine PIREPs with model forecasts of temperature, relative humidity, SLW, and vertical velocity. The current and forecast icing products (CIP and FIP, respectively) resulting from this comprehensive approach are proving useful to the aviation community and are available over the contiguous United States (CONUS) and southern Canada in near–real time as supplementary information at the National Oceanic and Atmospheric Administration (NOAA) Aviation Weather Center. Although research is under way for incorporating satellite-derived cloud properties in the CIP (Haggerty et al. 2008), the current version only uses satellite data in a rudimentary way as in Thompson et al. (1997). Smith et al. (2000) employed a theoretically based cloud parameter retrieval system to identify SLW clouds and found excellent correspondence with icing PIREPs provided that high-level ice clouds did not obscure the satellite field of view. Smith et al. (2003) found reasonably good correspondence between the cloud liquid water path (LWP) and effective radius R_e derived for SLW clouds from *GOES-8* data and similar parameters derived from

surface-based remote sensors and aircraft in situ measurements. They also found a weak correlation between the LWP and PIREP icing intensity. Minnis et al. (2004) exploited these relationships and developed a satellite-based icing algorithm that is based on satellite-derived cloud parameters. Bernstein et al. (2006) found that it was particularly useful for directing a research aircraft into icing conditions. That algorithm was selected as the prototype candidate algorithm for the NOAA GOES-R program. NOAA is developing a suite of algorithms to derive geophysical parameters from its next-generation geostationary satellite system to improve weather forecasting and diagnoses of hazardous weather. Under sponsorship by the GOES-R Algorithm Working Group, an advanced version of the algorithm has been developed, demonstrated, tested, and delivered to the GOES-R program office.

The purpose of this paper is to describe the first-generation FIT algorithm developed for GOES-R and efforts to validate and demonstrate the potential utility to the aviation community using current GOES data. The theoretical basis for the algorithm is discussed, and the current formulation is described. The satellite-based icing diagnoses are compared with icing PIREPs, Tropospheric Airborne Meteorological Data Reporting (TAMDAR), and National Aeronautics and Space Administration (NASA) Icing Remote Sensing System (NIRSS) data. The paper concludes with a summary of the validation work and expectations for future improvements. Note that the algorithm and nomenclature presented here refer to the icing hazard associated with naturally occurring SLW in the atmosphere. A more mysterious icing hazard known to cause jet engine power loss and damage as a result of cloud ice particle ingestion (e.g., Mason et al. 2006) is a different phenomenon that is being addressed elsewhere and in future studies.

2. Data

Although aircraft icing conditions can form anywhere, they are most commonly found in two geographical regions over North America (Bernstein et al. 2007). The first includes the Pacific Northwest, western British Columbia in Canada, and Alaska. The second extends from the Canadian Maritimes stretching west and southwest to encompass the Great Lakes region, Ohio River Valley, and Hudson Bay. Much of this area is within the observation domain of the GOES imagers (*GOES-W* and *GOES-E*), which are well suited to monitor the evolution of clouds and associated weather conditions because of their relatively high spatial and temporal resolutions, nominally 4 km (1 km) in the

infrared (visible), and every 15 min. There fortunately are a number of other observing systems in this domain that characterize icing conditions that can be used to develop, demonstrate, and corroborate the satellite-based FIT. Icing PIREPs, TAMDAR, and NIRSS, respectively, offer direct subjective, direct objective, and ground-based remote observations of icing conditions. These data and their associated products are described in more detail below.

a. GOES-derived cloud products

For over a decade, NASA Langley Research Center (LaRC) has been routinely deriving cloud parameters from GOES imager data and has made these products available to the scientific and weather forecasting communities (Minnis et al. 2008a). The cloud retrieval methods were developed for application to the Moderate Resolution Imaging Spectroradiometer (MODIS) for the Clouds and the Earth's Radiant Energy System (CERES) global climate program (Minnis et al. 2011a) and have been adapted for application to GOES data beginning with *GOES-8* in the late 1990s. The primary algorithms used to derive cloud properties from GOES radiance data are the visible–infrared–solar-infrared–split-window technique (VISST) and solar-infrared–infrared–split-window technique (SIST). The VISST operates during the daytime using the 0.65-, 3.9-, 11-, and 12- (or 13.3) μm channels, whereas the SIST operates at night using the 3.9-, 11-, and 12- (or 13.3) μm channels. Cloudy pixels are determined using the method described by Minnis et al. (2008b). Cloud parameters are derived for the cloudy pixels using a set of parameterizations of the Earth–atmosphere solar reflectance (during daytime) and infrared emittance (day and night) models that incorporate cloud contributions for each relevant wavelength to match the observed satellite radiances with radiative transfer calculations using the assumption that each cloud layer is composed of either ice crystals or water droplets (Minnis et al. 2011a). In the real-time processing system, the GOES imager data are sampled from 4 km to 8 km to reduce the latency in producing the cloud products that is due to limited computational resources. In addition to LWP and R_e, the GOES-derived cloud products (GDCP) include the cloud phase, effective ice particle diameter D_e, ice water path (IWP), optical depth (COD), effective temperature T_c, height Z_c, and pressure P_c; cloud thickness ΔZ; and cloud-top height Z_t and pressure P_t. The cloud optical properties can be derived for a wide range of cloud thicknesses during the daytime since the solar reflectance at visible wavelengths is sensitive to changes in COD from values of less than 1 to values over 100. Since only infrared channels are available from

GOES at night, there is little sensitivity to variations in COD for optically thick clouds. Thus, at night, cloud optical properties are only derived for optically thin clouds (COD < 6).

The LaRC CERES and GOES cloud products have been rigorously validated with cloud parameters derived from ground-based remote sensing and in situ data collected at the U.S. Department of Energy (DOE) Atmospheric Radiation Measurement (ARM) Program sites (Dong et al. 2002, 2008; Smith et al. 2008, Xi et al. 2010, and others). They have also recently been favorably compared to cloud parameters derived from active remote sensors aboard the *Ice, Cloud, and Land Elevation Satellite* (*ICESat*), the *Cloud–Aerosol Lidar and Infrared Pathfinder Satellite Observations* (*CALIPSO*) and *CloudSat* satellites (e.g., Minnis et al. 2008c, 2011b). An example of the LaRC cloud products derived from *GOES-10* and *GOES-12* is shown in Fig. 1, which depicts the retrieved cloud-top phase, Z_t, COD, R_e, LWP, and the cloud-base altitude Z_b, which is from the difference between Z_t and ΔZ. These parameters provide unique information about clouds that can be used to infer the potential for aircraft icing. For example, the cloud-top temperature (not shown) and cloud-top phase can be used to detect the presence of SLW. In this example, a large area of SLW (denoted by the cyan color in Fig. 1a) is detected over much of the upper Midwest and southern Canada in association with a storm system centered over the Great Lakes. The associated SLW droplet sizes and their densities can be inferred from the R_e and LWP images in Figs. 1d and 1e while Z_t and Z_b, shown in Figs. 1b and 1f, respectively, provide upper and lower altitude boundaries for the potential icing layers. These satellite-derived parameters are critical inputs to the FIT algorithm described below.

b. Icing PIREPs

PIREPs constitute the most widely available direct observations of in-flight icing conditions, particularly over the CONUS, and thus are used extensively in algorithm development and validation despite the fact that they have known deficiencies (Kane et al. 1998). They are spatially and temporally biased, and the biases are not systematic. Many years of experience with icing research aircraft, from which icing PIREPs were routinely filed, indicate that geolocation errors are on the order of 10–20 km [F. McDonough, University Corporation for Atmospheric Research (UCAR), 2010, personal communication]. PIREPs include intensity reports, which should be useful for validating the satellite algorithm. The intensity reports are subjective, however, and are based on pilot experience as well as on airframe and flight characteristics, and thus they can be difficult to
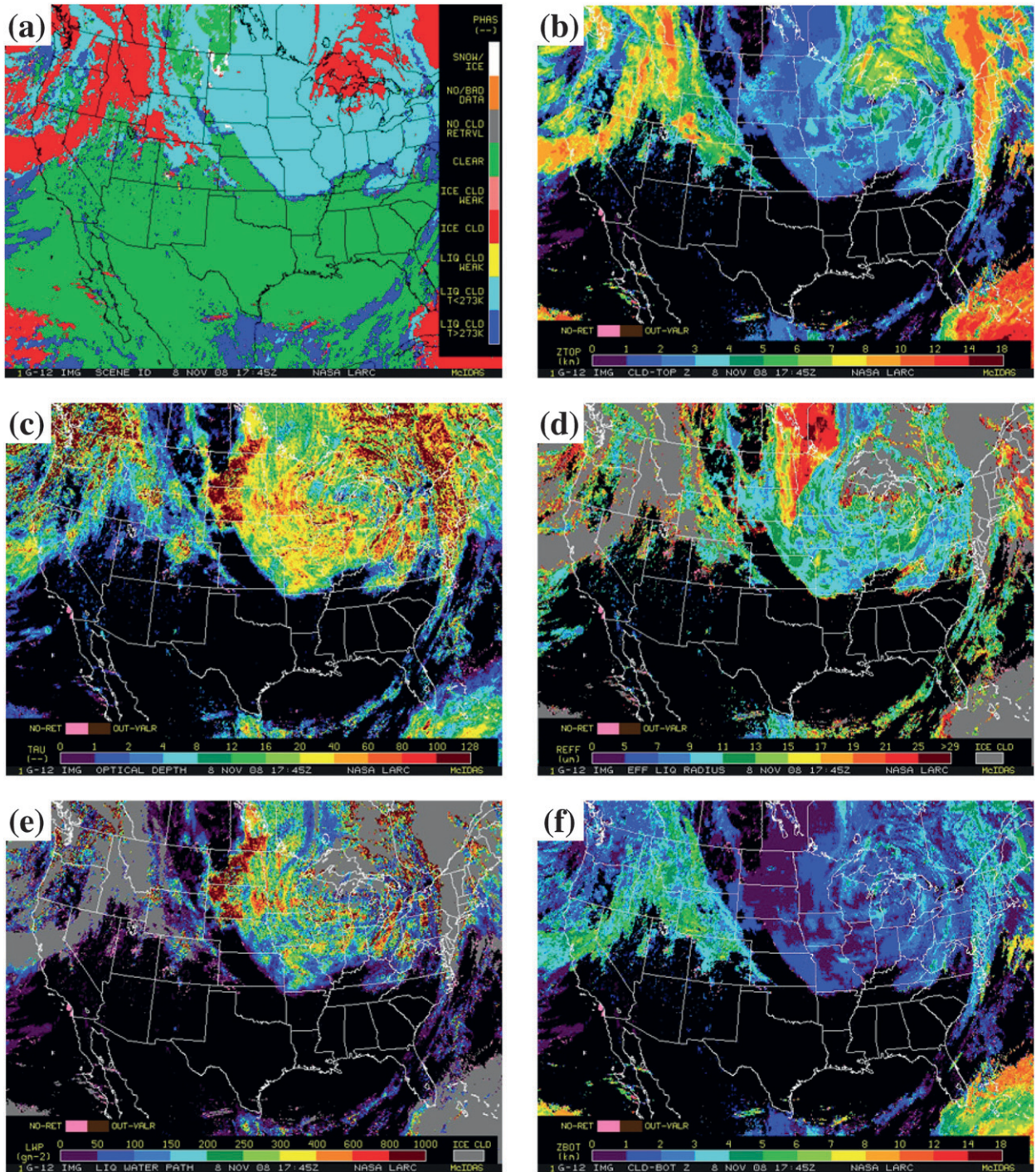
FIG. 1. Select cloud parameters derived from *GOES-E* and *GOES-W* at 1745 UTC 8 Nov 2008: (a) cloud-top phase, (b) cloud-top altitude (kft; 1 ft = 0.3048 m), (c) COD, (d) effective droplet size (μm) for liquid clouds, (e) LWP (g m^{-2}), and (f) base altitude (kft). These and other satellite-derived products are available online (http://angler.larc.nasa.gov).

interpret. A typical distribution of icing-intensity PIREPs shown in Fig. 2 for two winter periods over the CONUS indicates that most of the positive reports fall into only two of the eight possible intensity categories and that

there are relatively few negative ("no icing") reports. Icing PIREPs have been found to be useful for validating icing detection (Smith et al. 2000) but are inappropriate to compute standard measures of
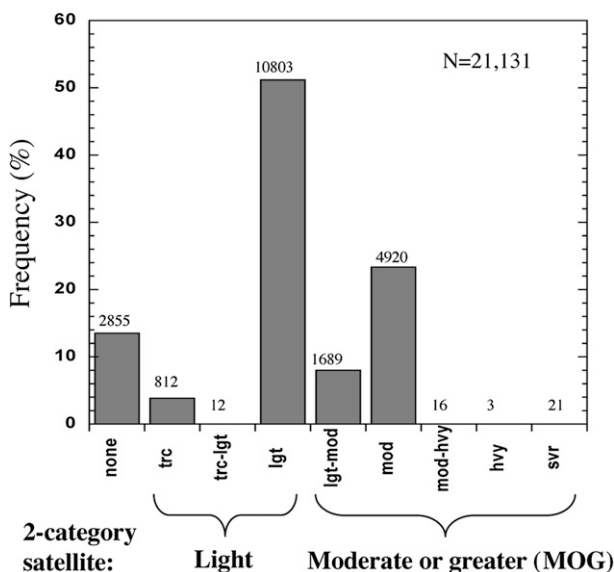
FIG. 2. PIREP icing intensity for two winter periods (November–March 2006/07 and 2007/08) over the CONUS. The classification strategy for the two-category satellite technique is also indicated.

overwarning, such as the false-alarm ratio (FAR; Brown and Young 2000).

c. TAMDAR

TAMDAR is the sensor currently deployed on approximately 400 commercial aircraft operating over the CONUS, Alaska, and Canada. TAMDAR is a low-cost sensor that was developed by AirDat, LLC, for NASA. It is designed to measure and report winds, temperature, humidity, turbulence, and icing from regional commercial aircraft (Daniels 2002). The TAMDAR icing sensor contains two independent infrared emitter–detector pairs mounted on the probe to detect ice accretion. The accretion of at least 0.5 mm of ice on the leading edge surface will block the beams and result in a positive detection. When ice is detected, internal heaters mounted within the probe melt the ice and the measurement cycle repeats. The heaters are powered for at least 1 min and the deicing cycle occurs each time ice is detected. The icing data are given as yes (icing) or no (no icing) reports. Thus, TAMDAR provides a direct, objective measure of the occurrence of in-cloud icing. Potential information on the icing intensity is not currently being extracted from the measurements. Data collected during the Great Lakes Fleet Experiment (GLFE) in 2005 are analyzed here to provide an initial assessment of their utility for validating the satellite FIT. The current TAMDAR deployment has shifted to include the western states and Alaska. These data will be analyzed in a future study.

d. NIRSS

The NIRSS has been collecting valuable information on icing conditions since 2005 at the NASA Glenn Research Center in Cleveland, Ohio. This location is well situated for observing icing conditions because it lies in the heart of a climatological icing bull's-eye (Bernstein et al. 2007). The NIRSS was developed to demonstrate a ground-based remote sensing system concept that could provide accurate detection and warning of in-flight icing conditions in the near-airport environment. The system fuses data from radar, lidar, and multifrequency microwave radiometer sensors to quantify the icing environment and compute the icing hazard (Reehorst et al. 2009) on the basis of the expected ice accretion severity for the measured environment (Politovitch 2003). Although the system does not measure icing directly, this remote sensing concept appears to offer some advantages for satellite validation that are not found elsewhere. For example, it appears that these unique data could help to quantify the FIT algorithm FAR, which cannot be done reliably with PIREPs or TAMDAR data. Several years of NIRSS data have been analyzed, and comparisons with the FIT derived from GOES are presented below.

3. Satellite methods

The potential for in-cloud aircraft icing and its severity depend on many factors related to the particular aircraft and the weather conditions. Some aircraft will accumulate ice in certain conditions while other aircraft will remain ice free in the same cloud. These aircraft-related factors are not considered here. Meteorological factors that contribute to icing intensity and severity include the concentration of supercooled water droplets and the droplet sizes. In general, larger droplets and/or larger concentrations of droplets or higher liquid water content (LWC) contribute to more severe icing. The satellite-derived R_e is related to the cloud droplet sizes while the derived LWP is related to the concentration since it is an estimate of the vertically integrated LWC. Correlations found between the satellite-derived LWP and R_e with icing PIREPs (Smith et al. 2003; Minnis et al. 2004) suggest that some information on icing intensity may be contained in the satellite data. The current version of the FIT algorithm has been developed 1) to exploit these relationships during the daytime for clouds that can be determined to pose an icing threat to aircraft because of the presence of SLW and 2) to take advantage of the capability to resolve highly variable cloud properties with high-resolution satellite data, as depicted in Fig. 1.

TABLE 1. Logic table for mapping the cloud phase and optical depth products to the icing mask.

Cloud phase	COD	Icing mask
Clear	—	No icing
Water	All	No icing
SLW	COD > 1.0	Icing
SLW	COD ≤ 1.0	No icing
Ice	COD ≤ 6.0	No icing
Ice	COD > 6.0	Unknown

a. Icing mask

Because SLW is a prerequisite for aircraft icing, the first step in the satellite FIT algorithm is to identify cloudy areas where SLW is likely to exist. An icing mask is constructed for each geolocated pixel with valid radiance data and for which the cloud algorithms have been properly executed and have returned valid retrievals. The purpose of the icing mask is to determine, to the extent possible, which cloudy pixels pose an icing threat to aircraft on the basis of the retrieved cloud-top temperature T_t, thermodynamic phase, and COD and to differentiate these pixels from clear and cloudy pixels that pose no icing threat or for which the icing threat cannot currently be determined (e.g., pixels composed of high-altitude optically thick ice-phase-topped clouds, or multilayered thin-ice-cloud-over-thick-liquid-cloud systems). The simple logic adopted to map the cloud-top phase and COD to the icing mask is shown in Table 1. A $T_t = 272$ K is used to distinguish warm water clouds from SLW clouds. For SLW clouds, a COD threshold of 1.0 is chosen to eliminate the very thinnest clouds associated with very low LWC values from the icing threat. For ice-phase-topped clouds, a COD threshold of 6.0 is

used to eliminate thin clouds that are unlikely to overlap SLW clouds, while the icing threat for optically thicker clouds (COD > 6), which may or may not overlap SLW clouds, is considered to be unknown. The icing mask derived using the data from Fig. 1 is shown in Fig. 3 along with the icing intensity reported by pilots near the same time. Good correspondence is apparent between the icing PIREPs and the cyan areas representing potential icing conditions in the satellite-derived icing mask. Areas where there is no icing and where the icing threat cannot be determined are denoted by the gray and white colors, respectively.

b. Supercooled liquid water path

A potential issue in using an integral parameter such as the LWP as a proxy for icing in clouds with SLW tops is that it may include the mass of warm cloud water for clouds that extend to altitudes below the freezing level. A simple approach is adopted to estimate the supercooled fraction of the total LWP (SLWP) to eliminate the warm cloud mass from the icing threat. The approach requires knowledge of the cloud geometric thickness, the freezing level, and the vertical distribution of liquid water. The freezing level Z_{fr} is obtained from the satellite-derived T_t and Z_t, assuming a moist-adiabatic lapse rate:

$$Z_{fr} = Z_t + (T_t - 273.15 \, \text{K})/6.5. \tag{1}$$

The cloud geometric thickness ΔZ is obtained using empirical formulas that depend on the COD (for water clouds) as described in Minnis et al. (2011a). For liquid water clouds,

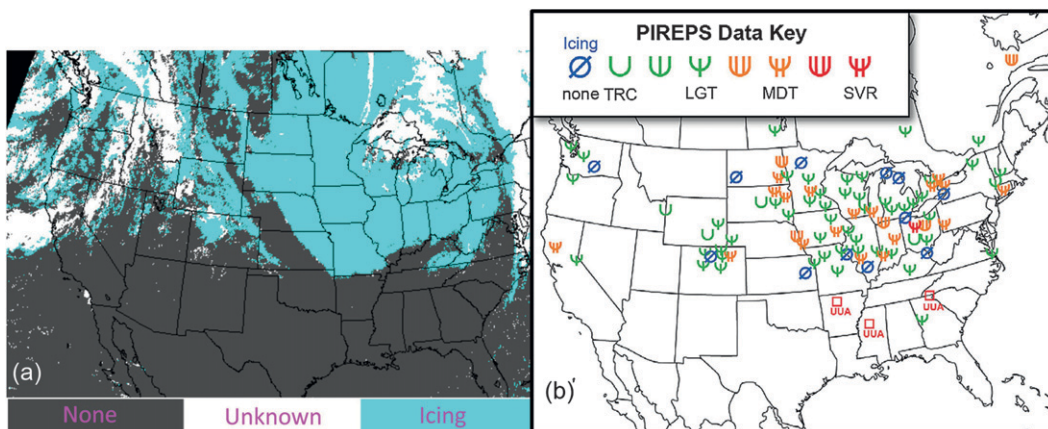$$\Delta Z = 0.39 \ln(\text{COD}) - 0.01. \tag{2}$$

FIG. 3. (a) Icing mask at 1745 UTC and (b) corresponding pilot reports of icing intensity from 1600 to 2000 UTC 8 Nov 2008. The PIREP image was obtained online from the NOAA/National Weather Service (NWS) Aviation Weather Center (http://aviationweather.gov/adds/pireps/java/).

The minimum allowable ΔZ is 0.02 km. The cloud-base altitude Z_b is

$$Z_b = Z_t - \Delta Z. \qquad (3)$$

For this study, a uniform vertical distribution of cloud liquid water is assumed. Thus, in this version, we define the SLWP as

$$\text{SLWP} = \text{LWP} \quad (Z_b \geq Z_{\text{fr}}) \quad \text{and} \qquad (4)$$

$$\text{SLWP} = \text{LWP}(Z_t - Z_{\text{fr}})/\Delta Z \quad (Z_b < Z_{\text{fr}}). \qquad (5)$$

c. Icing probability and intensity

Because of the nature of icing PIREPs and, in particular, of the fact that most positive icing-intensity reports fall into just two of the eight available intensity categories (light and moderate), a strategy is adopted to recategorize the eight intensity levels into two broader categories to serve as a more realistic target for the intensity component of the satellite algorithm. Hereinafter, "light" icing will be used to refer to reports in the first three PIREP intensity categories (trace, trace–light, and light), and "moderate or greater" (MOG) icing will refer to the other categories (light–moderate, moderate, moderate–heavy, heavy, and severe), as indicated in Fig. 2.

The icing PIREPs shown in Fig. 2 were matched with the coincident GDCP derived from *GOES-11* and *GOES-12* data taken over the CONUS to find relationships between icing and the satellite-derived cloud properties. Given the uncertainties in the PIREP locations, the satellite results were averaged in a 20-km-radius region centered at the location of each icing PIREP (about twenty-five 8-km pixels). This analysis was restricted to overcast SLW scenes as determined by the LaRC cloud-phase retrieval and to daytime [solar zenith angle (SZA) < 82°] data. Figure 4 depicts the frequency of occurrence of none, light, and MOG icing reports as a function of the GOES-derived SLWP. The results from the 1359 matches are binned in increments of 100 g m^{-2}. As SLWP increases, the number of negative and light icing reports decreases while the number of moderate or greater reports increases. Despite the aforementioned uncertainties associated with icing PIREPs and their superposition on high-resolution cloud fields such as the GOES-derived SLWP, which may be highly variable, the results in Fig. 4 are encouraging. Moreover, they are physically realistic considering that larger values of LWP are likely to be associated with larger values of LWC and/or larger cloud thickness. Thicker SLW clouds may be associated with an increased
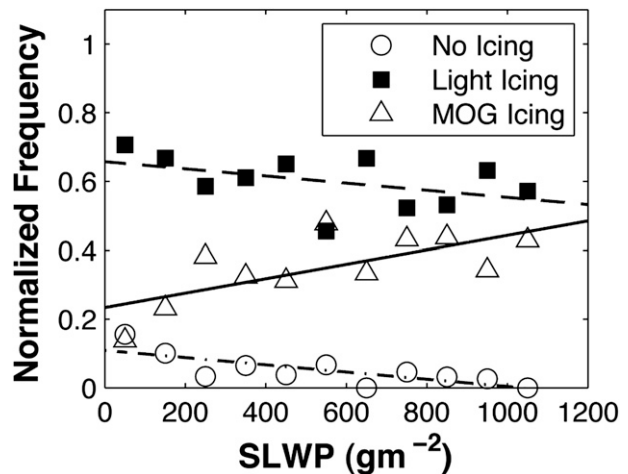
FIG. 4. Relative frequency of icing PIREPs vs GOES-derived SLWP for two winter periods (November–March 2006/07 and 2007/08) over the CONUS. The two-bin PIREP intensity categories are denoted as light and MOG, as in Fig. 2.

icing threat because of the likelihood that they increase the aircraft's exposure time to SLW as it passes through the cloud.

Using the data in Fig. 4, the probability of icing was computed as a function of SLWP. Those values were multiplied by the probability of icing found from the data for values of $R_e = 5$ μm (composed of data with $R_e < 8$ μm) and $R_e = 16$ μm (composed of data with $R_e \geq 16$ μm). These two sets of data were normalized to yield a 100% probability of icing for SLWP = 1050 g m^{-2} and $R_e = 16$ μm. These threshold values were chosen somewhat arbitrarily on the basis of visual interpretation of the data, since more definitive values could not be determined empirically. Thus, it is assumed that the combination of SLWP and R_e values at or above these thresholds yields a 100% probability for icing. The probabilities and best-fit curves for the two values of R_e, intended to represent the upper and lower limits, are shown in Fig. 5. In this procedure, the negative icing reports were duplicated several times to account for the sampling bias relative to positive icing reports that is apparent in Fig. 2. This bias in negative reports is due to the lack of incentive to report no icing. The results shown in Fig. 5 are consistent with our theoretical understanding of icing, indicating an increased likelihood of icing with increased SLWP and R_e. From these results, the icing probability (IP) is formulated in the FIT algorithm as

$$\text{IP} = 0.252 \log_{10}(\text{SLWP}) - 0.110 \quad (R_e = 5 \, \mu\text{m}) \quad \text{and}$$
$$(6)$$
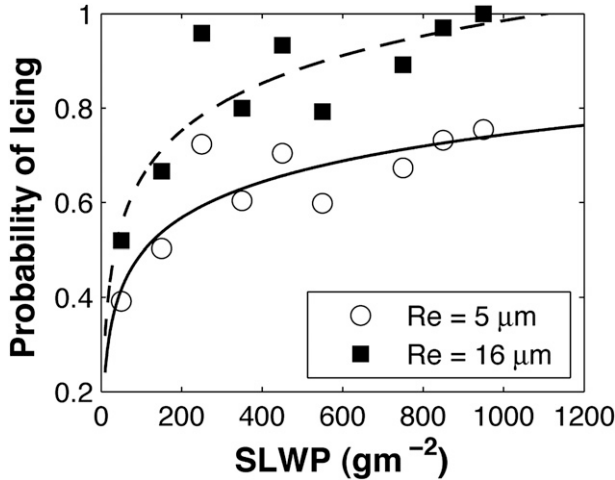
FIG. 5. Renormalized probability of in-cloud aircraft icing as a function of satellite-derived LWP and model fit for two values of R_e.

$$IP = 0.333 \log_{10}(SLWP) - 0.015 \quad (R_e = 16 \, \mu m). \qquad (7)$$

Linear interpolation between the results of (6) and (7) is used for pixels with R_e between 5 and 16 μm. Pixels with larger or smaller values of R_e are assigned the appropriate extreme value. Values of IP < 0.4 are classified as low probability. For values between 0.4 and 0.7, pixels are classified as medium probability, and values exceeding 0.7 are classified as high probability.

Table 2 lists the results of a statistical analysis performed on the matched satellite and icing PIREP dataset to determine any relationships between the GDCP and icing intensity. The mean and standard deviation for a number of satellite-derived cloud parameters are shown. When the values were computed with all of the matched data, the mean results indicate that, on average, there is little dependency found between icing-intensity PIREPs and R_e. There are several possible explanations for this result. In this analysis, R_e has been derived from the highly absorbing 3.9-μm channel, available on current GOES, which is mostly sensitive to cloud droplets very close to cloud top. It is possible that the cloud-top information extracted from this channel is not very representative of the droplet size spectra affecting icing conditions as reported by pilots, when the aircraft is well below cloud top. The scattering phase function for cloud hydrometeors is also very sensitive to droplet size when the solar angles and satellite viewing geometry are such that strong back-scatter occurs, which may result in larger uncertainties or noise in the R_e retrievals. This phenomenon occurs in the late morning (early afternoon) for *GOES-E* (*GOES-W*) over the CONUS in the autumn and winter months when icing is most prevalent. More work is needed to reduce uncertainties in R_e retrievals using other satellites, multiple-wavelength R_e retrievals, and perhaps improved forward models to better understand and quantify any relationships between R_e and aircraft icing. A stronger dependence is found for the LWP, but there is not much separation between the mean LWP found for the light and MOG categories shown in the mean results when using all of the data.

To reduce the potential ambiguity associated with temporal and spatial matching errors on the correlations shown in the results for all data in Table 2, a strategy was adopted to filter the data. In the filtering procedure, a set of conservative SLWP thresholds is set for specific PIREP icing intensities on the basis of the assumption that the two are positively correlated as shown in Fig. 4. Thus, in the filtered dataset, the matched data are eliminated for the following scenarios: 1) all positive icing reports, if SLWP < 50 g m^{-2}; 2) all positive icing reports with MOG icing intensity, if SLWP < 200 g m^{-2}; 3) all icing reports, if the intensity is less than light and the SLWP > 750 g m^{-2}; and 4) all icing reports with light or less intensity if SLWP > 1000 g m^{-2}. About 20% of the original matched data are absent in the filtered dataset. Much stronger sensitivity to LWP is found in the filtered dataset (Table 2) since the correlation

TABLE 2. Mean and standard deviation (in parentheses) found for satellite-derived cloud parameters matched with icing PIREPs during winters of 2006/07 and 2007/08 in three categories: 0 = no icing, 1 = light icing, and 2 = moderate or greater icing. Results are shown for the entire matched dataset ("all data") and for the filtered dataset ("filtered data").

| Cloud property (GOES)	PIREP intensity (all data)			PIREP intensity (filtered data)		
	0	1	2	0	1	2
COD	35.98 (25.41)	42.89 (28.49)	49.60 (29.32)	31.25 (22.52)	35.74 (21.98)	56.71 (27.64)
R_e (μm)	11.65 (3.17)	12.03 (3.11)	12.11 (3.02)	11.35 (2.68)	12.00 (3.15)	12.11 (2.95)
LWP (g m^{-2})	460.56 (569.58)	614.21 (653.18)	715.54 (678.19)	321.61 (369.75)	381.67 (317.59)	836.65 (694.14)
SLWP (g m^{-2})	332.31 (444.03)	530.65 (592.64)	671.68 (664.48)	193.16 (160.45)	338.91 (232.74)	805.90 (676.69)
T_c (K)	263.39 (4.44)	262.65 (3.96)	262.05 (3.62)	263.62 (4.45)	262.61 (3.87)	261.84 (3.50)
ΔZ (km)	1.23 (0.36)	1.34 (0.37)	1.43 (0.36)	1.17 (0.33)	1.27 (0.29)	1.51 (0.34)
No.	90	838	431	79	659	346
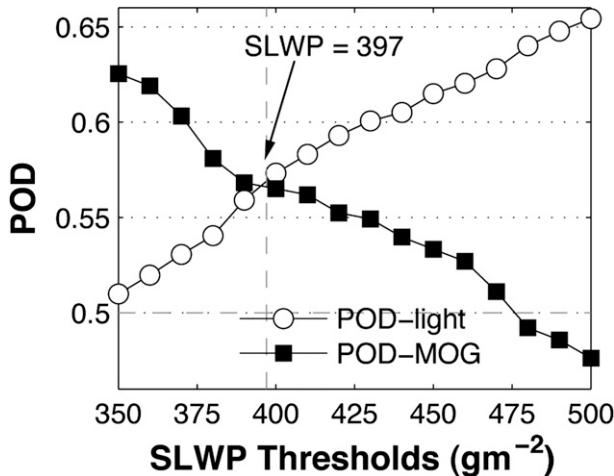
FIG. 6. Probabilities of detecting light and MOG icing conditions as a function of the GOES-derived SLWP in snow-free conditions during the winters of 2006/07 and 2007/08.

between the icing intensity and the LWP has increased. Also note that the filtered dataset generally produces much lower LWP standard deviations. From a statistical point of view, there is arguably good reason to employ the filtering procedure to both develop and validate the algorithm, but the procedure is somewhat arbitrary, and there is no guarantee or requirement that independent evaluators of the algorithm would also employ it. Thus, we have developed an approach to determine intensity thresholds for the current version of the FIT algorithm using all of the matched (unfiltered) data. We have, however, chosen to report the results that are shown in Table 2 to provide the mean cloud properties found for this icing dataset and to demonstrate the improved sensitivity of the LWP and SLWP to icing intensity reported by pilots when a simple filtering procedure is applied.

The filtering procedure is also employed in our validation studies (section 4) to help to bound the uncertainties. For the current algorithm, intensity thresholds were derived, using the unfiltered dataset, by iteratively determining the SLWP threshold that maximizes both the probability of detection for the light (PODL) and MOG (PODM) categories. Different thresholds were derived for snow and snow-free scenes since the snow albedo was not accounted for in this version of the LaRC cloud analyses. The bright snow background could bias the cloud microphysical property retrievals. An example for the snow-free dataset is shown in Fig. 6, which indicates a maximum POD of 0.55 for the two intensity categories at an SLWP threshold of 379 g m^{-2}. Daily snow maps obtained from the National Snow and Ice Data Center (now available from the National Ice Center: http://

TABLE 3. The two-category intensity thresholds and probability of detection found using the satellite-derived SLWP over snow (100% coverage), snow-free (0% coverage), and all surfaces for consecutive winters (November–March) between 2006 and 2008.

Surface	SLWP (g m^{-2})	POD (%)	N
All	405	58	2341
Snow	475	63	735
No snow	379	55	1310

www.natice.noaa.gov) are used to stratify the matched satellite–PIREPs dataset for snow and snow-free scenes. Table 3 summarizes the SLWP thresholds and the intensity POD (PODL is equal to PODM in this technique) found following this approach for snow, snow-free, and all surfaces.

d. Algorithm output

The satellite-derived icing mask, probability, and intensity are combined to form the FIT index, depicted in Table 4, which is the primary output of the FIT algorithm. The FIT index is color coded for display purposes and is illustrated in Fig. 7 for the 8 November 2008 case. In general, there is good correspondence between the FIT output and the icing-intensity PIREPs shown in Fig. 3b. That is, warmer colors associated with more severe icing and the cooler colors associated with less severe or no icing tend to match reasonably well on a large scale. It is apparent how much more information the current FIT product can provide during the daytime when compared with a binary yes/no icing product (e.g., icing mask in Fig. 3). The approach described here may resolve some of the natural variability in the FIT to a significant degree but, of course, needs to be validated to the extent possible.

4. Verification

To help to gain an understanding of the potential utility of the satellite-based FIT product to the aviation

TABLE 4. FIT index output from the satellite FIT algorithm.

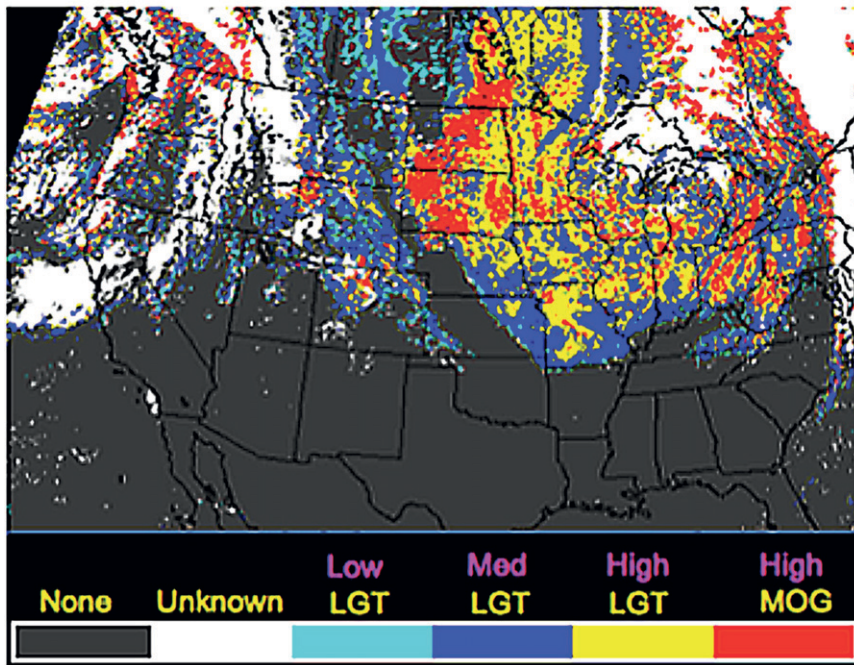| FIT index	Description
−7	No retrieval/bad data
−9	Missing data/other
0	No icing
1	Unknown
2	Low probability of light icing (daytime only: SZA < 82°)
3	Medium probability of light icing (daytime only: SZA < 82°)
4	High probability of light icing (daytime only: SZA < 82°)
5	High probability of MOG icing (daytime only: SZA < 82°)
6	Icing possible (Nighttime only: SZA ≥ 82°)

FIG. 7. Flight icing threat derived from GOES at 1745 UTC 8 Nov 2008.

community, icing information from PIREPs, TAMDAR, and NIRSS is used for intercomparison. Each dataset has unique advantages and disadvantages (described briefly in section 2), with their own associated uncertainties that may not be well understood in some cases. Because the satellite FIT algorithm has no vertical resolution and produces a bulk icing index limited to SLW-topped clouds (generally lower-level clouds with limited vertical extent that are not obscured by high-level clouds), and considering the uncertainties in satellite-derived boundary layer cloud heights and the uncertainties associated with the validation data, we have excluded altitude in our validation thus far. The matching approach that has been adopted here ensures to the extent possible that the satellite and validation data represent the same cloud volume. It is also important to emphasize again that aircraft icing is not just a meteorological phenomenon, but depends on characteristics of the airframe, flight trajectory, residence time, and other factors. Furthermore, there is currently no accepted definition for icing severity that is based on cloud microphysical parameters (e.g., LWC or R_e) or the accretion rate on an airframe (M. Politovitch, UCAR, 2010, personal communication).

Despite the somewhat ill-defined nature of aircraft icing, a method was developed to quantify the potential accuracy of the satellite product by correlating it with icing information extracted from PIREPs, TAMDAR,

and NIRSS data. The data were matched in time and space for overcast conditions to eliminate any ambiguity that might arise in partly cloudy conditions. Two-by-two contingency tables are constructed to help to quantify the intercomparisons with standard skill scores (e.g., Wilks 2006). Each cell in the table provides the frequency with which a particular observation or estimate occurs at a specific threshold. Two sets of contingency tables are formed. The first table is composed of yes or no icing frequencies to test the icing-detection capability, as in Table 5. The second table is composed of light or MOG icing frequencies to test the icing-intensity capability, as in Table 6. The set of skill scores computed, and discussed below, is defined in Table 7.

a. Comparisons with icing PIREPs

The FIT derived from *GOES-11* and *GOES-12* was compared with icing PIREPs over the CONUS between

TABLE 5. Contingency table describing possible outcomes for icing detection.

Icing detected by satellite	Icing observed	
	Yes	No
Yes	h (hit)	f (false alarm)
No	m (miss)	n (correct negatives)

TABLE 6. As in Table 5, but for icing intensity.

Satellite intensity	Observed intensity	
	Light	MOG
Light	hL (light hit)	mM (MOG miss)
MOG	mL (light miss)	hM (MOG hit)

1 November and 31 March 2008–09 and 2009–10. This dataset is independent from that used in the algorithm development (2006–08). In this analysis, all pixels within 20 km and 15 min of each icing PIREP were matched under the condition that the 20-km-radius region was completely overcast. Regions containing any SLW are considered to be positive detections from GOES. This strategy resulted in 22 551 and 9851 matches during the daytime and nighttime, respectively. The skill in detecting icing conditions was determined from the contingency tables shown in Tables 8 and 9. The PODY, PODN, and accuracy are 62%, 42% and 61% (56%, 54%, and 56%), respectively, during daytime (nighttime). False detections are common, but compose only a small percentage of the total (FAR = 5%–6%). These results are nearly identical to those found by Ellrod and Bailey (2007) during wintertime. The large number of misses is due to the fact that this version of the satellite FIT algorithm, like that of Ellrod and Bailey (2007), cannot detect icing conditions below high-level ice clouds. When these ''undetectable'' conditions are eliminated from the validation dataset, the satellite FIT algorithm performance is much better. Tables 10 and 11 depict the contingency tables for the same data used to construct Tables 8 and 9 but excluding the cases with high optically thick ice cloud. Under these conditions, the PODY, PODN, and accuracy are found to be 98%, 6%, and 93% (64%, 49%, and 63%), respectively, during daytime (nighttime). It is not possible to adequately quantify false alarms using icing PIREPs because of the low bias in ''no icing'' observations (Brown and Young 2000). PODN is also highly uncertain and misleading for the same reason. The high values of PODY and accuracy found for the daytime data indicate that the satellite technique has an excellent detection capability relative to positive icing PIREPs, provided high clouds do not obscure the satellite view. The skill at night is good but is less than that found during the daytime because of the availability of just a few infrared channels that have poor sensitivity to optically thick cloud microphysical properties.

A contingency table was formed to test the two-category intensity component of the FIT algorithm during daytime for overcast SLW regions (number $N = 5711$) and is shown in Table 12. The probabilities of detecting light (PODL) and moderate or greater (PODM) icing conditions are 59% and 57%, respectively, and the accuracy is 58%. Considering the uncertainties associated with icing PIREPs and the associated difficulties in accurately matching the reports to satellite data, these comparison results are probably reasonable. The data were also stratified for snow and snow-free scenes. The intensity accuracy was also found to be 57% for both, which is an encouraging consistency indicating that the LWP thresholds developed with the 2006–08 data (Table 3) worked relatively well for the 2008–10 dataset. Better results were found using the filtering procedure described in section 3, which eliminates about 15% of, what appear to be, the more ambiguous data and yields a PODL, a PODM, and an intensity accuracy of 67%, 69%, and 67% respectively.

Figure 8 depicts a frequency histogram of cloud-top temperatures for all of the matched satellite and icing PIREP data used in this study between November 2006 and March 2010. The percentage of clouds with bases estimated to be below the freezing level is indicated for each 5-K temperature bin and is found to occur about 25% of the time, overall. To gauge the impact of our strategy to partition the cloud mass for the subfreezing portion (SLWP), the algorithm was also evaluated with data using intensity thresholds developed in the same manner described earlier but using the LWP rather than the SLWP. The overall improvement in the intensity accuracy using the SLWP approach is just a few percent

TABLE 7. Contingency-table scoring definitions.

Score	Meaning	Formula
PODY	Probability of detecting icing	$h/(h + m)$
PODN	Probability of detecting no icing	$n/(f + n)$
FAR	False-alarm ratio	$f/(h + f)$
Accuracy	Icing-detection accuracy	$(h + n)/(h + m + f + n)$
TSS	True skill score	PODY + (1 − PODN).
PODL	Probability of detecting light icing	$hL/(hL + mL)$
PODM	Probability of detecting MOG icing	$hM/(hM + mM)$
Intensity accuracy	Icing-intensity accuracy	$(hL + hM)/(hL + mL + mM + hM)$

TABLE 8. Frequency of yes/no icing reports found for the matched GOES–PIREP dataset constructed over consecutive winters (November–March) between 2008 and 2010 for overcast regions during daytime.

Icing detected by satellite	Icing observed	
	Yes	No
Yes	13 075	790
No	8107	579

TABLE 10. Frequency of yes/no icing reports found for the matched GOES–PIREP dataset constructed over consecutive winters (November–March) between 2008 and 2010 for overcast regions with no high thick clouds during daytime.

Icing detected by satellite	Icing observed	
	Yes	No
Yes	13 075	790
No	237	46

when evaluating all of the data. However, when considering only the data for which SLWP and LWP differ (occurs 25% of the time), a relative accuracy improvement of about 20% is realized using the SLWP approach.

b. Comparisons with NIRSS

The NIRSS icing retrieval uses ground-based remote sensing data to estimate the FIT over a single surface site (Reehorst et al. 2009) in Cleveland, Ohio. Although icing is not measured directly, NIRSS provides an objective estimate using active and passive remote sensors (i.e., microwave radiometer, cloud radar, and ceilometer) and thus has the capability to provide vertical resolution, with some assumptions. In the NIRSS approach, the vertical distribution of supercooled liquid water is estimated using climatological profiles that are based partially on experience and measurements taken from the NASA Glenn Twin Otter during icing research aircraft missions, and using the cloud radar reflectivity measured at the site. The profiles are constrained with the integrated liquid water (LWP) inferred from the microwave radiometer and cloud boundaries derived from the radar and ceilometer. For the subfreezing portion of the cloud, LWC is converted to eight levels of icing intensity with relationships that were developed from an airfoil modeling study (Politovitch 2003). An example of the NIRSS icing retrieval is shown in Fig. 9 along with the corresponding cloud boundaries and FIT derived from GOES on 12 February 2010. For this case, there is reasonably good agreement between the satellite-derived cloud boundaries and FIT with the NIRSS results.

Three years of NIRSS icing retrievals taken between 2008 and 2010 were analyzed and matched with the satellite data when the GDCP indicated overcast conditions. The icing threat was estimated from the GOES data using pixels within 20 km of the site. A bulk icing intensity was computed from the NIRSS results, for direct comparison with the satellite FIT, by averaging the vertical mean NIRSS LWC over a 20-min period centered at the time when *GOES-12* scanned Cleveland. The mean LWC was converted to icing intensity using the NIRSS conversion factors and the same categorical partitioning shown in Fig. 2. Contingency tables were constructed as before to evaluate the estimates of satellite icing detection and intensity relative to the NIRSS data. For this dataset, there were 885 matches, including 174 cases with high ice cloud obscuration. PODY, PODN, FAR and TSS were found to be 76%, 62%, 10%, and 38%, respectively. With respect to NIRSS data, the FIT-algorithm icing-detection accuracy is 73%. As before, eliminating the "unknown" cases yielded different statistics. In that case, the accuracy is 90%, and the PODY, PODN, FAR, and TSS are found to be 100%, 22%, 10%, and 22%, respectively. The low values of PODN and TSS are due to the relatively low number of no-icing cases (most of the NIRSS data were obtained during winter), and to a significant number of false alarms due to thin cirrus contamination in the satellite retrievals. A detailed analysis of the satellite and cloud radar imagery for the false-alarm points indicated that many of these cases were thin cirrus over warm water clouds, which were misclassified as SLW pixels in the satellite analyses.

The severity component of the FIT algorithm was also tested relative to the NIRSS data. The PODL and PODM were found to be remarkably consistent, with values of 77% and 78%, respectively. The overall accuracy in the FIT intensity is 77%. These results are

TABLE 9. As in Table 8, but during nighttime.

Icing detected by satellite	Icing observed	
	Yes	No
Yes	5158	273
No	4104	316

TABLE 11. As in Table 10, but during nighttime.

Icing detected by satellite	Icing observed	
	Yes	No
Yes	5158	273
No	2859	261

TABLE 12. Frequency of the two-category icing intensity found for the matched GOES–PIREP dataset constructed over consecutive winters (November–March) between 2008 and 2010 for regions determined from GOES to contain overcast SLW clouds.

	Observed intensity	
Satellite intensity	Light	MOG
Light	2385	716
MOG	1675	935

encouraging considering that the FIT algorithm is tuned to icing PIREPs while the NIRSS intensity is tuned to an airfoil model, and considering the different sensitivities and assumptions associated with the satellite and ground-based remote sensing techniques.

c. Comparisons with TAMDAR

The FIT algorithm was applied to the GDCP derived from daytime *GOES-12* data from 1 to 26 April 2005 and was compared with TAMDAR data taken during the GLFE. The pixel-level icing parameters derived from GOES are averaged, by spatially weighting the four closest pixels to each TAMDAR observation taken within 15 min of the satellite observation. There were 440 542 TAMDAR observations, of which 13 321 indicated icing, 8951 indicated that the heater was on so that icing was not detectable at that time, and the rest indicated that no icing was observed. Unlike the relatively few PIREPs (most of which are reported during icing conditions), TAMDAR takes continuous data. As a result, about 95% of the TAMDAR reports indicate no icing. Thus, the GOES and TAMDAR comparison statistics in the results will be biased toward the TAMDAR no-icing category if filters are not properly applied to remove insignificant reports (e.g., from cloud-free areas).

Figure 10 shows an example of satellite-derived icing indices compared with the TAMDAR icing indicators on a Mesaba Airlines flight (with TAMDAR serial number 247) between 1800 and 1830 UTC 22 April 2005. Good agreement is found for this single-layer cloud case. The satellite FIT is a bulk index for the icing layer as indicated by the vertical bars. The TAMDAR measurements indicating yes or no icing are also plotted as a function of altitude. During the majority of the flight segment, the aircraft was inside the GOES-retrieved cloud boundaries and reported icing that corresponds well to the GOES analysis. During the descent below cloud base, the TAMDAR no longer reported icing while GOES still detected icing above the aircraft. This illustrates the need to ensure, to the extent possible, that only in-cloud TAMDAR reports be compared with the GOES FIT.
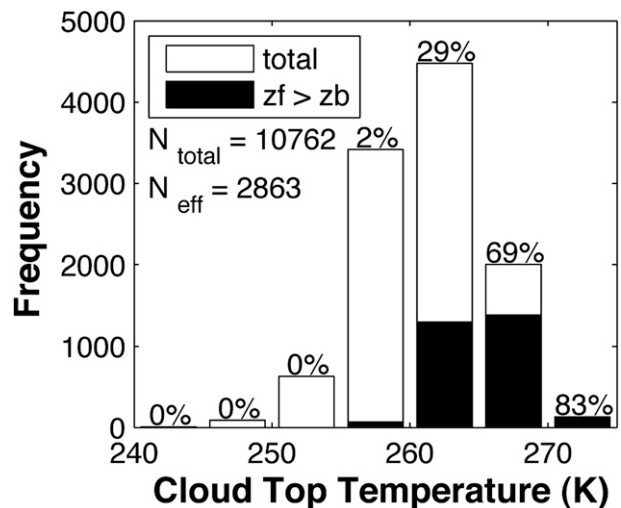

FIG. 8. Frequency histogram of cloud-top temperature for all of the matched satellite and icing PIREP data used in this study between November 2006 and March 2010. The percentage of clouds with bases estimated to be below the freezing level is indicated for each 5-K temperature bin.

To compare statistically the TAMDAR data with GOES without biasing the results, only TAMDAR reports at altitudes within the GOES-derived cloud boundaries are used. This condition reduced the total number of daytime TAMDAR reports (with heater off) to 17 140. This includes 5048 cases in which icing could not be determined from GOES because of obscuration by high ice clouds. If we classify these points as no icing from GOES, then the PODY, PODN, accuracy, and FAR are found to be 45%, 67%, 72%, and 85%, respectively. Eliminating the GOES unknown points yields values of 87%, 49%, 53%, and 85%. Thus, a reasonable value for PODY (87%) was found using TAMDAR, which agrees well with the values found with the other validation datasets, but the remaining statistics are relatively poor. This is due to the high number of false alarms (FAR is 84%), most of which were determined to arise as a result of inaccuracies in the cloud altitude boundaries derived from GOES. Because the retrieved cloud-base and -top heights have an uncertainty of about 1 km (Smith et al. 2008), it is likely that many of the TAMDAR no-icing reports outside of clouds are being included in the statistics with the GOES icing detections. Thus, the PODY appears to be the only derived metric with much value, considering the comparison method used here. We plan to use the temperature and humidity profiles in future analyses of TAMDAR data to try to improve the definition of the actual cloud boundaries penetrated by the instrumented aircraft and, it is
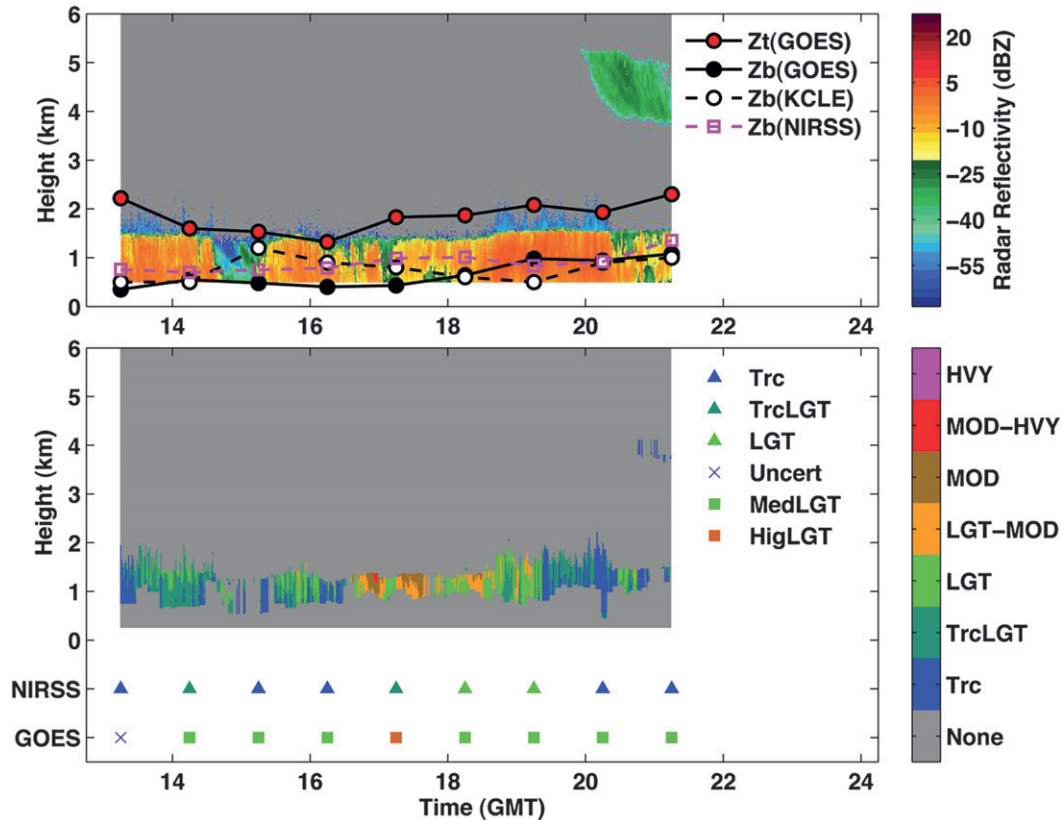
FIG. 9. Comparison of flight icing threats derived from NIRSS and GOES for 12 Feb 2010. (top) NIRSS radar reflectivity and (bottom) icing-intensity profiles with satellite-derived cloud boundary overlay (red and black circles). Cloud base measured by ceilometer is shown for the NIRSS site (pink squares) and at a nearby NWS Automated Surface Observing System station (white circles). Vertical and temporal aggregate NIRSS icing is indicated by colored triangles at the bottom of the bottom panel along with the FIT derived from GOES, which is indicated by the colored squares.

hoped, to improve the utility of TAMDAR data for satellite validation.

5. Summary

In this paper, a physically based empirical technique was developed to estimate from satellite data the FIT to aircraft. The technique is formulated to utilize satellite-derived cloud products as input, including T_c, cloud-top phase, LWP, and R_e. The satellite-based icing method has been applied to current GOES data, and the results were rigorously compared with icing observations contained in PIREP, TAMDAR, and NIRSS data. A summary of these comparisons is provided in Table 13. During the daytime, the satellite icing detection accuracies are found to range from about 60% to 75% using the various validation sets as ground truth in all cloud conditions. The results that are based on comparisons with icing PIREPs are nearly identical to those found by Ellrod and Bailey (2007), who used

a radiance thresholding technique. Much better results are obtained if we use the satellite-derived cloud microphysical properties to screen out the cases obscured by high ice clouds, since the presence of SLW below these clouds cannot be inferred with current single-layer satellite retrieval methods. Excluding these cases yields accuracies of 90% or better when compared with NIRSS and PIREPs. The poor accuracy found in the comparisons with TAMDAR can be attributed to insufficient knowledge of when the TAMDAR sensor is reporting no-icing conditions in cloud rather than in clear air. From the data shown in Tables 8–11, we estimate that roughly 35% of atmospheric icing remains undetected using single-layer techniques, because of high cloud obscuration. New techniques (e.g., Chang et al. 2010) to derive cloud properties in some multilayer conditions [i.e., thin cirrus over lower-level water clouds; see Chang and Li (2005)] can be exploited to estimate the FIT below high-level ice clouds with a promising degree of accuracy. This is a topic for future research that may
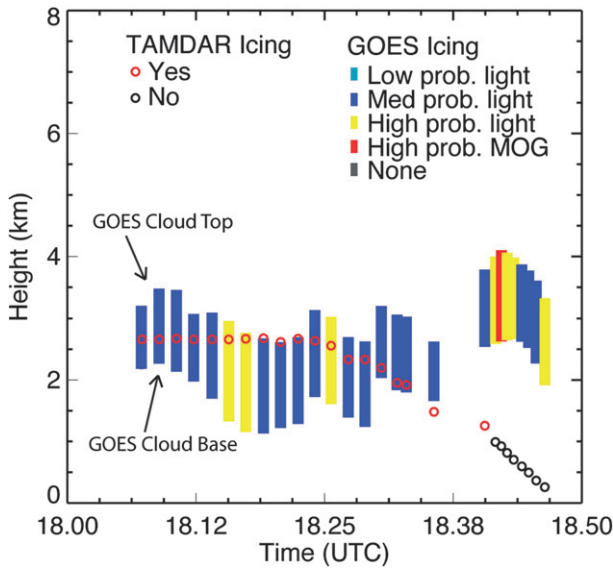
FIG. 10. Comparison of the GOES-derived flight icing threat to yes/no icing inferred using TAMDAR sensor measurements taken from a commercial aircraft on 22 Apr 2005 during the GLFE.

further improve the satellite-derived FIT under a wider range of cloud conditions.

A significant advance in the FIT algorithm developed here, relative to previous satellite-based icing analyses, is an estimate of icing probability and intensity that is based on derived cloud microphysical parameters. The technique significantly increases the information content extracted from the satellite observations, providing an improved dynamic range to the FIT that should be useful to the aviation community. Relative to icing PIREPs, the accuracy in the satellite two-category intensity estimates is between 58% and 68% depending on the degree of filtering used to reduce ambiguities that are likely due to poor spatial and temporal matching. Better agreement is found with NIRSS data (77% accuracy), which is also encouraging, keeping in mind that NIRSS is a ground-based remote sensing system and

does not provide a direct measure of icing intensity. The results presented here indicate that the satellite method has significant skill. Considering the somewhat ill-defined nature of icing intensity and severity, as well as many issues regarding the accuracy of the validation data used to characterize aircraft icing, it is possible that the practical utility of the method to the aviation community may be better than the validation data suggest, but this remains to be demonstrated.

Newer advanced imagers, with more channels and improved horizontal resolution and spectral information similar to that currently available on MODIS, such as the Visible Imaging Infrared Radiometer Suite on the Suomi National Polar-Orbiting Partnership, the Spinning Enhanced Visible and Infrared Imager (SEVIRI) on the Meteosat series deployed over Europe, and the Advanced Baseline Imager planned for GOES-R, are providing the impetus for research to further advance satellite-derived cloud characterizations for icing and other aviation weather hazards. For example, advanced imagers can provide some capability to improve the resolution of cloud vertical structure (e.g., Platnick 2000), which has not yet been exploited. It is also expected that the icing-detection accuracy at night and during the day/night transition will be somewhat better than that shown in Table 13 because of the availability of additional spectral information in the infrared with improved sensitivity to cloud-top phase (Pavolonis 2010). Despite the inherent bias toward "positive icing" reports found in the validation data used in this study, we were able to gain some understanding of potential false alarms, which appear to occur less than 10% of the time. A significant number of these cases appear to be due to the inability to detect thin cirrus clouds adequately with the current GOES imager in multilayer conditions. Improvements can be expected in the near future that take advantage of the improved resolution and spectral information available from advanced imagers, as well as improved cloud retrieval techniques, including the multilayer methods currently being developed.

TABLE 13. Summary of the FIT capability determined from GOES when compared with icing PIREP, TAMDAR, and NIRSS data for all cloud conditions, and under the condition that high-level overcast ice clouds do not obscure the satellite view. The intensity accuracy was only evaluated in overcast SLW conditions as determined from GOES.

		Icing detection				
		All clouds		Unobscured		
Validation data	Day/night	PODY (%)	Accuracy (%)	PODY (%)	Accuracy (%)	Icing-intensity accuracy (%)
PIREPs	Night	56	56	64	63	—
PIREPs	Day (all)	62	61	98	93	58
PIREPs	Day (filtered)	—	—	—	—	67
NIRSS	Day	76	73	100	90	77
TAMDAR	Day	45	72	87	53	—

The satellite-based icing product described here, as well as the icing altitude boundaries derived from Z_t, Z_b, and Z_{fr}, provide unique information about icing conditions over broad areas and at resolutions not available elsewhere that should contribute a substantial enhancement in aviation safety to regions susceptible to heavy supercooled liquid water clouds. These icing products, as well as many other cloud and radiation products being derived routinely from operational satellite data, are available in digital and graphical formats from NASA (http://angler.larc.nasa.gov).

REFERENCES

Bernstein, B. C., F. McDonough, M. Politovich, B. Brown, T. Ratvasky, D. Miller, C. Wolff, and G. Cunning, 2005: Current icing potential: Algorithm description and comparison with aircraft observations. *J. Appl. Meteor.,* **44,** 969–986.

——, C. A. Wolff, and P. Minnis, 2006: Practical application of NASA-Langley advanced satellite products to in-flight icing nowcasts. *Proc. 44th AIAA Aerospace Science Meeting and Exhibit,* Reno, NV, AIAA-2006-1220.

——, ——, and F. McDonough, 2007: An inferred climatology of icing conditions aloft, including supercooled large drops. Part I: Canada and the continental United States. *J. Appl. Meteor. Climatol.,* **46,** 1857–1878.

Brown, B. G., and G. S. Young, 2000: Verification of icing and turbulence forecasts: Why some verification statistics can't be computed using PIREPs. Preprints, *Ninth Conf. on Aviation, Range, and Aerospace Meteorology,* Orlando, FL, Amer. Meteor. Soc., 393–398.

Chang, F.-L., and Z. Li, 2005: A new method for detection of cirrus overlapping water clouds and determination of their optical properties. *J. Atmos. Sci.,* **62,** 3993–4009.

——, P. Minnis, B. Lin, M. M. Khaiyer, R. Palikonda, and D. A. Spangenberg, 2010: A modified method for inferring upper troposphere cloud top height using the *GOES 12* imager 10.7 and 13.3 μm data. *J. Geophys. Res.,* **115,** D06208, doi:10.1029/2009JD012304.

Curry, J. A., and G. Liu, 1992: Assessment of aircraft icing potential using satellite data. *J. Appl. Meteor.,* **31,** 605–621.

Daniels, T. S., 2002: Tropospheric airborne meteorological data reporting (TAMDAR) sensor development. *SAE General Aviation Technology Conf. and Exposition,* Wichita, KS, SAE International, 2002-02-153. [Available online at http://papers.sae.org/2002-01-1523.]

Dong, X., P. Minnis, G. G. Mace, W. L. Smith Jr., M. Poellot, R. T. Marchand, and A. D. Rapp, 2002: Comparison of stratus cloud properties deduced from surface, GOES, and aircraft data during the March 2000 ARM Cloud IOP. *J. Atmos. Sci.,* **59,** 3256–3284.

——, ——, B. Xi, S. Sun-Mack, and Y. Chen, 2008: Comparison of CERES-MODIS stratus cloud properties with ground-based measurements at the DOE ARM Southern Great Plains site. *J. Geophys. Res.,* **113,** D03204, doi:10.1029/2007JD008438.

Ellrod, G., and J. P. Nelson, 1996: Remote sensing of aircraft icing regions using GOES multispectral imager data. Preprints, *15th Conf. on Weather Analysis and Forecasting,* Norfolk, VA, Amer. Meteor. Soc., 9–12.

——, and A. P. Bailey, 2007: Assessment of aircraft icing potential and maximum icing altitude from geostationary meteorological satellite data. *Wea. Forecasting,* **22,** 160–174.

Haggerty, J., F. McDonough, J. Black, S. Landolt, C. Wolff, S. Mueller, P. Minnis, and W. L. Smith Jr., 2008: Integration of satellite-derived cloud phase, cloud-top height, and liquid water path into an operational aircraft icing nowcasting system. Preprints, *13th Conf. on Aviation, Range, and Aerospace Meteorology,* New Orleans, LA, Amer. Meteor. Soc., 3.13. [Available online at http://ams.confex.com/ams/pdfpapers/131893.pdf.]

Kane, T. L., B. G. Brown, and R. Bruintjes, 1998: Characteristics of pilot reports of icing. Preprints, *14th Conf. on Probability and Statistics,* Phoenix, AZ, Amer. Meteor. Soc., 90–95.

Mason, J. G., J. W. Strapp, and P. Chow, 2006: The ice particle threat to engines in flight. *Proc. 44th AIAA Aerospace Science Meeting and Exhibit,* Reno, NV, AIAA-2006-206.

Minnis, P., and Coauthors, 1995: Cloud Optical Property Retrieval (subsystem 4.3). Clouds and the Earth's Radiant Energy System (CERES) Algorithm Theoretical Basis Document: Cloud Analyses and Radiance Inversions (Subsystem 4), NASA RP 1376, Vol. 3, 135–176.

——, and Coauthors, 2004: Real-time cloud, radiation, and aircraft icing parameters from GOES over the USA. Preprints, *13th Conf. on Satellite Oceanography and Meteorolology,* Norfolk, VA, Amer. Meteor. Soc., P7.1. [Available online at http://ams.confex.com/ams/pdfpapers/79179.pdf.]

——, and Coauthors, 2008a: Near-real time cloud retrievals from operational and research meteorological satellites. *Remote Sensing of Clouds and the Atmosphere XIII,* R. H. Picard et al., Eds., International Society for Optical Engineering (SPIE Proceedings Vol. 7107), 710703, doi:10.1117/12.800344.

——, and Coauthors, 2008b: Cloud detection in non-polar regions for CERES using TRMM VIRS and *Terra* and *Aqua* MODIS data. *IEEE Trans. Geosci. Remote Sens.,* **46,** 3857–3884.

——, C. R. Yost, S. Sun-Mack, and Y. Chen, 2008c: Estimating the physical top altitude of optically thick ice clouds from thermal infrared satellite observations using *CALIPSO* data. *Geophys. Res. Lett.,* **35,** L12801, doi:10.1029/2008GL033947.

——, and Coauthors, 2011a: CERES edition-2 cloud property retrievals using TRMM VIRS and *Terra* and *Aqua* MODIS data, Part I: Algorithms. *IEEE Trans. Geosci. Remote Sens.,* **49,** 4374–4400.

——, and Coauthors, 2011b: CERES edition-2 cloud property retrievals using TRMM VIRS and *Terra* and *Aqua* MODIS data, Part II: Examples of average results and comparisons with other data. *IEEE Trans. Geosci. Remote Sens.,* **49,** 4401–4430.

National Aviation Safety Data Analysis Center, 2005: National Transportation Safety Board weather related accident study: 1994–2003. Federal Aviation Administration Study Rep. [Available online at http://www.asias.faa.gov/aviation_studies/weather_study/studyindex.html.]

Pavolonis, M. J., 2010: Advances in extracting cloud composition information from spaceborne infrared radiances—A robust alternative to brightness temperatures. Part I: Theory. *J. Appl. Meteor. Climatol.,* **49,** 1992–2012.

Platnick, S., 2000: Vertical photon transport in cloud remote sensing problems. *J. Geophys. Res.,* **105,** 22 919–22 935.

Politovich, M. K., 2003: Predicting inflight aircraft icing intensity. *J. Aircr.,* **40,** 639–644.

Rasmussen, R., and Coauthors, 1992: Winter Icing and Storms Project (WISP). *Bull. Amer. Meteor. Soc.,* **73,** 951–974.

Rauber, R., and A. Tokay, 1991: An explanation for the existence of supercooled water at the top of cold clouds. *J. Atmos. Sci.,* **48,** 1005–1023.

Reehorst, A., D. Brinker, M. Politovich, D. Serke, C. Ryerson, A. Pazmany, and F. Solheim, 2009: Progress towards the remote sensing of aircraft icing hazards. NASA Tech. Rep. NASA/TM-2009-215828, 12 pp. [Available online at http://icebox-esn.grc.nasa.gov/RSData/70880J.pdf.]

Smith, W. L., Jr., P. Minnis, and D. F. Young, 2000: An icing product derived from operational satellite data. Preprints, *Ninth Conf. on Aviation, Range, and Aerospace Meteorology,* Orlando, FL, Amer. Meteor. Soc., 256–259.

——, ——, B. C. Bernstein, F. McDonough, and M. M. Khaiyer, 2003: Comparison of super-cooled liquid water cloud properties derived from satellite and aircraft measurements. *Proc. In-Flight Icing/De-icing Int. Conf.,* Chicago, IL, Federal Aviation Administration 2003-01-2156.

——, ——, H. Finney, R. Palikonda, and M. M. Khaiyer, 2008: An evaluation of operational GOES derived single-layer cloud top heights with ARSCL over the ARM Southern Great Plains site. *Geophys. Res. Lett.,* **35,** L13820, doi:10.1029/2008GL034275.

Thompson, G., R. Bullock, and T. F. Lee, 1997: Using satellite data to reduce spatial extent of diagnosed icing. *Wea. Forecasting,* **12,** 185–190.

Wilks, D. S., 2006: *Statistical Methods in the Atmospheric Sciences.* Academic Press, 627 pp.

Xi, B., X. Dong, P. Minnis, and M. M. Khaiyer, 2010: A 10-year climatology of cloud cover and vertical distribution derived from both surface and GOES observations over the DOE ARM SGP site. *J. Geophys. Res.,* **115,** D12124, doi:10.1029/2009JD012800.